

Collaboration and Sustainability in Emergency Transport Resource Configuration

Lead Guest Editor: Yong Wang

Guest Editors: Zheng Wang and Xiangyang Guan





Collaboration and Sustainability in Emergency Transport Resource Configuration

Journal of Advanced Transportation

**Collaboration and Sustainability
in Emergency Transport Resource
Configuration**

Lead Guest Editor: Yong Wang





Guest Editors: Zheng Wang and Xiangyang Guan



Copyright © 2021 Hindawi Limited. All rights reserved.






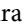

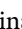


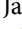




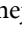


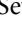


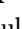
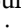
This is a special issue published in "Journal of Advanced Transportation." All articles are open access articles distributed under the Creative Commons Attribution License, which permits unrestricted use, distribution, and reproduction in any medium, provided the original work is properly cited.

Associate Editors

Juan C. Cano , Spain
Steven I. Chien , USA
Antonio Comi , Italy
Zhi-Chun Li, China
Jinjun Tang , China

Academic Editors

Kun An, China
Shriniwas Arkatkar, India
José M. Armingol , Spain
Socrates Basbas , Greece
Francesco Bella , Italy
Abdelaziz Bensrhair, France
Hui Bi, China
María Calderon, Spain
Tiziana Campisi , Italy
Giulio E. Cantarella , Italy
Maria Castro , Spain
Mei Chen , USA
Maria Vittoria Corazza , Italy
Andrea D'Ariano, Italy
Stefano De Luca , Italy
Rocío De Oña , Spain
Luigi Dell'Olio , Spain
Cédric Demonceaux , France
Sunder Lall Dhingra, India
Roberta Di Pace , Italy
Dilum Dissanayake , United Kingdom
Jing Dong , USA
Yuchuan Du , China
Juan-Antonio Escareno, France
Domokos Esztergár-Kiss , Hungary
Saber Fallah , United Kingdom
Gianfranco Fancello , Italy
Zhixiang Fang , China
Francesco Galante , Italy
Yuan Gao , China
Laura Garach, Spain
Indrajit Ghosh , India
Rosa G. González-Ramírez, Chile
Ren-Yong Guo , China


Yanyong Guo , China
Jérôme Ha#rri, France
Hocine Imine, France
Umar Iqbal , Canada
Rui Jiang , China
Peter J. Jin, USA
Sheng Jin , China
Victor L. Knoop , The Netherlands
Eduardo Lalla , The Netherlands
Michela Le Pira , Italy
Jaeyoung Lee , USA
Seungjae Lee, Republic of Korea
Ruimin Li , China
Zhenning Li , China
Christian Liebchen , Germany
Tao Liu, China
Chung-Cheng Lu , Taiwan
Filomena Mauriello , Italy
Luis Miranda-Moreno, Canada
Rakesh Mishra, United Kingdom
Tomio Miwa , Japan
Andrea Monteriù , Italy
Sara Moridpour , Australia
Giuseppe Musolino , Italy
Jose E. Naranjo , Spain
Mehdi Nourinejad , Canada
Eneko Osaba , Spain
Dongjoo Park , Republic of Korea
Luca Pugi , Italy
Alessandro Severino , Italy
Nirajan Shiwakoti , Australia
Michele D. Simoni, Sweden
Ziqi Song , USA
Amanda Stathopoulos , USA
Daxin Tian , China
Alejandro Tirachini, Chile
Long Truong , Australia
Avinash Unnikrishnan , USA
Pascal Vasseur , France
Antonino Vitetta , Italy
S. Travis Waller, Australia
Bohui Wang, China
Jianbin Xin , China



Hongtai Yang , China
Vincent F. Yu , Taiwan
Mustafa Zeybek, Turkey
Jing Zhao, China
Ming Zhong , China
Yajie Zou , China




Contents

Air Emergency Transport under COVID-19: Impact, Measures, and Future

Zhun Li 







Review Article (14 pages), Article ID 5560994, Volume 2021 (2021)

Two-Stage Humanitarian Logistics Deprivation Model for the Planning of Scarce KN-95 Facemask Supplies under Agent's Cooperation

Oscar L. Pineda-Martinez , Carlos D. Paternina-Arboleda , and Guisselle A. García-Llinás 

Research Article (10 pages), Article ID 6638266, Volume 2021 (2021)



Variable Speed Limit Strategies Based on the Macro Hierarchical Control Traffic Flow Model

Shubin Li , Tao Wang , Hualing Ren , Baiying Shi , Xiangke Kong , Jianyong Chai , and

Xuejuan Wang 


Research Article (10 pages), Article ID 9910097, Volume 2021 (2021)

Evaluation of Cruise Ship Supply Logistics Service Providers with ANP-RBF

Liling Huang , Yong Tan , and Xu Guan



Research Article (13 pages), Article ID 6645946, Volume 2021 (2021)

Optimization of Rider Scheduling for a Food Delivery Service in O2O Business

Guiqin Xue, Zheng Wang , and Guan Wang


Research Article (15 pages), Article ID 5515909, Volume 2021 (2021)

Vehicle Routing Problem for Collaborative Multidepot Petrol Replenishment under Emergency Conditions

Guangcan Xu  and Qiguang Lyu 

Research Article (20 pages), Article ID 5531500, Volume 2021 (2021)

A Multistage Dynamic Emergency Decision-Making Method considering the Satisfaction under Uncertainty Information

Yong Liu 

Research Article (14 pages), Article ID 5535925, Volume 2021 (2021)

An Optimization Model for Tramp Ship Scheduling considering Time Window and Seaport Operation Delay Factors

Ang Yang , Yu Cao , Kang Chen , Qingcheng Zeng, and Zigen Chen

Research Article (19 pages), Article ID 6650097, Volume 2021 (2021)

Application of the Bayesian Model Averaging in Analyzing Freeway Traffic Incident Clearance Time for Emergency Management

Yajie Zou, Bo Lin , Xiaoxue Yang, Lingtao Wu, Malik Muneeb Abid, and Jinjun Tang 





Research Article (9 pages), Article ID 6671983, Volume 2021 (2021)

An Improved Fuzzy Trajectory Clustering Method for Exploring Urban Travel Patterns

Fang Liu , Wei Bi , Wei Hao , Fan Gao , and Jinjun Tang 




Research Article (13 pages), Article ID 6651718, Volume 2021 (2021)

Cooperative Hypercube Queuing Model for Emergency Service Systems

Han Liu , Hao Yin , Yang Zhou , and Meng Li 

Research Article (12 pages), Article ID 6653573, Volume 2021 (2021)

Research on Operation Characteristics and Safety Risk Forecast of Bus Driven by Multisource Forewarning Data

Shejun Deng , Hongru Yu , and Caoye Lu 

Research Article (19 pages), Article ID 6623739, Volume 2020 (2020)

Review Article

Air Emergency Transport under COVID-19: Impact, Measures, and Future

Zhun Li ^{1,2}

¹*School of Economics and Business Administration, Chongqing University, Chongqing 400030, China*

²*Postdoctoral Programme, Chongqing Airport Group Co., Ltd., Chongqing 401120, China*

Correspondence should be addressed to Zhun Li; i-chn-e@163.com

Received 26 February 2021; Revised 30 July 2021; Accepted 31 August 2021; Published 22 September 2021

Academic Editor: Yong Wang

Copyright © 2021 Zhun Li. This is an open access article distributed under the Creative Commons Attribution License, which permits unrestricted use, distribution, and reproduction in any medium, provided the original work is properly cited.

The COVID-19 pandemic caused by SARS-CoV-2 dominated the year 2020 and has an unprecedented impact on global air transport. This paper tries to make an overall review on the interaction of air transport and the COVID-19 pandemic. Although the confirmed cases were first reported in China, the origin of the pandemic remains uncertain. China was the first country to control the COVID-19 pandemic, and domestic air traffic recovers at a fast pace. Compared to 2019 level, world scheduled capacity, passengers carried, and revenues for 2020 were reduced by 50%, 60%, and \$371 billion, respectively. Compared with domestic passenger traffic, international passenger traffic reduces more seats, passengers, and revenues. Because air transport contributes to economic growth, many countries or regions provide aviation bailout. The US provides most direct aid, while China mostly provides policy measures. In the post-COVID-19 period, IATA suggests that accepting vaccinated passengers is the best practice to reopen borders. Air cargo will play an important role in the distribution of COVID-19 vaccines. Meanwhile, air transport should be more digitalized, sustainable, and responsible in the future.

1. Introduction

In the past several years, global air transport rapidly develops. According to the World Bank, the number of passengers carried increased from 0.31 billion in 1970 to 4.40 billion in 2019 [1]. The increasing passenger demand promotes the industry revolution and changes the ecosystem. For example, low-cost airlines are gaining more market share, which are different from full-service airlines servicing in segmentation of passengers [2]. During the process of growth, the air transport industry is always under the exposure of endogenous risks [3] and has undergone disasters and crises, such as 911 terrorist attacks, severe acute respiratory syndrome (SARS), H1N1, and Middle East respiratory syndrome. But the growth almost never stopped before the coronavirus disease 2019 (COVID-19) pandemic [4]. The global air transport industry operated as many as 38 million commercial flights and serviced 4.3 billion passengers in 2018 [5]. In addition, the sector employed 65.5 million people including 10.5 million staff in airlines and airports in 2019 [6].

However, the growth of air transport peaked in 2019. The COVID-19 pandemic broke out at the end of 2019, which was caused by a novel coronavirus known as SARS-CoV-2 [7]. The COVID-19 pandemic dominated the year 2020 and still evolves in this year. The pandemic has extensive and far-reaching impacts on both individuals and society. The International Civil Aviation Organization (ICAO) shows that COVID-19 is an unprecedented shock and hits hard the air transport industry. Compared to the 2019 level before COVID-19, the world air passengers including international and domestic passengers declined 60% in 2020 [8]. According to the Center for Systems Science and Engineering at Johns Hopkins University, global confirmed COVID-19 cases surpassed 100 million by January 26, 2021 [9]. However, the waves of COVID-19 are not over yet. Several variants of the virus are creating concern. These SARS-CoV-2 variants first emerged in the UK, South Africa, and Brazil and have spread to the rest of the world [10].

COVID-19 is similar to SARS, both of which are airborne diseases resulting from human-to-human

transmission [11]. However, these two viruses are completely different [12]. Although COVID-19 is less severe than SARS, the former is found to be more contagious than the latter [13–16]. Before outbreak of the COVID-19 epidemic, SARS was the first deadly coronavirus pandemic with the ability of human-to-human transmission [17].

SARS is caused by SARS coronavirus (SARS-CoV) [18, 19]. A detailed chronology of SARS has been established [20]. The first known SARS case was confirmed in late 2002 in Guangdong province, China [21]. On February 21, 2003, a superspreader from Guangdong went to Hong Kong and communicated the virus to the nearby residents including 4 healthcare workers [22]. Because of international travel, the infected guests then carried SARS to Vietnam, Singapore, and Canada [23]. Within 6 months, the pandemic had spread to 28 more countries and regions in five continents: Asia, North America, Oceania, Europe, and Africa. Eventually, SARS disappeared rapidly benefiting from global cooperation and effective infection control measures. On April 28, 2003, Vietnam firstly ended SARS successfully. Hong Kong and China were declared SARS-free on June 23 and June 24, 2003, respectively. As the last human chain of SARS transmission was broken in Taiwan, China, the WHO announced the end of SARS epidemic on July 5, 2003. As of July 2003, the confirmed SARS cases were 8098 with 774 deaths across the world [24].

SARS did not hurt the air transport industry, as it rapidly bounced back. However, the air transport industry struggled to survive from the COVID-19 pandemic through the year 2020. Year 2020 was the most difficult year in history for the air transport industry. But it is the price we have to pay for controlling the COVID-19 pandemic. Travel restrictions play an important role in controlling the COVID-19 pandemic because international flights are one of the major drivers of international transmission of the pandemic [25]. By using COVID-19 air traffic visualization tool built by RAND Corporation, RAND found that about forty passengers per week exported this virus worldwide via international travel by the end of February 2020 [26].

It is necessary to summarize the economic impacts of COVID-19 on air transport, the roles of air transport in preventing COVID-19, and the future of air transport in the post-COVID-19 era. Tanriverdi et al. [27] reviewed the previous studies before COVID-19 published in the *Journal of Air Transport Management*. They used a bibliometric and visualization analysis and found that few studies focused on the combination of air transport and pandemics or crises. The results were surprising to Tanriverdi et al. [27]. The reason is that they expected that previous pandemics and crises never hit hard air transport like COVID-19 and thus the related studies are neglected. They also expected that the studies related to pandemic and transport would attract more attention in the future. Sun et al. [28] reviewed the short-term and long-term impact of COVID-19 on air transport and the role air transport plays in the spread of COVID-19. Meanwhile, they proposed 10 directions of future research regarding COVID-19 and air transport.

This paper first highlights some key moments during the COVID-19 pandemic, especially from the perspective of China. Second, this paper summarizes the roles of air

restrictions in controlling COVID-19 and analyzes the negative impact of COVID-19 on air transport industry, especially Chinese civil aviation markets. The negative operating losses make airlines face rapid cash burn and then bankruptcy. However, because the air transport industry contributes to economic growth, aviation bailout is provided to help the industry. Air transport industry needs to evolve actively to adapt to changes in the post-COVID-19 era. This paper predicts the future of air transport industry finally.

This paper tries to make an overall review on the interaction of air transport and COVID-19 pandemic. This paper summarizes the roles of air restrictions in controlling the COVID-19 pandemic and performance of air transport industry during the COVID-19 pandemic. Because air transport is important for economic development, it gets government assistance. This paper tracks aviation bailout.

This paper also tries to contribute to highlighting the timeline of COVID-19 pandemic from the perspective of China. There are five stages of fighting against the epidemic for China. Thanks to the effective control of COVID-19 and policy support for civil aviation in China, China's domestic aviation market is recovering fast.

The rest of the paper is structured as follows. Section 2 looks back at the evolution of COVID-19 pandemic. Section 3 presents the impact of air transport on transmission of COVID-19, and Section 4 presents the impact of COVID-19 on the air transport industry. Section 5 introduces aviation bailout and the effectiveness to support air transport. Section 6 summarizes the relationship between air transport and economic growth. Section 7 predicts the future of air transport, and Section 8 concludes the paper.

2. Timeline of COVID-19 Pandemic Developments

On December 27, 2019, Hubei Provincial Hospital of Integrated Chinese and Western Medicine reported cases of pneumonia of unknown cause to the Wuhan Jiangnan Center for Disease Prevention and Control. On December 31, China informed WHO about a cluster of pneumonia cases in Wuhan, Hubei province [29]. And, since that day, China began to release updates on the disease in accordance with the law. On January 7, 2020, a new type of coronavirus was identified as cause by Chinese authorities. As of January 19, 2020, China was in the first stage of fighting against the epidemic, where it was swift response to the public health emergency.

The second stage, between January 20 and February 20, was the initial progress in containing the virus. During this period, newly confirmed cases in China rapidly increased. China began an all-out battle to protect Wuhan and Hubei from the COVID-19 epidemic. China mobilized nationwide resources to assist Hubei province and Wuhan city. On January 20, the National Health Commission (NHC) confirmed that the novel coronavirus could transmit from human to human and brings the pneumonia under quarantinable infectious disease management. On January 23, the Wuhan city's outbound routes at its airports and railway stations were closed temporarily at 10 a.m. and passenger

traffic into Wuhan from other parts of China by road or waterway was suspended. On February 11, the WHO announced COVID-19 as the name of the disease and the virus causing COVID-19 was officially named "SARS-CoV-2." As the most comprehensive, stringent, and thorough epidemic prevention and control campaign was launched in China, the spread of the virus was curbed preliminarily. On February 19, newly cured and discharged cases outnumbered newly confirmed ones in Wuhan for the first time.

During the third stage, from February 21 to March 17, the rapid spread of virus was contained in Wuhan and Hubei province and the situation in other parts of China stabilized. However, the COVID-19 epidemic began to break out in other countries. On February 23, many Italian small towns entered a lockdown, and, on March 11, WHO declared COVID-19 a pandemic. However, from March 11 to March 17, the daily new confirmed cases in China remained in single digits and the epidemic peak had passed as a whole. To promote the stable development of air transport industry of China, on March 9, Civil Aviation Administration of China (CAAC) issues a series of support policies, including financial policies, charge reduction and burden alleviation, infrastructure investment, and so on. Some days later, US president Trump signed a \$2 trillion stimulus package called the CARES (Coronavirus Aid, Relief, and Economic Security) Act, in which air transport industry got more than \$60 billion.

The fourth stage, between March 18 and April 28, was an initial victory in a critical battle in defending Wuhan and Hubei against COVID-19. On March 18, there were no new domestic confirmed cases in China. However, on March 25, imported confirmed cases were reported in 23 provinces of China. To curb the spread of the virus, on April 1, nucleic acid testing was conducted on overseas arrivals at all points of entry. On April 8, Wuhan lifted 76-day outbound traffic restrictions and travel began to return to normal. By April 26, all COVID-19 patients in Wuhan hospitals had been discharged. Since this stage, China adopted an approach to guard against imported cases and a rebound in indigenous cases.

From April 29, China entered the fifth stage of ongoing prevention and control. The nationwide virus control was conducted on an ongoing basis. On May 1, WHO announced that the COVID-19 pandemic remains a public health emergency of international concern. However, on May 2, the public health emergency response was lowered to level 2 in Hubei province. It took China about 3 months to record a decisive victory in defending Wuhan city and Hubei province. This achievement did not come easily for China with its large population.

On May 14, global coronavirus death toll exceeded 300,000 according to Johns Hopkins University. On July 22, China launched the urgent use of COVID-19 vaccines. By the end of September, domestic air passengers carried nearly reached 2019 level in China [30]. As COVID-19 infections spiraled, Germany decided to impose national lockdown from November 2. Meanwhile, on December 14, a new SARS-CoV-2 variant was identified in UK, which could spread more readily between people [31]. On December 31,

Sinopharm COVID-19 vaccine got conditional market approval [32]. And, on February 6, 2021, China granted conditional market approval for Sinovac COVID-19 vaccine. In the United States, the U.S. Food and Drug Administration issued the first emergency use for Pfizer-BioNTech COVID-19 vaccine on December 11, 2020 [33].

Because of the increasing number of confirmed cases caused by virus imposed from abroad, on January 6, Shijiazhuang city imposed a lockdown to curb infection. During Spring Festival, Chinese people were encouraged to stay put. On January 29, Shijiazhuang ended the lockdown for residents in low-risk areas. A World Health Organization report published on March 30 said that SARS-CoV-2 most likely transmits from bats to humans through other emissary animals and that a lab leak was extremely unlikely [34]. From mid-March, there was a sudden rise in the number of confirmed cases in India. On May 1, India reported a record daily rise of 401,993 new confirmed cases. Some days later, India had a new record high of 414,188 confirmed cases on May 7. In May, the COVID-19 pandemic suddenly broke out in Taiwan, China. On May 26, Taiwan, China, reported a total of 6,091 confirmed cases.

As of May, Guangzhou reported some COVID-19 cases infected by the Delta variant, which was first detected in India and is known to be highly transmissible. On June 2, Guangzhou raised the COVID-19 risk level of neighborhoods in Liwan, Panyu, and Haizhu districts. On June 25, all high-risk areas in China were cleared. Figure 1 highlights the timeline of COVID-19 as of June 2021.

3. Roles of Air Restrictions in Containing COVID-19

Facing the outbreak of COVID-19 pandemic, there is no choice but to implement bundles of protective measures which are highly restrictive and sometimes even intrusive in response to the spread of worldwide COVID-19 pandemic. Air travel is assessed to be possible to accelerate the spread of pandemic [35]. RAND estimates that COVID-19 transmits worldwide via international air flights [26]. China firstly identified COVID-19 and firstly took public measures to control the virus and prevent its human-to-human transmission. As COVID-19 rapidly spreads around the world, most governments adopt measures at various levels, including movement and travelling restrictions. Many studies explore the role of transport in the spread of infectious diseases and assess the role of travelling restrictions in controlling and limiting the COVID-19 pandemic.

To effectively manage the infectious diseases and assess the role of transport, Muley et al. [36] reviewed the literature related to infectious diseases and transport and analyzed the interaction of transport and the spread of infectious diseases. They found that transport plays a crucial role in controlling the spread of infectious diseases and transport sector is worst affected by the movement restrictions. Browne et al. [37] reviewed the role of transportation in the transmission of influenza and coronaviruses and found that, compared with road transport and sea transport, the propagation of influenza can be accelerated and amplified by air transport.

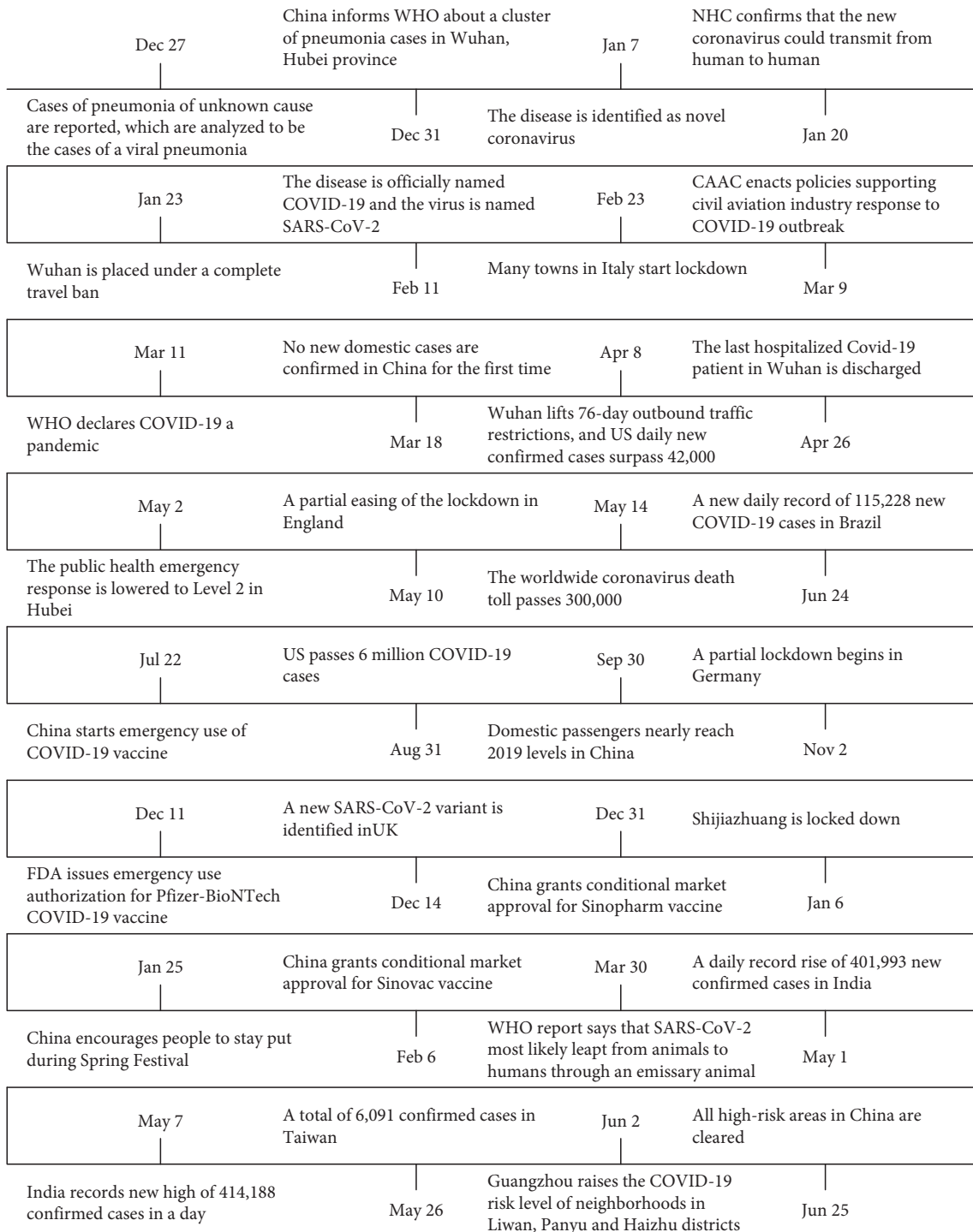


FIGURE 1: A timeline of COVID-19 during the period of 2019–2021.

The movement of travelers impacts the number of infected people and the duration of the epidemic [38]. Zhang et al. [39] found that the number of COVID-19 cases in the destinations was significantly related to the frequencies of air flights from Wuhan and that the speed of the spread of COVID-19 was also significantly associated with the presence of the airport. Many researches supported the view that travelling restrictions seem to be one of the most effective

measures in restraining the spread of COVID-19. Linka et al. [40] showed that if travelling restrictions were not implemented with regard to the recent COVID-19 outbreak, the spread of COVID-19 could have been more serious, especially in France, Spain, and Central Europe. A shutdown of highly connected hub airports in biggest cities is effective to inhibit the spread the epidemic [41]. At the domestic level, the travelling restrictions can delay the outbreak by some

days, and, at the international level, the travelling restrictions contribute to delaying the spread by a couple of weeks [42]. Especially at the early stage of the pandemic outbreak, travelling restrictions were found to be effective, while once the pandemic began to spread widely, the effectiveness of travelling restrictions became less [43]. Meanwhile, systematic reviews studied by Bielecki et al. [44] showed that the effect of travelling restrictions on limiting COVID-19 was limited generally and multiple factors affected the degree of impact, such as the extent and timing of restrictions, the epidemic size, the virus transmissibility, and travel patterns. They also pointed that temperature screening was not effective. Quarantine may delay the transmission of virus, but the effect is likely to be small. Saliva testing may be the best way to avoid quarantine after flight. Bajardi et al. [45] and Hollingsworth et al. [46] also found that travelling restrictions were of small a magnitude to affect the global spread of pandemic.

Apart from travelling restrictions, China was the first country to implement protective measures, some of which are worthy of reference. Shaw [47] overviewed the infection control practices during the 2003 SARS outbreak. The control measures included dedicated SARS hospitals [48], personal protective equipment [49, 50], isolation [51], physical space separation [52], handwashing [53], environmental decontamination [54], and education and training [55]. The lessons learned from 2003 SARS were helpful to control the spread of COVID-19.

Zhang et al. [56] summarized multiple levels of interventions including societal, community, organizational, and individual levels in Shanghai, China. Societal level strategy included reporting system and quarantine reinforcement, public health education, educational system support, and customs support. Both community health service centers and neighborhood committees played an important role in prevention efforts at a community level. Many public places were closed and all large public activities were suspended. Entertainment, exhibitions, lectures, and forums were provided online. Experts advised individuals to wear masks, open windows, wash hands frequently, and so on through mass media and social media. In addition, the use of serving chopsticks and spoons was called for by the government.

As the COVID-19 pandemic began to spread across the world, other countries and regions also implemented their protective measures. Several government interventions directly decreased contact probabilities, such as social distancing, bans on public events, self-isolation, and school closure. Meanwhile, other interventions included travelling restrictions and personal protective measures [57–61]. Haug et al. [62] ranked the effectiveness of these government interventions using a modelling approach that combines four different methods. Their study demonstrated that the imposed government interventions were necessary to suppress the spread of COVID-19, while there was a difference in their effectiveness. Among them, the most effective interventions comprised curfews, lockdowns, and gathering cancellations; and the highly effective and less intrusive measures included land border restrictions, support to the vulnerable, and risk-communication strategies.

4. Impact of COVID-19 on Air Transport

Global air transport sector makes great sacrifices to fight COVID-19. The social distancing and movement restriction measures, especially travelling restrictions, result in collateral damage to society, economy, and trade [62]. Due to the COVID-19 pandemic and travelling restriction measures, air transport suffers from a dramatic drop in demand. Bouali et al. [63] found that, in the period from January to April 2020, COVID-19 has significantly affected global passenger transport and air freight, resulting in losses and even bankruptcy. They are also expected to be worse in the coming years. In 2020, airlines were impacted by COVID-19, and many have ceased operation or gone bankrupt.

As expected by Bouali et al. [63], 2020 was a tough year for global air transport sector. Airports were estimated to lose approximately 64.2 of passenger traffic and 65% or more than 111.8 billion revenues in 2020 compared to business as usual [64], and airlines reduced revenue passenger kilometers by 65.9% in 2020 compared to 2019 [65]. Taken together, ICAO [8] reported that, compared to 2019 level, world scheduled capacity for year 2020 offered by airlines reduced by 50% overall, passengers carried reduced about 2.7 billion, and gross passenger operating revenues of airlines reduced about 371 billion dollars. Because travelling restrictions are mostly imposed on long-distant international flights, international flights suffer more seriously than domestic flights [66]. Therefore, compared with domestic passenger traffic, international passenger traffic reduces more seats and passengers and losses more revenues. Table 1 summarizes the scheduled passenger traffic for year 2020.

There is a difference in air passenger traffic by region. As shown in Table 2, Asia and Pacific region seriously suffers from reduction of passengers and losses of revenues, falling by 921 million and 120 billion dollars, respectively. Europe and North America regions are not far behind.

The numbers of passengers carried by China's civil flight in 2020 was 418 million, which is about 63% of 2019 level [67]. The monthly evolution of China's passenger traffic from 2019 to 2021 is shown in Figure 2. Figure 2 shows that the numbers of passengers carried by domestic flights in February bottom out. Thanks to the effective control of the COVID-19 pandemic, China's domestic market has been recovering at faster pace since then. Domestic passenger traffic in September 2020 almost reached the level of the same period of last year. After a brief drop during Spring Festival in 2021, domestic passengers carried quickly recovered. The domestic passengers carried in March 2021 exceeded the level of the same period of 2019. However, because international travelling is still restricted by most countries, China's international passenger traffic has been in a low level since February 2020.

The performance of global air transport is barely satisfactory, which is reflected in stock market as well. Depending on the GARCH model, Liu et al. [68] found that the holistic volatility of index of Chinese airport shipping set increased compared to the pre-COVID-19 period and that there were significant differences in volatility of airports. In addition, the further evidences indicate that the more positive attitude

TABLE 1: Change of world total air passenger traffic for year 2020 compared to 2019 level.

	Airlines seats	Passengers	Airlines gross operating revenues
Global	-50%	2,699 million (-60%)	-371 billion dollars
International	-66%	1,376 million (-74%)	-250 billion dollars
Domestic	-38%	1,323 million (-50%)	-120 billion dollars

TABLE 2: Change of air passenger traffic for year 2020 compared to 2019 level by region.

Region	Airlines seats	Passengers	Airlines gross operating revenues
North America	-43%	-599 million	-88 billion dollars
Asia and Pacific	-45%	-921 million	-120 billion dollars
Europe	-58%	-769 million	-100 billion dollars
Latin America and the Caribbean	-53%	-199 million	-26 billion dollars
Middle East	-60%	-132 million	-22 billion dollars
Africa	-58%	-78 million	-14 billion dollars

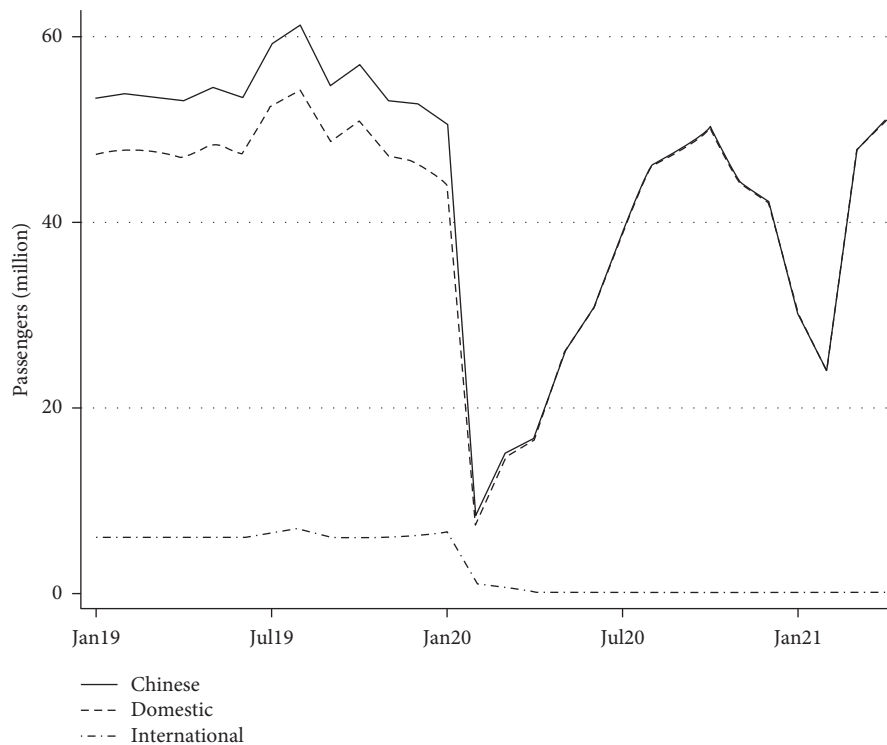


FIGURE 2: China's passenger traffic monthly evolution during the period of 2019–2021.

and more effective measures to mitigate risks of the diseases can decrease the stock price volatility. Maneenop and Kotcharin [69] demonstrated that the stock returns of 52 international listed airlines decrease more significantly than market returns and found that investors overreacted after the official announcements of WHO and President Trump.

The outbreak of COVID-19 also spilled over the employment in air transport industry and related industries, such as tourism. The reduction of capacity and loss of revenues of airlines rippled the airline employment. During the COVID-19 period, total airline employment is estimated to decrease by 7–13%, with major airlines being worst affected [70]. World Tourism Organization (UNWTO) reports that, compared to 2019 level, international tourist

arrivals reduced by 1 billion or by 74%, international tourism revenues decreased by 1.3 trillion dollars, and 100–120 million tourism jobs were directly impacted. Moreover, international tourist arrivals plunged to 381 million, lower than 1990 level [71].

5. Aviation Bailout

As global air traffic activity plummeted, the cash holding of airlines and airports is rapidly burnt for the high capital costs. The share of fixed and semifixed costs of air transport industry picked up to 61% in 2020 and amortization and depreciation became the largest fixed operating cost [72]. Most of airlines have cash to maintain operation for only

about two months [73]. However, civil aviation is seen as the strategic asset by many governments such as in Singapore, because it is closely related to other industries and economic growth. Meanwhile, during the COVID-19 pandemic, air transport plays an important role in stabilizing supply chains. Therefore, subsidies are provided to maintain air transport [74].

Many countries provide financial support to national airlines, airports and other participants in air transport sector. The support form can be divided into seven main categories, that is, government-backed commercial loans and government guarantees, recapitalization through state equity, flight subsidies and nationalization, deferral and/or waiver of taxes and charges, grants, and private equity [75]. Table 3 shows the government support provided by some countries and regions to airlines during the COVID-19 pandemic. As of August 2020, about 160 billion dollars were provided by governments to airlines [76]. The financial aid package for US airlines extends to more than 80 billion dollars, much more compared to other countries. Germany, France, Italy, and some other European countries intend to nationalize the large airlines in their countries to avoid being merged by other countries.

Abate et al. [75] explored the aim of government support to airlines in three dimensions of competition and liberalization, ownership and control, and environmental sustainability. In order to maintain essential connectivity and protect economy and employment, a few major airlines or/and state-owned airlines obtain biggest financial support. Meanwhile most of low-cost and regional airlines only get a small part, which leads to an unfair competition and bankruptcy of small airlines. As shown in Table 4, at least 31 airlines ceased operation, went bankrupt, or filed for bankruptcy in 2020, all of which were low-cost airlines or regional airlines.

Apart from airlines, governments also provide support to airports, cargo airlines, general aviation, workers, and so on. Tables 5–7 show the measures to support airports, cargo carriers and general aviation, and workers, respectively. As shown in Table 5, more policy measures are provided in China, while the US, Singapore, and Norway provide direct aid to airports. The US provides \$10 billion grants-in-aid, Norway fully compensates the loss of airport charges, and Singapore allows airport to defer payment of fees.

Different from passenger flight, the pandemic leads to the increase in air cargo demand. To keep supply chains in foreign trade smooth, China provides effective policy measures to increase international air freight capacity. The US provides \$4 billion loans and loan guarantees for cargo carriers. Singapore rebates 10% landing charge for all scheduled freighter flights. In air transport industry, general aviation has not received sufficient attention [77]. Only US general aviation airports get \$100 million.

The US provides a total of \$41.5 billion grants for employee wages, salaries, and benefits, with \$34.5 billion for passenger airline employees, \$4 billion for cargo airline employees, and \$3 billion for airline contractor employees. Hong Kong, China, earmarks HK\$50 million to provide training allowance to frontline airport staff on no-pay leave.

Singapore pays 75% of the first S\$4,600 of monthly salaries per employee.

Overall, China and the US almost pay attention to each part in air transport industry. However, China mostly provides fee exemptions and policy measures, while the US provides direct aid with conditions. US aviation companies should avoid layoffs, maintain certain air service, and limit dividends and executive compensation. Compared with the US, China should provide more direct aid to air transport industry.

6. Air Transport and Economic Growth

In Organization for Economic Co-operation and Development (OECD) countries, passenger and freight air transport only account for about 0.3% of value-added, yet the important roles in economic activity are made by the strong linkages with both upstream and downstream industries [76]. In addition, the economic growth also generates demand for air transport and accelerates the development of air transport. The key point in the field is whether there is causal relationship between air transport and the economy. Tam and Hansman [78], Britton et al. [79], and Laird and Mackie [80] established a conceptual framework consisting of major channels where air transport and economy interact. Air transport impacts economy through supply chain effect and spillover effect, and economy accelerates air transport through feedback effects.

Irwin and Kasarda [81], Button et al. [82], Brueckner [83], Button and Yuan [84], and Brida et al. [85] found that there is a unidirectional causal relationship from air transport to economic growth. Fernandes and Pacheco [86] only found feedback effect from economy to air transport. Most studies found the evidences of bidirectional effect between air transport and economy [87, 88]. Zhang and Graham [89] found that the bidirectional effect is more likely to present in developing countries and there is only unidirectional effect from air transport to economies growth in developed countries.

In order to overcome the endogeneity problem better, McGraw [90] employed a pooled synthetic control event study strategy and found that airports can increase total employment by 3.9% per decade. Tveter [91] used difference in difference approach and estimated that the population of the city near the airports increased by 5% from 1970 to 1980. Apart from most studies at macro level, recently questions related to air transport at firm level are studied. Ellis et al. [92] introduced direct flights as an exogenous shock and found that the mutual funds invest significantly more in firms more proximate due to direct flights and these investments perform better.

7. Development of Air Transport after COVID-19

COVID-19 vaccines are perhaps the best hope for limiting and even ending the epidemic. Before the presence of COVID-19 vaccines, the fresh waves of the epidemic continued. Gudmundsson et al. [93] showed that the most

TABLE 3: Measures to support airlines in some countries and regions.

Country/region	Measures	Effective date/ duration
China	Waiver of Civil Aviation Development Fund payable by airlines	1 Jan 2020
	A subsidy of CNY 0.0176 per available seat-kilometer for cooperated international routes, and a subsidy of CNY 0.0528 per available seat-kilometer for international routes covered by a sole airline	From 23 Jan to 30 Jun 2020
	Exemption of parking fees and 10% reduction of base price of landing & take-off fees at classes 1 and 2 airports; 10% reduction of route fares; 8% reduction of base price of jet fuel sales difference for domestic flights operated by domestic airlines	23 Jan 2020
	Support for airlines' reorganization and optimization of capacity as required	11 Feb 2020
Hong Kong, China	Full waiver for five months on parking and airbridge fees for idle passenger aircraft	From Feb to Jun 2020
	40% reduction of passenger aircraft landing charges for four months	
	Reduction of ramp handling, maintenance, and airside vehicle-related fees	
	Purchase of around 500,000 air tickets in advance from the four home-based airlines worth up to HK\$2 billion	8 Apr 2020
USA	\$25 billion in loans and loan guarantees available to passenger airlines	30 Mar 2020
	\$17 billion in loans and loan guarantees to Boeing and its suppliers	
Singapore	10% landing charge rebate for all scheduled passenger flights landing in Singapore	From Apr 2020 to Mar 2021
	50% rebate on rental paid for airlines' lounges and offices within Changi Airport and Seletar Airport terminal buildings	
	100% rebate on aircraft parking charges at Changi Airport and Seletar Airport	
	Waivers of the 1% increase in Landing, Parking, and Aerobridge (LPA) charges for all airlines and freighter flights	
	Deferred payment of certain fees such as certificates of airworthiness	26 Mar 2020
	Temasek Holdings will vote in favour of new issuance of shares and bonds and will buy all remaining shares and bonds	
Australia	\$715 m relief package to refund and waive aviation fuel excise, air service charges, and domestic and regional aviation security charges	17 Mar 2020
	\$198 million to maintain critical air services throughout regional Australia by securing operations to certain routes	28 Mar 2020
New Zealand	NZ\$163 million financial support to pay passenger-based government charges for the next six months	17 Mar 2020
	NZ\$37 million to cover airways related fees for the next six months	
	Any fee rises or pricing reviews from agencies that charge fees at the border are put on hold for 12 months	
	NZ\$900 million government loan to Air New Zealand over the next two years	20 Mar 2020
Germany	€9 billion bailout to take 20% stake of Lufthansa	25 May 2020
France & Netherlands	€10 billion bailout to Air France-KLM	24 Apr 2020
Italy	€600 million bailout to Alitalia	17 Mar 2020
Sweden and Denmark	\$300 million credit guarantees to SAS	17 Mar 2020

pessimistic estimate of the recovery of passenger demand to pre-COVID-19 level will be in 2026 in the absence of vaccines. The demand for vaccines is almost certain to exceed the supply in 2021 [94]. International Air Transport Association (IATA) suggests that accepting vaccinated passengers is the best practice to reopen borders [95]. However, vaccine passports may worsen vaccine inequality [96]. Some high-income countries are already stockpiling vaccines [97], while low-income and middle-income countries urgently need vaccines [98]. Because inequitable vaccine distribution can cost lives and the global economy [99, 100], vaccine inequality should be righted and vaccines should be distributed equitably [101]. Air cargo plays a crucial role in distributing vaccines [102]. While just providing a single dose to 7.8 billion people needs 8,000 Boeing

747 cargo aircraft, and diminished cargo capacity of the global air transport industry likely limits the distribution of vaccines [103], it is necessary for vaccine distribution to establish emergency logistics with cost reduction and quick emergency response under limited transportation resources [104].

Another challenge for COVID-19 vaccine distribution is the cold chain transportation [105]. To ensure the quality of vaccines, the transportation must be in line with international regulatory requirements. The temperatures should be controlled. In every corner of the world, cold chain facilities are required and the scale of cold chain transportation is vast.

Although COVID-19 hits hard air transport, it promotes the rapid development and application of digitalization

TABLE 4: List of bankruptcy of airlines in 2020.

Airlines	Country/region	Date
Trans States Airlines	USA	1 Apr 2020
Compass Airlines	USA	7 Apr 2020
Ravn	USA	Apr 2020
Miami Air International	USA	8 May 2020
Shoreline Aviation	USA	1 Apr 2020
ExpressJet	USA	30 Sep 2020
Air Italy	Italy	26 Feb 2020
Ernest Airlines	Italy	13 Jan 2020
Flybe	UK	5 Mar 2020
Germanwings	Germany	7 Apr 2020
German Airways	Germany	22 Apr 2020
SunExpress Deutschland	Germany	26 Jun 2020
LEVEL Europe	Austria	18 Jun 2020
Jet time	Denmark	21 Jul 2020
Go2Sky	Slovakia	21 Aug 2020
Montenegro Airlines	Republic of Montenegro	24 Dec 2020
AtlasGlobal	Turkey	12 Feb 2020
Cathay Dragon	Hong Kong, China	21 Oct 2020
NokScoot	Thailand	24 Jun 2020
Air Asia Japan	Japan	5 Oct 2020
Palestinian Airlines	Palestine	29 Dec 2020
Tigerair Australia	Australia	5 Aug 2020
South African airways	South Africa	6 Apr 2020
South African express	South Africa	29 Apr 2020
Avianca Perú	Peru	10 May 2020
TAME EP	Ecuador	19 May 2020
Flyest	Argentina	10 Jun 2020
LATAM Argentina	Argentina	19 May 2020
One Airlines	Chile	24 Jun 2020
Leeward Islands Air Transport	Antigua	27 Jun 2020

TABLE 5: Measures to support airports in some countries and regions.

Country/ region	Measures	Effective date/ duration
China	Restrictions on peak hour slots for cargo flights will be lifted at airports with strong cargo handling capacity	24 Mar 2020
	Existing airports will be modernized and better equipped with cold chain and parcel sorting facilities	
	Where conditions permit, international hub airports in Beijing, Tianjin, Hebei, the Yangtze River Delta, Guangdong, Hong Kong, Macao, Chengdu, and Chongqing will provide 24/7 customs clearance services and improve the efficiency of security checks and clearance procedures	
USA	\$10 billion in grants-in-aid	30 Mar 2020
Singapore	Deferred payment of certain fees such as licenses to provide air services	From Apr 2020 to Mar 2021
Norway	Fully compensating airports for the loss of airport charges	19 Mar 2020

technologies in air transport [106, 107]. Gallego and Font [108] used big data to assess the desire to travel and the intention to travel, demonstrating that big data should be widely used to improve management ability. Airports should accelerate implementation of biometric and contact-less capabilities to reduce human-to-human interactions after COVID-19 [109]. COVID-19 is rebuilding global economy and we cannot return to business as usual [110]. Digitalization is perhaps the only way out for air transport.

Global aviation is calculated to contribute to 3.5% of net anthropogenic effective radiative forcing in 2011 [111]. The

COVID-19 pandemic leads to the reduction in CO₂ emissions of global air transport. Daily CO₂ emissions by April 2020 declined by 60% in the aviation section compared with the mean 2019 level before COVID-19 [112]. However, air travel demand is estimated to continue to grow [8]. Green and sustainable transport receives more attention [113, 114]. ICAO adopted the Carbon Offsetting and Reduction Scheme for International Aviation (CORSIA) in 2016 in order to offset CO₂ emissions in international aviation [115]. Air transport should increase environmental sustainability [116, 117]. Low-carbon technologies should be introduced to

TABLE 6: Measures to support cargo carriers and general aviation in some countries and regions.

Country/region	Measures	Effective date/duration
China	Policy support to international cargo flights during the outbreak Encourage the merger and reorganization of air freight and logistics firms	24 Mar 2020
USA	\$4 billion in loans and loan guarantees for cargo carriers \$100 million for general aviation airports	30 Mar 2020
Singapore	10% landing charge rebate for all scheduled freighter flights	From Apr to Oct 2020

TABLE 7: Measures to support workers in some countries and regions.

Country/region	Measures	Effective date/duration
Hong Kong, China	HK\$50 million in training allowance to frontline airport staff who are on no-pay leave \$25 billion in grants for passenger airline employee wages, salaries, and benefits	24 Mar 2020
USA	\$4 billion in grants for cargo airline employee wages, salaries, and benefits \$3 billion in grants for airline contractor employee wages, salaries, and benefits \$9.5 billion in additional funds to air carriers	30 Mar 2020 25 Apr 2020
Singapore	75% wage subsidy	26 Mar 2020

the field of air transport, such as electric flight and sustainable alternative fuels [118, 119]. Gössling et al. [120] found that nonbiogenic synthetic fuels likely are the most viable option to completely phase out fossil fuels.

8. Conclusions

Air transport is hit hard by COVID-19 and plays an important role in containing COVID-19. This paper tries to make an overall review on the interaction of air transport and COVID-19 pandemic. The confirmed cases were firstly found in China in December 2019 and then found in other countries. International flight accelerates the worldwide spread of the COVID-19 pandemic. Dependent on the lessons learnt from previous pandemics such as SARS, China and then other countries or regions quickly respond and implement several involuntary measures including travel restrictions to prevent COVID-19.

This paper first highlights some key moments during the COVID-19 pandemic, especially from the perspective of China. China experiences five stages fighting against the epidemic. Thanks to the effective control of COVID-19 and policy support for civil aviation in China, China's domestic aviation market is recovering fast. Second, this paper analyzes the impact of air transport on transmission of COVID-19 and the roles of air restrictions in controlling COVID-19. As a result, the grounding of aircrafts causes immense operating losses of each part in air transport industry because the fixed costs of the sector are high.

Third, this paper summarizes the negative impact of COVID-19 on air transport industry, especially Chinese civil aviation markets. The data of Chinese passenger traffic shows that domestic passengers carried since February 2020 recovered. And domestic passenger traffic in September 2020 almost reached the level in the same period of the preceding year. Compared to 2019 level, world scheduled capacity for year 2020 offered by airlines reduced by 50% overall, passengers carried reduced about 2.7 billion, and gross passenger operating revenues of airlines reduced about 371 billion dollars.

The negative operating losses make airlines face rapid cash burn and then bankruptcy. Because air transport industry is seen as a key strategic asset and contributes to economic growth, aviation bailout is provided by governments to help air transport industry. Compared to other countries and regions, the US provided most direct aid. However, China mostly provides policy measures.

In the post-COVID-19 era, air transport industry itself needs to evolve actively to adapt to changes. For instance, more digitalization technologies should be applied and environmental sustainability be increased. In addition, air transport bears the burden of the distribution of COVID-19 vaccines. However, diminished cargo capacity of the global air transport industry likely limits the distribution of vaccines. Just providing a single dose to 7.8 billion people needs 8,000 Boeing 747 cargo aircraft. Meanwhile, the scale of cold chain transportation will be vast in the future.

Conflicts of Interest

The author declares that there are no conflicts of interest.

Acknowledgments

The author greatly acknowledges the helpful comments and suggestions of Professor Xu Maozeng from Chongqing Jiaotong University. This research was mainly sponsored by the Basic and Frontier Research Project of Chongqing (no. cstc2020jsyj-zdxwtBX0003), Chongqing Social Science and Planning Priorities Project (no. 2020TBWT-ZD02), and Key Research Project of Chongqing Airport Group Co., Ltd. (no. 2019-3).

References

- [1] World Bank, "Air transport, passengers carried," 2020, <https://data.worldbank.org/indicator/IS.AIR.PSGR?end=2019&start=1970&view=chart>.
- [2] J. Pearson and R. Merkert, "Airlines-within-airlines: a business model moving East," *Journal of Air Transport Management*, vol. 38, pp. 21–26, 2014.

- [3] R. Merkert and H. Swidan, "Flying with (out) a safety net: financial hedging in the airline industry," *Transportation Research Part E: Logistics and Transportation Review*, vol. 127, pp. 206–219, 2019.
- [4] L. H. Chung, "Impact of pandemic control over airport economics: reconciling public health with airport business through a streamlined approach in pandemic control," *Journal of Air Transport Management*, vol. 44, pp. 42–53, 2015.
- [5] International Civil Aviation Organization, "Aviation benefits report 2019," 2019, <https://www.icao.int/sustainability/Documents/AVIATION-BENEFITS-2019-web.pdf>.
- [6] Airports Council International and International Air Transport Association, "ACI and IATA call for urgent financial assistance to protect jobs and operations," 2020, <https://www.iata.org/en/pressroom/pr/2020-04-30-01/>.
- [7] N. J. Matheson and P. J. Lehner, "How does SARS-CoV-2 cause COVID-19?" *Science*, vol. 369, pp. 550–551, 2020.
- [8] International Civil Aviation Organization, "Effects of novel coronavirus (COVID-19) on civil aviation: economic impact analysis," 2021, https://www.icao.int/sustainability/Documents/COVID-19/ICAO_Coronavirus_Econ_Impact.pdf.
- [9] Johns Hopkins University, "COVID-19 dashboard by the Center for Systems Science and Engineering," 2020, <https://coronavirus.jhu.edu/map.html>.
- [10] J. Singh, J. Samal, V. Kumar et al., "Structure-function analyses of new SARS-CoV-2 variants B.1.1.7, B.1.351 and B.1.1.28.1: clinical, diagnostic, therapeutic and public health implications," *Viruses*, vol. 13, no. 3, p. 439, 2021.
- [11] Y. Yang, H. Zhang, and X. Chen, "Coronavirus pandemic and tourism: dynamic stochastic general equilibrium modeling of infectious disease outbreak," *Annals of Tourism Research*, vol. 83, Article ID 102913, 2020.
- [12] N. Zhu, D. Zhang, W. Wang et al., "A novel coronavirus from patients with pneumonia in China, 2019," *New England Journal of Medicine*, vol. 382, no. 8, pp. 727–733, 2020.
- [13] W. J. Tan, X. Zhao, and X. J. Ma, "A novel coronavirus genome identified in a cluster of pneumonia cases-Wuhan, China 2019-2020," *China CDC Weekly*, vol. 2, pp. 61–62, 2020.
- [14] C. I. Paules, H. D. Marston, and A. S. Fauci, "Coronavirus infections-More than just the common cold," *Journal of the American Medical Association*, vol. 323, no. 8, pp. 707–708, 2020.
- [15] V. J. Munster, M. Koopmans, N. van Doremalen, D. van Riel, and E. de Wit, "A novel coronavirus emerging in China-key questions for impact assessment," *New England Journal of Medicine*, vol. 382, no. 8, pp. 692–694, 2020.
- [16] The Novel Coronavirus Pneumonia Emergency Response Epidemiology Team, "The epidemiological characteristics of an outbreak of 2019 novel coronavirus diseases (COVID-19) in China," *Chinese Journal of Epidemiology*, vol. 41, no. 2, pp. 145–151, 2020.
- [17] P. Sampathkumar, Z. Temesgen, T. F. Smith, and R. L. Thompson, "SARS: epidemiology, clinical presentation, management, and infection control measures," *Mayo Clinic Proceedings*, vol. 78, no. 7, pp. 882–890, 2003.
- [18] C. Drosten, S. Günther, W. Preiser et al., "Identification of a novel coronavirus in patients with severe acute respiratory syndrome," *New England Journal of Medicine*, vol. 348, no. 20, pp. 1967–1976, 2003.
- [19] J. Peiris, S. Lai, L. Poon et al., "Coronavirus as a possible cause of severe acute respiratory syndrome," *The Lancet*, vol. 361, no. 9366, pp. 1319–1325, 2003.
- [20] J. D. Cherry, "The chronology of the 2002-2003 SARS mini pandemic," *Paediatric Respiratory Reviews*, vol. 5, no. 4, pp. 262–269, 2004.
- [21] M. Enserink, "SARS: chronology of the epidemic," *Science*, vol. 339, no. 6125, pp. 1266–1271, 2013.
- [22] M. Chan-Yeung and W. C. Yu, "Outbreak of severe acute respiratory syndrome in Hong Kong Special Administrative Region: case report," *BMJ*, vol. 326, no. 7394, pp. 850–852, 2003.
- [23] K. W. Tsang, P. L. Ho, G. C. Ooi et al., "A cluster of cases of severe acute respiratory syndrome in Hong Kong," *New England Journal of Medicine*, vol. 348, no. 20, pp. 1977–1985, 2003.
- [24] World Health Organization, "Summary of probable SARS cases with onset of illness from 1 November 2002 to 31 July 2003," 2003, http://www.who.int/csr/sars/country/table2003_09_23/en/.
- [25] Y. M. Sokadjo and M. N. Atchadé, "The influence of passenger air traffic on the spread of COVID-19 in the world," *Transportation Research Interdisciplinary Perspectives*, vol. 8, Article ID 100213, 2020.
- [26] C. A. Mouton, A. R. Grissom, J. P. Godes, and R. Hanson, "COVID-19 air traffic visualization: worldwide spread of COVID-19 accelerated starting on february 19," 2020, https://www.rand.org/pubs/research_reports/RRA248-6.html.
- [27] G. Tanriverdi, M. Bakır, and R. Merkert, "What can we learn from the JATM literature for the future of aviation post Covid-19? -A bibliometric and visualization analysis," *Journal of Air Transport Management*, vol. 89, Article ID 101916, 2020.
- [28] X. Q. Sun, S. Wandelt, C. H. Zheng, and A. M. Zhang, "COVID-19 pandemic and air transportation: successfully navigating the paper hurricane," *Journal of Air Transport Management*, vol. 94, Article ID 102062, 2021.
- [29] World Health Organization, "Novel coronavirus (2019-nCoV) situation report-1," 2020, <https://www.who.int/docs/default-source/coronaviruse/situation-reports/20200121-sitrep-1-2019-ncov.pdf>.
- [30] Civil Aviation Administration of China, "Statistics of key performance indicators for china's civil aviation industry in september 2020," 2020, http://www.caac.gov.cn/en/HYY/SJ/202011/t20201123_205327.html.
- [31] Department of Health and Social Care, "Sharp rise in coronavirus numbers and a new variant," 2020, <https://www.gov.uk/government/speeches/sharp-rise-in-coronavirus-numbers-and-a-new-variant>.
- [32] State Council, "China approves first self-developed COVID-19 vaccine," 2020, http://english.www.gov.cn/news/topnews/202012/31/content_WS5fed6440c6d0f72576942c83.html.
- [33] U.S. Food and Drug Administration, "Pfizer-BioNTech COVID-19 vaccine," 2021, <https://www.fda.gov/emergency-preparedness-and-response/coronavirus-disease-2019-covid-19/pfizer-biontech-covid-19-vaccine#:~:text=On%20December%2011%2C%202020%2C%20the%20U.S.%20Food%20and,in%20individuals%2016%20years%20of%20age%20and%20older>.
- [34] World Health Organization, "WHO-convened global study of origins of SARS-CoV-2: China part," 2021, <https://www.who.int/publications/i/item/who-convened-global-study-of-origins-of-sars-cov-2-china-part>.
- [35] R. F. Grais, J. Hugh Ellis, and G. E. Glass, "Assessing the impact of airline travel on the geographic spread of

- pandemic influenza,” *European Journal of Epidemiology*, vol. 18, no. 11, pp. 1065–1072, 2003.
- [36] D. Muley, M. Shahin, C. Dias, and M. Abdullah, “Role of transport during outbreak of infectious diseases: evidence from the past,” *Sustainability*, vol. 12, no. 18, Article ID 7367, 2020.
- [37] A. Browne, S. S. Ahmad, C. R. Beck, and J. S. Nguyen-Van-Tam, “The roles of transportation and transportation hubs in the propagation of influenza and coronaviruses: a systematic review,” *Journal of Travel Medicine*, vol. 23, no. 1, Article ID tav002, 2016.
- [38] A. Denphednong, S. Chinviriyasit, and W. Chinviriyasit, “On the dynamics of SEIRS epidemic model with transport-related infection,” *Mathematical Biosciences*, vol. 245, no. 2, pp. 188–205, 2013.
- [39] Y. Zhang, A. Zhang, and J. Wang, “Exploring the roles of high-speed train, air and coach services in the spread of covid-19 in China,” *Transport Policy*, vol. 94, pp. 34–42, 2020.
- [40] K. Linka, M. Peirlinck, F. Sahli Costabal, and E. Kuhl, “Outbreak dynamics of COVID-19 in Europe and the effect of travel restrictions” *Computer Methods in Biomechanics and Biomedical Engineering*, vol. 23, no. 11, pp. 710–717, 2020.
- [41] L. Hufnagel, D. Brockmann, and T. Geisel, “Forecast and control of epidemics in a globalized world,” *Proceedings of the National Academy of Sciences*, vol. 101, no. 42, pp. 15124–15129, 2004.
- [42] M. Chinazzi, J. T. Davis, M. Ajelli et al., “The effect of travel restrictions on the spread of the 2019 novel coronavirus (COVID-19) outbreak,” *Science*, vol. 368, no. 6489, pp. 395–400, 2020.
- [43] M. U. G. Kraemer, C.-H. Yang, B. Gutierrez et al., “The effect of human mobility and control measures on the COVID-19 epidemic in China,” *Science*, vol. 368, no. 6490, pp. 493–497, 2020.
- [44] M. Bielecki, D. Patel, and J. Hinkelbein, “Air travel and covid-19 prevention in the pandemic and peri-pandemic period: a narrative review,” *Travel Medicine and Infectious Disease*, vol. 39, Article ID 101915, 2021.
- [45] P. Bajardi, C. Poletto, and J. J. Ramasco, “Human mobility networks, travel restrictions, and the global spread of 2009 H1N1 pandemic,” *PLoS One*, vol. 6, Article ID 16591, 2011.
- [46] T. D. Hollingsworth, N. M. Ferguson, and R. M. Anderson, “Will travel restrictions control the international spread of pandemic influenza?” *Nature Medicine*, vol. 12, no. 5, pp. 497–499, 2006.
- [47] K. Shaw, “The 2003 SARS outbreak and its impact on infection control practices,” *Public Health*, vol. 120, no. 1, pp. 8–14, 2006.
- [48] P.-L. Ho, X.-P. Tang, and W.-H. Seto, “SARS: hospital infection control and admission strategies,” *Respirology*, vol. 8, no. s1, pp. S41–S45, 2003.
- [49] T. Svoboda, B. Henry, L. Shulman et al., “Public health measures to control the spread of the severe acute respiratory syndrome during the outbreak in Toronto,” *New England Journal of Medicine*, vol. 350, no. 23, pp. 2352–2361, 2004.
- [50] J. T. F. Lau, K. S. Fung, T. W. Wong et al., “SARS transmission among hospital workers in Hong Kong,” *Emerging Infectious Diseases*, vol. 10, no. 2, pp. 280–286, 2004.
- [51] E. Seow, “SARS: experience from the emergency department, Tan Tock Seng Hospital, Singapore,” *Emergency Medicine Journal*, vol. 20, no. 6, pp. 501–504, 2003.
- [52] G. Gopalakrishna, P. Choo, Y. S. Leo et al., “SARS transmission and hospital containment,” *Emerging Infectious Diseases*, vol. 10, no. 3, pp. 395–400, 2004.
- [53] W. Seto, D. Tsang, R. Yung et al., “Effectiveness of precautions against droplets and contact in prevention of nosocomial transmission of severe acute respiratory syndrome (SARS),” *The Lancet*, vol. 361, no. 9368, pp. 1519–1520, 2003.
- [54] World Health Organization, “Consensus document on the epidemiology of severe acute respiratory syndrome (SARS),” 2003, <http://www.who.int/csr/sars/en/WHOconsensus.pdf>.
- [55] M. R. Loutfy, T. Wallington, T. Rutledge et al., “Hospital preparedness and SARS,” *Emerging Infectious Diseases*, vol. 10, no. 5, pp. 771–776, 2004.
- [56] N. Zhang, T. Shi, H. Zhong, and Y. Guo, “Covid-19 prevention and control public health strategies in Shanghai, China,” *Journal of Public Health Management and Practice*, vol. 26, no. 4, pp. 334–344, 2020.
- [57] A. Arenas, W. Cota, and J. Gómez-Gardeñes, “Derivation of the effective reproduction number r for covid-19 in relation to mobility restrictions and confinement,” *medRxiv*, 2020.
- [58] K. A. Auger, S. S. Shah, T. Richardson et al., “Association between statewide school closure and COVID-19 incidence and mortality in the US,” *Journal of the American Medical Association*, vol. 324, no. 9, pp. 859–870, 2020.
- [59] J. Y. Wang, K. Tang, K. Feng, and W. F. Lv, “When is the COVID-19 pandemic over? Evidence from the stay-at-home policy execution in 106 Chinese cities,” *SSRN Electronic Journal*, 2020.
- [60] J. P. R. Soucy, S. L. Sturrock, and I. Berry, “Estimating effects of physical distancing on the COVID-19 pandemic using an urban mobility index,” *medRxiv*, 2020.
- [61] S. C. Anderson, A. M. Edwards, and M. Yerlanov, “Quantifying the impact of COVID-19 control measures using a Bayesian model of physical distancing,” *PLoS Computational Biology*, vol. 16, no. 12, Article ID 1008274, 2020.
- [62] N. Haug, L. Geyrhofer, A. Londei et al., “Ranking the effectiveness of worldwide covid-19 government interventions,” *Nature Human Behaviour*, vol. 4, no. 12, pp. 1303–1312, 2020.
- [63] S. Bouali, S. Douha, and N. Khadri, “To what extent is air freight affected by the corona virus pandemic?” *Journal of Sustainable Development of Transport and Logistics*, vol. 5, no. 2, pp. 98–108, 2020.
- [64] Airports Council International, *The Impact of COVID-19 on the Airport Business*, Airports Council International, Montreal, Canada, 2020, https://aci.aero/wp-content/uploads/2020/12/Advisory_Bulletin_The_impact_of_COVID_19_on_the_airport_business.pdf.
- [65] International Air Transport Association, “December 2020 air passenger market analysis,” 2020, <https://www.iata.org/en/iata-repository/publications/economic-reports/air-passenger-monthly-analysis--december-2020/>.
- [66] X. Q. Sun, S. Wandelt, and A. M. Zhang, “How did covid-19 impact air transportation? a first peek through the lens of complex networks,” *Journal of Air Transport Management*, vol. 89, Article ID 101928, 2020.
- [67] Civil Aviation Administration of China, “Statistical bulletin of civil aviation industry development in 2020,” 2021, http://www.caac.gov.cn/XXGK/XXGK/TJSJ/202106/t20210610_207915.html.
- [68] J. Liu, P. Qiao, J. Ding et al., “Will the aviation industry have a bright future after the covid-19 outbreak? evidence from

- Chinese airport shipping sector,” *Journal of Risk and Financial Management*, vol. 13, no. 11, p. 276, 2020.
- [69] S. Maneenop and S. Kotcharin, “The impacts of covid-19 on the global airline industry: an event study approach,” *Journal of Air Transport Management*, vol. 89, Article ID 101920, 2020.
- [70] J. B. Sobieralski, “Covid-19 and airline employment: insights from historical uncertainty shocks to the industry,” *Transportation Research Interdisciplinary Perspectives*, vol. 5, Article ID 100123, 2020.
- [71] World Tourism Organization, “COVID-19 and tourism,” 2021, <https://www.unwto.org/covid-19-and-tourism-2020>.
- [72] International Air Transport Association, “Shares of key cost items changed during the crisis,” 2021, <https://www.iata.org/en/iata-repository/publications/economic-reports/shares-of-key-cost-items-changed-during-the-crisis/>.
- [73] International Air Transport Association, “Industry losses to top \$84 billion in 2020,” 2020, <https://www.iata.org/en/pressroom/pr/2020-06-09-01/>.
- [74] J. Arellana, L. Márquez, and V. Cantillo, “COVID-19 outbreak in Colombia: an analysis of its impacts on transport systems,” *Journal of Advanced Transportation*, vol. 2020, Article ID 8867316, 12 pages, 2020.
- [75] M. Abate, P. Christidis, and A. J. Purwanto, “Government support to airlines in the aftermath of the covid-19 pandemic,” *Journal of Air Transport Management*, vol. 89, Article ID 101931, 2020.
- [76] Organization for Economic Co-operation and Development, “COVID-19 and the aviation industry: impact and policy responses,” 2020, <http://www.oecd.org/coronavirus/policy-responses/covid-19-and-the-aviation-industry-impact-and-policy-responses-26d521c1/>.
- [77] L. Tisdall, Y. Zhang, and A. Zhang, “COVID-19 impacts on general aviation – comparative experiences, governmental responses and policy imperatives,” *Transport Policy*, vol. 110, pp. 273–280, 2021.
- [78] R. Tam and R. J. Hansman, “Impact of air transportation on regional economic and social connectivity in the United States,” in *Proceedings of the AIAA Aircraft Technology, Integration, and Operations Forum*, Los Angeles, CA, USA, October 2002.
- [79] E. Britton, A. Cooper, and D. Tinsley, “The economic catalytic effects of air transport in Europe,” in *Proceedings of the ETC 2005*, Vilnius, Lithuania, November 2005.
- [80] J. Laird and P. Mackie, *Wider Economic Impacts of Regional Air Connectivity*, Department for Transport, London, UK, 2018.
- [81] M. D. Irwin and J. D. Kasarda, “Air passenger linkages and employment growth in U.S. Metropolitan areas,” *American Sociological Review*, vol. 56, no. 4, pp. 524–537, 1991.
- [82] K. Button, S. Lall, R. Stough, and M. Trice, “High-technology employment and hub airports,” *Journal of Air Transport Management*, vol. 5, no. 1, pp. 53–59, 1999.
- [83] J. K. Brueckner, “Airline traffic and urban economic development,” *Urban Studies*, vol. 40, no. 8, pp. 1455–1469, 2003.
- [84] K. Button and J. Yuan, “Airfreight transport and economic development: an examination of causality,” *Urban Studies*, vol. 50, no. 2, pp. 329–340, 2013.
- [85] J. G. Brida, D. Bukstein, and S. Zapata-Aguirre, “Dynamic relationship between air transport and economic growth in Italy: a time series analysis,” *International Journal of Aviation Management*, vol. 3, no. 1, pp. 52–67, 2016.
- [86] E. Fernandes and R. R. Pacheco, “The causal relationship between GDP and domestic air passenger traffic in Brazil,” *Transportation Planning and Technology*, vol. 33, no. 7, pp. 569–581, 2010.
- [87] M. Marazzo, R. Scherre, and E. Fernandes, “Air transport demand and economic growth in Brazil: a time series analysis,” *Transportation Research Part E: Logistics and Transportation Review*, vol. 46, no. 2, pp. 261–269, 2010.
- [88] M. M. Hakim and R. Merkert, “The causal relationship between air transport and economic growth: empirical evidence from South Asia,” *Journal of Transport Geography*, vol. 56, pp. 120–127, 2016.
- [89] F. Zhang and D. J. Graham, “Air transport and economic growth: a review of the impact mechanism and causal relationships,” *Transport Reviews*, vol. 40, no. 4, pp. 506–528, 2020.
- [90] M. J. McGraw, “The role of airports in city employment growth, 1950–2010,” *Journal of Urban Economics*, vol. 116, Article ID 103240, 2020.
- [91] E. Tveter, “The effect of airports on regional development: evidence from the construction of regional airports in Norway,” *Research in Transportation Economics*, vol. 63, pp. 50–58, 2017.
- [92] J. Ellis, L. Madureira, and S. Underwood, “The causal effects of proximity on investment: evidence from flight introductions,” *Journal of Financial and Quantitative Analysis*, vol. 55, no. 6, pp. 1978–2004, 2020.
- [93] S. V. Gudmundsson, M. Cattaneo, and R. Redondi, “Forecasting temporal world recovery in air transport markets in the presence of large economic shocks: the case of COVID-19,” *Journal of Air Transport Management*, vol. 91, Article ID 102007, 2021.
- [94] T. Burki, “Equitable distribution of COVID-19 vaccines,” *The Lancet Infectious Diseases*, vol. 21, no. 1, pp. 33–34, 2021.
- [95] International Air Transport Association, “Accepting vaccinated passengers should be best practice to reopen borders,” 2021, <https://www.iata.org/en/pressroom/pr/2021-05-19-01/>.
- [96] E. Stoye, “Daily briefing: vaccine passports could worsen inequality,” *Nature*, vol. 12, 2021.
- [97] A. D. So and J. Woo, “Reserving coronavirus disease 2019 vaccines for global access: cross sectional analysis,” *BMJ*, vol. 371, Article ID m4750, 2020.
- [98] Lancet Commission on COVID-19 Vaccines and Therapeutics Task Force Members, “Urgent needs of low-income and middle-income countries for COVID-19 vaccines and therapeutics,” *Lancet*, vol. 397, pp. 562–564, 2021.
- [99] J. Lambert, “Global inequity in COVID-19 vaccination is more than a moral problem,” *Science News*, vol. 199, no. 6, 2021.
- [100] World Health Organization, “Vaccine inequity undermining global economic recovery,” 2021, <https://www.who.int/news/item/22-07-2021-vaccine-inequity-undermining-global-economic-recovery>.
- [101] M. Bolcato, D. Rodriguez, and A. Feola, “COVID-19 pandemic and equal access to vaccines,” *Vaccines*, vol. 9, no. 6, 2021.
- [102] G. Nhamo, K. Dube, and D. Chodzi, *Counting the Cost of COVID-19 on the Global Tourism Industry*, Springer, Berlin, Germany, 2020.
- [103] International Air Transport Association, “The time to prepare for COVID-19 vaccine transport is now,” 2020, <https://www.iata.org/en/pressroom/pr/2020-09-09-01/>.

- [104] Y. Wang, S. G. Peng, and M. Xu, "Emergency logistics network design based on space-time resource configuration," *Knowledge-Based Systems*, vol. 223, Article ID 107041, 2021.
- [105] D. Dai, X. Wu, and F. Si, "Complexity analysis of cold chain transportation in a vaccine supply chain considering activity inspection and time-delay," *Advances in Difference Equations*, vol. 1, 2021.
- [106] J. Li, Z. Z. Peng, and A. Liu, "Analysis and future challenge of blockchain in civil aviation application," in *Proceedings of the IEEE 6th International Conference on Computer and Communications (ICCC)*, pp. 1742–1748, Chengdu, China, December 2020.
- [107] Y. L. Wang and J. Sarkis, "Emerging digitalisation technologies in freight transport and logistics: current trends and future directions," *Transportation Research Part E: Logistics and Transportation Review*, vol. 148, Article ID 102291, 2021.
- [108] I. Gallego and X. Font, "Changes in air passenger demand as a result of the COVID-19 crisis: using Big Data to inform tourism policy," *Journal of Sustainable Tourism*, vol. 2, pp. 1–20, 2020.
- [109] F. Serrano and A. Kazda, "The future of airports post COVID-19," *Journal of Air Transport Management*, vol. 89, Article ID 101900, 2020.
- [110] McKinsey & Company, "COVID-19: implications for business," 2021, <https://www.mckinsey.com/business-functions/risk/our-insights/covid-19-implications-for-business>.
- [111] D. S. Lee, D. W. Fahey, and A. Skowron, "The contribution of global aviation to anthropogenic climate forcing for 2000 to 2018," *Atmospheric Environment*, vol. 244, Article ID 117834, 2021.
- [112] C. Le Quéré, R. B. Jackson, M. W. Jones et al., "Temporary reduction in daily global CO₂ emissions during the COVID-19 forced confinement," *Nature Climate Change*, vol. 10, no. 7, pp. 647–653, 2020.
- [113] Y. Wang, S. G. Peng, and X. S. Zhou, "Green logistics location-routing problem with eco-packages," *Transportation Research Part E: Logistics and Transportation Review*, vol. 143, Article ID 102118, 2020.
- [114] H. Zhang, C. X. Zhuge, and J. M. Jia, "Green travel mobility of dockless bike-sharing based on trip data in big cities: a spatial network analysis," *Journal of Cleaner Production*, vol. 313, Article ID 127930, 2021.
- [115] International Civil Aviation Organization, "Carbon offsetting and reduction scheme for international aviation," 2021, <https://www.icao.int/environmental-protection/CORSIA/Pages/default.aspx>.
- [116] S. Gössling, "Risks, resilience, and pathways to sustainable aviation: a COVID-19 perspective," *Journal of Air Transport Management*, vol. 89, Article ID 101933, 2020.
- [117] L. Budd and S. Ison, "Responsible transport: a post-COVID agenda for transport policy and practice," *Transportation Research Interdisciplinary Perspectives*, vol. 6, Article ID 100151, 2020.
- [118] A. W. Schäfer, S. R. H. Barrett, K. Doyme et al., "Technological, economic and environmental prospects of all-electric aircraft," *Nature Energy*, vol. 4, no. 2, pp. 160–166, 2019.
- [119] P. Schmidt, V. Batteiger, A. Roth, W. Weindorf, and T. Raksha, "Power-to-liquids as renewable fuel option for aviation: a review," *Chemie Ingenieur Technik*, vol. 90, no. 1–2, pp. 127–140, 2018.
- [120] S. Gössling, A. Humpe, F. Fichert, and F. Creutzig, "COVID-19 and pathways to low-carbon air transport until 2050," *Environmental Research Letters*, vol. 16, Article ID 034063, 2021.

Research Article

Two-Stage Humanitarian Logistics Deprivation Model for the Planning of Scarce KN-95 Facemask Supplies under Agent's Cooperation

Oscar L. Pineda-Martinez , Carlos D. Paternina-Arboleda ,
and Guisselle A. García-Llinás 

Department of Industrial Engineering, Universidad del Norte, Barranquilla, Colombia

Correspondence should be addressed to Oscar L. Pineda-Martinez; omartines@uninorte.edu.co

Received 13 December 2020; Revised 31 March 2021; Accepted 22 June 2021; Published 2 July 2021

Academic Editor: Yong Wang

Copyright © 2021 Oscar L. Pineda-Martinez et al. This is an open access article distributed under the Creative Commons Attribution License, which permits unrestricted use, distribution, and reproduction in any medium, provided the original work is properly cited.

Humanitarian logistics encompasses a wide spectrum of conditions or constraints for supply chains, yet its focus on mitigating human suffering efficiently is what has motivated organizations and governments to make rapid decisions in real time. In this article, through the approach to an emergency such as COVID-19, we propose a two-stage model capable of considering human suffering, the cost of humanitarian logistics, and the benefit obtained by the interaction of suppliers that generally behave as oligopolies through a mathematical programming model and one of the cooperative games. Our main finding was the adaptability of a previously validated model for humanitarian logistics to the ongoing COVID-19 pandemic, where the externalities had greater relevance in social costs than private costs.

1. Introduction

In terms of attention to the occurrence of disasters or emergency situations similar to COVID-19, it is important to guarantee effective and efficient processes for the correct delivery of goods and services as well as meet the survival requirements of the affected population [1–3]. In this context, it is important to properly define operational models that optimize the logistics' behavior of the stakeholders.

The logistics processes involved either in disaster relief or in the health emergency caused by COVID-19 are made up of different stages and considerations in terms of humanitarian aid and critical supplies, according to Van Wassenhove [4] and Holguín-Veras et al. [5]. The components of international trade and incoterms are important aspects to consider because they can represent the free passage of supplies or the restriction of the same due to the reliability of the origin of the goods [1, 6]. Likewise, taking into account that the main objective is to satisfy and prioritize the attention of the affected population [7–9], there is a social cost

related to the human suffering produced by the lack of access to goods or services.

This article develops an extension to an operational model that was initially conceived for humanitarian logistics by Franco et al. [10] towards an environment where the actors involved share market participation and there is direct competition at the horizontal level in the logistics chain. The objective is to minimize logistics and social costs, considering penalties associated with the latter (deprivation costs). As an integral part of the model, cooperative participation is considered through cooperative games between the different suppliers (national or international) as a mechanism to optimize the processes and operating costs involved in the supply chain in order to obtain a global benefit [11–13]. In this order of ideas, the model to be treated in this article consists of 2 stages: a programming model and a cooperative games model. In the first, the distribution schemes are established along the supply network without considering last-mile activities; however, human suffering over time (deprivation) is considered. In the second model, the information resulting from the previous stage is taken, starting

from the fact that the actors involved in the first stage receive benefits from the deliveries made and different cooperation scenarios are recreated. The purpose of these scenarios is to analyze the interaction between the participants and draw conclusions about the distribution strategies adopted by the different possible coalitions.

2. Literature Review

In this article, we seek to relate or compare the behavior of the actors in the supply chains from an emergency or disaster situation that affects the population and makes the supply of goods and services necessary, so we focus on publications of related situations such as those experienced in the humanitarian logistics environment and the consequences in global supply chains. Despite the fact that the research related to the COVID-19 emergency is recent and has had a boom mainly in the health sciences [14], the impact it has caused on the behavior of the global supply chains and the economy has been notorious [15], which is why some authors have focused on the medium- and long-term effects on supply chains [16]. Complementary to the above and considering the fact that the emergency currently experienced is scalable or comparable to the humanitarian logistics response stage, there is a limited amount of goods or services (critical supply or humanitarian aid) that are necessary to overcome the eventualities of the emergency and whose lack of access or poor condition has consequences on the daily life of the affected population [17–19], considering sanitary regulations and measures adopted by governments and international organizations.

Despite the fact that humanitarian logistics is a subject with a relatively shorter study time than commercial logistics, the interest it has aroused due to its lack of effectiveness in previous years has led us towards the belief that the vision of commercial logistics could mean a contribution to humanitarian logistics in terms of supply chain performance [4]. Complementary, the budgetary support of organizations for disaster response indicates the need to develop efficient preparedness and response models [20]. Humanitarian logistics encompasses an extensive field of study, so it would not be correct to isolate it as apart from conventional logistics. It is worth noting the operating conditions in which organizations are involved in the response and recovery stages: scarcity of resources and urgent demand from the affected population [5]. In this article, we develop a humanitarian approach to a problem where suppliers generally behave like oligopolies, taking into consideration the profit obtained by the participants when carrying out their activity and the social cost (mainly deprivation costs) incurred in the attention of the affected areas.

Deprivation is understood as being in the absence of goods or services for a certain time, and then, the deprivation cost is defined as that caused by human suffering in the absence of humanitarian aids or critical supplies. Some interpret it as the externality impact of transport costs, paralleling the private cost of travel [21–23]; on the other hand, some define it as the willingness to pay for access to goods or services after a certain time [10].

The nonlinear behavior of deprivation costs implies approximations to represent the increment in human suffering over time; some authors adopted a perspective that proposes the use of penalties for incurring relatively high deprivation costs compared to expectations [24], while others developed variable penalties according to the level of deprivation to which the affected population is exposed [25]. It is worth highlighting the fact that hysteresis or the development of sequelae in the well-being of people due to the deprivation costs is not considered. In our contribution, we decided to relax the nonlinear complexity of deprivation into statistically grounded linear approximations that are representative of behavior caused by human suffering.

The conceptual differences with respect to some models developed with problems related to our contribution are shown in Table 1.

In relation to the interaction between actors, the need to share information and more effective supply chains has been seen in previous emergencies when supplying demand [10]. Additionally, the investigative contribution would be useful if we consider all these components in a single emergency: international commerce, relative shortage of critical supplies, human suffering caused by the lack of access, and the possible horizontal cooperation between suppliers that generally behave as oligopolies.

3. Model Description

This section describes the model's development, its limitations, and the research contribution, taking into account the aforementioned problem. The objectives to be met are based on minimizing the global costs of a humanitarian supply network under possible cooperation schemes and the benefit obtained by the participants.

3.1. First Stage: Programming Model. A mixed integer nonlinear programming operational model is developed, which proposes minimizing the social costs inherent to emergency care at the local level. The associated human suffering is taken into account as the deprivation cost; that is, given a known function of the deprivation costs, a series of thresholds are proposed over the time horizon and the penalty associated with delivery time is modified according to the elapsed time. The model considers variable penalties, which can be representative of the nonlinear nature of the deprivation costs [21]; consequently, the penalty value varies each time the time in deprivation exceeds one of the thresholds, having a terminal value where the growth in deprivation costs is diminished and the concavity of the function would begin to occur after the said value, also known as “value of life.” Concerning the supply chain, the traditional aspects of any network in commercial logistics are preserved, with the addition of considering duality in transport costs; that is, for a given transport, its cost is divided into a logistics component whose value is commonly associated with payment for the transport activity and a social component associated with the value of time seen as human suffering, since during transport, the affected people remain in lack of goods or service (deprivation status).

TABLE 1: Comparative table between the contribution made against different models developed.

Model to compare	Type of programming model	Stage within the humanitarian logistics cycle	Savings in cooperation	Competitive advantages
Franco et al. [10]	Tactical	Response	The cost savings in transportation can be based on productivity—saving time—and competitive costs of vehicle fleets.	It is assumed that each supplier has strength, with is given as follows: a Supplier A: lower production costs. b Supplier B: larger capacities. c Supplier C: lower transportation cost.
Pérez-Rodríguez [26]	Operational	Preparation/ response	Not captured, it focuses on last-mile distribution based on the fact that they already have inventories available.	There are no competitive advantages.
Cotes and Cantillo [27]	Operational	Response	Not captured, the model developed mentions cooperation but does not express it in the form of coalitions.	There are no competitive advantages.
Our contribution	Operational	Response	The savings in transportation costs come from economies of scale (quantity discount) and the valuation of time is subject to priorities.	There are no predefined competitive advantages for the participants, so we leave the value of the contribution in the coalitions to free will so as not to rule out the existence of a subadditive game.

Model assumptions: the demand is known, based on estimates in the affected area; there is knowledge of the demand and its behavior. The offer is also known, based on the fact that there is a group of commercially constituted manufacturers, which provide information on the quantities that they would be willing to mobilize. Horizontal cooperation is possible, in contrast to the previously validated model for a humanitarian environment—where a good part of the entities was non-for-profit—and for a commercial environment, it is necessary to establish coalitional interactions between the actors that in natural conditions represent oligopolies in their market sector. The supply network is predefined, since this article does not include location models and the previous existence of a supply network through which the products would be mobilized is assumed.

The social cost is penalized according to time, in the sense that there is a limited value of human suffering due to deprivation time. To avoid incurring in this situation, thresholds are established (considerably lower in time); in case of breaching a certain threshold, late deliveries would be subject to variable penalties, depending on the time elapsed above this [21]. The product used is not perishable over the time horizon so that the product condition does not become a risk factor in terms of cargo loss due to expiration. Last-mile distribution is not considered, since it is a programming model independent of an allocation model and it is assumed that the points of demand house groups of affected people; consequently, there is consolidated demand in those areas. Last but not least, a convex nature in deprivation costs is considered, since once the deprivation cost function and its convexity are known,

people would not develop sequelae after remaining deprivation of goods or services, for which their state of well-being would not be affected in time by secondary effects (hysteresis).

As previously mentioned, our model was validated with that developed by Franco et al. [10] with an extension to the problem of the COVID-19 emergency, for which we summarize the conceptual changes made as; unlike the model proposed by Franco et al. [10], our contribution went from taking a tactical model to an operational programming model that would be developed during the emergency response stage.

One of the most notable differences that we propose is related to the savings from belonging to a coalition and being in cooperation with other participants, where the time of the shipments and their respective rate vary according to the established priority. On the other hand, our model does not establish predefined competitive advantages, so we leave the contribution value of each participant to free will so as not to rule out the existence of a cooperative game of a subadditive nature.

The model is made up of several levels: manufacturers (I) and points of demand (J), according to Figure 1. Manufacturers refer to the suppliers of the products (water, food, medicines, etc.) necessary to supply the needs in the emergency (K). These suppliers represent direct competition in their natural market conditions and their interaction could mean economies of scale when forming a coalition (S). The points of demand would be the affected areas that could be cities or communities, where the impact to be considered is that resulting from the deprivation of the goods or services.

Considering the demand (D_{kj}) and the offer (O_{ki}), we propose a supply network in which the response capacity is

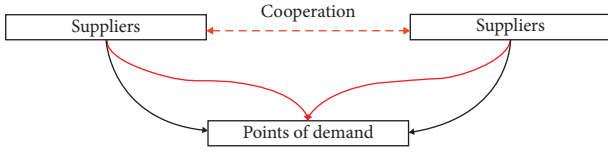


FIGURE 1: Graphic description of the programming model. The red line represents the consolidation of cargo from cooperation, while the black line represents an individualistic distribution scheme.

sufficient to meet the needs at the local level; in the case of unmet demand, we will denote it by UF_{kj} . Shipments made (X_{kijjt}) over time (T) are subject to priority parameters (Q) in transport cost (CT_{kijj}) and their contribution in time to deprivation (TV_{kijj}) at the time of being delivered at points of demand, so the deprivation is weighted in quantity delivered (Y_{kjt}) and time elapsed (TE_{kjt}). Regarding the nonlinear nature of deprivation, we opted to do a linear relaxation ($\beta(t)_{kt'}$) through a piecewise function whose segments (T') represent an approximation to the deprivation function (G_{kt}), according to Holguín-Veras et al. [21] such that

$$\beta(t)_{kt'} = \beta_{1kt'} * t + \beta_{2kt'}. \quad (1)$$

According to equation (1), it is considered that $\beta_{1kt'}$ and $\beta_{2kt'}$ are parameters of the linear regression performed on the deprivation function, remaining in the form of a piecewise function and depending on time. Additionally, of all the possible functions from the regression segments, there is a regression function that best fits a given period (T), which we will denote by G_{kt} . If there are shipments in a period (T), we check it in a binary way (BE_{kjt}), where the value of 1 is assumed in case of shipments, and apply the respective deprivation cost (G_{kt}) and 0 otherwise. In the case of unmet demand, the deprivation to be assigned would be equivalent to the maximum willingness to pay by the individual, which we will denote by P [21].

For its part, membership in a coalition (PC_{is}) is evaluated in a binary way, adopting the value of 1 when a player or manufacturer (I) is a participant in a specific coalition (S) and 0 otherwise. When applying the discount rates by quantity in the transports carried out by a coalition (DC_c), we choose to delimit the quantity intervals with lower (LI_c) and higher (LS_c) limits to select the rate to be applied in a binary way (BT_{sc}), which assumes the value of 1 when the quantity mobilized belongs to an interval and applies the corresponding rate (C) and 0 otherwise.

For the total cost of the objective function, we will denote it as follows:

$$\begin{aligned} \text{Min } F = & \sum_K \sum_I \sum_Q \sum_J \sum_T \sum_S \sum_C X_{kijjt} * \\ & CT_{kijj} - \sum_K \sum_I \sum_Q \sum_J \sum_T X_{kijjt} * PC_{is} * BT_{sc} * DC_c * \\ & CT_{kijj} + \sum_K \sum_J P * UF_{kj} + \sum_K \sum_J \sum_T Y_{kjt} * G_{kt}, \end{aligned} \quad (2)$$

subject to

$$\sum_Q \sum_J \sum_T X_{kijjt} \leq O_{ki}, \quad \forall k \in K, i \in I, \quad (3)$$

$$Y_{kjt} = \sum_I \sum_Q X_{kijjt} (t - TV_{kijj}), \quad \forall k \in K, j \in J, t \in T: t > TV_{kijj}, \quad (4)$$

$$UF_{kj} + \sum_T Y_{kjt} = D_{kj}, \quad \forall k \in K, j \in J, \quad (5)$$

$$UF_{kj} \leq D_{kj}, \quad \forall k \in K, j \in J, \quad (6)$$

$$Y_{kjt} \leq M * BE_{kjt}, \quad \forall k \in K, j \in J, t \in T, \quad (7)$$

$$TE_{kjt} = t * BE_{kjt}, \quad \forall k \in K, j \in J, t \in T, \quad (8)$$

$$\beta(TE_{kjt})_{kt'} \leq G_{kt}, \quad \forall k \in K, j \in J, t \in T, t' \in T', \quad (9)$$

$$\begin{aligned} \sum_K \sum_I \sum_Q \sum_J \sum_T X_{kijjt} * PC_{is} \leq M * (1 - BT_{sc}) + LS_c * BT_{sc}, \\ \forall s \in S, c \in C, \end{aligned} \quad (10)$$

$$\begin{aligned} \sum_K \sum_I \sum_Q \sum_J \sum_T X_{kijjt} * PC_{is} \geq -M * (1 - BT_{sc}) + LI_c * BT_{sc}, \\ \forall s \in S, c \in C, \end{aligned} \quad (11)$$

$$\sum_C BT_{sc} = 1, \quad \forall s \in S, \quad (12)$$

$$X_{kijjt}, Y_{kjt}, UF_{kj}, G_{kt}, TE_{kjt} > 0. \quad (13)$$

In equation (2), the objective function is found, where it is sought to minimize the social cost, either by the logistics cost component (related to the variables X_{kijjt} and Y_{mjt}), by the penalty applied to not meeting the demand (related to UF_{kj}), or by that from deprivation costs (related to G_{kt}); additionally, quantity discounts are considered in the rates of some national transports, right at the end of equation (2) [21]. The response capacity (offer) by producers is shown in equation (3), in which the flow of supplies is evidenced in equation (4). For its part, equations (5) and (6) describe the fulfillment of the demand. Equations (7)–(9) assign a delivery time and an equivalent deprivation cost, evaluated within all the piecemeal functions available to capture deprivation. Equations (10) and (11) evaluate the intervals for which it is possible to assign a rate, having M as a large value (big M). For its part, equation (12) is in charge of assigning discount rates by quantity based on the quantity of goods that a specific coalition has mobilized, which is palpable in the objective function. Finally, equation (13) proposes the nonnegativity of the variables.

Based on the results obtained from the previous programming model and assuming that the participants in the supply chain received benefits for the deliveries, the information would be used as input for a cooperative gaming model. The purpose of this would be related to the

interaction between actors involved in the supply chain (national or international) to justify the existence or not of coalitions between players, based on the total benefit obtained.

3.2. Second Stage: Cooperative Games Model. A series of scenarios are established, for which cooperation would imply benefits or cost reductions for some of the players. Next, the Shapley value is used to obtain information on the contributions provided by the players belonging to a specific coalition and make inferences regarding the expected value of the contribution for each player [28, 29]. To calculate the value of the contribution, we will use the following equation:

$$\phi_i(v) = \sum_{S \subseteq N \setminus \{i\}} \frac{|S|!(n-|S|-1)!}{n!} [v(S \cup \{i\}) - v(S)], \quad (14)$$

where S is a specific coalition within the set of feasible coalitions N , for its part, n is the total number of players, $v(S)$ is the value of the coalition S , and finally, i is the player who is being calculated by the Shapley value.

Our contribution to the research is based on how the cooperation between participants—who generally behave like oligopolies—can impact a commonly humanitarian problem either by generating economies of scale or by sharing information to generate benefits.

4. Case Study

To put the proposed model into practice, different scenarios were simulated, taking as a reference the emergency of COVID-19 due to the supply of protection elements for the areas of Barranquilla and Cali, Colombia, as of March 11, 2020. In this context, the national regulations declared the mask as a “*not available vital medical device*,” according to INVIMA [30]. In the following days, the country began to experience an over demand for protection products for the general population and imports had increased, with which the Government of Colombia found it necessary to impose taxes on the import of masks in order to protect national production and regulate prices, in accordance with Dinero [31, 32] and DANE [33]. The effects of uncertainty and social behavior were essential factors to address this case, since demand is encouraged by the consequences of the cultural environment in which the population lives, according to Gómez et al. [34].

Figure 2 shows the supply network used by national manufacturers and treated with a personal protection product (face mask); for transport costs, the tool of the Colombian transport ministry Sice-Tac was used. Finally, to determine the deprivation costs, the function developed by Macea et al. [35] and linear approximations were made in a piecewise function under a confidence level of 95%, according to Figure 3. The application case is made up of the following links: national producers, which are regional textile companies from the departments (provinces) of Antioquia and Cundinamarca and also points of demand which would be located in the cities of Barranquilla and Cali. Also, the product to be mobilized would be KN-95 reference

face masks (with a relatively good average performance) which should be delivered at the points of demand. The time horizon was discretized in 20 segments of 12 hours, for a total of 240 hours (10 days), thus ensuring a linear scaling to the nonlinear deprivation function; in the same way, the priorities in the shipments behave in the same way as follows: the higher the priority, the higher the cost of shipping and the shorter the travel time, classified under the categories of low, medium, and high priority. At the same time, as the quantity mobilized by a coalition increases, transport rates are exposed to reductions due to economies of scale, made up of 3 quantity intervals in our case.

In summary, there is a group of national manufacturers clustered in 2 regions (Antioquia and Cundinamarca) where a good part of the textile production is concentrated due to their considerable market share; these producers have autonomy in the mobilization of their products due to exclusive contracts with cargo operators. Likewise, there are a group of cities in a condition of deprivation of the mentioned product (KN-95 mask) whose demand must be supplied with the lowest possible overall cost (understood as the set of monetary costs and deprivation costs). Shipments made from the producing regions are subject to cost-time and quantity-cost rates in the form of priority shipments and quantity discounts.

Figure 4 shows the relationship of deaths per week at the national level from March 2 to October 4, 2020, leaving a balance of 29,787 confirmed deaths from COVID-19, where a peak of activity is seen for the month June [36]. Additionally, the impact of the measures adopted for emergency care is reflected in the population with the greatest vulnerability, taking into account that more than 85% of deaths come from socioeconomic classes with middle or low income [37], added to the threat of the hoarding of critical supplies and possible price speculation by suppliers or intermediaries, in accordance with the Superintendency of Industry and Commerce [38].

In an unfortunate and coincidental way, the peak of activity in deaths is probably due to the social indiscipline that had flooded the country in that period of time, where the national authorities intervened around 4 thousand social meetings and celebrations during a period of 2 weeks, which was becoming a risk factor in accordance with Portafolio [39] and El Tiempo [40]. Complementary to the above, we decided to apply the methodology based on the fact that the Colombian government had made the determination to protect the national production of masks, reducing or discouraging their imports, leading to the possible presence of an oligopoly in this market sector.

A series of scenarios are established, for which cooperation could imply benefits or cost reductions for some of the players. In scenario 1, the participants do not cooperate, and the players corresponding to the production of the regions of Antioquia (A) and Cundinamarca (B) act separately; in scenario 2, participants A and B cooperate.

The cooperation of the different manufacturers implies a consolidation of cargo or a greater volume to be mobilized in the different coalitions (depending on the number of members). By belonging to a coalition, the members have



FIGURE 2: Georeferencing the supply network: manufacturers are located in the areas pointed in red, while the points of demand are located in the areas pointed in blue.

access to different national transport rates; due to the quantity discounts, each transport rate includes an interval for which a discount is applied, and the amount to be taken into account is the one mobilized by the coalition.

4.1. Results. The first stage model belongs to a mixed integer nonlinear programming problem; it was solved by coding

the General Algebraic Modeling System (GAMS) program and it was executed on the Network-Enabled Optimization System (NEOS) platform for approximately 9,000 variables and just over 15,000 constraints for each scenario, making computational execution time span less than 100 seconds to show the optimal supply network that minimizes social costs. The second stage model uses the outputs resulting from the first stage to define the value of each participant's

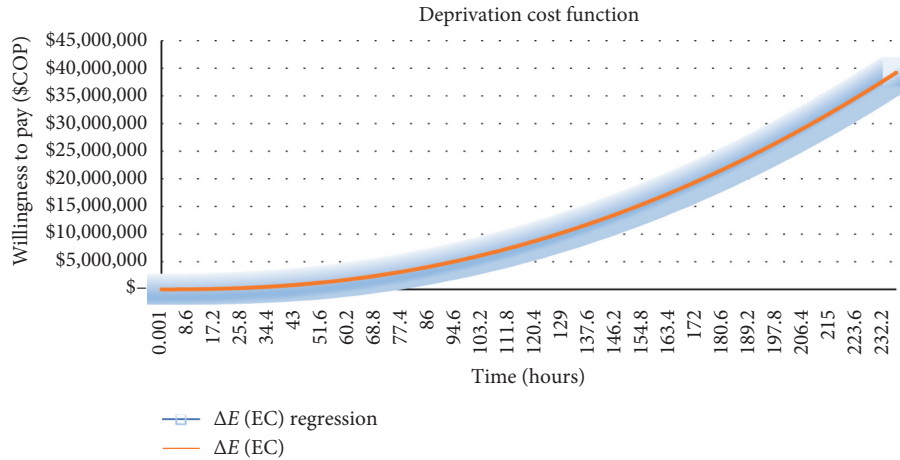


FIGURE 3: Comparison of the behavior between the nonlinear deprivation function ΔE (EC) and the linear regressions of the proposed piecewise function.

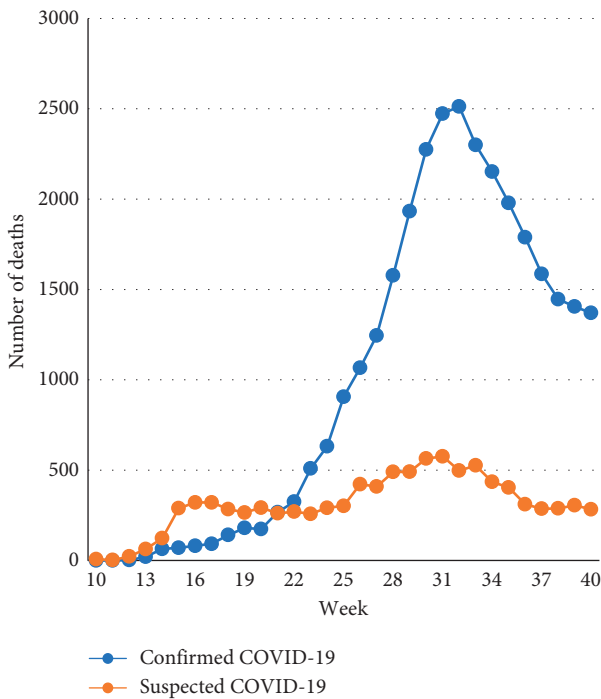


FIGURE 4: Weekly deaths from confirmed and suspected COVID-19 according to DANE [36, 37] (the time horizon between March 2 and October 10, 2020.).

contribution, according to the quantities mobilized in the first stage and the market value of the critical supply.

The results obtained from the aforementioned information can be seen in Tables 2 and 3, from which it can be inferred that there were scenarios where, due to the weighing of costs, the manufacturers chose to consolidate deliveries in a single period, acting separately and incurring a lower overall cost, in accordance with scenario 1. On the other hand, in scenario 2, we notice a change in the quantities to be distributed by the manufacturers mainly due to the economies of scale to which they would access; a longer delay in

the delivery of the masks can also be noted, which would imply a higher cost associated with deprivation. Regarding the priorities of shipments, a low level of alert or concern about carrying out the mobilizations of masks may be noted, which responds to the problem of over demand and a possible case of “bullwhip effect,” which would be understandable due to the fact that the valuation given to this product comes mainly from the care of life and not precisely because of its monetary value, in accordance with Figure 3 where the incremental behavior of human suffering is explained over time. Surprisingly, the scenario that incurred the lowest total cost was the one where the participants decided not to cooperate (scenario 1).

Regarding the cooperative game model, it is assumed that the players or participants would receive benefits for their activity [9], which commonly happens in a commercial environment in the presence of oligopolies. The results obtained for the cooperation scenarios can be seen in Tables 4 and 5.

Paradoxically, scenario 2 coincided in having the highest social cost incurred in the objective function and the highest benefit obtained in the cooperative game, so the possibility that the benefits of coalitions are adversely related to social costs is not ruled out. With the above, it is implied that there must be control over the number of members that would make up the coalitions, since they could not guarantee the lowest social cost.

Table 5 describes the Shapley value of each of the players, assuming that they belonged to the AB coalition and their respective contributions to the coalition in a percentage way, where the national producer (located in Antioquia) obtains around 80% of the total benefits from the coalition.

4.2. Sensitivity Analysis. Likewise, Figure 5 shows the sensitivity analysis carried out on the programming model, where a change of up to 100 times the value of the objective function can be noticed with only varying less than 5% of the time horizon (10 hours), so the proposed model is capable of capturing the nonlinear behavior of delays to delivery

TABLE 2: Results of the programming model under scenario 1.

Individualistic scenario (A-B)					F (\$COP)
Variable $X(k, i, q, j, t)$	MB	U	TS	TL	
Antioquia-Low-Barranquilla	A	1,072,350	5	28	
Antioquia-Low-Cali	A	1,519,650	16	28	
Cundinamarca-Low-Barranquilla	B	0	—	—	
Cundinamarca-Low-Cali	B	461,450	14	28	
Total		3,053,450			\$ 895,918,833,000

MB: player or participant; U : units mobilized; TS: period of delivery of the supply; TL: period of receipt of the supply; F : value of the objective function.

TABLE 3: Results of the programming model under scenario 2.

Cooperation scenario (AB)					F (\$COP)
Variable $X(k, i, q, j, t)$	MB	U	TS	TL	
Antioquia-Medium-Barranquilla	A	208,350	5	25	
Antioquia-Low-Cali	A	1,981,100	12	24	
Cundinamarca-Medium-Barranquilla	B	864,000	121	143	
Cundinamarca-Baja-Cali	B	0	—	—	
Total		3,053,450			\$ 11,200,890,000,000

MB: player or participant; U : units mobilized; TS: period of delivery of the supply; TL: period of receipt of the supply; F : value of the objective function.

TABLE 4: Benefits obtained (\$COP) by the players in each of the scenarios.

Player\benefit	Scenario 1 A-B	Scenario 2 AB
A	\$1,907,712,000	\$1,611,435,200
B	\$369,021,565	\$690,940,800
Total	\$2,276,733,565	\$2,302,376,000

TABLE 5: Calculation of the Shapley value (\$ COP and percentage) for each of the players.

Player	$\phi(w)$	%
A	\$ 1,920,533,217, 50	83,42
B	\$ 381.842.782, 50	16,58
Total	\$ 2,302,376.000, 00	100

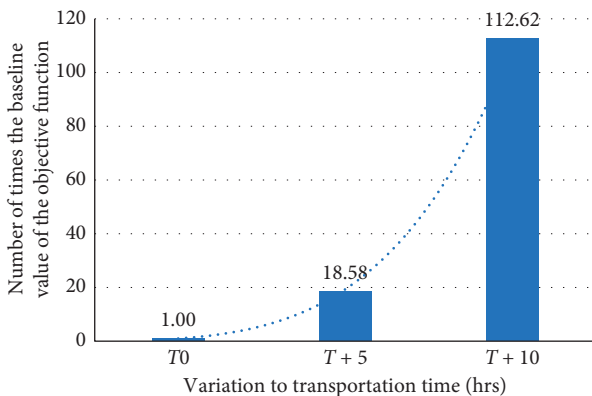


FIGURE 5: Sensitivity analysis performed on delivery times.

times—generally attributed to disruptions in the supply network—and its contribution as a deprivation cost in the objective function. The cost-time relationship coincided with that proposed by Arellana et al. [41], where a proportional behavior is expressed between travel times and the

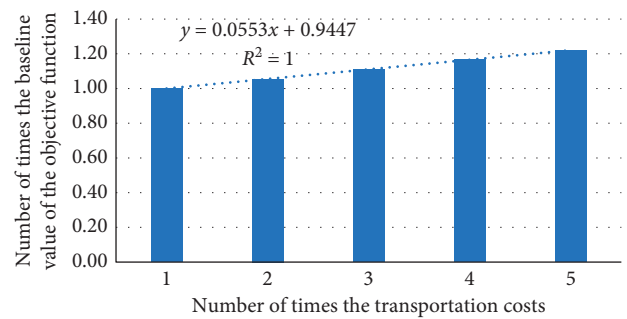


FIGURE 6: Sensitivity analysis performed on transportation costs.

impact of transport externalities; in this case, it is attributed to the nonlinear nature of deprivation costs.

In addition, what is expressed by Figure 5 reflects the opportunity cost of not having opted for foreign trade, where delivery times are generally longer, and therefore the associated deprivation, leaving us with the following contrast: by allowing imports of critical supplies, we expose ourselves to a possible spread of the disease and higher social costs due to delivery times, while reducing or prohibiting them will result in the possible hoarding, price speculation, and greater socioeconomic vulnerability of the affected population.

On the other hand, by varying the transport costs, an incremental relationship was obtained in the social costs, according to Figure 6, where by varying the size of the transport costs 5 times, an increase of just over 20% was obtained in the social costs.

In summary, we found a behavior in the social costs derived from transport where private costs have a relatively minor importance compared to the externalities caused by delays in deliveries. Finally, considering that the local response capacity was sufficient to meet the demand, the formation of coalitions allowed access to economies of scale in transportation and reductions in social cost.

5. Conclusions and Future Research

Regarding the proposed approach, the methodology offers a tool to evaluate the distribution networks of critical supplies from a humanitarian perspective, avoiding last-mile distribution, but it is capable of considering the nonlinear impact of time on total costs of the distribution strategy, where a slight change to delivery times generated a drastic change to total costs, due to deprivation costs. Likewise, the approach analyzes the risks to which the affected population is exposed when considering the possible participation of international suppliers as well as the possible hoarding of critical supplies by actors that generally behave as oligopolies. The information pertaining to the COVID-19 emergency could be represented through the proposed and statistically based approach towards deprivation costs, which played a fundamental role in the decision-making of the programming model, in accordance with the trend on the part of the players to make the deliveries as early as possible efficiently, showing a behavior in transport costs where the externalities caused by deprivation time obtained greater importance than private costs. By adding delays equivalent to 5% of the time horizon, we obtained a change in social costs of more than 100 times its value, while by varying up to 5 times the value of private costs, we obtained a change of little more than 20% in social costs.

On the other hand, the recreation of possible cooperation scenarios allowed the evaluation of the different types of coalitions regarding the benefit that they could offer to the players; by not ruling out the possibility of a subadditive game, it is probable that some participants could reduce the global benefit when participating in a coalition. Additionally, the proposal of a possible contrast between the benefit obtained and the overall cost of the distribution schemes proved that having the highest benefit does not guarantee the lowest social cost.

For future research, we hope to improve the parameters' accuracy, which involve human suffering since they are approximations. We also contemplate the possibility of additional disruptions to the supply networks while the response stage is developing, either in the transport routes or in the number of actors involved (usually due to regulations), uncertainty in demand and supply, and last-mile distribution. Last, but not least, we hope to recreate scenarios where there are variations in the price of critical supply and the deprivation cost function over the time horizon, in relation to the changes that occur in reality regarding foreign trade policies and the impact they would have on global costs, the benefit obtained, and the affected population.

Data Availability

The data used to support the findings of this study are available from the corresponding author upon request.

Conflicts of Interest

The authors declare no conflicts of interest.

References

- [1] W. Shin, T. R. Tan, P. Stoller, W. Yew, and D. Lieo, "Issues on the logistics challenges in the pandemic period," *Journal of Critical Reviews*, vol. 7, no. 8, pp. 776–780, 2020.
- [2] S. Babatunde, R. Oloruntoba, and K. Agho, "Healthcare commodities for emergencies in Africa: review of logistics models, suggested model and research agenda," *Journal of Humanitarian Logistics and Supply Chain Management*, vol. 10, no. 3, 2020.
- [3] L. Sperling, "Seed security response during COVID-19: building on evidence and orienting to the future," *Food Security*, vol. 12, no. 4, pp. 885–889, 2020.
- [4] L. N. Van Wassenhove, "Humanitarian aid logistics: supply chain management in high gear," *Journal of the Operational Research Society*, vol. 57, no. 5, pp. 475–489, 2006.
- [5] J. Holguin-Veras, M. Jaller, L. N. Van Wassenhove, N. Pérez, and T. Wachtendorf, "On the unique features of post-disaster humanitarian logistics," *Journal of Operations Management*, vol. 30, no. 7, pp. 494–506, 2012.
- [6] D. Ivanov, "Predicting the impacts of epidemic outbreaks on global supply chains: a simulation-based analysis on the coronavirus outbreak (COVID-19/SARS-CoV-2) case," *Transportation Research Part E: Logistics and Transportation Review*, vol. 136, Article ID 101922, 2020.
- [7] J. Pacheco and M. Laguna, "Vehicle routing for the urgent delivery of face shields during the COVID-19 pandemic," *Journal of Heuristics*, vol. 26, no. 5, pp. 619–635, 2020.
- [8] Y. Wang, Y. Yuan, X. Guan et al., "Collaborative two-echelon multicenter vehicle routing optimization based on state-space-time network representation," *Journal of Cleaner Production*, vol. 258, Article ID 120590, 2020.
- [9] Y. Wang, X. Ma, Z. Li, Y. Liu, M. Xu, and Y. Wang, "Profit distribution in collaborative multiple centers vehicle routing problem," *Journal of Cleaner Production*, vol. 144, pp. 203–219, 2017.
- [10] V. B. Franco, C. D. P. Arboleda, V. Cantillo, L. F. Macea, and D. G. R. Ríos, "A collaborative supply chain model for non-for-profit networks based on cooperative game theory," *International Journal of Logistics Systems and Management*, vol. 26, no. 4, pp. 475–496, 2017.
- [11] L. N. C. Vellojin, D. G. R. Rios, M. C. H. Hernandez, C. D. P. Arboleda, and W. A. Miller, "A fictitious play algorithm applied to a retailer's replenishment decision problem in a two-echelon supply chain," *International Journal of Logistics Systems and Management*, vol. 8, no. 3, pp. 247–266, 2011.
- [12] D. G. Ramí, N. A. Rez, J. M. D. Escorcía, J. V. Martínez, C. D. P. Arboleda, and A. García, "The dynamic demand game: a Markov state fictitious play approach to a two-echelon supply chain problem under demand uncertainty," *International Journal of Industrial and Systems Engineering*, vol. 10, no. 3, pp. 319–335, 2012.
- [13] L. G. Acuña, D. R. Ríos, C. P. Arboleda, and E. G. Ponzón, "Cooperation model in the electricity energy market using bi-level optimization and Shapley value," *Operations Research Perspectives*, vol. 5, pp. 161–168, 2018.
- [14] J. S. Lee and A. Godard, "Critical care for COVID-19 during a humanitarian crisis—lessons learnt from Yemen," *Critical Care*, vol. 24, no. 1, p. 572, 2020.
- [15] L. L. Albu, C. I. Preda, R. Lupu, C. E. Dobrotă, G. M. Călin, and C. M. Boghicevici, "Estimates of dynamics of the Covid19 pandemic and of its impact on the economy," *Romanian Journal for Economic Forecasting*, vol. 23, no. 2, pp. 5–17, 2020.

- [16] M. M. Queiroz, D. Ivanov, A. Dolgui, and S. Fosso Wamba, "Impacts of epidemic outbreaks on supply chains: mapping a research agenda amid the COVID-19 pandemic through a structured literature review," *Annals of Operations Research*, pp. 1–38, 2020.
- [17] M. L. Ranney, V. Griffith, and A. K. Jha, "Critical supply shortages - the need for ventilators and personal protective equipment during the covid-19 pandemic," *New England Journal of Medicine*, vol. 382, no. 18, p. e41, 2020.
- [18] E. Livingston, A. Desai, and M. Berkwitz, "Sourcing personal protective equipment during the COVID-19 pandemic," *JAMA*, vol. 323, no. 19, pp. 1912–1914, 2020.
- [19] G. M. G. Pacheco, C. D. P. Arboleda, R. A. B. Correa, and H. L. Solano, "Non-linear programming model for cost minimisation in a supply chain, including non-quality and inspection costs," *International Journal of Operational Research*, vol. 14, no. 3, pp. 301–323, 2012.
- [20] P. H. Tatham and S. J. Pettit, "Transforming humanitarian logistics: the journey to supply network management," *International Journal of Physical Distribution & Logistics Management*, vol. 40, no. 8/9, pp. 609–622, 2010.
- [21] J. Holguín-Veras, N. Pérez, M. Jaller, L. N. Van Wassenhove, and F. Aros-Vera, "On the appropriate objective function for post-disaster humanitarian logistics models," *Journal of Operations Management*, vol. 31, no. 5, pp. 262–280, 2013.
- [22] J. Holguín-Veras, J. Amaya-Leal, V. Cantillo, L. N. Van Wassenhove, F. Aros-Vera, and M. Jaller, "Econometric estimation of deprivation cost functions: a contingent valuation experiment," *Journal of Operations Management*, vol. 45, no. 1, pp. 44–56, 2016.
- [23] A. G. Chapman and J. E. Mitchell, "A fair division approach to humanitarian logistics inspired by conditional value-at-risk," *Annals of Operations Research*, vol. 262, no. 1, pp. 133–151, 2016.
- [24] D. Khayal, R. Pradhananga, S. Pokharel, and F. Mutlu, "A model for planning locations of temporary distribution facilities for emergency response," *Socio-Economic Planning Sciences*, vol. 52, pp. 22–30, 2015.
- [25] T. Zhang, H. Zhao, and X. Bai, "A dynamic PD-HL model with various penalty parameters," in *Proceedings of the 5th International Conference on Risk Analysis and Crisis Response (Emerging Economies, Risk and Development, and Intelligent Technology)*, p. 277, Tangier, Morocco, 2015 June.
- [26] N. Pérez-Rodríguez, "Inventory allocation models for post-disaster humanitarian logistics with explicit consideration of deprivation costs," Doctoral dissertation, Rensselaer Polytechnic Institute, Troy, NY, USA, 2011.
- [27] N. Cotes and V. Cantillo, "Including deprivation costs in facility location models for humanitarian relief logistics," *Socio-Economic Planning Sciences*, vol. 65, pp. 89–100, 2019.
- [28] S. Lozano, P. Moreno, B. Adenso-Díaz, and E. Algaba, "Cooperative game theory approach to allocating benefits of horizontal cooperation," *European Journal of Operational Research*, vol. 229, no. 2, pp. 444–452, 2013.
- [29] D. G. Ramirez-Rios, C. M. Rodríguez Pinto, J. Visbal Martínez et al., "A bi-criteria optimization model for parallel machine scheduling: game theoretic vs genetic algorithms," *International Journal of Management Science and Operations Research*, vol. 1, no. 1, pp. 20–30, 2016.
- [30] Instituto Nacional de Vigilancia de Medicamentos y Alimentos (INVIMA), 2020, March 16, Invima declara tapabocas como dispositivo médico vital no disponible durante la emergencia por COVID-19, Invima.Gov.Co, <https://www.invima.gov.co/invima-declara-tapabocas-como-dispositivo-medico-vital-no-disponible-durante-la-emergencia-por-covid-19#:~:text=En%20atenci%C3%B3n%20de%20declaraci%C3%B3n,m%C3%A9dico%20vital%20no%20disponible%2C%20permitiendo>.
- [31] Dinero, (2020a, July 30), Fabricantes colombianos de elementos de protección están "al borde de quebra." Dinero.Com, <https://www.dinero.com/empresas/articulo/fabricantes-de-tapabocas-colombianos-estan-al-borde-de-quebrar/294061>.
- [32] Dinero, (2020b, April 18), Colombia restablece arancel a tapabocas para proteger empresas locales, Dinero.Com, <https://www.dinero.com/economia/articulo/arancel-para-importaciones-de-tapabocas-en-colombia/294561>.
- [33] Departamento Administrativo Nacional de Estadística (DANE), *Precios de Venta al Público de Artículos de Primera Necesidad (PVPAPN)*, Departamento Administrativo Nacional de Estadística (DANE), Bogotá, Colombia, 2020, <https://www.dane.gov.co/index.php/estadisticas-por-tema/precios-y-costos/precios-de-venta-al-publico-de-articulos-de-primera-necesidad-pvpapn>.
- [34] Á. C. Gómez, M. P. R. Sánchez, M. C. R. Díaz, and G. Arias, *Indisciplina Social Análisis Y Aproximación Causal*, Academia Nacional de Medicina de Colombia, Bogotá, Colombia, 2020.
- [35] L. F. Macea, J. Amaya, V. Cantillo, and J. Holguín-Veras, "Evaluating economic impacts of water deprivation in humanitarian relief distribution using stated choice experiments," *International Journal of Disaster Risk Reduction*, vol. 28, pp. 427–438, 2018.
- [36] Departamento Administrativo Nacional de Estadística (DANE), *Informe de Seguimiento - Defunciones por COVID-19*, Departamento Administrativo Nacional de Estadística (DANE), Bogotá, Colombia, 2020, <https://www.dane.gov.co/index.php/estadisticas-por-tema/demografia-y-poblacion/informe-de-seguimiento-defunciones-por-covid-19>.
- [37] Departamento Administrativo Nacional de Estadística (DANE), *Defunciones Por COVID-19*, Departamento Administrativo Nacional de Estadística (DANE), Bogotá, Colombia, 2021, <https://www.dane.gov.co/files/investigaciones/poblacion/defunciones-covid19/boletin-defunciones-covid-2020-02mar-2021-09may.pdf>.
- [38] Superintendencia de Industria y Comercio (SIC), (2020, April 23), Superindustria ordena a propietarios de todas las tiendas del país cesar prácticas que vulneran los derechos de los consumidores | Superintendencia de Industria y Comercio, <http://www.sic.gov.co>. <https://www.sic.gov.co/slider/superindustria-ordena-propietarios-de-todas-las-tiendas-del-pais-cesar-practicas-que-vulneran-los-derechos-de-los-consumidores>.
- [39] Portafolio, (2020, June 23), El coronavirus anda de rumba en Colombia, <https://www.portafolio.co/tendencias/noticias-coronavirus-el-coronavirus-anda-de-rumba-en-colombia-542009>.
- [40] El Tiempo, (2020, June 16), ¡Insólito! Policía intervino más de 1.800 fiestas este fin de semana, <https://www.eltiempo.com/justicia/delitos/coronavirus-colombia-fiestas-que-fueron-intervenidas-por-la-policia-en-fin-de-semana-507292>.
- [41] J. Arellana, L. Márquez, and V. Cantillo, "COVID-19 outbreak in Colombia: an analysis of its impacts on transport systems," *Journal of Advanced Transportation*, vol. 2020, Article ID 8867316, 16 pages, 2020.

Research Article

Variable Speed Limit Strategies Based on the Macro Hierarchical Control Traffic Flow Model

Shubin Li ^{1,2}, Tao Wang ³, Hualing Ren ⁴, Baiying Shi ², Xiangke Kong ²,
Jianyong Chai ⁵ and Xuejuan Wang ⁶

¹Department of Traffic Management Engineering, Shandong Police College, Jinan 250014, China

²Department of Traffic Engineering, Shandong Jianzhu University, Jinan 250101, China

³Department of Automation and Electronic Engineering, Qingdao University of Science and Technology, Qingdao 266061, China

⁴MOE Key Laboratory for Urban Transportation Complex Systems Theory and Technology, Beijing Jiaotong University, Beijing 100044, China

⁵Shandong High-Speed Information Group Co., Ltd, Jinan 250013, China

⁶Department of Rail Transportation, Shandong Jiaotong University, Jinan 250357, China

Correspondence should be addressed to Shubin Li; li_shu_bin@163.com, Tao Wang; wangtao@qust.edu.cn, Hualing Ren; hlren@bjtu.edu.cn, Baiying Shi; shibaiying@sdjzu.edu.cn, and Xiangke Kong; 15621852679@163.com

Received 26 March 2021; Revised 6 June 2021; Accepted 15 June 2021; Published 24 June 2021

Academic Editor: Yong Wang

Copyright © 2021 Shubin Li et al. This is an open access article distributed under the Creative Commons Attribution License, which permits unrestricted use, distribution, and reproduction in any medium, provided the original work is properly cited.

The superior traffic control system can promote the efficiency of mainstream expressway. As the effective method to smooth traffic system, the variable speed limits (VSL) strategies are discussed in an expressway traffic network. The dynamic OD estimation model is used to produce the real traffic information, which is loaded to the traffic network. Then, the prediction information of traffic variables and the VSL strategy are introduced to macro hierarchical control traffic flow model. A solution algorithm is further developed to find the optimal parameters of VSL by minimizing the total travel time and delay. The simulation results show that the proposed strategy perfects well, the traffic congestion is effectively alleviated, and the traffic efficiency of the road section is significantly improved. This framework can be adopted by transit managers for traffic efficiency.

1. Introduction

The expressway is a modern transportation infrastructure which has its specific characteristics, such as high flow and high speed. Building expressway becomes a major project to relieve traffic congestion and traffic delay. This project could improve regional development and promote industrial restructuring and social progress. However, it also attracts more traffic demand for its high efficiency. Then, the problem of traffic congestion and traffic safety occurred inevitably. According to the survey results of Baidu Map in 2020, the degree of highway congestion in China has increased significantly, and the number of traffic jams has also increased. This phenomenon is especially obvious during holidays and peak travel periods. Therefore, it is urgent to take effective control measures to address these problems.

At present, the static speed limit sign is widely used in the speed limit control of expressways, but the determination of the static speed limit value is often based on ideal traffic conditions, and the influence of variable factors such as road traffic flow and weather conditions on the safe driving speed of vehicles is seldom considered. In order to overcome the deficiency of static speed limit control, the dynamic traffic control method represented by variable speed limit (VSL) has gradually become a control strategy considered by scholars and traffic control departments. A large number of studies have found that a smooth traffic flow can effectively improve the safety of vehicles and the efficiency of road sections. Variable speed limit can consider the influence of the change of traffic environment on safe speed more comprehensively and carry out real-time control by adjusting the speed limit value, which is of great significance

to improve the traffic safety and operation efficiency of expressways.

The dynamic traffic control is an effective method to relieve traffic congestion, which is mainly divided into two types: global control strategy and local control strategy. Both of them play essential roles in relieving the congestion of expressway and ensuring the travel safety [1–3]. Compared with local control, the global control measures have many advantages from the network level, such as global logistics network optimization [4] and global state space-time network model [5, 6], take the solution of local traffic congestion as an example for analysis. The local control mitigates the congestion of a specific location on the traffic network. However, this good result comes at the cost of worse congestion at other links in the traffic network, while the control strategy on the network level could avoid this deficiency and reduce the adverse impact of local control on the traffic states of other links. Local controllers only use part of the traffic information, while in the controller on the traffic network level, the real origin-destination (OD) is crucial. The predictions of traffic flow will be easily applicable to control on the network level when the dynamic OD is available.

Therefore, how to implement variable speed limit control strategy in expressway from the perspective of global control becomes the focus of this paper. In addition, in order to adapt the control strategy to the future traffic situation, this paper studies the combination of traffic volume prediction and control of expressway trunk line with variable speed restriction. The paper is divided into eight sections. Section 1 introduces the background and research significance of the problem. Section 2 reviews previous research. Section 3 states the traffic demand estimation and prediction. Section 4 gives the proposed control model and the improved macroscopic traffic flow model. Section 5 presents the simulation method and algorithm. Section 6 shows the numerical examples. Section 7 compares the research results of this model with other models. Section 8 draws the conclusion.

2. Literature Review

In variable speed limits research, scholars have done a lot of excellent research. Lin et al. [7] proposed VSL algorithms which were combined with ramp control (RM) with the aim of improving traffic efficiency. Hegyi et al. [8] used the variable speed limit strategy to study the traffic wave and it can compress the wave. Bertini et al. [9] studied the variable speed limit and traveler information system provided by overhead dynamic information signs in order to improve the understanding of how these systems affect driver behavior and bottleneck formation and location. Abdel et al. [10] analyzed the relationship between the implementation of variable speed limit and the possibility of vehicle collision under different traffic conditions and gave some suggestions on the implementation of variable speed limit. Yao proposed a trajectory smoothing method based on individual variable speed limits with location optimization (IVSL-LC) and verified that the method can improve traffic efficiency and

fuel consumption [11]. Ellen proposed a variable speed limit system based on connected vehicles and verified that, in most cases, the VSL system can improve traffic efficiency through microsimulation software [12]. In addition, some other applications and studies have also demonstrated the important role of variable speed limit in the safety and efficiency of expressways [13–16].

Besides the direct application of VSL on traffic system, it is also introduced into micro- and mesotrafic flow model [17, 18] and other optimization models [19–22]. Abdel et al. used microscopic simulation models to analyze the effects of different speed limit strategies on alleviating and improving road safety [17]. Inanjko established a microscopic simulation framework to analyze the layout and application scenarios of the VSL controller using travel time and vehicle emissions as indicators [18]. Fang proposed a VSL control algorithm based on the model predictive control (MPC) framework. The improved model reduces the speed prediction accuracy error and improves the performance of the system [19]. Alasiri used microscopic simulation software to combine the cell transmission model (CTM) and variable speed limit strategy to verify the effectiveness of the robust VSL controller [20]. Qu used the proposed single-lane cellular automaton model to simulate the traffic flow characteristics under VSL control. The simulation results are consistent with the actual situation, which verifies the validity of the model [21]. Li et al. combined the variable speed limit strategy with the cellular conveyor model to optimize the traffic flow of expressways [22].

The good performance of VSL combined with traffic flow model is demonstrated in their work [23–26], but there are still some unresolved problems need to be addressed. The gaps need to be filled are listed as follows: (1) the research area is small, and a large number of studies mainly focus on the ramp area of expressways, lacking the research on long-distance trunk lines; (2) the simulation data are mainly based on historical traffic volume, and lack of prediction of future traffic volume changes, resulting in low reference of simulation results. At present, the research on traffic flow modeling and prediction has also made great progress [27, 28], but it is rarely applied to VSL; (3) a large number of studies start from the microperspective, but there is lack of analysis from the macro perspective. In view of the above-mentioned problems, this paper selects the expressway trunk line as the main research area from a macro point of view and introduces the traffic flow prediction into the control strategy before the implementation, so as to predict the future traffic changes.

Therefore, this paper studies the combination of traffic volume prediction and control of expressway trunk line with VSL strategy. The contributions of this paper are as follows: (1) this paper simulates the overall situation of vehicles on the road based on the macroscopic traffic flow model and gives the control strategy from the macro level, which fills up the gaps in related research and (2) generates real-time dynamic demand that can be loaded on the transportation network through traffic estimation and forecasting technology. The dynamic road network traffic demand can more realistically verify the effect of the control strategy. (3) An optimal speed control strategy for highway arterials is proposed, based on optimization models and design

algorithms. (4) The feasibility of the proposed model is verified by traffic simulation technology.

3. Traffic Demand Estimation and Prediction

Based on the prediction of traffic demand, the real-time traffic demand is obtained. Also, the traffic demand can be obtained by performing OD prediction function. The decision about the boundary of the queue length should be made in advance. Thus, the estimated or predicted traffic demand will be loaded on traffic network, and then the traffic state can be acquired to realize active management for dynamic traffic.

The key to real-time dynamic traffic demand forecasting is to obtain the OD amount in the future time period based on the historical time-varying OD matrix. Okutani [29] first established a state space model for dynamic OD estimation and verified the effect of the model through Kalman filtering. Kachroo [30] studied the applicability of the Kalman filter method in estimating the origin-destination of travelers within the network from the link traffic. On this basis, Ashok [31] made further corrections and analyzed the deviation between the predicted OD value and the historical value. In this paper, the state space model of Ashok is used as the estimation and prediction of real-time OD matrix. Using deviation to define state variable, $\delta x_h = x_h - x_h^H$, clearly, x_h^H is the OD vector. The corresponding historical estimate is x_h^H . The deviation shows an autoregressive process:

$$x_{h+1} = \sum_{p=h+1-q}^h f_{h+1}^p \delta x_p + w_h. \quad (1)$$

As an autoregressive coefficient matrix, f_{h+1}^p is the impact of δx_p on δx_{h+1} ; q is the autoregressive process times; w_{h+1} is the white Gaussian noise. Satisfying $E(w_{h+1}) = 0$, $E(w_h w_h^T) = Q_h \delta_{hh}$, the error covariance matrix is Q_h , $\delta_w = \begin{cases} 1, & h = 1, \\ 0, & h \neq 1. \end{cases}$

$$\delta y_h = \sum_{p=h-p'}^h a_h^p \delta x_p + v_h. \quad (2)$$

In the formula, $\delta y_h = y_h - y_h^H = y_h - \sum_{p=h-p'}^h a_h^p x_p^H$. y_h means the volume that is obtained during the interval of h , y_h^H serves as the historical values. a_h^p is an assignment dynamic OD matrix, which is the contribution of δx_p to δy_p . The fraction of r in OD departs from the original place during the interval of p . Then, during the interval h , it crosses the counting point. $p' + 1$ stands for the maximum time intervals in travelling between the OD pairs of the traffic network. v_h is the error measurement, $E(v_h) = 0$. To achieve the estimation and prediction of the dynamic OD, equations (1) and (2) are employed for the construction of the state space model. Also, the Kalman filter [32] is helpful for solving this problem.

4. The Improved Control Model

4.1. The Improved Traffic Flow Model Integrated with VSL. Generally, there are three types of traffic flow models: macro-, micro- and mesoscopic models. The macroscopic

model focuses on the collect behaviour of vehicles, the speed and density are the research objects. The microscopic model aims to describe the behaviour of individual vehicle in detail. The description range of mesotrafic model is between micro and macro, which is suitable for medium-sized traffic network. In this paper, the macro hierarchical control model [33] will be explored and improved based on the characteristics of highway. At present, the research on variable speed control strategy is not thorough. Besides, the control models employed in these studies are only based on few control strategies. A comprehensive and effective variable speed decision system is not established yet. To develop an effective decision system, the VSL control strategy is introduced in the macro hierarchical traffic flow control model. The speed-density relation will change if the speed limits are added to the macro hierarchical control model. The definitions of indexes and variables are shown in Table 1.

The improved macromodel-integrated VSL is proposed as follows:

$$p(i, k+1) = p(i, k) + \frac{T}{l_1 \bullet n_i} [q(i-1, k) - q(i, k) - e(i, k)],$$

$$q(i, k) = p(i, k) \cdot \min\{v(i, k), v_{\text{lim}}(i, k)\} \cdot n_i, \quad (3)$$

$$v[p(i, k)] = \min\left\{v_f \left[1 - \left(\frac{p(i, k)}{P_{\text{jam}}}\right)^\alpha\right]^\beta, v_{\text{lim}}(i, k)\right\}. \quad (4)$$

At the entrance and exit of the boundary ramp, namely, $i = 1$ and $i = N$,

$$p(1, k+1) = p(1, k),$$

$$v(1, k+1) = \min\{v[p(1, k)], v_{\text{lim}}(1, k+1)\},$$

$$p(N, k+1) = p(N, k),$$

$$v(N, k+1) = \min\{v[p(N, k)], v_{\text{lim}}(N, k+1)\}. \quad (5)$$

The queue length of the on-ramp is as follows:

$$p(i, k+1) = p(i, k) + T[d(i, k) - r(i, k)]. \quad (6)$$

In addition to the state equation (6), $r(i, k)$ must meet the following constraints:

$$r_{i \min} \leq r(i, k) \leq r_{i \max}. \quad (7)$$

So, $V = \{v_{\text{lim}}(i, j), i = 1, 2, \dots; j = 1, 2, \dots\}$, is the variable speed limits strategy.

The relationship between density and speed on a segment can be described by equation (4) (see Figure 1).

In addition to the presented model, the dynamic characteristics of the vehicles are described. In this paper, the control objective is to minimize the total delay and the total travel time of all vehicles. This is a global optimal control algorithm on the basis of the mentioned state equations of the traffic flow model.

4.2. The Optimization Control Model. The multiobjective optimization control model, in this paper, aims to minimize

TABLE 1: Table of definitions of variables.

Variables	The definitions of variables
i	$i = 1, \dots, N$
k	A period of time, $k = 1, 2, \dots, k$
l_i	It is the length of segment i
n_i	It is the number of lanes on segment i
T	The sampling period
v_f	The free flow speed
ρ_{jam}	The traffic jam density
ρ_c	The critical density
α, β	Model parameters
$\rho(i, k)$	At time k , on segment i , the vehicle density (veh/km/Lane)
$r(i, k)$	At time k , on segment i , the entrance ramp traffic flow
$e(i, k)$	At time k , on segment i , the exit ramp traffic flow
$v(i, k)$	At time k , on segment i , the average speed of vehicles (km/h)
$p(i, k)$	At time k , on segment i , the queue length
$d(i, k)$	At time k , on segment i , the traffic demand
$q(i, k)$	At time k , on segment i , the number of vehicles (veh/h/lane)
$v_{\text{lim}}(i, k)$	At time k , on segment i , the limited speed

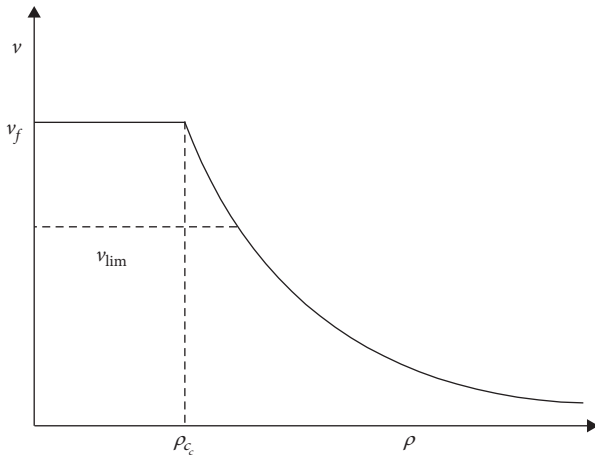


FIGURE 1: Speed and density relationship.

the total delay and the total travel time of all vehicles of all simulation intervals through the network. In other words, the objective is to ensure all vehicles reach destinations in the shortest possible time. One of the best variable speed limit strategies can be selected by means of simulation method. The following notations are used to provide a clear description of the problem.

The traffic network consists of nodes and connecting lines. The lines are divided into segments, which are represented by j . The total simulation time is divided into several intervals, which are represented by h , $Q(j, h)$ is the average traffic flow in h interval on j segment, $V(j, h)$ is the average traffic speed in h interval on j segment, and $p(j, h)$ is the average traffic density in h interval on j segment. Equation (8), formula of the objective function, reads

$$\begin{aligned} \min L(\cdot) &= \sum_{jh} (C_j - Q(j, h) + V(j, h)), \\ &\text{s.t. } C_{\min} \leq C \leq C_{\max}, \\ &Q(j, h), V(j, h), \rho(j, h) \geq 0, \end{aligned} \quad (8)$$

where C_{\min} is the minimum traffic capacity and C_{\max} is the maximum capacity. The constraints are up threshold and nonnegative.

5. The Simulation Method

The feasibility of online macroscopic traffic simulation and optimal traffic control is demonstrated in this paper. This approach can adapt to the changeable traffic conditions. A situation is proposed in which the VSL can be used in upstream main roads. The following is how the approach performs its function. The VSL can prevent traffic congestion at the bottleneck by creating a free flow zone at the upstream section. The existence of VSL changes the fundamental diagram shown in Figure 1 and reduces the output capability of this segment.

The following section shows the process of executing the proper simulation with VSL. A closed cycle scheme plays an important part in solving the problem (see Figure 2). VSL is integrated into the mesoscopic traffic simulator to estimate network operation state. The optimal objective is the optimal control speed limits strategy by minimizing the total delay. In order to improve the estimation accuracy of macroscopic model parameters (such as $\alpha, \beta, k_{\text{jam}}$ etc.), it has a process of parameter correction. A point deserves noting that the parameters usually become constant when the parameter calibration horizon passes. The procedure reduces the number of variables and enhances the stability of the traffic system. The parameters calibration process is chosen with the purpose of correcting system parameters. In this way, the network description and traffic dynamics characteristics can be obtained more accurately. In the following, a new optimization's performing functions are triggered to find the best strategy. In this regard, traffic estimation and prediction are of great help to this. A more comprehensive network state results from their interaction. Known as rolling horizon, this scheme enables updating the state from measurement and it can even update the model in every iteration step.

6. The Simulation Study

6.1. The Simulation Environment. As shown in the simulation structure diagram in Figure 3, the highway network is divided into 9 sections. Each section is a one-way four-lane connecting line. On this highway, there are 4 entry ramps and 4 exit ramps. The section of each road is 3 km.

The proposed model is used in the modeling and simulation. In order to simulate the real traffic situation and reveal its essence, the parameters of the traffic flow model are set according to the specific characteristics of the road section (length, width, level, capacity, and traffic flow), where $\alpha = 1.7$, $\beta = 2$, $r_{\text{max}} = 900$ veh/h, $r_{\text{min}} = 180$ veh/h, $v_f = 100$ km/h, $p_{\text{jam}} = 130$ (veh/km)/Lane, and the

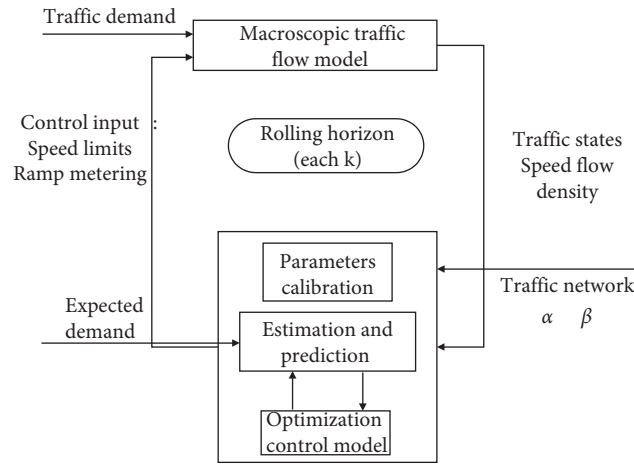


FIGURE 2: Simulation structure.

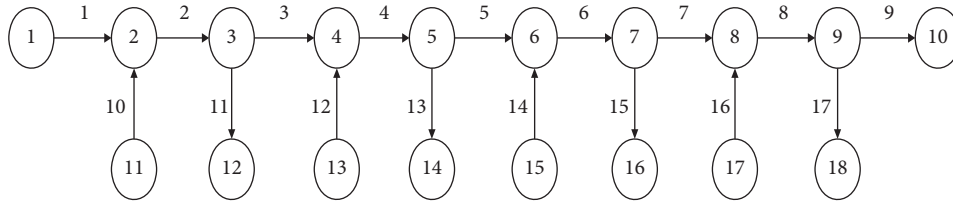


FIGURE 3: Simulation structure.

TABLE 2: The OD pairs in network.

OD	Origin-destination	Average exit rate
1	1-12	60
2	1-14	100
3	1-16	250
4	1-18	420
5	1-10	1500
6	11-12	50
7	11-14	300
8	11-16	360
9	11-18	220
10	11-10	300
11	13-14	40
12	13-16	120
13	13-18	840
14	13-10	420
15	15-16	60
16	15-18	100
17	15-10	500
18	17-18	80
19	17-10	360

TABLE 3: Dynamic OD prediction result.

O	D									
	1	2	3	4	5	6	7	8	9	10
1			21.00		20.00		56.00		52.00	198.00
2			5.00		10.00		26.00		33.00	60.00
3							21.00		14.00	100.00
4										
5					3.00		48.00		55.00	102.00
6										
7							7.00		17.00	36.00
8										
9										30.00
10										

simulation time is 3 hours. The OD and exit average rate are shown in Table 2. The average exit rate is a time variable, which reflects the average starting rate between OD pairs. A greater value indicates that the adjacent vehicle's departure time interval is shorter. In the simulation, we placed three variable message boards on road sections numbered 3, 5, and 7. the VSL strategy is as follows: {70, 60, 50}; {60, 50, 50}. In the simulation time of 15-25 minutes and 35-45 minutes,

the limit strategies are implemented. Vehicle detectors are installed at the middle of each section, so as to mark the traffic volume and average speed and density on the segment.

6.2. *The Simulation Results.* According to the traffic demand estimation and forecasting method, the dynamic traffic demand of the study area can be obtained. The prediction results are shown in Table 3. After completing the traffic demand forecast, we first distribute the forecast results to the road network in the study area to obtain the traffic flow status and traffic flow parameters of each road section. Then, on this basis, the changes of traffic flow parameters before and after the implementation of the VSL strategy under the

TABLE 4: Simulation results.

Internal	The network average density without VSL	The network average density with VSL
1	0.00288	0.00285
2	0.00681	0.00688
3	0.00793	0.00804
4	0.00845	0.00859
5	0.00843	0.00839
6	0.00847	0.00853
7	0.00830	0.00861
8	0.00817	0.00866
9	0.00835	0.00851
10	0.00850	0.00864
11	0.00854	0.00870
12	0.00853	0.00863
Average	0.00778	0.00792

overall network are compared, and the effect of the model in this paper has been verified.

Table 4 shows the traffic density of each road section in the network before and after the implementation of the VSL strategy. What is worth noting here is that the entire network is taken into consideration in obtaining the simulation results. Obviously, before the VSL comes into play, the overall average density of the network is 0.00778. After it is performed, the value is 0.00792, a slight increase in density indicates that a decrease in speed results in an increase in the number of vehicles stranded on the network. The average traffic and speed of road sections in the network before the implementation of VSL were 387.4769 and 20.7170. However, after the implementation of VSL, the average network traffic was 387.2130 and the average speed was 20.5129. Due to the implementation of the variable speed limit strategy, the speed of the vehicle in the network has become lower, so the driving time of the vehicle in the network has increased.

The following two-dimensional and three-dimensional distribution map, respectively, depicts the average density and speed of each segment in each time period. Figure 4 is the three-dimensional distribution of the average density on each segment in each interval without VSL. Figure 5 is the three-dimensional distribution of the average density on each segment in each interval with VSL. Figures 6 and 7 are their two-dimensional representations.

According to Figures 4–7, the average density of segments which are implemented with the VSL strategy increases significantly. But overall the other segments’ average density becomes smoother. Because of the proposed method with VSL strategy, the simulation results present a better queue formation than those without a non-VSL. Owing to the VSL, it is convenient for vehicles to keep the earlier speed, because they can adjust speed according to the network state. In this way, the queue can be transferred from the bottleneck to upstream timely. However, the queue without the help of VSL cannot achieve that goal. Although after using VSL, the mean speed, especially during the rush hour, of most sections is lower than that in the non-VSL case, there is no negative impact on travel time. This highlights the advantages of the VSL in enabling the network to operate at a more stable speed. A comparison of the average speed of each interval from the eighth to twelfth interval implies

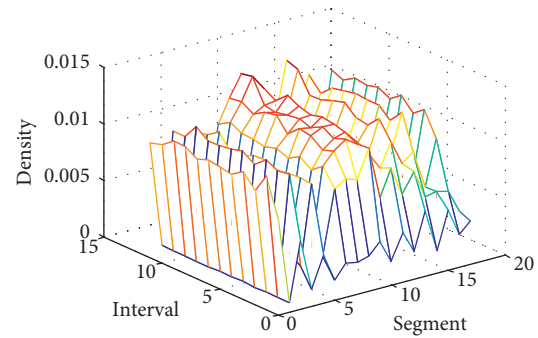


FIGURE 4: The density distribution without VSL.

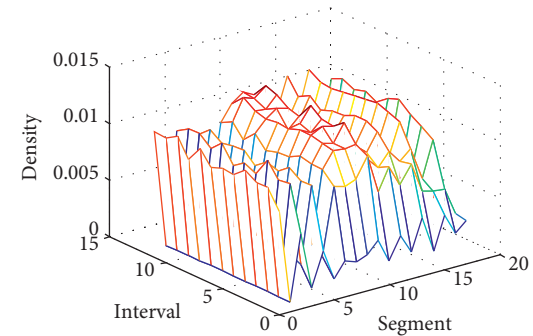


FIGURE 5: The density distribution with VSL.

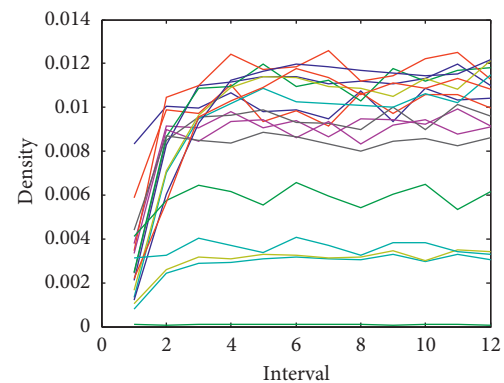


FIGURE 6: Two-dimensional density without VSL.

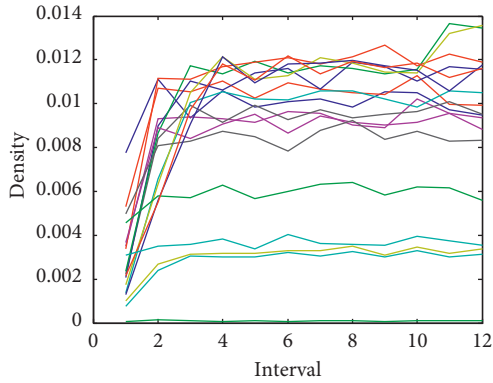


FIGURE 7: Two-dimensional density with VSL.

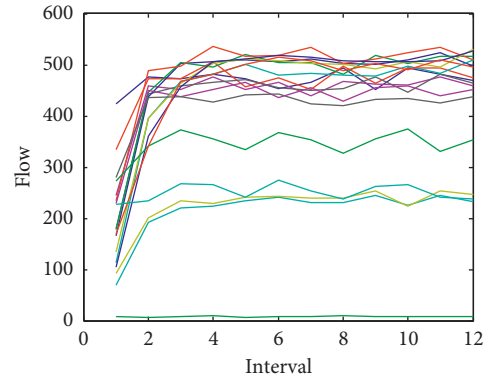


FIGURE 8: Two-dimensional flow without VSL.

that the values are 17.7258, 16.7817, 16.9283, 18.6175, and 18.9500, when there is no VSL. The values become, however, 17.8033, 17.5525, 17.0200, 17.5867, and 17.0967, when the VSL is used. The network of traffic flow becomes more stable than that in the previous time. The traffic flow of some segments becomes less congested. Theoretically, the more stable the traffic flow is, the better the operation efficiency of the traffic system will be.

In the same way, Figures 8–15 show the average flow and speed of each segment in each interval in three-dimensional and two-dimensional forms.

In the four locations, the values of variable speed limit are set 100 km/h, 80 km/h, 80 km/h, and 90 km/h, respectively. Different values should be taken to be in line with limiting strategies. Because traffic congestion does not occur at those segments, variable speed limit strategies are acceptable in relieving traffic density while the overall traffic flow remains stable. When critical density appears on traffic network, the VSL plays an important role in avoiding potential danger. Both traffic density and traffic flow on the sections are far away from variable speed limit sections which undergo no changes. It can be concluded that without reducing road capacity, the variable speed limit strategies contribute to traffic safety.

Undoubtedly, if the vehicle speed is stable, it benefits to traffic flow operation. This avoids the risk of traffic accidents. To sum up, the variable speed limit strategies can effectively prevent the potential risk factors and improve the operation efficiency of the system in some cases. Although it does not show obvious effect in relieving traffic congestion, it is the best application in traffic management.

On the basis of the abovementioned research, in order to further verify the effectiveness of the method proposed in this article, we adopted a method of randomly perturbing the test data, that is, randomly changing each OD pair with a range of 30%. Since the traffic demand of the expressway network is time-varying, adding random disturbances can better describe the dynamic changes of the traffic volume on the road network and then verifies the effectiveness of the method in this paper more realistically. The simulation results show that when the demand increases by 30% on individual road sections with high OD demand, the variable speed limit has little effect on the traffic flow of the road section. This is because the density of the road section

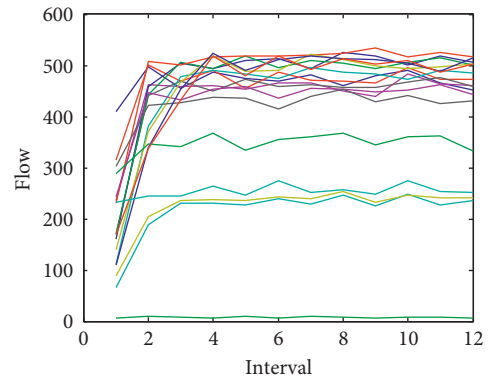


FIGURE 9: Two-dimensional density with VSL.

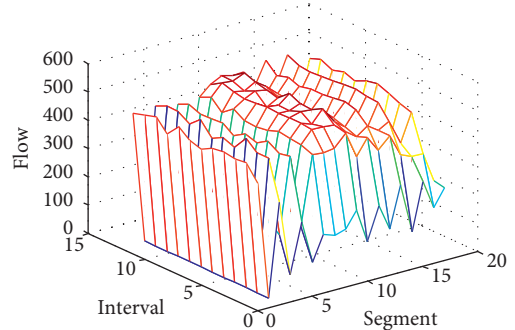


FIGURE 10: The flow distribution without VSL.

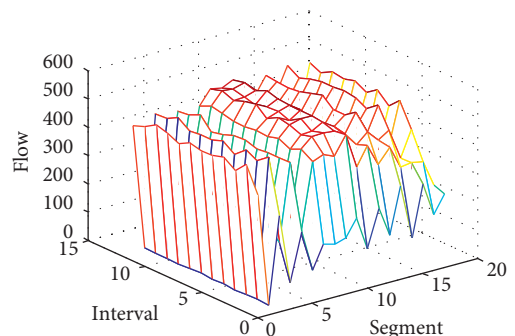


FIGURE 11: The flow distribution with VSL.

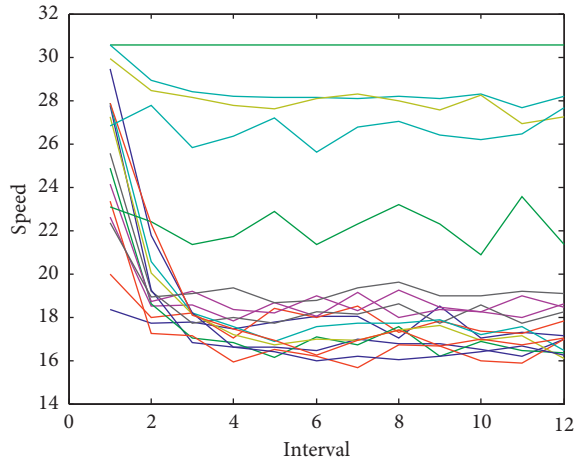


FIGURE 12: Two-dimensional speed without VSL.

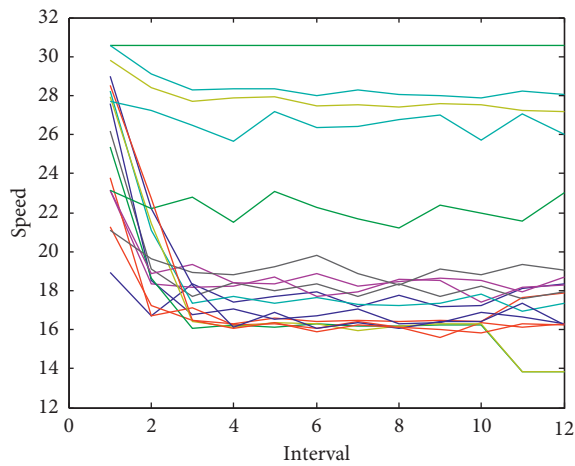


FIGURE 13: Two-dimensional speed with VSL.

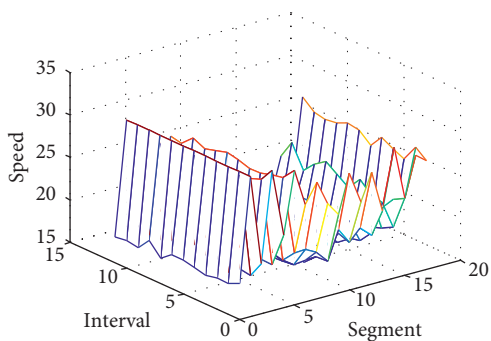


FIGURE 14: The speed distribution without VSL.

roughly makes the speed of the road section much lower than the dynamic speed limit value. When the demand is reduced by 30%, the speed of the vehicles on the road section is greater than the speed limit value. At this time, the variable speed limit value can act on most vehicles on the road section, thus producing a more obvious improvement and

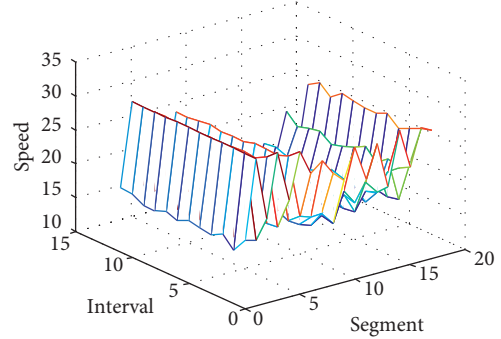


FIGURE 15: The speed distribution with VSL.

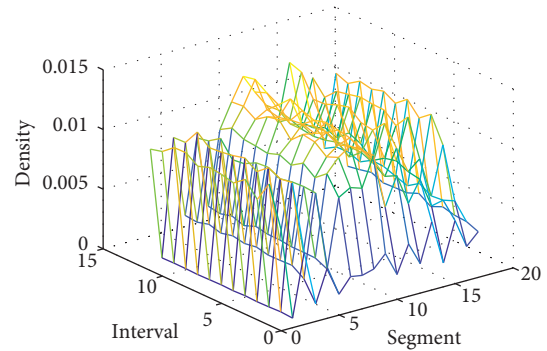


FIGURE 16: The VSL-integrated mesomodel.

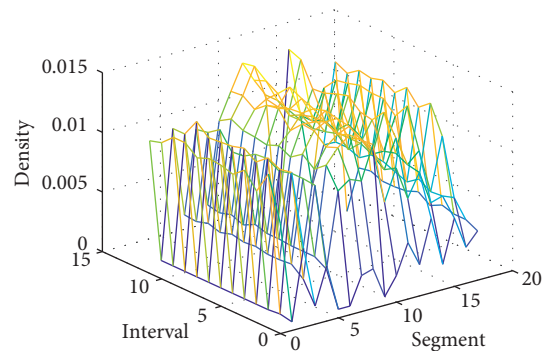


FIGURE 17: The VSL-integrated LTM.

regulation effect. In general, it can be concluded through simulation: on the one hand, the variable speed limit method proposed in this paper can increase the traffic in some road sections, and the density is evenly distributed in the overall road network. On the other hand, the model has a more obvious improvement effect before the occurrence of congestion, so the implementation of the strategy needs to cooperate with accurate traffic state prediction methods. In addition, if the OD is adjusted again, the control measures of closed ramp can be adopted, combined with the variable speed limit of this article to adjust the main line traffic flow, and better control effect is desirable.

7. Comparing with Other Research Results

The proposed method in this paper is suitable for specific sections of the expressway. We used the assumed theoretical data to verify it. In this section, we compared the results of this paper with three other traffic flow models integrated with VSL, namely, the mesotrafic flow model, CTM (the cell transport model), and LTM (the link transport model) [14, 34, 35]. CTM is suitable for studying the micromotion of urban road vehicles and is combined with VSL to control the congestion at the intersection at the same time ensuring traffic safety. LTM is suitable for studying the traffic conditions at the section level which can nip the traffic congestion in the bud according to the speed limit strategy of different road sections. The mesoscopic traffic flow model integrated with VSL can control regional urban traffic. At the same traffic environment, we use VSL-integrated CTM and the VSL-integrated mesoscopic traffic flow model to study the traffic flow parameters such as density, and the results are shown in Figures 16 and 17.

From the abovementioned results, there is little difference among the two types of models. The density calculated by the LTM-based model is a little higher than any one of others. Although the optimization effect of the traffic flow on the road is not very different, it is worth noting that the research scope of the expressway in this paper is very large, which shows that the calculation speed of the model in this paper is faster than other methods, so it is suitable for the macrotraffic flow based on VSL.

8. Research Conclusions and Prospects

This paper explores the VSL strategy on expressway by means of traffic simulation method, and the real-time traffic demands are estimated and predicted. With the help of motion equation, a cooperative systems extension is developed. Then, a new speed limits strategy is proposed by using the proposed method. The recommendations of speed are provided in advance for the vehicles at predefined points. Additionally, according to the actual speed of the vehicles, the location of releasing speed limits strategy is determined.

According to the simulation results, the proposed method produces some different queue formations under the VSL strategy. These vehicles adapt their earlier speed to guiding vehicle speed, which continuously produces a queue that moves upstream from the bottleneck. In the non-VSL case, however, the queue is stationary and the front of the queue grows upstream from the bottleneck, which reduces the capacity of bottleneck. The new control method can also smooth the density oscillation of traffic flow. Then, the traffic flow is in a stable state. In the cooperative VSL case, the mean speed of most road segments during the rush hour is lower than that in the non-VSL case. But the lower mean speed does not affect the total travel time. This provides a new way to control the traffic flow with a stable speed pattern. It can be concluded that the proposed VSL strategy could harmonize traffic flow, promote traffic efficiency, and then improve the regional traffic conditions.

Data Availability

The data of this study come from mesoscopic simulation software.

Conflicts of Interest

The authors declare that there are no conflicts of interest regarding the publication of this paper.

Acknowledgments

This work was supported by the National Natural Science Foundation of China (Grant nos. 71871130, 71471104, 71771019, and 71971125); University Science and Technology Program Funding Projects of Shandong Province (Grant no. J17KA211); Social Science Foundation of Shandong Province (Grant no.12BJJJ13); and Science and Technology Program Funding Projects of Shandong Police College (Grant no. YSKYB2005).

References

- [1] Z. Z. Tian, "Modeling and implementation of an integrated ramp metering-diamond interchange control system," *Journal of Transportation Systems Engineering and Information Technology*, vol. 1, no. 7, pp. 61–72, 2007.
- [2] X. R. Liang, Z. Y. Liu, J. M. Xu et al., "Design and simulation of coordinated ramp control system on expressway," *Information and Control*, vol. 3, no. 7, pp. 308–311, 2005.
- [3] O. J. Chen, *A Dynamic Traffic Control Model for Real Time Expressway Operations*, Massachusetts Institute of Technology, Boston, MA, USA, 1996.
- [4] Y. Wang, X. L. Ma, Z. B. Li, Y. Liu, M. Xu, and Y. Wang, "Profit distribution in collaborative multiple centers vehicle routing problem," *Journal of Cleaner Production*, vol. 144, pp. 203–219, 2017.
- [5] Y. Wang, S. G. Peng, X. S. Zhou, M. Mahmoudi, and L. Zhen, "Green logistics location-routing problem with eco-packages," *Transportation Research Part E: Logistics and Transportation Review*, vol. 143, Article ID 102118, 2020.
- [6] Y. Wang, Y. Y. Yuan, X. Guan et al., "Collaborative two-echelon multicenter vehicle routing optimization based on state-space-time network representation," *Journal of Cleaner Production*, vol. 258, Article ID 120590, 2020.
- [7] P. W. Lin, K. P. Kang, and G. L. Chang, "Exploring the effectiveness of Variable Speed Limit controls on highway work-zone operations," *Intelligent Transportation Systems*, vol. 8, no. 3, pp. 155–168, 2004.
- [8] A. Hegyi, B. D. Schutter, and J. Hellendoorn, "Optimal coordination of variable speed limits to suppress shock waves," *IEEE Transactions on Intelligent Transportation Systems*, vol. 1852, no. 1, pp. 167–174, 2003.
- [9] R. L. Bertini, S. Boice, and K. Bogenberger, "Dynamics of a variable speed limit system surrounding a bottleneck on a German autobahn," in *Proceedings of the 85th TRB Annual Meeting*, Washington DC, WA, USA, January 2006.
- [10] A. M. Abdel, J. Dilmore, and A. Dhindsa, "Evaluation of variable speed limits for real-time expressway safety improvement," *Accident Analysis and Prevention*, vol. 38, no. 7, pp. 335–345, 2006.
- [11] H. D. Yao, J. X. Cui, X. P. Li, Y. Wang, and S. An, "A trajectory smoothing method at signalized intersection based on

- individualized variable speed limits with location optimization,” *Transportation Research Part D*, vol. 62, 2018.
- [12] F. G. Ellen and T. Andreas, “Using connected vehicles in a variable speed limit system,” *Transportation Research Procedia*, vol. 27, pp. 85–92, 2017.
- [13] M. D. Robinson, “Examples of variable speed limit applications. Speed management workshop,” in *Proceedings of the 79th TRB Annual Meeting*, Washington DC, WA, USA, January 2000.
- [14] S. B. Li and D. N. Cao, “Variable speed limit strategies’ analysis with cell transmission model on expressway,” *Modern Physics Letters B*, vol. 31, no. 24, Article ID 1750219, 2017.
- [15] S. B. Li and D. N. Cao, “Variable speed limit strategies analysis with link transmission model on urban expressway,” *Modern Physics Letters B*, vol. 32, no. 6, Article ID 1850077, 2018.
- [16] S. B. Li, D. N. Cao, W. X. Dang, T. Sun, and W. Dang, “Intersection-movement-based traffic incidents detected method and run state evaluation of expressway network,” *Journal of Transportation Safety and Security*, vol. 11, no. 6, pp. 642–660, 2018.
- [17] A. M. Abdel, R. Cunningham, V. Gayah, and L. Hsia, “Dynamic variable speed limit strategies for real-time crash risk reduction on freeways,” *Transportation Research Record Journal of the Transportation Research Board*, vol. 2078, no. 2078, pp. 108–116, 2009.
- [18] E. Ivanjko, K. Kušić, and M. Gregurić, “Simulation analysis of two controllers for variable speed limit control,” *Proceedings of the Institution of Civil Engineers—Transport*, 2020.
- [19] J. Fang, H. X. Ye, and S. M. Easa, “Modified Traffic Flow Model with Connected Vehicle Microscopic Data for Proactive Variable Speed Limit Control,” *Journal of Advanced Transportation*, vol. 2019, Article ID 8151582, 11 pages, 2019.
- [20] F. Alasiri, Y. H. Zhang, and A. I. Petros, “Robust variable speed limit control with respect to uncertainties,” *European Journal of Control*, vol. 59, pp. 216–226, 2021.
- [21] Q. Xu, L. H. Li, Z. W. Yi, P. Mao, and M. Yang, “Traffic flow modeling of freeway variable speed limit control based on the big data of driving behavior,” *Journal of Advanced Transportation*, vol. 2020, Article ID 8859494, 11 pages, 2020.
- [22] S. B. Li, J. J. Wu, Z. Y. Gao et al., “Bi-dynamic analysis of traffic congestion and propagation based on complex network,” *Acta Physica Sinica*, vol. 60, no. 11, Article ID 050701, 2011.
- [23] J. C. Long, Z. Y. Gao, and P. Orenstein, “Control strategies for dispersing incident-based traffic jams in two-way grid networks,” *IEEE Transactions on Intelligent Transportation Systems*, vol. 13, no. 2, pp. 469–481, 2012.
- [24] A. M. H. Zhang, Z. Y. Gao, and H. L. Ren, “Incident-based traffic congestion control strategy,” *Science China Technological Sciences*, vol. 54, no. 5, pp. 1338–1344, 2011.
- [25] H. W. Guo, W. H. Wang, W. W. Guo, X. Jiang, and H. Bubb, “Reliability analysis of pedestrian safety crossing in urban traffic environment,” *Safety Science*, vol. 50, no. 4, pp. 968–973, 2012.
- [26] W. H. Wang, W. Zhang, H. W. Guo, H. Bubb, and K. Ikeuchi, “A behavioural car-following safety model for microscopic simulation of traffic flow with various driving characteristics,” *Transportation Research Part C*, vol. 19, pp. 1202–1214, 2011.
- [27] J. J. Tang, F. Liu, Y. J. Zou, W. Zhang, and Y. Wang, “An improved fuzzy neural network for traffic speed prediction considering periodic characteristic,” *IEEE Transaction On Intelligent Transportation Systems*, vol. 18, no. 9, pp. 2340–2350, 2017.
- [28] J. J. Tang, J. Zeng, Y. W. Wang, H. Yuan, F. Liu, and H. Huang, “Traffic flow prediction on urban road network based on license plate recognition data: combining attention-LSTM with genetic algorithm,” *Transportmetrica A: Transport Science*, vol. 17, no. 4, pp. 1217–1243, 2021.
- [29] I. Okutani and J. Y. Stephanedes, “Dynamic prediction of traffic volume through Kalman filtering theory,” *Transportation Research Part B: Methodological*, vol. 18, no. 1, pp. 1–11, 1984.
- [30] P. Kachroo, K. Ozbay, and A. Narayanan, “Investigating the use of Kalman filtering approaches for dynamic origin-destination trip table estimation,” *Electrical and Computer Engineering*, vol. 1, pp. 138–142, 1997.
- [31] K. Ashok and A. M. Ben, “Dynamic origin-destination matrix estimation and prediction for real-time traffic management systems,” in *Proceedings of 12th International Symposium on Transportation and Traffic Theory*, Amsterdam Elsevier Science, Berkly, CA, USA, July 1993.
- [32] Y. S. Suh, V. H. Nguyen, and Y. S. Ro, “Modified Kalman filter for networked monitoring systems employing a send-on-delta method,” *Automatica*, vol. 43, no. 2, pp. 332–338, 2007.
- [33] Z. Y. Liu, *Theory and Application of Intelligent Traffic Control*, Science Press, Beijing, China, 2003.
- [34] S. B. Li, D. N. Cao, W. X. Dang, and L. Zhang, “Variable speed limit strategies analysis with mesoscopic traffic flow model based on complex networks,” *International Journal of Modern Physics C*, vol. 29, no. 2, Article ID 1850014, 2018.
- [35] S. B. Li, T. Wang, H. L. Ren, X. Kong, and X. Wang, “Coordination optimization of VSL strategy on urban expressway and main road intersection signal,” *IEEE Access*, vol. 8, pp. 223976–223987, 2020.

Research Article

Evaluation of Cruise Ship Supply Logistics Service Providers with ANP-RBF

Liling Huang ¹, Yong Tan ¹ and Xu Guan²

¹School of Management, Wuhan Polytechnic University, Wuhan 430048, China

²School of Management, Huazhong University of Science and Technology, Wuhan 430074, China

Correspondence should be addressed to Liling Huang; huangliling@whpu.edu.cn and Yong Tan; 11857985@qq.com

Received 22 December 2020; Revised 29 April 2021; Accepted 19 May 2021; Published 29 May 2021

Academic Editor: Yong Wang

Copyright © 2021 Liling Huang et al. This is an open access article distributed under the Creative Commons Attribution License, which permits unrestricted use, distribution, and reproduction in any medium, provided the original work is properly cited.

To overcome challenges like market dynamic configuration, information integration, and quick response, it is necessary to build an efficient, stable, and well-coordinated supply chain relationship for cruise ship supply. This requires building of a solid evaluation index system of logistics service providers (LSPs) in the cruise ship supply chain. In this paper, we introduce an evaluation index system that consists of four dimensions, based on the characteristics of cruise ship supply and the connotation and type of cruise ship supply LSPs. The four dimensions are business level, collaborative capacity, service price, and information level, including ten subcriteria. We first establish an evaluation decision model for the interdependence and feedback relationship between the criteria by using analytic network process (ANP) for weight definition of each index; then, we use Super Decisions software to simulate the results, combine RBF neural network training and validation, and extract implicit knowledge and laws. We propose an incremental algorithm that can effectively avoid the influence of subjective factors and increase the dynamic nature of evaluation. The results show that the ANP-RBF method has strong practicability in the evaluation of cruise ship supply LSPs.

1. Introduction

Since the end of the 20th century, the international cruise tourism industry has developed rapidly, with an average annual growth rate of 8%–9%, ranking the fastest in the global tourism market. As the growth of cruise economic throughout the world continues to lead to the problem of cruise ship supply chain, solutions to supply chain issues of supporting facilities planning, marketing mix customer satisfaction, and logistics supply process are becoming increasingly urgent [1]. The majority of previous research studies had focused on supporting facilities planning and logistics supply process, while limited attention had been paid to partnership issues [2–4]. However, partnership issues are becoming more and more urgent as partnership selection quantity has increased rapidly owing to the explosive growth of global purchasing. Cruise ship supply chain has some unique characteristics such as complexity, time validity, irreversibility, and high supply variability [5]. The time of a cruise port calling is limited, and there are only

a few hours for cruise ship replenishment on a tight schedule. The cruise ship supply includes local procurement and overseas procurement, with the supplies being of various varieties and large amount. Therefore, the cruise ship supply chain needs an efficient, stable, and well-coordinated supply chain relationship. It can overcome challenges like dynamic market configuration, information integration, and quick response. The outsourcing of cruise ship logistics service is conducive for the cruise companies to maintaining a stable source of goods and prices. To a certain extent, this can ensure quality [6]. In recent years, the upsurge of cruise tourism has promoted the development of cruise ship supply logistics. An appropriate evaluation of LSPs is an important step towards creating successful alliance and avoiding failure of relationships afterwards. Because the cruise industry is emerging industry, the evaluation of cruise ship supply LSPs has become an urgent problem for decision makers of cruise companies.

Traditional LSPs evaluation has focused on providing a low price and high quality. However, these can no longer be

met owing to the unique characteristics of cruise. To solve this problem, the evaluation of cruise ship supply LSPs should consider the characteristics of cruise ship supply. Otherwise, unrealistic criteria can hardly contribute to handling the problem.

This study focuses on partnership evaluation problem. An index system will be useful for the determination of the cruise ship supply LSPs. Without reliable evaluation results of the index system, it will be difficult for the partnership resources in cruise ship supply to remain stable. As a result, it will become occasionally difficult to ensure efficiency and quality owing to the lack of organization and management. At the same time, some tourists will be lost as a result of the unbalanced cruise service.

This paper enriches the field of cruise ship supply logistics management by making the following contributions. First, we put forward the special research perspective and objects. Cruise tourism is an emerging industry in China, and the research on its operation process supply chain is the current research trend. However, there is little research on the index system of cruise ship supply LSPs. This paper introduces the evaluation study of LSPs into the specific field of cruise industry. Second, we analyze the characteristics of cruise ship supply and further construct the index system. It fills the gap that deals with provider evaluation index of cruise ship supply chain. Finally, this study recognizes the requirement of diversified expertise both on technical and domain knowledge for making a right decision, proposing to use this expertise in group decision-making; it is of great practical significance to realize the planning of the cruise ship supply industry chain, improve the efficiency of the cruise ship supply chain, and realize the stable and healthy development of the cruise economy.

The remainder of this paper is organized as follows. In Section 2, we survey a relevant literature review from cruise ship supply and LSPs evaluation. In Section 3, we introduce definition and types of service supply chain to cruise ship supply and build the evaluation index system from four dimensions and ten subcriteria. Then, Section 4 presents the method. Later, Section 5 gives a numerical example to verify the evaluation method. Eventually, Section 6 concludes this article and suggests possible research directions in the future.

2. Literature Review

This paper will address LSPs evaluation problem of the cruise ship supply through cruise ship supply chain, and LSPs evaluation methods.

In terms of cruise ship supply chain, most of research is macroscopic. For example, Véronneau and Roy analyzed the planning process of the cruise supply chain and proposed that the cruise operation focused on logistics supply [7]. Due to the characteristics of cruise supply point movement, the distance between the port of call and the raw material supply point further increased the lead time of supply [6]. According to Boyd tactical cycle theory, replenishment lead time should be shorter than cruise length to maintain the responsiveness within a certain period. Shortening the

delivery time was the main solution to provide more flexibility, and this was further transferred to the pull supply system [8]. Furthermore, with the large-scale development of cruise ships, ship tonnage and passenger capacity gradually increase, which brings many challenges to cruise ship operation management [9]. The distribution problem of cruise ship supply, which had the characteristics of large quantity, high value, and strict time requirement, required specialized cruise distribution centers and supporting facilities to centralized procurement, centralized supervision, centralized distribution, and centralized settlement for the distribution development. It was proposed that if a port could provide comprehensive cruise logistics service for international cruise lines, such as complete port facilities, transport buildings, supplies services, and integrate related industries, the port is promoted as the cruise logistics service hub [10, 11].

LSPs selection and optimization are the source of the construction of service supply chain to cruise ship supply. Besides, the evaluation of LSPs includes supplier quantity optimization decision, supplier evaluation, and logistics task allocation, which is a typical multiobjective decision-making problem [12]. In the existing literature, many works are devoted to the evaluation of LSPs at domestic and foreign level. For example, Ding, Kuo, and Tai [13] use the fuzzy analytic hierarchy process (AHP) method to empirically study the key competency and capabilities affecting the selection of middle managers for global shipping logistics service providers (GSLSPs). Jain and Khan [14] formulated the reverse logistics service provider selection as a multi-criteria decision-making problem and developed a methodology to select the best two reverse logistics service providers for an injection moulding parts manufacturer company using analytical hierarchy process (AHP). Third-party logistics service providers (3PLSPs) evaluation and selection for a long-term as well as a strategic partnership constituted a very crucial and critical task, and they were continually associated with uncertain challenges. In order to measure and compare the relative efficiency of the existing 3PLSPs based on the technical and sustainable criteria, a data envelopment analysis (DEA) was used to find the best among the 3PLSPs portfolios, for the purpose of selection [15]. Celik, Erdogan, and Gumus [16] determined the criteria of green logistics service providers, and the criteria weights were determined by fuzzy AHP, based on expert opinions. Then, a new method was proposed, which was the combination of fuzzy TOPSIS and GRA, and used to evaluate green 3PLs based on different separation measures, Chen, Yu, and Yang [17] established an evaluation index system for the reverse logistics service provider selection and proposed a new multiattribute decision-making method, GI-TOPSIS, based on combinational weight determination. In terms of weight determination, they combined ANP with entropy method to consider the dependency of evaluation indexes and the information of evaluation data; then, they introduced the degree of grey incidence into TOPSIS and used relative similarity degree to reflect the distance differences and shape changes. Seongtae, Ramkumar, and Subramanian [18] focused on an assessment framework that

combines two MCDM techniques: decision-making trial and evaluation laboratory (DEMATEL) based analytic network process (ANP) (hereafter “DANP”) and complex proportional assessment of alternatives to grey relations (COPRAS-G) technique. Abdel-Baset et al.[19] provided a multicriteria group decision-making (MCGDM) proposed technique of the ANP (analytical network process) method and the VIKOR (ViseKriterijumska Optimizacija I Kompromisno Resenje) method under neutrosophic environment for dealing with incomplete information and high order imprecision.

From the perspective of research content, domestic and foreign scholars have gradually deepened their research on cruise ship supply, ranging from planning process to supporting facilities on board. In addition, the research on cruise ship supply is limited to the form of summary, and a good relationship is essential in cruise ship supply chain. The research on the evaluation of LSPs mainly focused on the selection and evaluation of third-party logistics enterprises. However, China cruise tourism is still in its infancy, and the development of the cruise industry is not yet perfect. In parallel to the increasing trend in LSPs evaluation research literature towards analyzing method, model, and related problems, the evaluation of cruise ship supply LSPs emerges as one of the appealing research topics in this area, and there are few related empirical studies. For example, from the six aspects of supply quality, price, service, technology, and competition, the supplier evaluation index system of cruise companies was established under the supply chain management environment [20]. The deployment problem of the liner ship fleet with uncertain demand was different from other logistics problems with uncertain demand [21, 22].

Generally, such a problem is an issue of great concern to decision makers. Most of relevant research studies on LSPs evaluation ignored integration, personalization, and network demand features of the logistics service chain. Therefore, the innovation of this paper is based on previous studies; an evaluation index system of cruise ship LSPs is constructed from the perspective of the features, connotation, and types of cruise ship supply LSPs.

From the viewpoint of research methods, overall, the research methods of LSPs evaluation include qualitative method, quantitative method, and both of them. Moreover, the common methods are AHP, DEA, TOPSIS, ANN, ANP, and the combination of these methods [23–30]. Generally speaking, these methods have different principles, and each has its own advantages and disadvantages in solving practical problems, as shown in Table 1.

Through the above summary, we find that each method has advantages and shortcomings, and there are three characteristics in the research of provider selection methods. First, AHP and DEA are most widely used; second, two or even three different methods are used comprehensively to solve the problem of supplier selection as objectively and accurately as possible; third, new intelligent methods become a research trend. The traditional AHP method cannot fully meet the needs of this study, because the relationship between the evaluation indexes of cruise ship LSPs is not nonlinear and independent. The ANP method is the

development and extension of the AHP. Therefore, we choose to apply ANP method due to the characteristics of mutual feedback and connection among the indexes, and Super Decisions software is used for its shortcoming. At the same time, the evaluation of cruise ship supply LSPs is a typical multiattribute decision group evaluation problem. After comparing other LSPs evaluation methods, the ANP method can take into account the characteristics of the relevance between all indexes and realize weight to each index. We propose an incremental algorithm that can effectively avoid the influence of subjective factors in ANP method, increase the dynamic nature of evaluation, combine RBF neural network training and validation, and extract implicit knowledge and laws. The combination of ANP and RBF method will make the weight more objective and scientific, and this method is feasible and practical.

3. Evaluation Index System

3.1. Definition and Types. Cruise ship supply, namely, material supply for cruise liner, in a broad sense, refers to the supply of food, beverage, liquor, fuel, hotel supplies and equipment, and navigation and communication equipment offered to customers in cruise liner operations. In a narrow sense, cruise ship supply refers to the supply of food and daily necessities used and consumed by cruise crew and passengers during the voyage. Specifically, cruise ships provide food for passengers and crew during the voyage, such as fresh fruits and vegetables, meat products, and fresh water; the cruise ship also involves daily necessities like toiletries and bed sheets [31]. In order to cater the diversified consumption demands of cruise passengers from all over the world, cruise companies purchase different flavors of food from different countries to achieve a five-star experience. There is also the need for international cruise ships to meet the high standards of five-star hotels and provide first-class services. At present, there are more than 60 cruise ships with more than 100000 gross tonnage, which can carry 2500 passengers and crew. And there are many giant cruise ships that can carry 8800 passengers and crew. For example, ocean symphony is the largest cruise ship in the world with 18 decks, 22 restaurants, 24 swimming pools, 2759 guest rooms, and other entertainment facilities; it can be called a maritime city. In the next ten years, there will be 40 giant cruise ships on cruise market. The large scale of ship size and the large quantity of passengers would bring huge demand for cruise ship supplies.

Compared with the supply of ordinary cargo ships, the purchase of cruise ship supplies has the following characteristics:

- (1) *Global Procurement.* Compared with ordinary cargo ships, cruise ships carry a large number of passengers. For example, there are more than 8,000 people in the quantum of the sea, which needs a large number of living materials and other spare parts. In order to ensure quality and reduce procurement cost, cruise ship supplies are purchased all over the world.
- (2) *High Supply Frequency.* Cruise ships usually have a period of several days or weeks to realize the cycle of

TABLE 1: Summary of LSPs evaluation methods.

Method	Advantages	Shortcomings
AHP	It can simplify complex problems; there are few requirements for quantitative data information.	It is too subjective, and too many indexes will lead to large data statistics and uncertain weight. With the increase of indexes, the accurate calculation of eigenvalues and eigenvectors will be more complex.
DEA	It selects high quality suppliers by measuring the relative efficiency of evaluation objects, and it is simple to apply.	It is usually a subjective value determined in advance and specific to a certain degree of randomness.
TOPSIS	It requires less sample data and is easy to understand and simple to operate.	The distance as a scale can only reflect the position relationship between data curves and cannot reflect the dynamic changes of data series.
BP neural network	It can solve any complex nonlinear problems and has the ability to self-learn and self-adapt.	It has low learning efficiency and slow convergence speed, is easy to fall into local minimum state, and so on.
Fuzzy comprehensive evaluation	It is simple and easy to understand, and the evaluation effect is ideal for complex problems with multiple indexes and multiple levels.	The calculation of the weight of each index is highly subjective, and it is difficult to determine the membership function.
Grey relational analysis	The grey information and white information are treated differently, which can ensure the integrity and accuracy of information; they do not need many samples and normalization processing.	The theoretical basis is relatively narrow, the standardization lacks comprehensiveness, and it is unable to deal with the information duplication caused by relevant indicators.
ANP	An interactive risk evaluation system is incorporated into the supplier selection process. The triangular fuzzy number is used to construct the linguistic evaluation set to avoid the negative impact of subjective judgment.	It is a very complex operation process to solve the hypermatrix problem.

departure and return. Compared with freighters, materials are consumed quickly and need to be replenished in a short time. Besides, cruises are often berthing, and frequent replenishment and formalities are required in cruise ports.

- (3) The cruise lines purchase directly from the suppliers, while the cargo ships purchase from the agent companies.
- (4) The standard of cruise ship supplies is uniform, and supplies are high-end, differentiated, and centrally sourced. The supply system should be stable, and food should be secure.

Cruise ship supply logistics refers to a series of logistics activities, such as storage, transportation, loading and unloading, processing, packaging, information processing, and distribution in the process of material flow from manufacturer/ship supplier to cruise ship. Due to the mobility and tourism properties of cruise ships, cruise ship supply logistics is more complex than general logistics. In the general sense, LSPs are not traditional logistics services providers for cruise ship supply, but suppliers that provide operational logistics services for the core cruise enterprises in the cruise ship supply chain, that is, functional LSPs, including LSPs of transportation, storage, distribution, and customs clearance, which act as upstream service providers of the cruise enterprise in the ship supply chain and provide the logistics service with its core advantages. In addition, they have established a long-term strategic cooperative relationship with the port enterprises, which is also the most fundamental feature different from traditional LSPs.

The service supply chain of cruise ship supply is a kind of capability cooperation, which takes cruise ship as the core

enterprise and integrates other types of cruise ship LSPs. According to the types of cruise ship supply LSPs, the functional LSPs of cruise ship supply could be divided into single type and composite type: the single type is LSPs that only provide single logistics service capability, such as warehouse operators or distributors; the composite type is LSPs that provide multiple logistics service capabilities simultaneously. For example, the third-party integrated logistics enterprise could provide a variety of service capabilities such as transportation, storage, and distribution. The composite type of LSPs is studied on cruise ship supply chain in this paper.

3.2. Evaluation Index System Construction. Most of the existing evaluation index systems of LSPs only studied capability evaluation of LSPs in the traditional supply-demand management mode, such as quality, delivery time, and cost. However, they cannot fully reflect the requirements of LSPs in supply chain management mode. Hence, they cannot adapt to the global characteristics of the cruise ship supply chain, and the strategic partnership of information sharing and risk sharing cannot be realized. Meanwhile, a long-term, stable, and it is necessary to establish sustainable strategic partnership between the cruise ship supply LSPs and the port enterprises, so the evaluation of the collaborative ability should not be ignored for LSPs of cruise ship supply, which would affect the stable and benign operation of the whole logistics service supply chain. Besides, there is a lack of evaluation at the information level of LSPs in many index systems. In the network economy environment, the response time and the personalization degree of supply chain are closely related to information. In the mature evaluation of

LSPs, information level is an important prerequisite to ensure the success and stability of cooperation. Numerous available studies provide information on the evaluation criteria to be chosen for the cruise ship supply LSPs. Hence, while cruise companies select LSPs for cruise ship supply, they should evaluate them from the perspective of the whole logistics service supply chain, which should not only investigate the service price and business level of LSPs, but also pay attention to their synergies and competitiveness with upstream and downstream members.

When establishing the evaluation index system for cruise ship supply LSPs, we should pay attention to the following principles.

- (1) *Simplicity*. The evaluation index should be simplified, focused, and easy to operate
- (2) *Independence*. There is no inclusion relationship between all levels of evaluation indexes in the index system
- (3) *Scientificity*. The actual situation should be accurately reflected so that cruise companies can make an objective and comprehensive evaluation of shipping LSPs
- (4) *Generality*. The established index system should reflect the commonness of cruise ship service providers

In this paper, we establish an index system from the characteristics of cruise ship logistics service. It comprehensively reflects what cruise enterprises should consider in the evaluation of LSPs.

3.2.1. Service Price. In the traditional supply chain, price is often an important index for enterprises to select and evaluate suppliers. Besides, price is also an important index that cannot be ignored in the field of service supply chain [32, 33]. An effective price control can enhance the competitiveness of the whole service supply chain for cruise companies. The service price of LSPs mainly includes three indexes: The first is the transportation cost [34], because cruise ship supplies are mainly global sourcing. The second is cost elasticity, including storage costs, handling costs, sorting costs, handling expenses, sorting costs, and packing costs; it can reflect not only the coordination of the logistics links, but also the operation of the supply chain. The third is logistics supporting facilities; it directly affects the quality of logistics services.

3.2.2. Business Level. A strong business level is the guarantee for high quality services to LSPs. It mainly includes two aspects: The first is on-time delivery; cruise ship supplies are mostly consumables for people on board, the supply volume is huge in a short time, and most of them belong to refrigerated and fresh-keeping food. Therefore, they require high timeliness, and the cruise liner has a short replenishment time at home port and midway port, so LSPs should deliver the supplies to the cruise ships in the short time window; otherwise, the loss of shortage cost is immeasurable

[28]. The second is logistics network; due to mobility and irreparability of cruise ship supply logistics, it needs professional logistics parks, logistics nodes, transport channels, and distribution facilities [35]. Besides, logistics network plays an important role in supply chain, and the optimization of logistics network would affect the logistics service level and cost of providers [36–41].

3.2.3. Collaborative Capacity. Collaborative capacity is the collaboration ability of LSPs in the process of cooperation with port enterprises, government enterprises, and other LSPs, which is mainly reflected in the communication and coordination ability and cooperation efficiency of LSPs. [6, 7]. Hence, it can be embodied from the three aspects of supply time flexibility, risk response ability, and collaborative development capability [42–44].

3.2.4. Information Level. Cruise ship supply chains are global and are composed of a variety of products and streams, which render the process of tracking burdensome. Visibility of the production transit is essential to keep track of replenishment in this “just-in-time” environment. Hence, information level can highlight the advantages of LSPs and ensure the irreplaceable role in the cruise ship logistics service. Information investment and system integration capability reflect the informatization level of LSPs to some extent; for example, the information service system, real-time monitoring, cargo access, and passenger flow separation can ensure the smooth operation of the goods and tourists required for the cruise liner [5, 7]. Information level can guarantee the accuracy and timeliness of information communication between ship supply LSPs and port enterprises, to improve the cooperation efficiency and maintain a long-term and stable cooperative relationship.

Based on the above analysis, we can construct the evaluation index system of cruise ship supply LSPs, as shown in Table 2.

4. Methods

There are many factors affecting the evaluation of cruise ship service providers. For ease of analysis processing, we choose a limited number of representative indexes to evaluate and analyze according to the unique characteristics of cruise ship logistics service industry in this paper. In addition, because of the certain mutual relationship and influence among the indexes in the logistics system, we apply the analytic network process (ANP) to ascertain the weights of indexes. Meanwhile, in order to avoid the influence of subjective factors in the decision-making process by using ANP model, we use integrated ANP and RBF neural network to evaluate cruise ship supply LSPs.

4.1. The Analytic Network Process. Analytic Network Process (ANP) is a decision-making method proposed by Professor Thomas L Saaty, Professor of University of Pittsburgh, Pennsylvania, in 1996. It is suitable for nonindependent

TABLE 2: Dimensions and subcriteria for cruise ship LSPs.

Dimensions	Criteria	Reference
Business level (B1)	On-time delivery (C1)	Véronneau and Roy (2009) [5]; Vukonic, Bielic, and Russo (2016) [9] Budiartha and Adnyana (2016) [22]
	Logistics network (C2)	
	Information investment (C3)	
Information level (B2)	System integration capability (C4)	Véronneau and Roy (2009) [5], [7]
	Supply time flexibility (C5)	
Collaborative capacity (B3)	Risk response ability (C6)	Véronneau, Roy, and Beauieu (2015) [6]; Véronneau and Roy (2009) [7]; Erkoc, Iakovou, and Spaulding (2005) [42]
	Collaborative development capability (C7)	
	Cost elasticity (C8)	
	Transportation cost (C9)	
Service price (B4)	Logistics supporting facilities (C10)	Regina Galo et al. (2018) [25]; Mohamed et al. (2020) [34]

“hierarchy structure” [24]. Based on the traditional linear analytic hierarchy process (AHP), which considers the interrelation and internal dependence of each factor, the network form is used for elaboration and development, and then the objectives of organization and its optimal weight value are confirmed systematically for reaching decisions. The specific steps are as follows:

Step 1: establishing the hierarchical structure of decision issues. The decision-making system can be divided into two parts by ANP: The first part is the control layer, which confirms the goal according to the nature of the problem. Then, through literature analysis, this study selects the decision-making dimensions and subcriteria and establishes the hierarchical structure of decision-making. All the decision-making criteria are considered to be independent of each other and only controlled by the objective factors. The weight of each criterion can be ascertained by ANP. The second part is the network layer, which is composed of all the elements dominated by the control layer. The inner part is the network structure of mutual influence. The elements depend on and dominate each other, and the inner part of the elements and the layers are independent of each other. Each criterion dominates a pair of interdependent and feedback network structures in the hierarchical structure. In this study, decision-making experimental analysis method is used to establish the external dependence of the structural layer and the internal and external dependence of the criteria. Finally, ANP network hierarchy diagram is established according to all the influence relationships (network layer) and hierarchy.

Step 2: designing and filling the ANP questionnaire. After the establishment of ANP network hierarchy in step 1, an ANP questionnaire is made according to the internal and external dependence between dimensions and subcriteria. The content of the questionnaire can be divided into three parts: the first part is the comparison of the relative importance of evaluation criteria under the dimensions or levels for the structural layer; the second part is the comparison of the dependence ratio

between the dimensions of the structural layer; and the third part is the comparison of the dependence between the evaluation criteria. In any part, the format is a paired comparison of two elements. In the part of evaluation scale, Saaty (1980) divided the evaluation scale into four levels, with a nominal 1-9 scale representing nine categories from “equal importance” to “absolute importance.”

Step 3: constructing the pairwise comparison matrix. The pairwise comparison matrix is the pairwise comparison between the structural layer and the criterion layer, respectively. Under certain factors of each network hierarchy, the relative importance of pairwise comparison is measured by using the name scale as the ratio. The ratio is the constituent element of the constructed comparison matrix, as shown in the following formula:

$$X = [x_{ij}]_{n \times n} = \begin{bmatrix} 1 & x_{12} & \cdots & x_{1n} \\ x_{21} & 1 & \cdots & x_{2n} \\ \vdots & \vdots & \ddots & \vdots \\ x_{n1} & x_{n2} & \cdots & 1 \end{bmatrix}_{n \times n}, \quad (1)$$

where $x_{ij} = 1/x_{ji}$ {when $i \neq j$, $x_{ij} = [1/9, 1/8, 1/7, 1/6, 1/5, 1/4, 1/3, 1/2, 1, 2, 3, 4, 5, 6, 7, 8, 9]$, when $i = j$, $x_{ij} = 1$, $i = 1, 2, \dots, n$, $j = 1, 2, \dots, n$.

Step 4: eigenvalues and eigenvectors. Normalization of the geometric mean of the rows (NGM) method is adopted, which is a method of calculating eigenvectors proposed by Saaty (1980). The geometric mean of matrix column vectors is standardized, geometric average is shown in (2), and eigenvalue and eigenvalue vector can be defined as

$$g_{cn} = \sqrt[n]{1 \times a_{12} \times \cdots \times a_{1n}}, \quad (2)$$

$$w_{xn} = \frac{g_{cn}}{G}, \quad G = \sum_{y=1}^n g_{cy}, \quad 1 = \sum_{y=1}^n w_{xy}, \quad (3)$$

$$w_i = \begin{bmatrix} w_{X1} \\ w_{X2} \\ \vdots \\ w_{Xn} \end{bmatrix}. \quad (4)$$

Step 5: consistency test. The consistency of the results of the comparison matrix is tested, and the consistency index and the consistency ratio are compared in pairs to determine whether there is unreasonable judgment and whether the degree of decision-making is consistent.

The consistency ratio (CR) is derived from the consistency index (CI) divided by random variables RI , as shown in

$$CI = \frac{\lambda_{\max} - n}{n - 1}, \quad (5)$$

$$CR = \frac{CI}{RI}. \quad (6)$$

The larger the value of CI is, the greater the deviation of the judgment matrix from the complete consistency is; the smaller the value of CI is (close to 0), the better the consistency of the judgment matrix is. When the judgment matrix is completely consistent, $CI = 0$; when the judgment matrix is satisfactorily consistent, the average random consistency index value, RI , of the judgment matrix should be introduced.

If the order is greater than 2, the ratio of the consistency index, CI , of the judgment matrix to the average random consistency index, RI , is called the random consistency ratio, CR ; if $CR \leq 0.10$, it can be considered that the judgment matrix is satisfactorily consistent; otherwise, it needs to be adjusted.

Step 6: constructing the super matrix.

Step 7: building the limit super matrix to ascertain the index weight value.

4.2. RBF Neural Network. Radial basis function (RBF) neural networks, being inherited from the perceptual model on visual hyperacuity, are well-known for the simple topological structure and universal approximation ability. Since the approximation ability has been proved, they have drawn much attention to various areas, such as classification, nonlinear system modeling, and adaptive control [45–47]. Nevertheless, RBF neural networks still face challenges and open problems on how to model nonlinear systems accurately and fast [48, 49]. The primary questions for designing RBF neural networks involve two aspects [50]: (1) the construction of a network structure (the hidden layer size and initial parameters); (2) the optimization of all the parameters (centers, radii, and weights). Compared with BP network, the main difference lies in the use of different functions. In BP network, the hidden layer is sigmoid function, which is a neural network with global approximation. The function is Gaussian basis function in RBF

network, which is a neural network with local approximation. Therefore, RBF network can greatly accelerate the learning speed and avoid the local minimum problem, which is suitable for the requirements of timely control and can effectively improve the accuracy, robustness, and self-adaptability of the system.

RBF neural network has three layers: input layer, hidden layer, and output layer. A schematic for an RBF neural network, which is a type of receptive-field neural network, is shown in Figure 1. There are N neurons in the input layer, J neurons in the hidden layer, and M neurons in the output layer. The input layer receives information $x = (x_1, x_2, \dots, x_N)^T$ from the environment.

Locally sensitive hidden neurons are usually described by the Gaussian function:

$$\theta_j(X) = e^{-\frac{\|X - c_j\|^2}{\sigma_j^2}}, \quad (7)$$

where c_j is the center vector of the j th neuron and σ^2 denotes its radius.

The output neurons combine information from the hidden layer and calculate the following:

$$y_m(X) = \sum_{j=1}^J w_{jm} \theta_j(X), \quad (8)$$

where w_{jm} is the weight of the connection from hidden neuron j to output neuron m , and $y_m(X)$ is the output of the m th neuron in the output layer.

4.3. ANP-RBF. First of all, according to the experience and the actual situation of the candidate LSPs, enterprise experts need to score each index of the candidate LSPs, and the sum of each index score and its weight product is the total score. Second, it is easy to train RBF neural network after dimensional conversion of the score data. The building process of ANP-RBF neural network model is shown in Figure 2.

5. Experimental Testing and Analyses

5.1. Experimental Data. We select the data of a cruise company for empirical test and analysis, a world-famous large cruise company whose headquarter is located in the United States. Since June 2012, in order to open up the Chinese cruise market, it has set up cruise China branch with Shanghai as its home port. In order to maintain stable relations in the cruise supply chain, it needs to select suitable long-term strategic partners from multiple LSPs for cruise ship supply. Based on the bidding sample data of 12 cruise ship supply LSPs, the score of each index is shown in Table 3, and the full mark is 10.

5.2. Simulation Results and Analysis

5.2.1. Weight Fixing by ANP. Firstly, we classify the evaluation indexes of LSPs and evaluate the importance of each index from the research results and experience of relevant

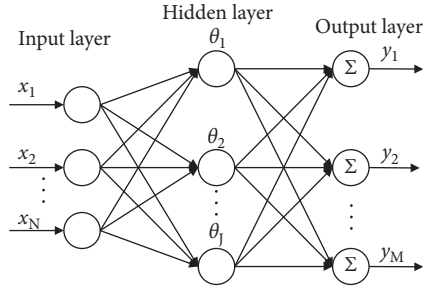


FIGURE 1: The RBF neural network structure diagram.

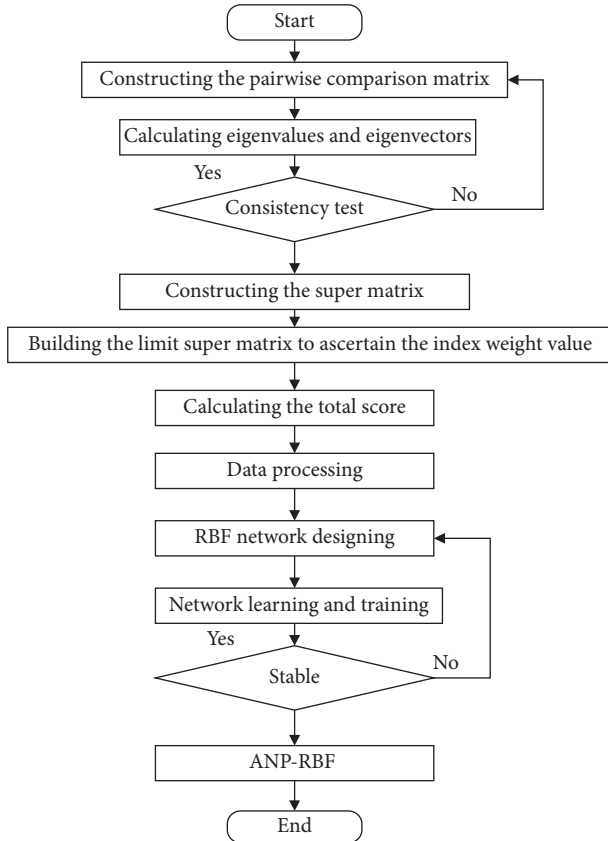


FIGURE 2: Building process of the ANP-RBF neural network model.

experts. Secondly, the internal experts establish an evaluation matrix based on the comprehensive evaluation indexes of the actual situation for the cruise enterprise. Thirdly, we determine the network structure diagram of the evaluation index system and construct the pairwise comparison judgment matrix. The judgment matrix of major criteria with respect to business level (B1) and information level (B2) is shown in Tables 4 and 5. We establish the network structure diagram of the evaluation index system by using Super Decisions 2.10 and construct element groups, elements, and related relations shown in Figure 3.

As can be seen from Table 4, the business level is higher than the collaborative ability, and the competitiveness is higher than the collaborative ability. Then, we establish the other judgment matrix of major criteria one by one according to this step and establish the judgment matrix for the target layer based on the subcriteria, as shown in Table 6.

TABLE 3: The score of each index for candidate LSPs.

Providers	C1	C2	C3	C4	C5	C6	C7	C8	C9	C10	C11
1	7	8	6	6	7	6	8	9	6	4	7
2	8	9	7	8	6	8	7	7	6	5	6
3	8	8	8	5	7	7	6	5	5	3	6
4	9	8	7	8	8	7	7	6	6	3	7
5	8	7	6	7	8	7	6	8	6	4	7
6	8	7	8	5	6	5	6	6	7	5	6
7	6	7	7	6	5	6	7	6	5	4	7
8	5	4	5	4	5	6	6	6	3	4	3
9	7	6	7	6	6	5	7	5	7	3	7
10	8	3	4	6	3	3	7	3	3	4	5
11	8	7	8	7	6	7	6	6	5	3	4

TABLE 4: The judgment matrix of major criteria with respect to business level (B1).

B1	B1	B2	B4
B1	1	5	3
B2	1/5	1	1/3
B4	1/3	3	1

TABLE 5: The judgment matrix of major criteria with respect to information level (B2).

B2	B1	B2	B3	B4
B1	1	5	1/3	1/4
B2	1/5	1	1/6	1/7
B3	3	6	1	1/5
B4	4	7	2	1

In the same way, we get the other second-grade index matrices one by one according to the above methods and use software paired comparison commands to compare the relationships between elements.

Finally, we execute the command of “Priorities” under “Computations” to bring on the global weight of each index, as shown in Table 7.

5.2.2. RBF Training and Validation. Due to the different dimensions of the sample indexes, it is necessary to carry out dimensional transformation. The service price is transformed by (9), and the business level, coordination capacity, and competitiveness are transformed by

$$y_i = \frac{\max\{x_i\} - x_i}{\max\{x_i\} - \min\{x_i\}}, \quad (9)$$

$$y_i = \frac{x_i - \min\{x_i\}}{\max\{x_i\} - \min\{x_i\}}. \quad (10)$$

After dimensional conversion of the data of the LSPs in Table 3, we get the evaluation results of each provider according to the weight results of each index above, as shown in Table 8. Hence, we can see that the logistics service provider 9 is the best one for the cruise company.

Using MATLAB software, we take the score of 10 element indexes as the input layer of RBF, the score of LSPs as

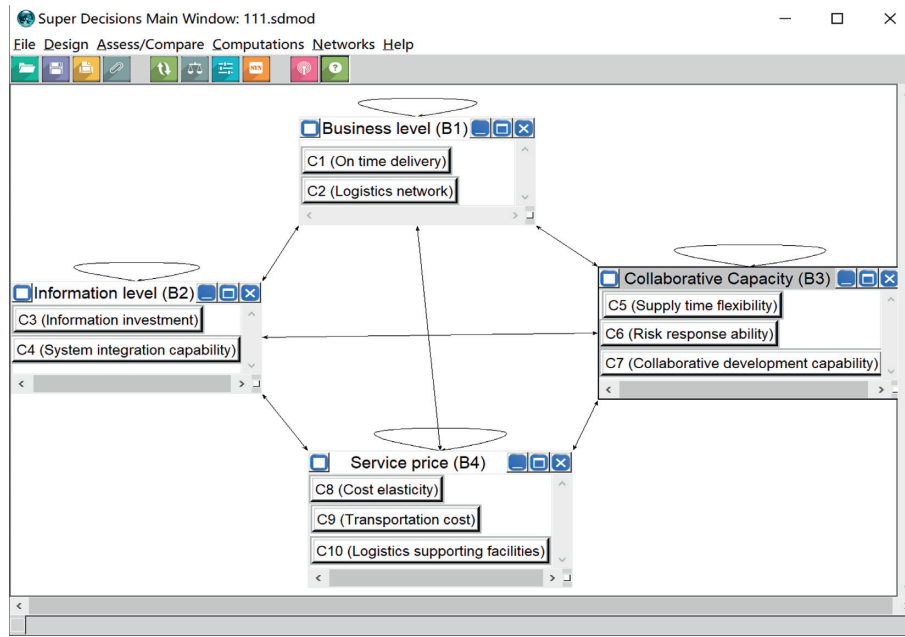


FIGURE 3: The network structure diagram of the evaluation index system for cruise ship supply LSPs.

TABLE 6: The judgment matrix under risk response ability (C3).

C2	C1	C2
C1	1	5
C2	1/5	1

TABLE 7: The weight value of each index.

Dimensions	Criteria	Weight value (ANP)
Business level (B1)	On-time delivery (C1)	0.2080
	Logistics network (C2)	0.2080
Information level (B2)	Information investment (C3)	0.0184
	System integration capability (C4)	0.0179
Collaborative capacity (B3)	Supply time flexibility (C5)	0.1018
	Risk response ability (C6)	0.0611
	Collaborative development capability (C7)	0.0516
Service price (B4)	Cost elasticity (C8)	0.0443
	Transportation cost (C9)	0.1568
	Logistics supporting facilities (C10)	0.1320

TABLE 8: The evaluation results of LSPs.

Provider	1	2	3	4	5	6	7	8	9	10	11
Score	0.526	0.600	0.739	0.738	0.634	0.262	0.693	0.599	0.799	0.644	0.712

the output layer, and the data after dimensional processing as the training sample. Then, we get the network fitting comprehensive evaluation results of LSPs, as shown in Figure 4.

As can be seen from Figure 4, after dimensional processing of different types of data, we use RBF neural network model to input, and the mean square error (MSE) is 0.0043. The result value is close to the fitted value, which shows that the effect is

very good. The RBF neural network evaluation is used to verify and fit the training data and extract the hidden knowledge and rules, which can reduce the influence of subjective factors in the process of supplier evaluation. Therefore, the learning speed is fast, the error is small, and the method can better solve the evaluation problem of cruise ship LSPs.

On the basis of the above, we apply the trained network to make a comprehensive evaluation of the three new LSPs,

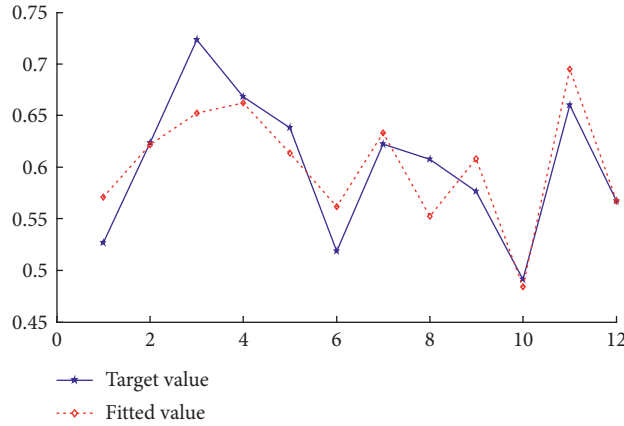


FIGURE 4: Network fitting comprehensive evaluation results.

TABLE 9: The evaluation index score of LSPs.

Provider	C1	C2	C3	C4	C5	C6	C7	C8	C9	C10
1	7	5	6	7	8	6	4	7	6	7
2	7	6	6	8	7	6	8	9	9	6
3	6	5	7	8	7	6	6	7	6	8

TABLE 10: The comprehensive score results of cruise ship supply LSPs.

Provider	1	2	3
Target value	0.5515	0.1496	0.3869
RBF fitted value	0.5495	0.1488	0.3764
Absolute error	0.0020	0.0008	0.0105

and the scores are shown in Table 9. We obtain the target value through ANP model and the comprehensive evaluation results of RBF neural network method, as shown in Table 10.

As can be seen from Table 10, the target values are dimensionless and weighted according to the weights of each index and the scores of 3 groups of LSPs. The first logistics service provider is the best one; its value is 0.5515. The RBF fitted value is very close to the target value of three LSPs, and the maximum absolute error is 0.0105. Therefore, the trained RBF neural network model has better learning effect and nonlinear mapping ability for LSPs evaluation.

The above analysis shows that the solution algorithm of ANP-RBF model is incremental algorithm, and the model has good scalability, which increases the dynamic of evaluation.

5.3. Comparison Analysis. AHP method can be also used to solve the problem of multicriteria decision-making [10, 11]. It is applied in many studies of LSPs evaluation, and we will not explain its principle and steps in detail here. We construct the judgment matrix, as shown in Table 11 and Table 12.

Then, using Super Decisions 2.10, we can get the weight value of each index by AHP method, and the comparison results are as shown in Table 13 and Figure 5.

As can be seen from Table 10 and Figure 5, ANP method considers the relationship of interdependence and feedback between the criteria and the specific indexes in the criteria. Compared with the weights using AHP method, there are two main differences: First, the weight of business level in the criteria layer is increased, replacing output service price as the most important factor in the evaluation of LSPs; second, the weight of transportation cost and logistics supporting facilities is significantly higher than that of cost elasticity in the criteria.

In contrast, the weight value using ANP method is reasonable. In the four dimensions of LSPs for cruise ship supply, business level is the basis of the others. Meanwhile, business level is also affected by the feedback and influence of service price and collaborative capacity; its weight value is higher than the other three. Due to the difference in standards and examination procedures among countries, the weight value of demand response timeliness will be lower. We can conclude that ANP method is more suitable for complex system problems such as LSPs for cruise ship supply and it is more realistic.

5.4. Managerial Insights. Cruise ship supply logistics has received considerable attention from operational managers and top management decision makers. It is closely related to economics, environmental regulation, and strategy. The case

TABLE 11: The judgment matrix of major criteria with respect to information level (B2).

B2	B1	B2	B3	B4
B1	1	5	1/3	1/4
B2	1/5	1	1/6	1/7
B3	3	6	1	1/5
B4	4	7	2	1

TABLE 12: The judgment matrix of subcriteria with respect to business level (B1).

B1	C1	C2
C1	1	5
C2	1/5	1

TABLE 13: The weight value comparison of AHP and ANP.

Dimensions	Criteria	Weight value (AHP)	Weight value (ANP)
Business level (B1)	On-time delivery (C1)	0.121	0.2080
	Logistics network (C2)	0.024	0.2080
Information level (B2)	Information investment (C3)	0.012	0.0184
	System integration capability (C4)	0.036	0.0179
	Supply time flexibility (C5)	0.165	0.1018
Collaborative capacity (B3)	Risk response ability (C6)	0.104	0.0611
	Collaborative development capability (C7)	0.044	0.0516
	Cost elasticity (C8)	0.333	0.0443
Service price (B4)	Transportation cost (C9)	0.050	0.1568
	Logistics supporting facilities (C10)	0.111	0.1320

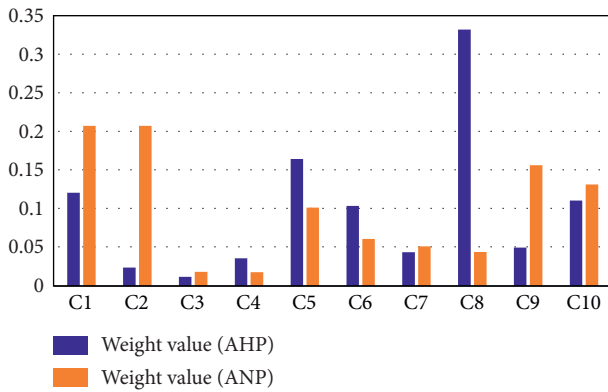


FIGURE 5: Network fitting comprehensive evaluation results.

studied in this paper has significant managerial implications. In this study, the ANP-RBF methodology adopted provides managers, responsible for selecting cruise ship supply LSPs for their organization, with insights about the various factors that need to be considered while selecting LSPs. The selected approach also aids them in prioritizing the criteria. Managers can utilize the hierarchical structure of adopted LSPs evaluation methodology suggested in this study to rank LSPs on the basis of various factors/criteria.

The sensitivity analysis performed in this study also analyzes the effect of changing the weights of the main criteria on the ranking of logistics providers for the cruise company, which will help managers in decision-making. This approach will also help managers in dividing the complex problem into simpler hierarchy.

6. Conclusions

In this paper, we put forward an evaluation model based on ANP-RBF method to study the evaluation of cruise ship LSPs. Firstly, we use ANP model to ascertain the weights of indexes. Secondly, we apply the RBF neural network to verify and fit the data. This method extracts the hidden knowledge and rules, and it can avoid the influence of subjective factors in the decision-making process. Through case study, we can see that on-time delivery and logistics network are the important criteria for evaluation of cruise ship supply LSPs. Hence, it is necessary to build a supporting collection and distribution logistics network to realize the information data exchange of cruise ship supplies procurement, transportation, and distribution in cruise ship supply service chain. As a result, it can improve the efficiency and reliability of the supply chain and effectively reduce the inventory of cruise companies. This is the real value of logistics network optimization and construction, and it is also the direction for the further development of China's cruise ship supply system; it has practical significance for the evaluation of cruise ship supply LSPs to China cruise lines. However, the factors affecting the supply logistics of cruise ships are complex, and the relevant indexes are qualitative and are not quantified. Therefore, this has a certain impact on the evaluation of LSPs. Besides, due to the influence of cruise port supporting infrastructure and related policies, local cruise ship supply companies are uneven, so it may be more complicated in practical application.

The proposed methodology has limitations though. First of all, ANP relies heavily on expert opinions, which may be

biased by the subjectivity and transitivity associated with the decision maker. Therefore, there is a need for a better aggregation methodology. For example, the same problem can be analyzed with ANP-RBF, so that the vagueness of the opinion of the decision maker can be taken care of. On top of that, a user-friendly interface needs to be developed to simplify the ANP calculations so as to use the proposed approach in real-life problems more easily, so we use Super Decisions software to solve it. The outcome of the model presented is purely dependent on the inputs provided by the experts of the cruise company. Thus, further refinement of the model can be done by carrying out additional field studies or by conducting surveys with other organizations.

Furthermore, the cruise ship is a special kind of vessel for international navigation. In the broad sense, cruise ship supplies are basically the same as ship materials, which can be divided into fuel, materials, consumables, and duty-free goods, and their procurement would be profoundly different. The current research needs to be further explored and refined, and the score of pairwise comparison matrix can be further standardized to avoid human subjective influence to the greatest extent. It can establish scoring rules for specific cruise ship supplies and relative importance of each index to guide evaluators to make objective evaluation.

Data Availability

The data used to support the findings of this study are included within the article.

Conflicts of Interest

The authors declare that they have no conflicts of interest.

References

- [1] S. Ros Chaos, A. A. Pallis, S. Saurí Marchán, D. Pino Roca, and A. Sánchez-Arcilla Conejo, *Economies of Scale in Cruise Shipping*, Maritime Economics and Logistics, Rotterdam, Netherlands, 2020.
- [2] J. Esteve-Perez and A. Garcia-Sanchez, "Cruise market: stakeholders and the role of ports and tourist hinterlands," *Maritime Economics & Logistics*, vol. 17, no. 3, pp. 371–388, 2015.
- [3] G. Michaël and D. Michaël, "An analysis of the CSR portfolio of cruise shipping lines," *Research in Transportation Business & Management*, vol. 8, Article ID 100615, 2020.
- [4] G. W. Y. Wang, A. A. Pallis, and T. E. Notteboom, "Incentives in cruise terminal concession contracts," *Research in Transportation Business & Management*, vol. 13, pp. 36–42, 2014.
- [5] S. Véronneau and J. Roy, "RFID benefits, costs, and possibilities: the economical analysis of RFID deployment in a cruise corporation global service supply chain," *International Journal of Production Economics*, vol. 122, no. 2, pp. 692–702, 2009.
- [6] S. Véronneau, J. Roy, and M. Beaulieu, "Cruise ship suppliers: a field study of the supplier relationship characteristics in a service supply chain," *Tourism Management Perspectives*, vol. 16, pp. 76–84, 2015.
- [7] S. Véronneau and J. Roy, "Global service supply chains: an empirical study of current practices and challenges of a cruise line corporation," *Tourism Management*, vol. 30, no. 1, pp. 128–139, 2009.
- [8] S. Véronneau and Y. Cimon, "Maintaining robust decision capabilities: an integrative human-systems approach," *Decision Support Systems*, vol. 43, no. 1, pp. 127–140, 2007.
- [9] D. Vukonic, T. Bielic, and A. Russo, "Organizational factors in management of "Mega Cruise Ships" from crowd management control aspect," *Scientific Journal of Maritime Research*, vol. 30, pp. 58–66, 2016.
- [10] J. Wang, J. B. Yin, R. U. Khan, S. Q. Wang, and T. Zheng, "A study of inbound logistics mode based on JIT production in cruise ship construction," *Sustainability*, vol. 13, no. 1588, p. 1588, 2021.
- [11] C.-A. Chen, "How can Taiwan create a niche in Asia's cruise tourism industry?" *Tourism Management*, vol. 55, pp. 173–183, 2016.
- [12] H. William, X. W. Xu, and K. D. Prasanta, "Multi-criteria decision making approaches for supplier evaluation and selection: a Literature Review," *European Journal of Operational Research*, vol. 202, pp. 16–24, 2010.
- [13] J.-F. Ding, J.-F. Kuo, and W.-H. Tai, "Using fuzzy AHP method to evaluate key competency and capabilities of selecting middle managers for global shipping logistics service providers," *Pomorstvo*, vol. 33, no. 1, pp. 3–10, 2019.
- [14] V. Jain and S. A. Khan, "Application of AHP in reverse logistics service provider selection: a case study," *International Journal of Business Innovation and Research*, vol. 12, no. 1, pp. 94–119, 2017.
- [15] N. Choudhury, R. D. Raut, B. B. Gardas, M. G. Kharat, and S. Ichake, "Evaluation and selection of third party logistics services providers using data envelopment analysis: a sustainable approach," *International Journal of Business Excellence*, vol. 14, no. 4, pp. 427–453, 2018.
- [16] E. Celik, M. Erdogan, and A. T. Gumus, "An extended fuzzy TOPSIS-GRA method based on different separation measures for green logistics service provider selection," *International Journal of Environmental Science and Technology*, vol. 13, no. 5, pp. 1377–1392, 2016.
- [17] K. Chen, X. Yu, and L. Yang, "GI-TOPSIS based on combinational weight determination and its application to selection of reverse logistics service providers," *Journal of Grey System*, vol. 25, no. 3, pp. 16–33, 2013.
- [18] K. Seongtae, M. Ramkumar, and N. Subramanian, "Logistics service provider selection for disaster preparation: a socio-technical systems perspective," *Annals of Operations Research*, vol. 283, no. 1-2, pp. 1259–1282, 2019.
- [19] M. Abdel-Baset, V. Chang, A. Gamal, and F. Smarandache, "An integrated neutrosophic ANP and VIKOR method for achieving sustainable supplier selection: a case study in importing field," *Computers in Industry*, vol. 106, pp. 94–110, 2019.
- [20] S. Wang, T. Wang, X. Qu, Z. Liu, and S. Jin, "Liner ship fleet deployment with uncertain demand," *Transportation Research Record: Journal of the Transportation Research Board*, vol. 2409, no. 1, pp. 49–53, 2014.
- [21] T. Wang, Q. Meng, S. Wang, and Z. Tan, "Risk management in liner ship fleet deployment: a joint chance constrained programming model," *Transportation Research Part E: Logistics and Transportation Review*, vol. 60, pp. 1–12, 2013.
- [22] R. M. Budiarta and I. P. A. Adnyana, "The development of marine transportation system in supporting sustainable tourism—case study: nusa Penida Island, Bali Indonesia,"

- Journal of Sustainable Development*, vol. 9, no. 4, pp. 89–95, 2016.
- [23] H. Li, Z. K. He, Q. Li, and Q. B. Sun, “Applications of the improved TOPSIS decision-making method in the supplier selection,” *Mathematics in Practice and Theory*, vol. 46, no. 16, pp. 93–101, 2016.
- [24] H. Danai, S. Hashemnia, R. Ahmadi, and S. H. Bazazzadeh, “Application of fuzzy ANP method to select the best supplier in the supply chain,” *International Journal of Operational Research*, vol. 35, no. 1, pp. 1–19, 2019.
- [25] Ö. Uygun, H. Kaçamak, and Ü. A. Kahraman, “An integrated DEMATEL and Fuzzy ANP techniques for evaluation and selection of outsourcing provider for a telecommunication company,” *Computers & Industrial Engineering*, vol. 86, pp. 137–146, 2015.
- [26] B. Guo, J. P. Liang, and Y. P. Liu, “Supplier evaluation and selection of the research based on ANP-TOPSIS in green supply chain,” *Science and Technology Management Research*, vol. 11, pp. 229–234, 2015.
- [27] A. Dargi, A. Anjomshoae, M. R. Galankashi, A. Memari, and M. B. M. Tap, “Supplier selection: a FUZZY-ANP approach,” *Procedia Computer Science*, vol. 31, pp. 691–700, 2014.
- [28] N. R. Galo, P. C. C. Ribeiro, R. C. Mergulhão, and J. G. V. Vieira, “Selección de proveedor de servicios logísticos: alineación entre criterios e indicadores,” *Innovar*, vol. 28, no. 69, pp. 55–70, 2018.
- [29] J. Fan, X. Liu, M. Wu, and Z. Wang, “Green supplier selection with undesirable outputs DEA under Pythagorean fuzzy environment,” *Journal of Intelligent & Fuzzy Systems*, vol. 37, no. 2, pp. 2443–2452, 2019.
- [30] B. Patricija, T. S. Danijela, and Z. Eva, “A distance-based AHP-DEA super-efficiency approach for selecting an electric bike sharing system provider: one step closer to sustainability and a win-win effect for all target groups,” *Sustainability*, vol. 13, no. 549, p. 549, 2021.
- [31] L. Huang and J. Yang, “An optimization approach to a two-stage replenishment strategy in cruise liner operations under dynamic demand,” *Journal of the Operational Research Society*, pp. 1–12, 2020.
- [32] S. Ghosh, L. H. Lee, and S. H. Ng, “Bunkering decisions for a shipping liner in an uncertain environment with service contract,” *European Journal of Operational Research*, vol. 244, no. 3, pp. 792–802, 2015.
- [33] H. P. Paryhiban, Z. Abdul, and P. G. Chintamani, “A multi criteria decision making approach for supplier selection,” *Procedia Engineering*, vol. 38, pp. 2312–2328, 2012.
- [34] K. M. Mohamed, F. Kjetil, M. Frank, and L. Elizabeth, “Analyzing different designs of liner shipping feeder networks: a case study,” *Transportation Research Part E: Logistics and Transportation Review*, vol. 134, 2020.
- [35] L. Huang and J. Yang, “Location-distribution of cruise ship supply logistics distribution centre considering time window,” *Systems Science & Control Engineering*, vol. 7, no. 1, pp. 338–345, 2019.
- [36] Y. Wang, S. G. Peng, X. S. Zhou, M. Mahmoudi, and L. Zhen, “Green logistics location-routing problem with eco-packages,” *Transportation Research Part E: Logistics and Transportation Review*, vol. 143, pp. 102–118, 2020.
- [37] Y. Wang, Y. Y. Yuan, X. Y. Guan et al., “Collaborative two-echelon multicenter vehicle routing optimization based on state-space-time network representation,” *Journal of Cleaner Production*, vol. 258, pp. 0958–6526, 2020.
- [38] Y. Wang, X. Ma, Z. Li, Y. Liu, M. Xu, and Y. Wang, “Profit distribution in collaborative multiple centers vehicle routing problem,” *Journal of Cleaner Production*, vol. 144, pp. 203–219, 2017.
- [39] L. Zhen, Y. Wu, S. Wang, and G. Laporte, “Green technology adoption for fleet deployment in a shipping network,” *Transportation Research Part B: Methodological*, vol. 139, pp. 388–410, 2020.
- [40] K. F. David, D. Guy, and R. Stefan, “Integrated liner shipping network design and scheduling,” *Transportation Science*, vol. 54, no. 2, pp. 512–533, 2020.
- [41] C. Marielle, H. Erik, P. David, S. David, and V. Charlotte, “Liner shipping network design,” *European Journal of Operational Research*, vol. 286, no. 1, pp. 1–20, 2020.
- [42] M. Erkoç, E. T. Iakovou, and A. E. Spaulding, “Multi-stage onboard inventory management policies for food and beverage items in cruise liner operations,” *Journal of Food Engineering*, vol. 70, no. 3, pp. 269–279, 2005.
- [43] M. Bennett, “Competing with the sea,” *Performance Research*, vol. 21, no. 2, pp. 50–57, 2016.
- [44] Y. M. Bandara and H.-O. Nguyen, “Influential factors in port infrastructure tariff formulation, implementation and revision,” *Transportation Research Part A: Policy and Practice*, vol. 85, pp. 220–232, 2016.
- [45] J. Qiao, X. Meng, and W. Li, “An incremental neuronal-activity-based RBF neural network for nonlinear system modeling,” *Neurocomputing*, vol. 302, pp. 1–11, 2018.
- [46] A. Bielecki and M. Wójcik, “Hybrid system of ART and RBF neural networks for online clustering,” *Applied Soft Computing*, vol. 58, pp. 1–10, 2017.
- [47] X. Li and Y. Sun, “Application of RBF neural network optimal segmentation algorithm in credit rating,” *Neural Computing and Applications*, 2020.
- [48] F. Cheshmberah, H. Fathizad, G. A. Parad, and S. Shojaeifar, “Comparison of RBF and MLP neural network performance and regression analysis to estimate carbon sequestration,” *International Journal of Environmental Science and Technology*, vol. 17, no. 9, pp. 3891–3900, 2020.
- [49] Q. Liu, P. Sun, X. Fu et al., “Comparative analysis of BP neural network and RBF neural network in seismic performance evaluation of pier columns,” *Mechanical Systems and Signal Processing*, vol. 141, 2020.
- [50] H. Wei, W. X. Xie, and J. H. Pei, “An incremental learning algorithm for the hybrid RBF-BP network classifier,” *EURASIP Journal on Advances in Signal Processing*, vol. 2016, no. 1, pp. 1–15, 2016.

Research Article

Optimization of Rider Scheduling for a Food Delivery Service in O2O Business

Guiqin Xue,¹ Zheng Wang ,¹ and Guan Wang^{1,2}

¹School of Maritime Economics and Management, Dalian Maritime University, Dalian, China

²Technical University Bergakademie Freiberg, Akademiestraße, Freiberg 6,09599, Saxony, Germany

Correspondence should be addressed to Zheng Wang; drwz@dlut.edu.cn

Received 25 February 2021; Revised 6 April 2021; Accepted 1 May 2021; Published 25 May 2021

Academic Editor: David Rey

Copyright © 2021 Guiqin Xue et al. This is an open access article distributed under the Creative Commons Attribution License, which permits unrestricted use, distribution, and reproduction in any medium, provided the original work is properly cited.

Services such as Meituan and Uber Eats have revolutionized the way the customer can find and order from restaurants. Numerous independent restaurants are competing for orders placed by customers via online food ordering platforms. Ordering takeout food on smartphone apps has become more and more prevalent in recent years. There are some operational challenges that takeout food service providers have to deal with, e.g., customer demand fluctuates over time and region. In this sense, the service providers sometimes ignore the fact that some riders may be idle in several periods in regions, while, in contrast, there may be a shortage of riders in other situations. In order to address this problem, we introduce a two-stage model to optimize scheduling of riders for instant food deliveries. A service provider platform expectantly schedules the least quantity of riders to deliver within expected arrival time to satisfy customer demand in different regions and time periods. We introduce a two-stage model that adopts the method of mixed-integer programming (MIP), characterize relevant aspects of the scenario, and propose an optimization algorithm for scheduling riders. We also divide the delivery service region and time into smaller parts in terms of granularity. The large neighborhood search algorithm is validated through numerical experiments and is shown to meet the design objectives. Furthermore, this study reveals that the optimization of rider resource is beneficial to reduce overall cost of the delivery. Takeout food service platforms decide scheduling shifts (start time and duration) of the riders to achieve a service level target at minimum cost. Additional sensitivity analyses, such as the tightness of the order time windows associated with the orders and riders' familiarity with delivery regions, are also discussed

1. Introduction

Ordering takeout food on smartphone apps is becoming more and more popular in China in the past several years. In a recent survey, 68% of diners order takeout food at least once a day, with 33% order at least once a week [1]. The takeout delivery business is regarded as an online-to-offline (O2O) business model applied by the food industry. In the past few years, Chinese consumers have widely accepted this model. Consumers could get rid of the hassle of going to restaurants but can get more food choices and faster services through online ordering mode. In China, online takeout food service platforms such as Meituan and Baidu provide takeout ordering services to most of the working population. Firstly, customers make orders on smartphone apps, meals

are then prepared and packaged by restaurants, and the takeout delivery platform assigns independent contracting riders to deliver the food. Compared with other foodservice providers such as McDonald's and KFC, online food ordering platforms do not hire a full-time employee to do the delivery job. Thus, a key issue faced by all takeout delivery platforms is how to formulate a timetable and route for riders to deliver food so that customers can get food as quickly as possible within the desired time [2]. Besides, taking into account the fluctuations in customer demand with regions and time periods, the scheduling of takeaway platforms will become more complicated. For example, the order arrival rate usually fluctuates more during the peak dining period (soaring during the meal times and dropping to deficient levels in other mealtimes) in the business district

than in the suburbs [3, 4]. Furthermore, to prevent or mitigate any adverse effects of the uncertainty associated with riders' delivery capacity, the service platform may also choose to have a scheduled delivery workforce that they can utilize more effectively.

Takeout service providers always try their best to fulfill customer requirements in the delivery process. Customers usually expect reliable and fast service within the expected time [5]. Therefore, in this study, we developed and evaluated a new approach to address order assignment and riders' service sequence. For the sake of simplicity, the rider starts from the central depot to the restaurant in the relevant pickup region. Generally, riders provide delivery service for customers within a radius of 3 km. Customers always place orders before each deadline, such as dividing the day into equidistant service periods, 10:00–12:00, 12:00–14:00, 15:00–17:00, and 17:00–19:00. We assume that a restaurant receives an order at 10:30 with the deadline as 11:30. In this case, the service provider observes that the service region does not have adequate rider resources, so the order is not assigned to the available rider to serve as fast as possible. The number of riders required varies in different periods in each region, and different regions have different order requests in the same period. Therefore, the delay of customer requests seems inevitable with the deadline. Furthermore, the delayed service also leads to lower service quality and more customer complaints [6]. Hence, a service platform needs to design reasonable scheduling plan to allocate riders' resources for instant food deliveries with respect to the fluctuations of customer demand over time and space. As shown in Figure 1, colors from light to dark indicate customers' ordering demand at the same ordering time. Meanwhile, it can be seen that the greater the customers demand near the central region, the smaller the demand in the edge region.

Due to the practical challenges, instant logistics is facing many difficulties, while developing rapidly. Foodservice providers face the complex problem as to control the cost of scheduling riders, while maintaining high quality of customers' service. That is, takeout service providers struggle to efficiently assign orders to riders for instant food deliveries. The issue is an inherent contradiction between the undulated distribution of order time, space locations, and available riders' stability. Several regions will have excess idle riders/riders without delivery tasks during the trough, resulting in a waste of resources. However, during peak dining periods, the order volume shows an increasing trend relative to nondining periods, and existing riders cannot satisfy the delivery demands of customers. This phenomenon is called insufficient rider resources. For example, in a day, the two peak periods of ordering takeout are usually 12:00 to 13:00 and the dinner is 17:00 to 19:00, respectively. Moreover, the number of existing riders assigned by the service platform in regions is insufficient to meet the growing customer requests. In this case, this phenomenon always causes many orders which are not delivered by the available rider resources for instant deliveries with fluctuation of customer requirements over

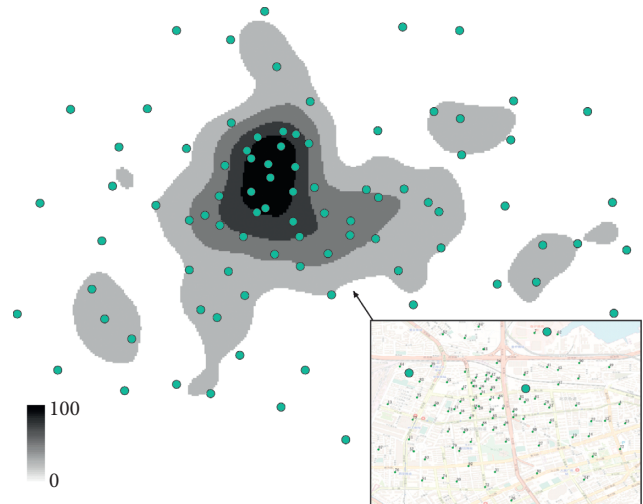


FIGURE 1: The fluctuation of customer requirements over time and space.

time and space. However, in the nonmeal periods of a day, some riders do not receive orders from the service provider. There is excess capacity in this case. The expected delivery time of orders is concise to a certain extent (the expected time refers to the customer placing the order to delivering the order). Customers have more stringent requirements than before the previous delivery system on speed, safety, and service quality. Therefore, the freshness of meals in the instant logistics delivery is becoming more significant than the traditional transportation [6].

Different types of ordering takeout have requirements for distribution conditions and ways. Hence, they also increase the difficulty of distribution processes for riders. Besides, riders will flexibly adjust their routes according to their own experience and real-time road conditions. In doing this, the rider route usually deviates from the actual routes, and thus, this phenomenon delays the customer's delivery service. A two-stage programming model is formulated to address the challenges mentioned above. In the first stage of the model, the rider's fixed cost and the rider's travel cost are considered, and the second stage of the model is to dispatch the rider to work in a specific area during a certain period. The study intends to provide a reasonable solution heuristic to optimize the rider resources of service providers. We use the time series analysis method to generate the initial route scheme according to the order quantity transmitted to the service provider. The consideration of the available riders in different periods and regions highlights the importance of punctuality [7]. Therefore, the objective of the first-stage is to minimize the total cost, including fixed cost and traveling cost of riders in the subregion periods. The objective of the second-stage is to minimize the rider scheduling times. The ordering takeout usually combines customer requests into a big order pool associated with the ordering time, space location, food category, and freshness to deal with the order requests. Specifically, a service provider adopts a way to assign orders and then schedules riders to deliver the

distribution tasks in each period and subregion. This way usually refers to distribution regions.

The rest of the paper is organized as follows. In Section 2, we review the related literature. We present the problem formally in Section 3 and formulate a multi-objective integer programming model and its related definitions in Section 3. Section 4 details the solution to the proposed problem. We use the proposed algorithm to perform the case study, of which the data comes from a takeout platform in China. Section 6 details the conclusion of this study and prospects for future research opportunities.

2. Literature Review

The delivery service providers deliver goods to customers over a given planning period [8]. They estimate the importance of transport capacity in the service regions to assign riders to deliver orders by the deadlines [5, 9]. To gain a competitive advantage, the instant delivery company tries the best to offer increasingly narrower delivery deadlines [10]. However, the trend towards shorter delivery lead-times increases transport resources cost for the instant food delivery of customer requirements over period and space, since the service provider has to recruit more riders [11] or seeks the assistance of the third logistics, such as crowdsourcing [12–16] or spare social transport capacity [2], to release the transport resources pressure. Hence, transport capacity management is significant for the instant delivery providers. [17–19]. Besides, Zhang et al. [20] analyzed the influence of the pickers' learning effects in the online integrated order picking and delivery application. They also consider the pickers' learning effect essential for the order fulfillment process's accuracy and predictability. However, the riders will be passive entities that are subject to a digital "panopticon" [7], as the effect is used to tame algorithms. Decisioners providing services need to maintain a balance by optimizing existing capacity resources, that is, the balance between existing rider resources and service quality. In the case of rider resources and no additional riders are rented, the order requests of customers are delivered by scheduling riders from other regions, while also ensuring the quality of customer service.

The problem of instant delivery is closely related to the pickup and delivery problem [21] and the dial-a-ride problem [22]. Each order has a pickup node and delivery node, respectively. Hence, the customer requires to be serviced by the rider within an hour or less. For example, all riders must deliver the orders to customers within 45 minutes to take out the delivery. Moreover, the rider must start from the depot, visit some new pickup nodes that come up as a result of new delivery nodes, and then return to the depot within the given time windows [23]. Otherwise, they may be subject to additional penalties due to delivery delays [24]. Usually, by using precise algorithms, we may work out the optimal solution, and by using the heuristic method, we may get a near-optimal solution to the delivery problem. [25] discussed the rider consistency in the dial-a-ride problem and proposed a branch-and-cut algorithm to solve two mathematical formulations. To the best of our knowledge, by exact methods, we may obtain the optimal solution. However, the computational time is too long for solving middle-size problems. Therefore, the exact

algorithm is unreasonable to address the proposed problem, because the high timeliness of instant delivery. Therefore, in the real-world scenario, the heuristics approach is adopted. Ghiani [26] introduced the order assignment and vehicle scheduling in the dynamic dial-a-ride problem. Li (2016) proposed a large neighborhood search algorithm to address the share-a-ride problem and determined the time slack. Klapp [27] formulated an arc-based integer programming model, and they also designed local search heuristics to solve a dynamic dispatch waves problem where the order arrival times are known. Gschwind [28] and Azi [29] developed a large neighborhood search heuristic to optimize the pickup and delivery problem.

Gu [30] presented the benefits of the truck-drone combination associated with the ordering takeout delivery of two advanced ant colony heuristics and a method to minimize the number of dispatched vehicles and the total travel time. Besides, the same-day delivery is another subtopic of research worthy of attention. When it comes to instant delivery, goods are usually delivered within the same-day [6, 31]. These delivery activities always occur in the form of online behavior [32]. It is worth noting that the pickup node and delivery node are usually located in the same city. Ulmer [33, 34] analyzed the drones combined with regular delivery vehicles to improve same-day delivery performance based on geographical districting. Klapp [35] discussed the request acceptance and distribution decisions in same-day delivery. They split the time horizon into four-periods. Bent [36] applied the multiple-scenario approach (MSA) to sample a set of scenarios for obtaining future customer requests, and the samples can determine a suitable route. Furthermore, in Table 1, we compare existing research works with this study to show the main differences.

The differences between this study and previous research are as follows. Firstly, we formulate a two-stage model to address the problem of configuring transport resources of delivery riders and optimize both quantity and travel routes of the riders for fluctuations of customer demand over time and space in any period of the entire region. Secondly, we design an LNS approach to generate the delivery rider's route given the determined minimum number of delivery riders in the first stage of our model. Then, the second stage of our model is addressed by the Gurobi 9.1, a commercial solver. Thirdly, the service region and the whole day are divided into some subregions and subperiods.

Our contributions are as follows. Firstly, we present the optimization of rider scheduling for a food delivery service (ORSFDS) problem based on a dataset from an online-to-offline takeout food service provider in China. Then, we formulate two MIP models and propose the LNS algorithm to generate the near-optimal solution. After that, an empirical study and extended computation are carried out on data provided by Dalian, China. Finally, this study includes the sensitivity analysis on the tightness of order time windows and the rider's familiarity with the region.

3. Problem Definition and Formulation

In this section, we first present a formal description of the ORSFDS. We then define the rider routing and rider scheduling. Suppose a set of customers $D = \{1, \dots, d\}$ that need to be

TABLE 1: Comparison between the existing literature and this study.

Reference	Transport capacity	Rider assignment	Rider scheduling	Two-stage model	Heuristic algorithm
Ulmer et al. [33]	✓		✓		
So et al. [11]	✓		✓		
Berbeglia [21]	✓		✓		✓
Cordeau et al. [22]			✓		✓
Li et al. [37]			✓		✓
Archetti [8]		✓	✓		✓
Huang et al. [5]	✓	✓			✓
Steever et al. [38]			✓		✓
Sun [7]	✓		✓		✓
Wang [39]	✓		✓		✓
Yildiz et al. [4]	✓		✓		✓
Liao [9]			✓	✓	✓
This study	✓	✓	✓	✓	✓

served by riders during time periods in regions, and they are located in a connected graph, $G = (V, E)$, where $V = \{0\} \cup N$ is the set of vertices, E is the set of edges and $N = P \cup D = \{1, \dots, n\}$ is a group of nodes including restaurants and customers. The node 0 represents the rider's origin, and nodes 1 to n represent, respectively, the locations of restaurants and customers. For each order $i = (o_i, d_i)$, we use O_s to denote the set of order sub-regions. In this study, we divide the distribution region into several sub-regions and the rider service horizon into small time periods throughout the day.

We present the fluctuation of customer demand with time in a certain service region in Figure 2. The example is depicted in Figure 2. The figure shows the fluctuation of customer demand with time in a specific service region. We discretize the working horizon of a day for riders and take every three hours as a period for riders to deliver meals. It can be seen from Figure 2 that there is excess capacity at $T1$ and $T3$ between the relationship of rider's supply and customer's demand. Excess capacity refers to customers' low demand at $T1$ and $T3$, resulting in some idle riders having no orders to deliver. However, at $T2$ and $T4$, there is insufficient capacity to meet customers' demands. Insufficient transport capacity refers to the surge of customer demand in the region at $T2$ and $T4$, and the existing riders cannot complete the delivery of orders. Similarly, this phenomenon also exists in other regions. Additionally, to make rational use of the existing resources, this study mainly considers integrating the existing regional riders' resources in a certain period to minimize the scheduling cost and meet the needs of customers and service quality. Therefore, we develop a two-stage scheduling model to optimize the rider scheduling problem.

In practice, however, due to the sharp increase of order demand in the peak period (11:00–13:00 and 17:00–19:00), a service provider (e.g., Meituan) usually assigns more riders to deliver orders within the expected time. To assign resources more reasonably and thus attain low operation costs, we have developed a large neighborhood search to solve the problem. In our study, in order to alleviate the large amount of orders in the business district, the existing rider resources cannot satisfy customers' order requests. Thus, we propose to schedule some idle riders from a subregion with a small order volume to another subregion with a large order volume to satisfy the needs of customers in a timely manner.

Throughout this study, two decisions are to be made in this problem: the number of routes of riders and the service periods and subregions of riders in the first stage of the model. For the number of riders and the traveling routes of riders' decisions, we use $x_{r0j} = 1$ to indicate that riders deliver directly from 0 to j , that is, riders start from the origin to work; and, $x_{rij} = 1$ indicates that the rider travels from i to j in the route, and $x_{r0j} = 0$ and $x_{rij} = 0$; otherwise, $i, j = 0, 1, \dots, n$. We also use $x_{rst} = 1$ to denote that the rider r provides delivery service for customer requests in the period t in the subregion s during the working horizon. For the sake of brevity, we formulate a two-stage model to optimize the rider scheduling problem. The rider scheduling model is to determine the delivery route and number of riders in each subregion during a time period and to determine the working period and working region of a rider.

In practice, we consider several reasonable assumptions to guarantee model availability. (1) For each order, it has a certain pickup quantity. Riders load the customer's ordered meals at the pickup node and unload them at the delivery node. (2) The pickup node is visited by the rider exactly once later than the delivery node. Significantly, the pickup node and the delivery node must be accessed by the same rider. (3) Each vehicle begins service at an initial position. As riders are independent contractors, each rider determines how assigned orders are sequenced and routed. (4) These routing and sequencing procedures are known to the dispatchers. Since the order requests are known to the service providers in advance, dispatchers and riders communicate via mobile phones. (5) Riders accept all orders assigned during the order horizon. The related notations and definitions used to formulate the ORSFDS are shown in Table 2.

$$\min : \sum_{r \in R_s} \sum_{j \in N \cup \{0\}} \gamma_1 x_{r0j} + \sum_{r \in R_s} \sum_{i \in N} \sum_{j \in N} \gamma_2 d_{ij} x_{rij}, \quad (1)$$

$$y_{ro_i} = y_{rd_i}, \quad \forall r \in R_s, i \in O_s, \quad (2)$$

$$\sum_{r \in R_s} y_{ro_i} = 1, \quad \forall i \in O_s, \quad (3)$$

$$t_{ij} + \alpha_{ir} \leq \alpha_{jr} + M(1 - x_{rij}), \quad \forall r \in R_s, i, j \in N \cup \{0\}, \quad (4)$$

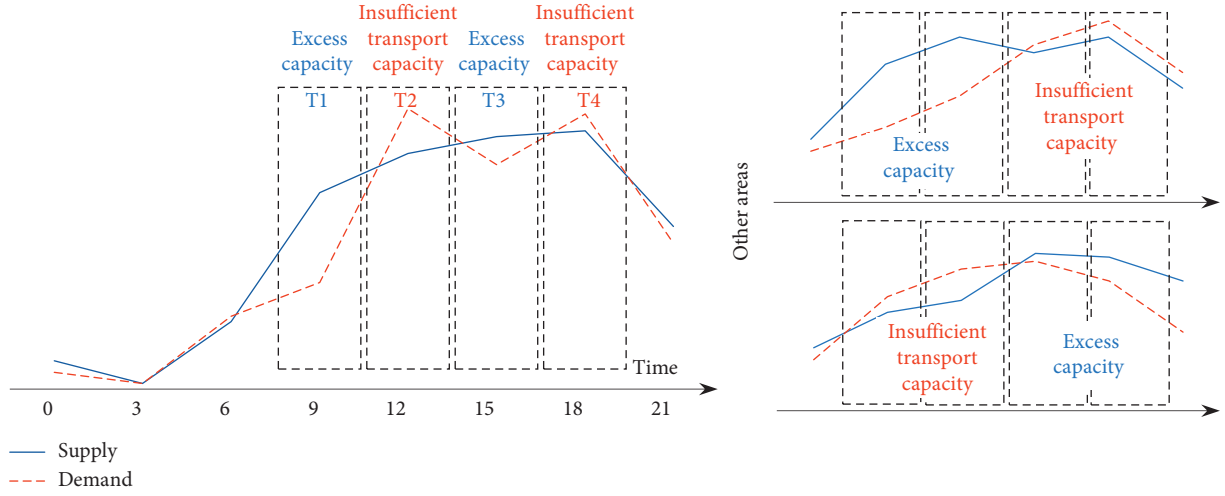


FIGURE 2: The fluctuation of customer demand with time in a certain service region.

TABLE 2: Sets, parameters, and decision variables.

Notation	Description
<i>Sets</i>	
R_s	Set of assigned riders in subregion
O_s	Set of orders in subregion, for any order i , it consists of two nodes, denoted by (o_i, d_i) .
D	Set of customers
S	Set of sub-regions serviced by riders, $S = 1, \dots, s$
$N = P \cup D \cup O$	Set of all nodes including pickup nodes (restaurant's locations) and delivery nodes (customer's locations) and the depot (the starting node of the rider)
<i>Parameters</i>	
a_i, b_i	The order placed time by customer i and the expected delivery time by customer i , respectively
u_{ir}	The load quantity of rider r arriving at node i
α_{ir}	Departure time of rider r at node i
q_i	The demand at node i
c_r	The capacity of the vehicle owned by the rider r
t_{ij}	Each arc (i, j) is associated with a travel time
d_{ij}	Distance of the arc (i, j) , unit: meter
γ_1	Fixed costs for each rider, unit: CNY
γ_2	The traveling cost, unit: CNY
<i>Decision variables</i>	
x_{rij}	Binary decision variable equals 1 if the rider r travels from node i to node j ; 0 otherwise.
x_{rst}	Binary decision variable equals 1 if rider r is assigned to deliver food delivery by the service platforms in the period t in the subregion s
y_{ir}	Binary decision variable equal 1 if the rider r services node i

$$\alpha_{ir} \leq b_i, \quad i \in D, \quad (5)$$

$$\alpha_{ir} \geq a_i, \quad \forall i \in P, \quad (6)$$

$$\alpha_{o_i r} + t_{o_i d_i} \leq \alpha_{d_i r}, \quad \forall i \in O_s, \quad r \in R_s, \quad (7)$$

$$x_{rd_i o_i} = 0, \quad \forall i \in O_s, \quad r \in R_s, \quad (8)$$

$$u_{ir} - q_i \leq u_{jr} + M(1 - x_{rij}), \quad \forall i \in D, \quad j \in N \cup \{0\}, \quad r \in R_s, \quad (9)$$

$$u_{ir} + q_i \leq u_{jr} + M(1 - x_{rij}), \quad \forall i \in P, \quad j \in N \cup \{0\}, \quad r \in R_s, \quad (10)$$

$$0 \leq u_{ir} \leq C, \quad \forall i \in N, \quad r \in R_s, \quad (11)$$

$$\sum_{i \in N} \sum_{j \in N} x_{rij} = \sum_{i \in N} y_{ri}, \quad \forall r \in R_s, \quad (12)$$

$$\sum_{r \in R_s} \sum_{j \in N} x_{rij} = 1, \quad \forall i \in N, \quad = \sum_{i \in N} y_{ri}, \quad \forall r \in R_s, \quad (13)$$

$$\sum_{r \in R_s} \sum_{i \in N} x_{rij} = 1, \quad \forall j \in N, \quad (14)$$

$$\sum_{r \in R_s} \sum_{j \in N} x_{r0j} = \sum_{r \in R_s} \sum_{j \in N} x_{r0j} \leq |R_s|, \quad (15)$$

$$\sum_{j \in N} x_{r0j} = \sum_{j \in N} x_{rj0} \leq 1, \quad \forall r \in R_s, \quad (16)$$

$$\alpha_{ir} > 0, \quad \forall i \in N, r \in R_s, \quad (17)$$

$$x_{rij} \in \{0, 1\}, \quad \forall r \in R_s, i, j \in N \cup \{0\}, i \neq j, \quad (18)$$

$$y_{ri} \in \{0, 1\}, \quad \forall i \in N, r \in R_s, \quad (19)$$

The objective function (1) seeks to minimize the total costs, including fixed cost and riders' travel cost [40]. Constraints (2) and (3) ensure that each order in the subregion is serviced exactly once by the same rider from the pickup node to the delivery node. Constraint (4) satisfies the travel time requirement between two adjacent nodes. Constraint (5) guarantees that customer requests are delivered before the order expected delivery time. The rider arrives at the restaurant to pickup food or leaves the restaurant to deliver food after placing the order is presented in constraint (6). Constraint (7) presents the time relationship between the same rider visiting the pickup node and delivery node; That is, the delivery time when the rider leaves the delivery node cannot be earlier than the total time. It is determined by the pickup time and traveling time from the pickup node to the delivery node. The arc does not travel directly from the pickup to the delivery node, as in Constraint (8). Payload capacities are presented in Constraints (9)-(11). Constraints (9) and (10) define the payload capacity of the vehicle owned by a rider. Constraint (11) determines the payload does not exceed the capacity of the vehicle. Constraint (12) shows the relationship between the node and the rider's ownership. Constraints (13) and (14) ensure the connectedness of the order nodes. Similarly, constraints (15) and (16) indicate that each rider starts from the depot, goes to the restaurant to pickup food, delivers the customer request, and returns to the same depot. Constraints (17)-(19) are decision variable definitions.

Riders' shifts are crucial for the optimization of the scheduling of riders. However, in the real-world scenario, the number of riders required is different in each period and each subregion. For example, at two peaks throughout the day, the number of order requests increased almost exponentially. In this case, the number of riders required for each period in the same region varies over time. Therefore, we propose a new way of scheduling riders. In other words, we schedule idle riders from several subregions to other subregions with less transport capacity in the same period so that the problem attaining the case of short riders in some subregions during the peak period could be solved.

For the sake of simplicity, in the second stage of the model, we suppose a set of subregions that need to be serviced by riders during the period. In our discussion, we assume a set of periods $T = \{t_1, t_2, \dots, t_{|T|}\}$, and the payload capacity of

riders at any subperiod in any subregion is denoted by q_{st} . There are $|R|$ available riders in the distribution, denoted by $R = \{1, 2, \dots, r\}$. We assume that each rider can only serve familiar subregions $S_r \subseteq S, S_r \neq \emptyset$. Because of the fluctuations of order requests in different subregions and periods, riders who may transfer among subregions are denoted by $s \in S$ to another $s' \in S$. Each arc is associated with a transfer cost by $c_{ss'}$. Riders are not allowed to serve subregions far from their original region, and the rider has the maximum transfer distance L_{\max} . For the rider's shift decision, the decision variable is denoted by $x_{rst} = 1$, and the rider r provides delivery service for customer requests at a period t in the subregion s . To satisfy the customer requirements and obtain the minimum scheduling times, the model is as follows.

$$\min = \sum_{r \in R} \sum_{s \in S} \sum_{t \in T} x_{rst}, \quad (20)$$

$$\sum_{s \in S} x_{rst} \leq 1, \quad \forall r \in R, t \in T, \quad (21)$$

$$\sum_{r \in R} x_{rst} \geq q_{st}, \quad \forall s \in S, t \in T, \quad (22)$$

$$\sum_{s \in S_r} x_{rst} = 0, \quad \forall r \in R, t \in T, \quad (23)$$

$$x_{rst} + x_{rs'(t+1)} \leq 2, \quad \forall r \in R, s, s' \in S, t \in T, c_{ss'} \leq L_{\max}, \quad (24)$$

$$x_{rst} + x_{rs'(t+1)} \leq 1, \quad \forall r \in R, s, s' \in S, t \in T, c_{ss'} > L_{\max}, \quad (25)$$

$$x_{rst} \in \{0, 1\}, \quad \forall r \in R, s \in S, t \in T. \quad (26)$$

The objective function (20) minimizes the overall scheduling time of riders [16]. Constraints (21) ensure that each rider can serve at most one subregion at a period. Constraints (22) indicate that the number of riders required by each sub-region in each period is not greater than the total number of assigned riders. Constraints (23) state that each rider has a fixed familiar region and cannot go to the unfamiliar sub-regions. Constraints (24) and (25) govern the transfer distance relationship for riders. Finally, Constraints (26) denote the decision variable.

4. Solution Heuristic

This section introduces the proposed large neighborhood search algorithm in detail. There are some metaheuristic algorithms that may have several drawbacks such as premature convergence and to tramp in local optimal or stagnation. To overcome these disadvantages, this study attempts to develop a hybrid heuristic algorithm that enables it to acquire high computational efficiency. Furthermore, heuristics and metaheuristics are widely applied for different research domains, such as online learning, scheduling, multiobjective optimization, medicine, passenger and freight terminal operations, data classification, and others.

As far as we know, the proposed rider scheduling model is an extension of the dial-a-ride problem, a well-known NP-hard problem [41]. Therefore, it is crucial to obtain high-

quality optimization results in a reasonable calculation time. A large neighborhood search algorithm is a widely verified resource scheduling algorithm [42]. The constructed initial solution improves the existing solution by iteratively executing the destroy and repair operators and generates an approximately optimal solution.

In the rider scheduling model, we optimize both the number of riders and the route of riders. Firstly, we design an insertion heuristic method to construct feasible initial solutions quickly; in the subsequent iterations, the existing solutions are destroyed by the removal operator, and then the removed orders are inserted by the repair operator. After this operation, a new neighborhood solution can be generated from the current solution. When the termination condition is satisfied, the algorithm outputs the optimal solution. Table 3 shows the pseudo-code for designing a large neighborhood algorithm.

4.1. Insertion Heuristic to Design Initial Solution. Cordeau et al. [41] constructed an initial solution using the completely stochastic method. However, the downside of this method is sometimes the infeasible solution may also be obtained. Therefore, in the proposed, we consider the time window of orders and the proximity of orders to generate a rider's feasible route quickly. First, all orders are sorted ascendingly based on the expected arrival time of the orders; then, each order is assigned to the rider's delivery route to generate $|R|$ initial sequences according to expected arrival time (from early to late). Finally, we merge the orders into the same delivery route by taking care of the four metrics listed below:

- (1) Calculate the distance between two pickup nodes.
- (2) Calculate the distance between two delivery nodes.
- (3) Calculate the distance between a delivery node and a pickup node.
- (4) Calculate the distance between a pickup node and a delivery node.

Delivery route merging is performed iteratively. In each iteration, an order is randomly selected from the remaining uninsured orders, one of the four metrics is randomly selected, the minimum distance based on these two random features is then calculated, and the order is inserted into the route with the minimum distance. During the insertion process, we also need to do a feasibility check according to the constraints of the order assignment's model to ensure the feasibility of the initial solution. A feasible initial scheduling plan is obtained until all orders are inserted into the route.

4.2. Neighborhood Search. In this section, to obtain a new neighborhood solution, the removal operation and repair operation are designed by destroying and reconstructing the current solution. In the removal operation, we use four removal operators: natural sequence removal operator, maximum time window removal operator, worst order removal operator, and cluster removal operator. As with each removal operation, the output result is only a part of the solution. Therefore, we

TABLE 3: The pseudo code of the heuristic algorithm.

Input: The order dataset
Output: The numbers of the riders and the rider's route
Step 1: generate initial route s_{ini} by using insertion heuristic
Step 2: set initial solution s_{ini} as the current solution, neighborhood solution s_{nei} , and best solution s_{best}
Step 3: implement remove operation on current solution s_{cur} to obtain partial solution s_{part}
Step 4: use repair operator to obtain neighborhood solution s_{nei} from partial solution s_{part}
Step 5: if s_{nei} outperforms s_{best} , accept the inferior solution according to the principle of simulated annealing
Step 6: check if the termination condition is fulfilled, that is, after N consecutive iterations, the value of S_best no longer changes. Then, jump to step 6 if yes, otherwise to step 3
Step 7: output the optimal solution

implement repair operators to construct a new feasible solution from partial solutions. In this study, useful repair operators are the optimal insertion operator, regret insertion operator, and maximum waiting time insertion operator.

4.2.1. Remove Operator. The purpose of the neighborhood search is to remove some orders from the current solution based on specific criteria. There are four neighborhood operations applied in this study as follows.

Natural sequence removal operator: the node in the route with "0" rider load is referred to as the natural sequence. In general, the rider route consists of two natural sequences, respectively. That is, sequence $1 \rightarrow 2 \rightarrow 1+n \rightarrow 3 \rightarrow 2+n \rightarrow 3+n$ and sequence $4 \rightarrow 5 \rightarrow 5+n \rightarrow 4+n$, namely. Randomly selects a natural sequence from the removal operator and removes it from the current rider route.

Maximum time window removal operator: select the order with the largest time window in all routes and remove them because orders with larger time windows have more time flexibility.

Worst order removal operator: for the rider route, the removed route's cost-saving value calculates one by one and removes the order with the most considerable saving value.

Cluster removal operator: randomly select a root node and threshold, and then remove the order on each route closest to the root node.

4.2.2. Repair Operator. The purpose of the repair operation is to reinsert the removed orders into the rider route. The repair operator performs iteratively in the repair process until all orders insert into a set of routes. In this study, we use the following three kinds of repair operators.

Optimal insertion operator: this way is similar to the insertion heuristics operation in section 4.2, in which the unserviceable orders insert to the location of the minimum cost increment.

Regret insertion operator: considering the optimal cost value insertion, the most challenging order usually puts to the final processing. Therefore, for all unserviceable orders, the optimal insertion location's cost value is calculated and generated by the cost value vector. Then, randomly select a

value from the vector and insert its corresponding order into the route.

The maximum waiting time insertion operator is to insert orders into the rider route with a more considerable buffer time. The waiting time refers to the time difference $\Delta t_{wait} = \alpha_{ir} - t_i, \forall i \in P$, between the rider's arrival time and the pickup node's opening time.

4.3. Selection and Stopping Criterion. The optimal and regret insertion is used to generate the initial feasible solution based on its current number. At each iteration of the algorithm, we randomly select removal and repair operators to destruct and reconstruct the current solution and obtain a new solution. Moreover, the simulated annealing criterion is used to determine if the new solution is accepted. Therefore, by adopting this criterion, we can accept a suboptimal solution for the time being to search for a universally optimal solution rather than a locally optimal solution.

5. Computational Experiments and Analysis

5.1. Benchmark Example Test. The LNS algorithm is implemented in C# and tested on a system with 64bit Windows 10 OS, Intel i7 processor (2.60 Hz), and 16 GB RAM. Then, we use the Gurobi 9.1.0 commercial solver to verify our model, but it can only handle less than ten orders. Therefore, we need to adopt the proposed heuristic to solve medium-sized problems.

The DARP has been studied for decades, associated with many benchmark instances that have been given. The standard instance provided by Cordeau [22] is used to verify the proposed mathematical model and heuristic method.

The difference between the proposed algorithm and DARP is that the pickup node and delivery node have only a one-sided time window. Therefore, the standard DARP instance can quickly be transformed into a test instance based on the first-stage of the model. We can set the time window on the right side of the pickup node and the delivery node's left side as positive infinity and 0, respectively.

We have compare the tabu search with the proposed LNS algorithm, and the results are shown in Table 4. The first column shows the instance name. The second column enumerates the order requests. Inset A, the quantity of customer requests is one unit. However, set B is subject to the uniform distribution. The third column is the capacity of the rider's vehicle. Column 4 indicates the minimal number of riders obtained from the model. Columns 5 to 6 and 7 to 8 denote the tabu search and LNS algorithm's solution and computational time, respectively.

According to Table 4, the proposed algorithm and tabu search method are two implementations of the first stage of the model. The performance of the proposed algorithm is better than the tabu search algorithm. We could obtain an optimal solution for 16 of the 24 instances by using the LNS algorithm; however, by employing the TS algorithm, we could only get an optimal solution of 13 instances. However, in terms of the computational time, the LNS algorithm is slightly longer than the tabu search algorithm. Moreover, the

TABLE 4: Summary of results on different scale instances.

Ins.	q_i	Q	The optimal solution	TS		LNS	
				Solution	Time	Solution	Time
a2-16	1	3	2	2	10	2	17
a2-20	1	3	2	2	16	2	16
a2-24	1	3	2	2	20	2	29
a3-30	1	3	3	3	26	3	30
a3-36	1	3	3	3	28	3	32
a4-40	1	3	4	4	32	4	34
a4-48	1	3	4	5	35	5	43
b3-24	U[1, 6]	6	3	3	18	3	25
b3-30	U[1, 6]	6	3	3	24	3	30
b3-36	U[1, 6]	6	3	3	27	3	29
b4-16	U[1, 6]	6	4	4	10	4	12
b4-32	U[1, 6]	6	4	4	26	4	30
b4-48	U[1, 6]	6	4	4	35	4	41
b5-40	U[1, 6]	6	5	6	32	5	32
b5-50	U[1, 6]	6	5	6	38	5	40
b5-60	U[1, 6]	6	5	5	42	6	50
b6-48	U[1, 6]	6	6	7	34	7	39
b6-60	U[1, 6]	6	6	7	40	7	49
b6-72	U[1, 6]	6	6	8	44	7	45
b7-56	U[1, 6]	6	7	8	41	7	44
b7-70	U[1, 6]	6	7	9	46	8	46
b7-84	U[1, 6]	6	7	9	55	8	60
b8-64	U[1, 6]	6	8	9	43	8	52
b8-80	U[1, 6]	6	8	9	53	9	68
b8-96	U[1, 6]	6	8	9	73	9	82

LNS algorithm is stochastic in nature, and their performance often fluctuates, so for test instance (a) and instance (b), we run the proposed algorithm for 1000 iterations. The convergence processes are shown in Figure 3; although the convergence rate of the LNS algorithm is slow, the solution approach has good stability. It should be noted that instance (a) and instance (b) are the benchmark examples, whose convergence is shown in, namely, Figures 3(a) and 3(b). In the real-world scenario, the time difference between the two algorithms can be ignored. Therefore, the LNS algorithm in this study can better solve the first stage of the model.

5.2. Data Source. This section is about ride optimization scheduling problems for on-demand food deliveries with a computational experiment from Dalian, China. Section 4.2.1 analyzes the delivery company's order data in half a month to illustrate customer demand fluctuations in time and space. In Section 4.2.2, this study carries out a specific calculation test to optimize riders' transport capacity. Section 4.3 discusses sections of discusses window tightness and riders' familiarity with distribution regions based on capacity assignment.

5.2.1. Description Of Real-World Cases. In this section, numerical experiments are performed based on data from an online-to-offline food delivery platform located in Dalian, China. To demonstrate the proposed algorithm's effectiveness in the configuration of transportation resources of delivery riders for on-demand food deliveries with the

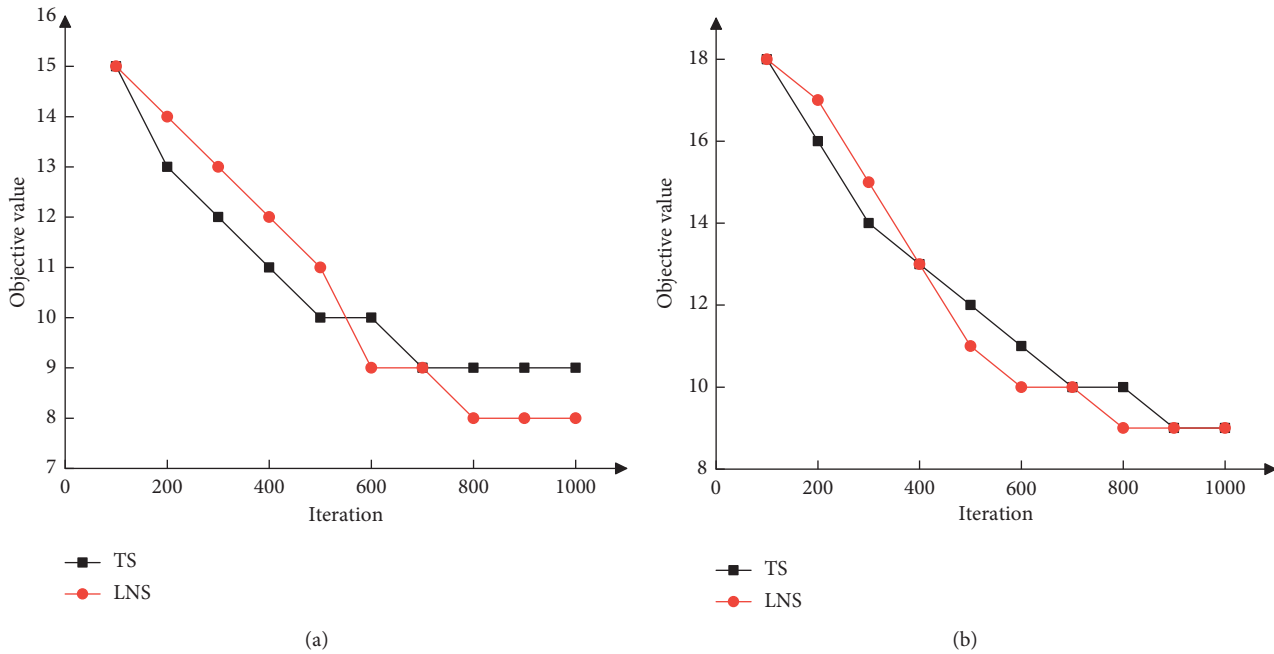


FIGURE 3: The convergence processes for instances. (a) Instance b8-64 (b) Instance b8-96.

fluctuations of customer demand over time and space, we take the customer order requests of a takeout food service provider from January 1 to 15, 2017, as the data source. Data sources include order IDs, restaurant names, customer locations, rider names, order times, delivery times, navigation distances, order regions, and rider regions. Then, we use the *Python* pandas package to process the data and get all order requests from the first 15 days of Jan 2017, as shown in Figure 4. It can be observed that the average number of daily orders is more than 5000.

Furthermore, the business districts with more than 100 orders on January 1, 2017, are selected as our research regions. Then we get 23 sub-regions, and their detailed information is shown in Figure 5. There are very few orders taken before 8:00 AM and 20:00. The peak hours are 11:00–12:00, 14:00–15:00, and 16:00–17:00. As a result, we focus on the delivery period from 8:00–20:00. We divide the whole day into six sub-periods, and each sub-period is 2 hours.

To analyze the order requests imbalance among the different sub-periods and sub-regions. We select four business districts: Luosifu, Xi'an Road, Wanda, and Shandong Road, to depict the order variations in Figure 6. We could see that the number of orders made by customers varies in regards to both time and region. Therefore, the takeout food delivery platform needs reasonably schedule riders to deliver customer requests and maintain the transportation capacity at a suitable level.

5.2.2. Optimization of Rider Scheduling. This section selects 46 orders from 10:00 to 12:00 in the Luosifu business district to determine the optimal number of delivery riders

required. The coordinates of the rider resource based on the Baidu Map are shown in Figure 7. No. 0 stands for the depot. The order pickup nodes are from No. 1 to No. 46, and the corresponding delivery nodes are from No. 47 to No. 92. The demand for each order is 1 unit, and the capacity of the rider is six units. The fixed cost of the rider is 150 CNY.

The proposed LNS algorithm is implemented in C# and run on an environment with Intel(R) Core (TM) i7-9750H CPU, 2.60 GHz, and 16 GB of RAM. The minimum number of riders is 13 in the above instance. The routes of riders are shown in Table 5 and Figure 8. Therefore, the first stage of the proposed model and the LNS heuristic are effective for the takeout food service provider in reducing the number of delivery drives required in the given period.

Moreover, in Table 6, we present the minimal number of riders obtained by the proposed heuristic and the number of dispatched riders in an original dataset in the 23 subregions from 10:00 to 12:00. The results show that, in 20 out of 23 subregions, our method outperforms the current system in use. Therefore, we conclude that the proposed model and LNS algorithm are superior to the current assignment method. Furthermore, we optimize the number of riders in the six time periods and 23 subregions. We assume that the transfer distance between two adjacent subregions is 3 km. The maximal allowed transfer distance for each rider is 9 km between two consecutive subperiods. The Gurobi 9.1 solver is used to generate the optimal solution for the second stage of the model. The corresponding results are presented in Table 6.

Table 7 presents the minimal number of riders required of the 23 subregions in the six subperiods. However, the instant delivery network needs 300 riders, and all riders schedule 1800 times. However, in the real scenario, a

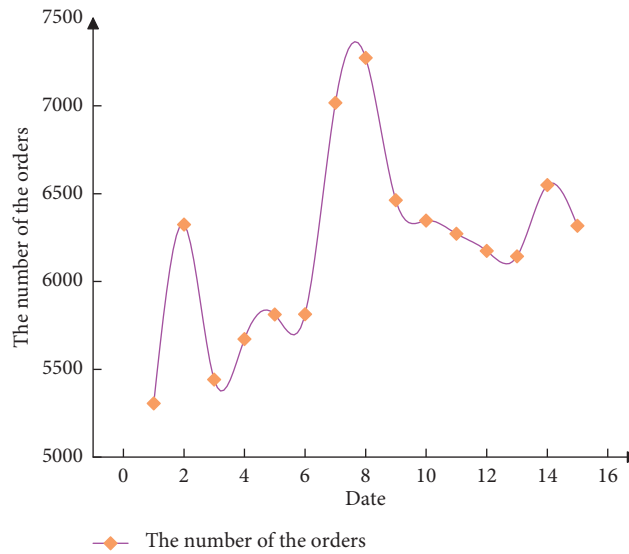


FIGURE 4: The average daily orders in the first half of January 2017 based on the historical dataset.

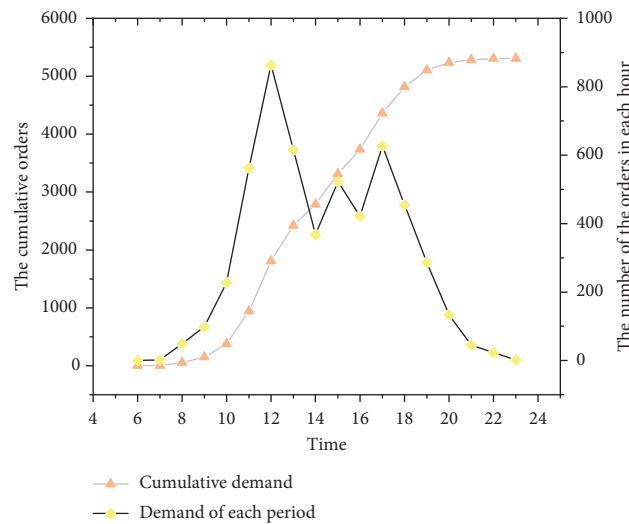


FIGURE 5: The statistics chart of the orders in January 2017.

service provider assigns 328 riders and schedules 2180 times to deliver customer requests. In order to address the fact that existing riders cannot satisfy the customer's ordering demands during the peak meal period, in our study, we proposed to schedule idle riders from some subregions to other subregions with high rider's demand. In this way, the total number of riders has been reduced by 8% compared to the previous scheduling scheme (each subregion has sufficient riders), and the cost of scheduling riders has also been saved by 4200 CNY. Hence, good capacity optimization is practical and economical for service providers. Randomly select ten riders and discuss the rider's changes in the service area in subperiods, and the results are shown in Table 8. The results show that the number of riders required in different time periods in different subregions is different. This is due to the fluctuation of orders in the same time period in different regions and different

time periods in the same region. For example, No. 1 assigns a rider to deliver orders in 6 different subregions. Hence, configuring riders' transport resources for instant deliveries with the imbalance of customer requirements over time and space is extremely critical.

5.3. Sensitivity Analysis. In this section, we conduct sensitivity analysis on the tightness of the order time windows and regional familiarity.

5.3.1. Analysis on the Tightness of the Order Time Windows. Punctuality is crucial to on-demand food delivery businesses since the freshness of meals must be preserved within the scheduled arrival time to meet the customers' expectations. Besides, by introducing an optimal delivery riders schedule,

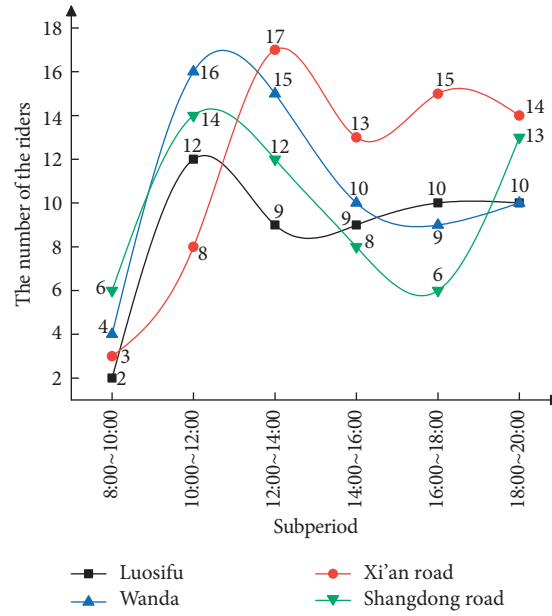


FIGURE 6: Statistical chart of transport capacity demand in each subperiod of the business circle.

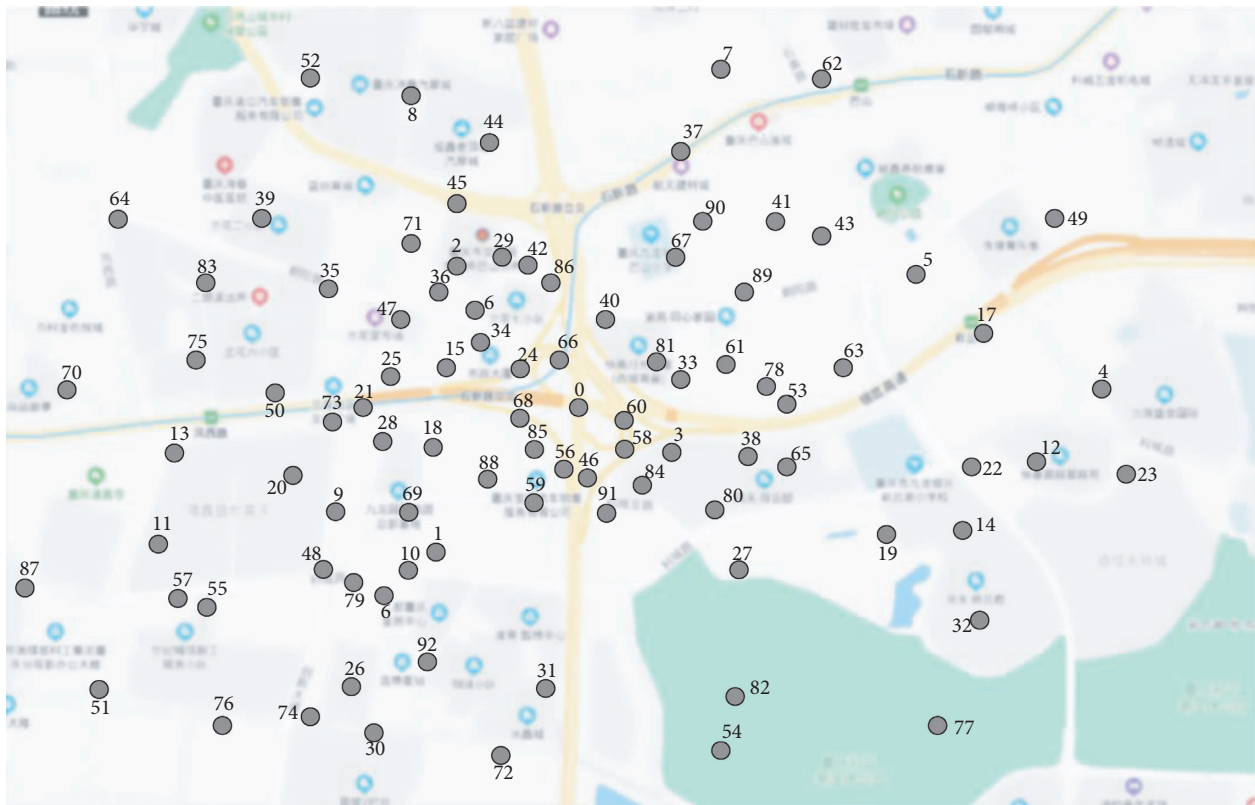


FIGURE 7: The spatial distribution of 46 orders.

more operation costs can be saved for the delivery platforms. However, in the most extreme cases, one order is assigned to one delivery rider only by the takeout service platform since

the objective is to satisfy all customer requests to obtain a good service reputation. We simulate three different order time windows and discuss the number of riders required.

TABLE 5: Optimization of rider scheduling.

Rider index	Rider routes
1	0-1-21-25-47-71-67-0
2	0-12-22-14-58-60-68-0
3	0-4-23-27-69-73-50-0;
4	0-41-5-30-76-51-87-11-57-0
5	0-24-70-13-59-20-66-0
6	0-16-45-44-62-43-90-89-91-0
7	0-37-39-83-15-85-61-0
8	0-33-46-92-6-79-18-64-52-0
9	0-29-8-75-31-54-77-32-19-65-78-0
10	0-40-86-2-36-28-48-74-82-0
11	0-34-42-35-88-80-81-0
12	0-3-7-49-17-63-53-38-84-0
13	0-9-55-26-72-10-56-0

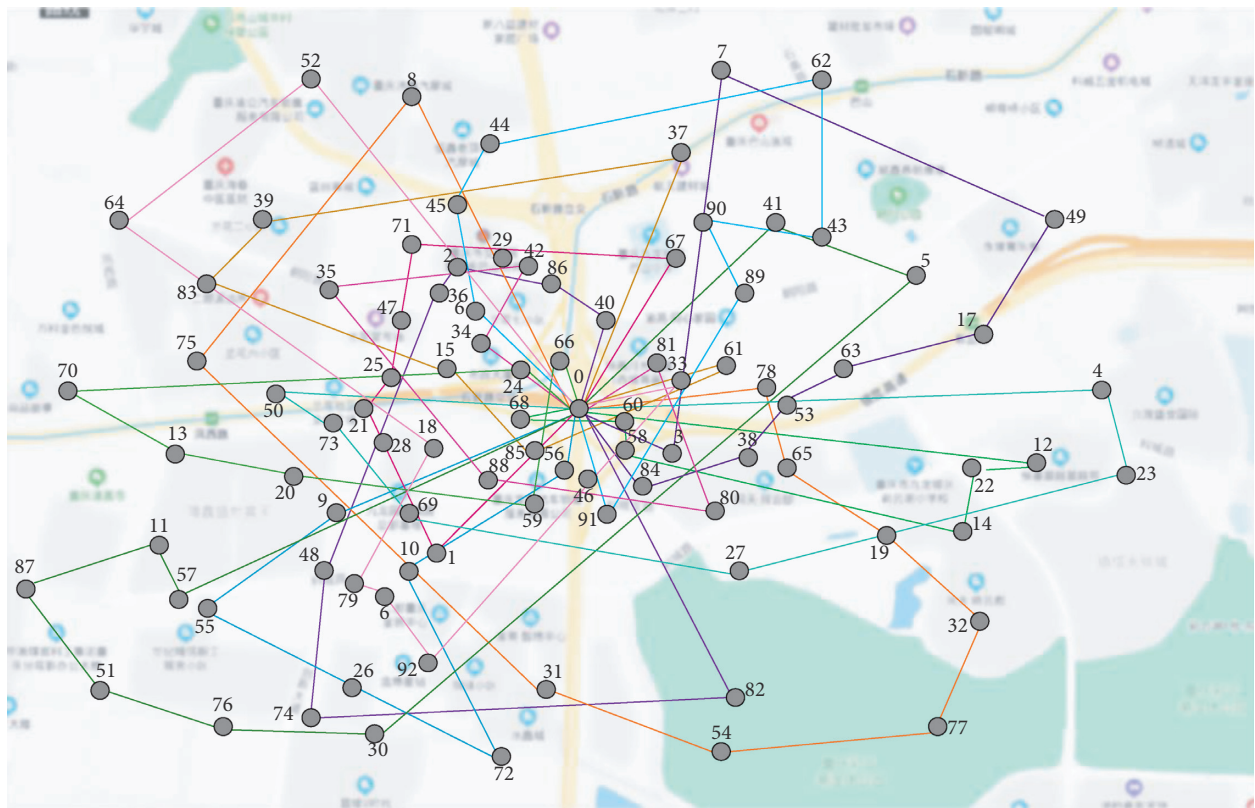


FIGURE 8: Visualization of the rider’s scheduling route.

Case 1 is the relaxed time windows, and the rider only has 60 minutes. Case 2 is the standard time window, and the rider has to go from the pickup node to the delivery node in 45 minutes. Case 3 is the tight time windows, and only 30 minutes is allowed. We test the three different time windows in the Luosifu business district, and the corresponding results are shown in Figure 9.

As the time window tightens, Figure 8 displays an opposite trend between the number of dispatched riders and each rider’s average order number. A more relaxed time window means fewer riders and more orders for each rider. Overall, the results show that the tightness of the order time windows and the

number of riders are closely related. More importantly, tighter time windows will inevitably make the distribution of transport capacity more imbalanced because the food delivery platforms have to assign more riders in peak periods.

5.3.2. *Analysis on the Regional Familiarity.* In the second-stage of the model, we prohibit the riders from visiting the sub-regions’ orders they are not familiar with regions. Because riders may spend less time to finish orders in a more familiar region, in the previous instance, we use the routes provided by Baidu Map, but there may be other shorter

TABLE 6: Number of riders in 23 sub-regions for instant deliveries.

No.	The number of the riders after optimization	The actual used riders
1	18	19
2	16	17
3	17	18
4	14	15
5	13	16
6	14	15
7	17	19
8	14	17
9	14	14
10	17	18
11	14	16
12	15	15
13	18	21
14	13	14
15	14	15
16	14	17
17	16	16
18	13	15
19	15	16
20	12	14
21	14	16
22	17	20
23	14	16

TABLE 7: The minimum number of riders required for each sub-region and each period of the whole delivery day.

Sub region number	Subperiod number					
	1	2	3	4	5	6
1	7	13	7	9	12	7
2	14	6	7	8	7	13
3	13	15	13	9	7	13
4	12	5	7	12	8	8
5	11	13	13	13	14	12
6	13	12	10	13	11	6
7	10	13	9	11	14	10
8	12	9	10	14	8	6
9	6	11	9	8	14	14
10	5	14	7	14	13	6
11	12	19	12	14	12	20
12	14	19	18	18	14	15
13	12	18	16	20	12	18
14	12	15	13	17	13	14
15	10	12	13	15	20	12
16	18	12	19	10	10	18
17	14	15	12	16	13	15
18	17	17	18	13	17	16
19	18	12	19	15	20	17
20	15	10	10	15	14	20
21	5	8	7	9	13	6
22	7	15	12	14	15	10
23	14	6	9	13	6	14

TABLE 8: Regional scheduling of some riders in each period.

Sub region number	The rider number									
	1	2	3	4	5	6	7	8	9	10
1	0	0	0	0	0	0	0	1	1	1
2	3	1	0	2	0	1	0	0	0	0
3	6	4	1	1	2	4	2	0	0	0
4	9	1	2	3	3	6	4	1	0	0
5	11	1	2	1	1	4	6	4	0	0
6	13	4	2	3	4	4	8	2	0	1

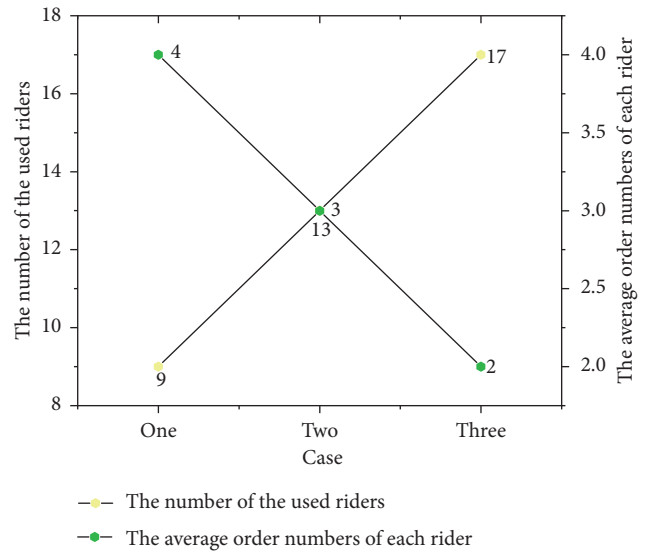


FIGURE 9: Relationship between the number of riders and the number of orders per capita under different time windows.

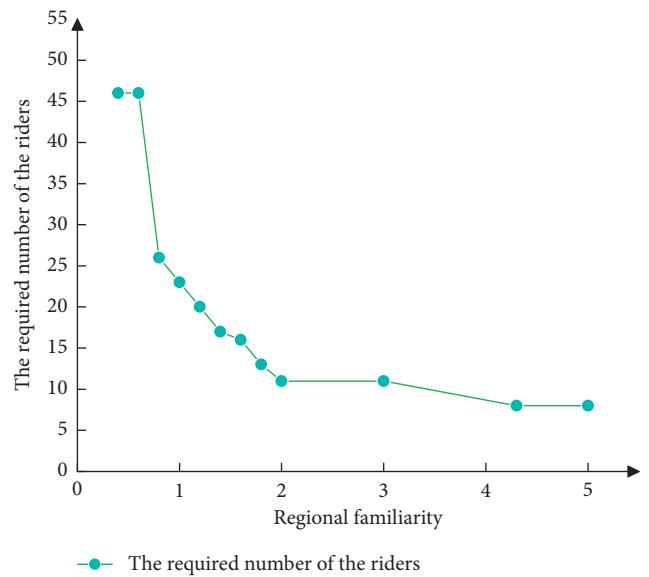


FIGURE 10: Relationship between regional familiarity and the required number of riders.

routes in practice. Therefore, we define the regional familiarity to describe the ratio between the Baidu Map distance and the rider's actual travel distance. It is evident that the smaller the familiarity, the larger the actual travel distance. We still take the Luosifu as an example and discuss the transportation capacity fluctuations in different regional familiarity. The results are depicted in Figure 10.

In Figure 10, the delivery system's number of delivery riders increases with the regional familiarity. When the rider maintains a higher regional familiarity, the required rider will be smaller, which will reduce the transportation capacity demand. Otherwise, the company assigns more riders, or the rider must travel a longer distance, which will increase the transportation capacity burden.

6. Conclusions

This study introduced a two-stage model to tackle riders' optimization problems in the on-demand food delivery business. Considering the intensively fluctuating demand of customer orders regarding period and region, the whole municipal level region is divided into smaller sub-regions while the whole period is divided into several sub-time periods. For each subregion, we formulate a dial-a-delivery rider model (first-stage of the model of our model) to minimize the delivery riders' number in each period. Furthermore, the imbalance of transportation capacity in different sub-regions and sub-periods is considered, and a transportation capacity allocation model (the second-stage of our model) is then built to minimize the time of the delivery rider's schedule. Due to the computational complexity of the first-stage of the model, we develop an ALNS heuristic to generate a near-optimal solution. In the next step, we have compared our proposed heuristic with results from other studies. Finally, the second-stage of the model is solved by Gurobi 9.1, a commercial solver. The dataset from an O2O foodservice platform in China is used to conduct the case study.

The results show that fewer delivery riders are required than the current delivery system in use by applying the first-stage of the model. The cost of saving after applying our model is 4200 CNY, and the new plan of delivery rider scheduling reduces the total delivery times by 328. Hence, the proposed model and algorithm could optimize the number of delivery riders in each subregion and improve the delivery rider scheduling. Besides, we find that the tightness of the order time windows and the number of delivery riders are closely related, and a tighter time window means more delivery riders and fewer orders for each delivery rider. Riders are found to travel significantly less distance when they are more familiar with the task subregion. However, in this study, we only focus on static order demand and ignore potential customer requirements. Moreover, in terms of riders' capacity, this paper mainly considers how to divide the whole region into small sub-regions, and separate the planning horizon into small subperiod. Furthermore, the division of rider service sub-regions depends on the area where the business circle is located, since this way is more intuitive in assessing customer demand. Meanwhile, an appropriate resource partition, with many reasonable

considerations, may outperform the proposed way in this study model, in terms of optimizing service resources.

There are several directions for further research. Firstly, we will consider the order demand mode of different delivery areas and the historical fluctuations of order demand in peak and off-peak periods, weekdays, and holidays. Secondly, appropriate resource partition methods are designed to optimize the allocation and scheduling of distribution-driven subareas. At last, the uncertainty in the delivery process may be considered (such as the uncertainty of order extraction (unexpected delay and real-time traffic conditions) to propose a more robust solution. Overall, considering more uncertainties, the on-demand food distribution-driven scheduling problem may also be worth studying.

Data Availability

The data used to support the findings of this study are available from the corresponding author upon request.

Conflicts of Interest

The authors declare that there are no conflicts of interest regarding the publication of this paper.

Acknowledgments

This work was supported by the National Natural Science Foundation of China (71971036, 71421001, and 71531002), the Major Program of Key Disciplines in Dalian (2019J11CY002), the Key R&D Project of Liaoning Provincial Department of Science and Technology (2020JH2/10100042), and the Humanities and Social Sciences Program of the Ministry of Education of China (19YJA630084).

References

- [1] Iimedia, "Research report on china's online catering takeout industry in the first half of 2017," 2017, <https://www.iimedia.cn/c400/54716.html>.
- [2] B. Kin, T. Ambra, S. Verlinde, and C. Macharis, "Tackling fragmented last mile deliveries to nanostores by utilizing spare transportation capacity-A simulation study," *Sustainability*, vol. 10, no. 3, p. 653, 2018.
- [3] Reuters, "How Amazon Is Making Package Delivery Even Cheaper," 2016, <https://fortune.com/2016/02/18/amazon-flex-deliveries>.
- [4] B. Yildiz and M. Savelsbergh, "Service and capacity planning in crowd-sourced delivery," *Transportation Research Part C: Emerging Technologies*, vol. 100, pp. 177–199, 2019.
- [5] W. Huang, Z. Zhang, X. An, and G. Min, J. Li, "Dynamic scheduling for urban instant delivery with strict deadlines," in *Proceedings of the ICC 2020 - 2020 IEEE International Conference on Communications*, pp. 1–6, Dublin, Ireland, 2020.
- [6] V. C. S. Yeo, S.-K. Goh, S. Rezaei, and Y. Sern, "Consumer experiences, attitude and behavioral intention toward online food delivery (OFD) services," *Journal of Retailing and Consumer Services*, vol. 35, no. 35, pp. 150–162, 2017.
- [7] P. Sun, "Your order, their labor: an exploration of algorithms and laboring on food delivery platforms in China," *Chinese Journal of Communication*, vol. 12, no. 3, pp. 308–323, 2019.

- [8] C. Archetti and M. G. Speranza, "The inventory routing problem: the value of integration," *International Transactions in Operational Research*, vol. 23, no. 3, pp. 393–407, 2016.
- [9] W. Liao, L. Zhang, and Z. Wei, "Multi-objective green meal delivery routing problem based on a two-stage solution strategy," *Journal of Cleaner Production*, vol. 258, p. 120627, 2020.
- [10] M. W. Ulmer, "Delivery deadlines in same-day delivery," *Logistics Research*, vol. 10, no. 3, pp. 1–15, 2017.
- [11] K. C. So and J.-S. Song, "Price, delivery time guarantees and capacity selection," *European Journal of Operational Research*, vol. 111, no. 1, pp. 28–49, 1998.
- [12] A. M. Arslan, N. Agatz, L. Kroon, and R. Zuidwijk, "Crowdsourced delivery-A dynamic pickup and delivery problem with ad hoc drivers," *Transportation Science*, vol. 53, no. 1, pp. 222–235, 2019.
- [13] V. E. Castillo, J. E. Bell, W. J. Rose, and A. M. Rodrigues, "Crowdsourcing last mile delivery: strategic implications and future research directions," *Journal of Business Logistics*, vol. 39, no. 1, pp. 7–25, 2018.
- [14] I. Dayarian and M. Savelsbergh, "Crowdshipping and same-day delivery: employing in-store customers to deliver online orders," *Production and Operations Management*, vol. 29, no. 9, pp. 2153–2174, 2020.
- [15] N. Kafle, B. Zou, and J. Lin, "Design and modeling of a crowdsource-enabled system for urban parcel relay and delivery," *Transportation Research Part B: Methodological*, vol. 99, pp. 62–82, 2017.
- [16] Y. Wang, S. Peng, X. Guan et al., "Collaborative logistics pickup and delivery problem with eco-packages based on time-space network," *Expert Systems with Applications*, vol. 170, Article ID 114561, 2021.
- [17] E. P. Jack and T. L. Powers, "A review and synthesis of demand management, capacity management and performance in health-care services," *International Journal of Management Reviews*, vol. 11, no. 2, pp. 149–174, 2009.
- [18] A. F. Veinott and H. M. Wagner, "Optimal capacity scheduling-II," *Operations Research*, vol. 10, no. 4, pp. 533–546, 1962.
- [19] J. Yoon, H. Yildiz, and S. S. Talluri, "Risk management strategies in transportation capacity decisions: an analytical approach," *Journal of Business Logistics*, vol. 37, no. 4, pp. 364–381, 2016.
- [20] J. Zhang, F. Liu, J. Tang, and Y. Li, "The online integrated order picking and delivery considering Pickers' learning effects for an O2O community supermarket," *Transportation Research Part E: Logistics and Transportation Review*, vol. 123, pp. 180–199, 2019.
- [21] G. Berbeglia, J.-F. Cordeau, and G. Laporte, "Dynamic pickup and delivery problems," *European Journal of Operational Research*, vol. 202, no. 1, pp. 8–15, 2010.
- [22] J.-F. Cordeau and G. Laporte, "The dial-a-ride problem: models and algorithms," *Annals of Operations Research*, vol. 153, no. 1, pp. 29–46, 2007.
- [23] G. Clarke and J. W. Wright, "Scheduling of vehicles from a central depot to a number of delivery points," *Operations Research*, vol. 12, no. 4, pp. 568–581, 1964.
- [24] L. He, "Research on route optimization of takeout delivery vehicles considering occasional road congestion," *Frontiers in Economics and Management*, vol. 1, no. 10, pp. 96–102, 2020.
- [25] K. Braekers and A. A. Kovacs, "A multi-period dial-a-ride problem with driver consistency," *Transportation Research Part B: Methodological*, vol. 94, pp. 355–377, 2016.
- [26] G. Ghiani, E. Manni, A. Quaranta, and C. Triki, "Anticipatory algorithms for same-day courier dispatching," *Transportation Research Part E: Logistics and Transportation Review*, vol. 45, no. 1, pp. 96–106, 2009.
- [27] M. A. Klapp, A. L. Erera, and A. Toriello, "The dynamic dispatch waves problem for same-day delivery," *European Journal of Operational Research*, vol. 271, no. 2, pp. 519–534, 2018.
- [28] T. Gschwind and M. Drexel, "Adaptive large neighborhood search with a constant-time feasibility test for the dial-a-ride problem," *Transportation Science*, vol. 53, no. 2, pp. 480–491, 2019.
- [29] N. Azi, M. Gendreau, and J.-Y. Potvin, "A dynamic vehicle routing problem with multiple delivery routes," *Annals of Operations Research*, vol. 199, no. 1, pp. 103–112, 2012.
- [30] Q. Gu, T. Fan, F. Pan, and C. Zhang, "A vehicle-UAV operation scheme for instant delivery," *Computers & Industrial Engineering*, vol. 149, p. 106809, 2020.
- [31] B. Yildiz, M. Savelsbergh, and M. Savelsbergh, "Provably high-quality solutions for the meal delivery routing problem," *Transportation Science*, vol. 53, no. 5, pp. 1372–1388, 2019.
- [32] S. A. Voccia, A. M. Campbell, and B. W. Thomas, "The same-day delivery problem for online purchases," *Transportation Science*, vol. 53, no. 1, pp. 167–184, 2019.
- [33] M. W. Ulmer and B. W. Thomas, "Same-day delivery with heterogeneous fleets of drones and vehicles," *Networks*, vol. 72, no. 4, pp. 475–505, 2018.
- [34] M. W. Ulmer and S. Streng, "Same-Day delivery with pickup stations and autonomous vehicles," *Computers & Operations Research*, vol. 108, no. 8, pp. 1–19, 2019.
- [35] M. A. Klapp, A. L. Erera, and A. Toriello, "Request acceptance in same-day delivery," *Transportation Research Part E: Logistics and Transportation Review*, vol. 143, p. 102083, 2020.
- [36] R. W. Bent and H. Van, "Scenario-based planning for partially dynamic vehicle routing with stochastic customers," *Operations Research*, vol. 52, no. 6, pp. 977–987, 2004.
- [37] B. Li, D. Krushinsky, T. Van Woensel, and H. A. Reijers, "An adaptive large neighborhood search heuristic for the share-a-ride problem," *Computers & Operations Research*, vol. 66, pp. 170–180, 2016.
- [38] Z. Steever, M. Karwan, and C. Murray, "Dynamic courier routing for a food delivery service," *Computers & Operations Research*, vol. 107, pp. 173–188, 2019.
- [39] W. Wang and L. Xie, "Optimal pricing of crowdsourcing logistics services with social delivery capacity," *Journal of Combinatorial Optimization*, pp. 1–23, 2021.
- [40] P. Toth and D. Vigo, "Models, relaxations and exact approaches for the capacitated vehicle routing problem," *Discrete Applied Mathematics*, vol. 123, no. 1-3, pp. 487–512, 2002.
- [41] J.-F. Cordeau and G. Laporte, "A tabu search heuristic for the static multi-vehicle dial-a-ride problem," *Transportation Research Part B: Methodological*, vol. 37, no. 6, pp. 579–594, 2003.
- [42] F. Lehuédé, R. Masson, S. N. Parragh, O. Péton, and F. Tricoire, "A multi-criteria large neighbourhood search for the transportation of disabled people," *Journal of the Operational Research Society*, vol. 65, no. 7, pp. 983–1000, 2014.

Research Article

Vehicle Routing Problem for Collaborative Multidepot Petrol Replenishment under Emergency Conditions

Guangcan Xu ¹ and Qiguang Lyu ²

¹School of Economics and Management, Chongqing Jiaotong University, Chongqing 400074, China

²School of Business Administration, Chongqing University of Science & Technology, Chongqing 401331, China

Correspondence should be addressed to Guangcan Xu; xgc@cqjtu.edu.cn and Qiguang Lyu; lvresearch@163.com

Received 29 January 2021; Revised 26 March 2021; Accepted 8 April 2021; Published 19 April 2021

Academic Editor: Zheng Wang

Copyright © 2021 Guangcan Xu and Qiguang Lyu. This is an open access article distributed under the Creative Commons Attribution License, which permits unrestricted use, distribution, and reproduction in any medium, provided the original work is properly cited.

In recent years, emergency events have affected urban distribution with increasing frequency. For example, the 2019 novel coronavirus has caused a considerable impact on the supply guarantee of important urban production and living materials, such as petrol and daily necessities. On this basis, this study establishes a dual-objective mixed-integer linear programming model to formulate and solve the cooperative multidepot petrol emergency distribution vehicle routing optimization problem with multicompartment vehicle sharing and time window coordination. As a method to solve the model, genetic variation of multiobjective particle swarm optimization algorithm is considered. The effectiveness of the proposed method is analyzed and verified by first using a small-scale example and then investigating a regional multidepot petrol distribution network in Chongqing, China. Cooperation between petrol depots in the distribution network, customer clustering, multicompartment vehicle sharing, time window coordination, and vehicle routing optimization under partial road blocking conditions can significantly reduce the total operation cost and shorten the total delivery time. Meanwhile, usage of distribution trucks is optimized in the distribution network, that is, usage of single- and double-compartment trucks is reduced while that of three-compartment trucks is increased. This approach provides theoretical support for relevant government departments to improve the guarantee capability of important materials in emergencies and for relevant enterprises to improve the efficiency of emergency distribution.

1. Introduction

The collaborative multidepot petrol distribution vehicle routing problem under emergency conditions (CMPDVRPE) is an extension of the multidepot petrol station replenishment problem (MPSRP) [1]. Factors such as blocked roads under emergency conditions, cooperation among petrol depots (PDs), and distribution resources sharing are considered. CMPDVRPE optimizes vehicle routing arrangement in emergency environments through multicompartment vehicle sharing and demand time window coordination (TWC) and then reduces the total network operating cost and shortens the total delivery time. As early as 1995, multicompartment vehicle has been used to study oil distribution [2], and it is widely used in oil supply. In recent years, various emergencies, such as earthquakes

and traffic accidents, have been occurring all over the world and cause road traffic blocks or closures and affect the use of several road lines. In particular, the 2019 novel coronavirus (COVID-19) outbreak in 2020 has spread around the world, causing road closures in many cities and communities and severely affecting the transportation and supply of important production and daily necessities. Such cases show the importance of the efficient and timely supply of petrol, an important material for production and daily life.

In the existing petrol distribution network, each depot is only responsible for specific petrol stations (PSs) in the region. PDs are independent of each other and lack coordination and sharing of distribution business and resources. In an emergency, roadblocks cause detours for several distribution trucks, resulting in low distribution efficiency and timeliness of the entire network. Furthermore, in such

cases, petrol is an important and necessary material, such as the replenishment demand of vehicles for disaster relief and medical treatment, and thus, ensuring its efficient and timely supply is of considerable significance for rescue and recovery. Therefore, cooperation between regional PDs must be enhanced and the routing arrangement of distribution trucks should be optimized through resource sharing and business coordination of multidepots on the premise of partial road blocking. This cooperation can effectively reduce the operation cost of the entire petrol distribution network, improve the efficiency of emergency petrol distribution in the region, shorten the total distribution time in the region, and ensure the timely supply of important production and living materials such as petrol.

In this study, multicompartment truck sharing (TS), TWC, truck route detour, and a cooperation mechanism are integrated into the traditional MPSRP as CMPDVRPE. An optimal mathematical model is established to minimize the total operating cost and total delivery time to optimize the CMPDVRPE and get good results. An improved multi-objective particle swarm optimization (MOPSO) algorithm considering genetic variation (GV) is designed to achieve the near-optimal solution. Correlation results before and after optimization are compared and analyzed, and the solution of CMPDVRPE can improve the efficiency and rationality of vehicle routing arrangement of petrol distribution networks. First, petrol products have special distribution natures, such as product diversification, and cannot be mixed. Second, multidepot cooperation, multicompartment vehicle use, different TWC mechanisms, and vehicle routing optimization are comprehensively considered to propel the sustainable development of vehicle routing problem (VRP) theory [3, 4] and emergency urban transportation system.

The remaining parts of this paper are organized as follows. In Section 2, relevant studies on petrol distribution optimization considering multidepot cooperation and vehicle routing optimization are reviewed. In Section 3, a practical example of CMPDVRPE is presented and a mathematical model is established using notations and definitions to minimize total operating costs and total delivery time. In Section 4, an improved heuristic algorithm is introduced to solve CMPDVRPE. In Section 5, a small-scale example and a case study in Chongqing City in China are conducted to verify the applicability of the proposed methodology. In Section 6, the conclusions and future directions are provided.

2. Literature Review

In the past few decades, relatively little research has been carried out on petrol replenishment in academic circles. Existing research focuses on the distribution of petrol in a single depot and the variations of PS replenishment problem. For example, the multiperiod, time window (TW), trip packing, and multidepot with TWS are separately considered for PSRP [1, 5–7], which with its related problems attract increasing research focus for their practical importance. Popović et al. [8] proposed a heuristic algorithm based on variable neighborhood search to solve the multiproduct

and multiperiod inventory routing problem (IRP) for multicompartment homogeneous vehicles. Their method proved superior to other optimization methods. Vidović et al. [9] developed a mixed-integer programming model and a heuristic method to observe its effects on multiproduct multiperiod IRP in fuel supply. Wang et al. [10] proposed a mathematical model considering petrol trucks returning multiple times to a depot, solved using a heuristic algorithm according to a local branch-and-bound search with a Tabu list and the Metropolis acceptance criterion. Wang et al. [11] constructed an adaptive large neighborhood search (ALNS) to solve the fuel replenishment problem (FRP) and performed sensitivity analysis on different features, including the number of vehicles, products, and vehicle compartments and capacities.

The above studies directly relate to the replenishment problem of PSs. However, the models mainly considered the multicompartment vehicle transportation and time window assignment (TWA). Huang [12] proposed the Tabu search to solve an advanced capacitated location routing problem in a distribution network with multiple pickup and delivery routes. Derigs et al. [13] introduced a formal model, an integer programming formula, and reference set of 200 examples for a class of delimited general VRP with compartments and presented a set of heuristic component solvers. Lahyani et al. [14] optimized a rich multiproduct, multiperiod, and multicompartment vehicle route for the collection of olive oil in Tunisia using mathematical formulas, especially a precise branch-and-cut algorithm. Coelho and Laporte [15] defined and compared four main categories of the multicompartment delivery problem (MCDP). The study proposed formulas and models for specific MCDP cases and versions and then described a branch-and-cut algorithm that works for all variants. Ostermeier and Hübner [16] identified vehicle-related costs in empirical data collection and used a large neighborhood to solve grocery delivery for an extended multicompartment vehicle routing problem (MCVRP). Qi et al. [17] proposed a VRP method for large-scale TW based on spatiotemporal partitioning using a genetic algorithm (GA) to cluster large-scale customers with K-medoid. Moreira et al. [18] presented a new method to solve the time window assignment vehicle routing problem (TWAVRP) where TWS is defined for multiple product segments. A mathematical heuristic method based on fixed optimization is used to solve the two-stage stochastic optimization problem. Martins et al. [19] extended research on MCVRP by tackling a multiperiod environment with a product-oriented TWA and proposed an adaptive large neighborhood search as a solution. Esh-tehadi et al. [20] studied the VRP with multicompartment vehicles operating from a single depot to visit customers within the chosen time period by minimizing major operational costs.

One part of CMPDVRPE literature focuses on the cooperation in distribution networks, which largely influences the arrangement of vehicle routes and the entire network efficiency. Wang et al. [21] established an intraregional oil distribution model with allocation quantity and route as decision variables to extend the multidepot half-open VRP

with TWS and then used GA as a solution. Wang et al. [22] used a mixed-integer linear programming model to minimize the total operating cost of the nonempty two-echelon heterogeneous cooperative logistics network alliance and the GA-particle swarm optimization (PSO) algorithm to reallocate customer clustering units. Wang et al. [23] established a biobjective programming model to optimize the total operation routing cost and the total number of delivery vehicles for collaborative multidepot VRP with TWA (CMDVRPTWA). The model was solved using a hybrid heuristic algorithm consisting of K-means clustering, Clark–Wright (CW) saving algorithm, and an extended nondominated sorting genetic algorithm-II (E-NSGA-II).

Another part of the CMPDVRPE literature focuses on the VRP in emergency distributions. Sheu [24] presented a hybrid fuzzy clustering-optimization approach to the emergency logistics codistribution response to the urgent relief demands in the crucial rescue period. Zhang and Xiong [25] studied the routing optimization problem of grain emergency vehicle scheduling with three objectives and presented a hybrid algorithm as a solution based on combining artificial immune and ant colony optimization (ACO) algorithms. Huizing et al. [26] described a mixed-integer linear program and several increasingly refined heuristics for the optimization problem of timetabling jobs and moving responders over a discrete network. A large set of benchmark instances, both from real-life case study data and from a generator, was created for the study.

Generally speaking, the mathematical model of VRP is hard NP, which requires solutions using appropriate algorithms. Kuo et al. [27] proposed a hybrid PSO with GA (HPSOGA) for solving capacitated VRP with fuzzy demand (CVRPFD). Wang et al. [28] minimized the total cost of the two-echelon logistics distribution network using a hybrid extended PSO and GA (EPSO-GA), which combines the merits of global and local search capabilities. Zhou et al. [29] proposed two partheno GA (PGA) and adapted PSO and one state-of-the-art method to solve the multiple traveling salesman problem (MTSP).

The above studies tackle plentiful MPSRP aspects but suffer from the following issues. (1) The vehicle routing optimized design procedure rarely considers the cooperation among PDs by regional partitioning. (2) Minimal attention is paid to distribution TS, multicompartment truck application, roadblocks, and transship transportation in a collaborative multidepot optimization network. (3) Single intelligent algorithm and heuristic approach are difficult to apply directly to a specific scale of CMPDVRPE with numerous PSs.

Combining observations in Table 1, the main contributions of the present study lie in the following aspects. (1) A cooperation mechanism is proposed based on the regional partitioning method and a collaborative multidepot PS replenishment VRP with emergency conditions is constructed. (2) A mixed-integer linear programming model is established on the basis of the minimum total operating cost and total delivery time for CMPDVRPE. (3) An improved MOPSO algorithm is designed to effectively address the optimization model. (4) Finally, a small-scale example and a

real-world case study are used to assess the applicability of the proposed model and approach and then compare the costs and delivery time before and after the vehicle routing optimization. In addition, this study lays a foundation and strategy for optimizing the VRP in emergencies and is conducive to improving its application range.

3. Problem Statement and Model Formulation

3.1. Problem Statement. CMPDVRPE integrates the problems of cooperative VRP, TS, roadblocks, and TWAs. Figure 1 illustrates a noncooperative petrol distribution network in which PDs operate independently and serve only their own customers. Roads blocked in an emergency can severely affect the timely supply of petrol. As such, long-haul deliveries are inevitable. A single PD also needs a large number of delivery petrol tankers to meet the different demands and TW requirements of its customers. This case results in a substantial decrease in distribution efficiency and increase in distribution costs. Given the numerous cross-transportations, delivery times dramatically increase and cannot be controlled.

Figure 2 displays an optimized petrol distribution network with cooperation, vehicle routing optimization, roadblocks, TS, and TWAs. In this network, large tankers transfer petrol across depots and are responsible for petrol delivery to many or a single PS. This cooperation leads to more efficient and reasonable distribution routes than the noncooperative distribution network. The delivery times, required number of petrol distribution trucks, and service scope of each PD are likewise reduced.

Based on the regional partitioning method, the transport time between PDs and stations is used to cluster corresponding PSs. Then appropriate distribution trucks are selected and distribution routes are arranged according to the demand of different petrol, demand TW, and roadblocks to each PS.

Seven assumptions underline the corresponding mathematical model. (1) In a relatively short working period, each PS only generates one distribution order for petrol demand. For each kind of petrol, the demand does not exceed the maximum loading capacity of most distribution truck compartments. (2) Each customer (PS) can only be served once in a working period, that is, only one distribution truck is used for its delivery service. (3) The petrol transfer and distribution trucks have constant transportation speed. (4) During a working period, distribution trucks may be dispatched repeatedly if time permits, regardless of the transfer time across PDs. (5) The loading and unloading service times of PDs and stations are related not to the petrol type but to the truck type and operational quantity. (6) Every 10 minutes is the time unit. (7) No consideration is given to the restriction of road geometry on multicompartment vehicles.

3.2. Model Formulation. The proposed model is mathematically formulated as an optimization problem to minimize the total cost and delivery time when each PD is assigned to serve a group of PSs and VRP with different

TABLE 1: Comparison between existing literature and the present study.

Study	Regional partitioning	Stations per trip	Time windows	Multicompartment	Fleet sharing	Emergency conditions
Cornillier et al. [1]	No	Several	Yes	Yes	No	No
Govindan et al. [30]	No	Several	Yes	No	No	No
Lahyani et al. [14]	No	Several	No	Yes	No	No
Wang et al. [28]	No	Several	Yes	No	Yes	No
Zhang et al. [25]	No	Several	No	No	No	Yes
Wang et al. [31]	No	Several	No	Yes	No	No
Xu et al. [32]	Yes	One	Yes	Yes	Yes	No
This study	Yes	Several	Yes	Yes	Yes	Yes

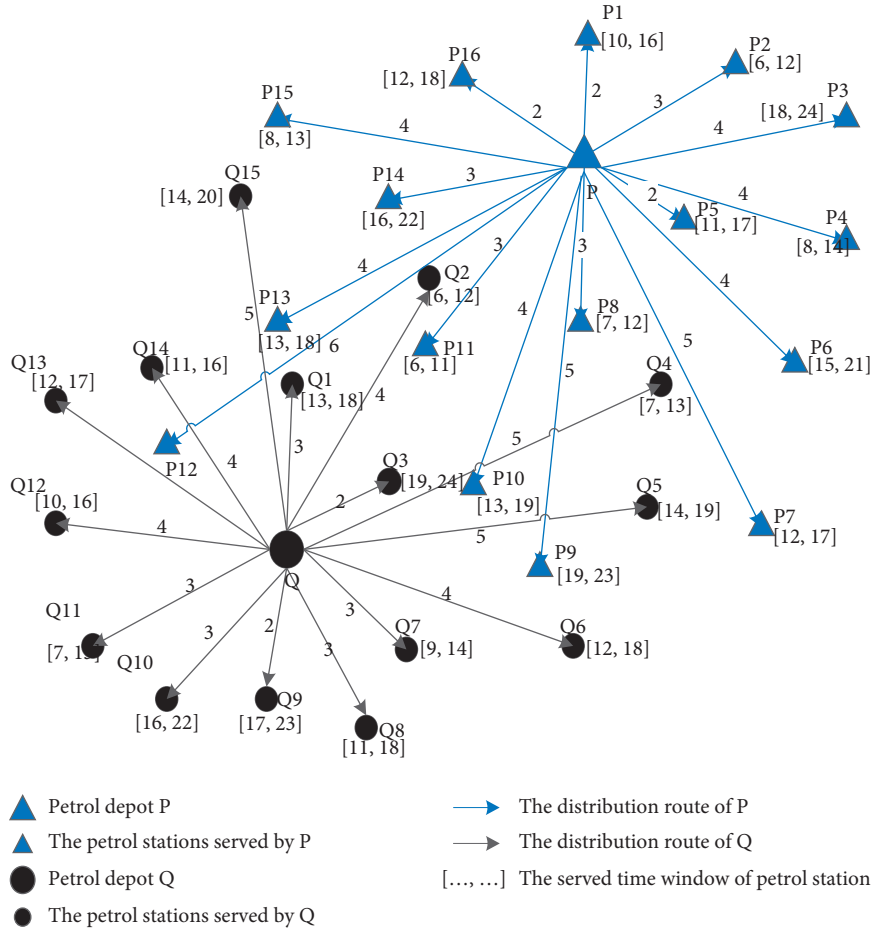


FIGURE 1: Noncooperative petrol distribution network.

trucks and TWS [20, 33]. Tables 2 and 3 list the related notations and definitions in the CMPDVRPE optimization and the judgement variables, respectively.

CMPDVRPE is formulated as a mixed-integer linear programming model to minimize the total cost and delivery time. The cost function contains four components, namely, C_1 , C_2 , C_3 , and C_4 , which are described below.

Equation (1) shows the formulation for C_1 , which denotes the transport cost of tankers that transfer petrol between PDs during a working period:

$$C_1 = \sum_{g,h \in D} \sum_{o \in O} \sum_{p \in P} (f_o \times P_F \times t_{gh}^D \times x_{gho}^p). \quad (1)$$

Equation (2) shows the formulation for C_2 , which denotes the transportation costs of petrol distribution trucks during a working period, including transportation costs from the PD to the PS and from PS to PS:

$$C_2 = \sum_{i \in DUS} \sum_{j \in S} \sum_{k \in K} (f_k \times P_F \times t_{ij}^{DUS} \times x_{ijk}). \quad (2)$$

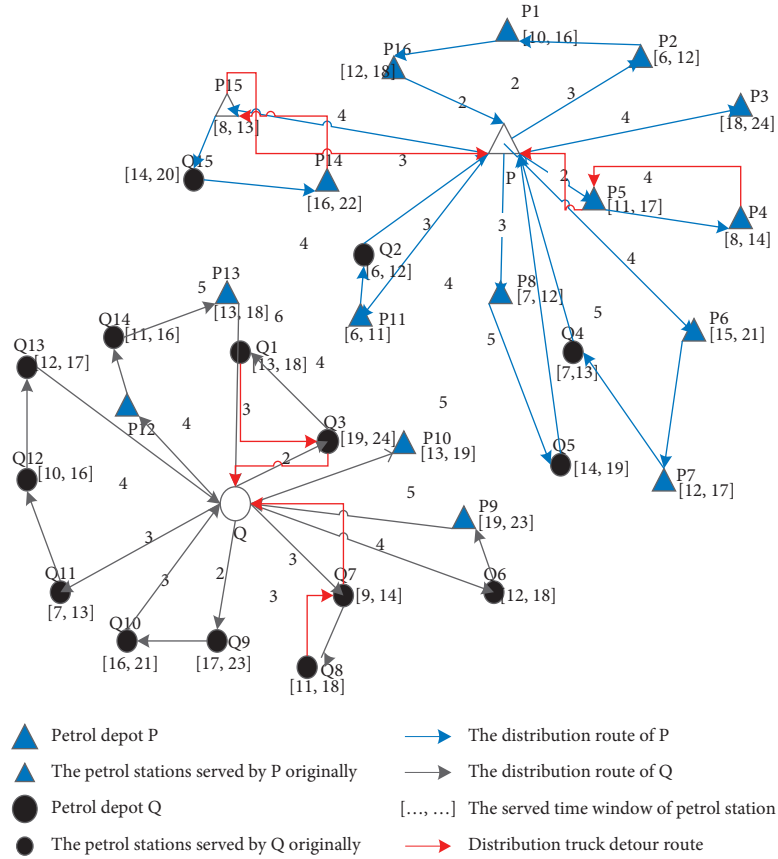


FIGURE 2: Cooperative petrol distribution network.

Equation (3) shows the formulation for C_3 , which denotes the penalty cost of the distribution truck arriving early or late at the PS, that is, the impact of the distribution truck

arrival time on the cost under the premise of fixed service TW at the PS:

$$C_3 = \sum_{i \in DUS} \sum_{j \in S} \sum_{k \in K} x_{ijk} \times \mu_e \times [\max\{\alpha_j - tr_{jk}, 0\}] + \sum_{i \in DUS} \sum_{j \in S} \sum_{k \in K} [\max\{tr_{jk} - \beta_j\}]. \quad (3)$$

Equation (4) shows the formulation for C_4 , which denotes the maintenance cost of all petrol tankers in a working period, and the fixed cost of the PD after considering the

incentive of the government competent authority or leader of the cooperative alliance:

$$C_4 = \sum_{g,h \in D} \sum_{o \in O} \sum_{p \in P} \left(\frac{xd_{gho}^p \times q_{ghp}}{Q^o} \times \frac{M_o}{N_w} \right) + \sum_{i \in D} \sum_{j \in S} \sum_{k \in K} \left(x_{ijk} \times \frac{M_k}{N_w} \right). \quad (4)$$

The optimization model of CMPDVRPE is defined as follows:

subject to

$$\min TC_1 = C_1 + C_2 + C_3 + C_4, \quad (5)$$

$$\sum_{i \in DUS} \sum_{j \in S} x_{ijk} \leq 1, \quad \forall k \in K, \quad (7)$$

$$\min TC_2 = \sum_{k \in K} \sum_{i \in DUS} \sum_{j \in S} t_{ijk}, \quad (6)$$

$$\sum_{j \in DUS} x_{ijk} - \sum_{j \in DUS} x_{jik} = 0, \quad \forall i \in DUS, \forall k \in K, \quad (8)$$

TABLE 2: Notations and definitions in CMPDVRPE.

Symbol	Description
D	Set of petrol depot, $i \in D$
S	Set of petrol station, $j \in S$
P	Set of petrol, $p \in P$
O	Set of petrol tanker, $o \in O$
K	Set of petrol distribution truck, $k \in K$
f_o	Fuel consumption per time unit of a petrol tanker, $o \in O$
f_k	Fuel consumption per time unit of petrol distribution truck, $k \in K$
P_F	Fuel price
Q^o	Loading capacity of petrol tanker, $o \in O$
Q^k	The loading capacity of single compartment of truck k , $k \in K$
t_{gh}^D	The transport time from petrol depot g to h , $g, h \in D$
$t_{ij}^{D \cup S}$	The transport time from the depot to the petrol station or from the petrol station to another, $i \in D \cup S, j \in S$
$[m_i, n_i]$	The working hours of petrol depot i , $i \in D$
$[\alpha_i, \beta_j]$	The service time window of petrol station, $j \in J$
t_{ik}	The departure time of distribution truck k from petrol depot i , $i \in D, k \in K$
tr_{ik}	The time of distribution truck k returning to the petrol depot i or arriving at the petrol station i , $i \in D \cup S, k \in K$
t_{ijk}	The driving time of distribution truck k from petrol depot i to petrol station j or petrol station i to j , $i \in D \cup S, j \in S, k \in K$
T	The maximum travel time allowed for each distribution truck
μ_e	The penalty cost per unit of time for distribution trucks arriving early
μ_d	The penalty cost per unit of time for distribution trucks arriving late
M_o	The annual maintenance cost of a petrol tanker, $o \in O$
M_k	The annual maintenance cost of distribution truck k , $k \in K$
q_{ghp}	During a working period, the amount of petrol p is transferred from depot g to h , $g, h \in D, p \in P$
q_{jp}	During a working period, the demand of petrol station j for petrol p , $j \in J, p \in P$
q_j^{kp}	During a working period, the amount of petrol p delivered to the petrol station j by the distribution truck k , $j \in S, k \in K, p \in P$
C^{kp}	Integer variable, the number of compartments of distribution truck k loaded with petrol p , $k \in K, p \in P$
Q_d	Service capacity of depot d during a working period, $d \in D$
FI_i	The fixed cost of petrol depot i in a working period, that is, when the petrol depot i joins the cooperative network, the fixed cost can be covered by the rewards given to the partners by the government authorities or the cooperative alliance leaders, $i \in D$
N_i	The number of distribution trucks at petrol depot i serving petrol stations during a working period, $i \in D$
N_k	The number of compartments for distribution trucks, $k \in K$
N_w	The number of working periods per year

TABLE 3: Judgement variables.

Decision variables	Definition
x_{ijk}	When the distribution truck k serving route (i, j) , the variable value is 1; otherwise, it is 0, $i \in D \cup S, j \in S, k \in K$
xd_{gho}^p	When the petrol tanker o transfers the petrol p from the petrol depot g to h , the variable is 1; otherwise, it is 0, $g, h \in D, o \in O, p \in P$
y_j^k	When the petrol station j is visited by the distribution truck k , the variable is 1; otherwise, it is 0, $j \in J, k \in K$
ω_{ijkd}	When the distribution truck k starts from the petrol depot d and passes through the route (i, j) , the variable is 1; otherwise, it is 0, $d \in D, i, j \in S, k \in K$
r_{gjh}	When the serving petrol depot of petrol station j is adjusted from g to h after the petrol distribution network optimization, the variable is 1; otherwise, it is 0, $g, h \in D, j \in S$
CO_i	When depot i agrees to join the cooperative petrol distribution network, the variable is 1; otherwise, it is 0, $i \in D$

$$\sum_{p \in P} C^{kp} \leq N_k, \quad \forall k \in K, \quad (9) \quad \sum_{j \in S} q_j^{kp} \leq C^{kp} Q^k, \quad \forall k \in K, p \in P, \quad (13)$$

$$0 \leq C^{kp} \leq N_k, \quad \forall k \in K, p \in P, \quad (10) \quad 0 \leq q_j^{kp} \leq \min\{Q^k N_k, q_{jp}\}, \quad \forall j \in S, k \in K, p \in P, \quad (14)$$

$$\sum_{k \in K} y_j^k q_j^{kp} = q_{jp}, \quad \forall j \in S, p \in P, \quad (11) \quad \sum_{p \in P} \sum_{k \in K} y_j^k q_j^{kp} = \sum_{p \in P} q_{jp}, \quad \forall j \in S, \quad (15)$$

$$q_j^{kp} \leq y_j^k Q^k N_k, \quad \forall j \in S, k \in K, \quad (12) \quad \sum_{j \in S} \sum_{p \in P} y_j^k q_j^{kp} \leq Q^k N_k, \quad \forall k \in K, \quad (16)$$

$$\sum_{g,h \in D} \sum_{p \in P} x d_{gho}^p q_{ghp} \leq Q^o, \quad \forall o \in O, \quad (17)$$

$$q_{ghp} = \sum_{j \in S} r_{gjh} q_{jp}, \quad \forall g, h \in D, p \in P, \quad (18)$$

$$m \leq t_{ik} \leq n, \quad \forall i \in D, \forall k \in K, \quad (19)$$

$$m \leq tr_{ik} \leq n, \quad \forall i \in D, k \in K, \quad (20)$$

$$\sum_{i \in D \cup S} \sum_{j \in S} t_{ijk} \leq T, \quad \forall k \in K, \quad (21)$$

$$t_{ik} + t_{ijk} = tr_{jk}, \quad \forall i \in D \cup S, \forall j \in S, \forall k \in K, \quad (22)$$

$$\alpha_j \leq tr_{jk} \leq \beta_j, \quad \forall j \in S, \forall k \in K, \quad (23)$$

$$\sum_{i,j \in S} x_{ijk} \leq |s| - 1, \quad \forall s \subset S, |s| \geq 2, \forall k \in K, \quad (24)$$

$$x_{ijk} = \{0, 1\}, \quad \forall i \in D \cup S, \forall j \in S, \forall k \in K, \quad (25)$$

$$x d_{gho}^p = \{0, 1\}, \quad \forall g, h \in D, \forall o \in O, \forall p \in P, \quad (26)$$

$$y_j^k = \{0, 1\}, \quad \forall j \in S, \forall k \in K, \quad (27)$$

$$\omega_{ijkd} = \{0, 1\}, \quad \forall d \in D, \forall i, j \in S, i \neq j, \forall k \in K, \quad (28)$$

$$r_{gjh} = \{0, 1\}, \quad \forall g, h \in D, \forall j \in S, \quad (29)$$

$$CO_i = \{0, 1\}, \quad \forall i \in D. \quad (30)$$

Equations 5 and (6) show the objective functions that minimize the total cost and total delivery time of the regional petrol distribution network, respectively. Constraint (7) stipulates that each distribution truck is required to serve at most one PD and one distribution route. Constraint (8) ensures flow conservation. Constraint (9) ensures that only one kind of petrol can be loaded into each distribution truck compartment, that is, the petrol cannot be mixed. Constraint (10) ensures that the number of compartments of the distribution truck k loaded with petrol p is less than the total number of compartments. Constraint (11) indicates that the total amount of all distribution trucks that deliver to PS j is equal to the station demand for petrol p . Constraint (12) ensures that the amount of petrol p distributed by the distribution truck k to PS j is not greater than the total truckload. Constraint (13) ensures that the distribution truck does not deliver more petrol p than it loads. Constraint (14) indicates that the amount of petrol p delivered by the distribution truck to PS j should not be greater than the smaller value between its maximum loading and the demand of the PS j for petrol p . Constraint (15) ensures that the PS demand for a product can only be delivered by one distribution truck. Constraint (16) stipulates that the distribution truck k is required to deliver no more petrol than its total loading

capacity to all the stations visited. Constraint (17) ensures that the amount of petrol transferred between depots is not greater than the loading capacity of tankers. Constraint (18) indicates that the amount of petrol p transferred from PD g to h is equal to the demand for p from the newly added service stations after optimization of the cooperative network. Constraints (19) and (21) specify the service time of the PD and the maximum duration constraint of the distribution truck travel. Constraints (22) and (23) constrain the time of distribution truck serving PS. Constraint (24) represents the elimination of subloop constraints. Equations (25) and (30) are judgement and decision variables.

4. Solution Methodology

4.1. PSO. As a method of evolutionary computing, PSO was proposed in 1995 by Eberhart, an American electrical engineer, and Kennedy, a social psychologist. By observing the foraging behavior of birds, the authors believed that at first, the birds do not know where the food but come closer and closer to the food through a kind of information exchange. This information includes the adaptability of each bird to estimate its own position according to certain rules, ability of each bird to remember its best position, and the best position found by all the birds in the flock. The best position found by the bird group is called individual optimal “*pbest*,” while the best position found by the whole bird group is called global optimal “*gbest*” [34].

In PSO, the entire population is called particle swarm, and each individual in the population is called a particle. The target is a search space, and the position of each particle is a potentially feasible solution. Each particle in space adjusts its flight path based on personal and group experience to find the optimal solution.

Suppose the population is composed of n particles, and in a D -dimensional target search space, each particle can be regarded as a point in space, then $x_i = \{x_{i1}, x_{i2}, \dots, x_{iD}\}$ represents the D -dimensional vector of particle i ($i = 1, 2, \dots, m$). A particle flies in space at a certain speed, as $v_i = \{v_{i1}, v_{i2}, \dots, v_{iD}\}$. Generally, the fitness represented by the objective function is used to calculate the current particle fitness value, to judge the advantages and disadvantages of the particle position. The local optimal particle position is $pbest = \{pbest_{i1}, pbest_{i2}, \dots, pbest_{iD}\}$. At the same time, the best adaptive value experienced by the entire particle swarm is the global optimal value, $gbest = \{gbest_{i1}; gbest_{i2}, \dots, gbest_{iD}\}$. The particle optimizes the search process iteratively, and for each of its generation, the d ($1 \leq d \leq D$) dimensional position and velocity are updated by the following equation iteration [34]:

$$v_{id}(t+1) = v_{id}(t) + c_1 r_1 (pbest_{id}(t) - x_{id}(t)) + c_2 r_2 (gbest_{id}(t) - x_{id}(t)), \quad (31)$$

$$x_{id}(t+1) = x_{id}(t) + v_{id}(t+1), \quad (32)$$

where c_1, c_2 are the learning coefficients, also known as the acceleration coefficients, and $r_1, r_2 = \text{rand}[0, 1]$, namely, r_1, r_2 are the random numbers between 0 and 1.

4.2. *MOPSO*. The single-objective optimization problem only needs to obtain a single or a set of continuous optimal solutions, while the multiobjective optimization problem generally obtains a set of continuous solutions. For the basic PSO, all particles converge in one direction following the best particle (leader), and thus, the single-objective optimization problem can be solved. When solving the multi-objective optimization problem, *pbest* (individual optimal solution) and *gbest* (globally optimal solution) cannot be directly determined due to the lack of a single optimal solution, and thus, the basic PSO method cannot be directly adopted.

In fact, the solution of the multiobjective optimization problem is composed of a set of noninferior solutions. Different particles seek different “leaders” in the optimization. The noninferior solutions are stored in the “external container” (archive). Furthermore, by evaluating the “quality” of these solutions, the *gbest* is determined to realize the guidance of particle iterative updating. Clearly, the archived solution can represent the optimal subset of particles that the algorithm finds in each generation of particle swarm, and thus, considering the archived set as a candidate set for the *gbest* is appropriate [35].

MOPSO is a cyclic process. When the algorithm starts, the first-generation noninferior solution is found from the initialized particle swarm and stored in the external archive. Subsequently, the *gbest* is selected from the external container by comparison, and then, the particle swarm updates the speed and position through equations (31) and (32). Then, the loop operation is repeated.

Based on the generation of new nondominant solutions after each particle iteration, the external archive set size, and thereby the computation, increases after multiple iterations. Therefore, considering the effect of computational complexity, limiting the size of external collections is necessary [35]. Once the number of solutions in the external archive collection reaches the upper limit set for the external container, the noninferior solutions in the external container are compared and a few are deleted according to certain rules.

In solving MOPSO, the evaluation criteria of particles, construction, and preservation of noninferior solutions, selection of optimal positions, and the processing of constraints are mainly used.

4.3. *IMOPSO*. PSO is characterized by rapid convergence speed, but for a multiobjective optimization problem, too fast convergence speed may cause particles to fall into the local optimal. Thus, achieving the global optimal becomes difficult. This problem may be prevented by introducing the mutation operation of particles.

In the early stage of the algorithm, the particle needs to search the entire target space to ensure the escape from the local optimal state and enhance the global search capability; in the late stage, a quick convergence is necessary to find the optimal solution. Thus, this study carries out mutation operation on particles through mutation probability. At the beginning of the algorithm, mutation should be carried out on all particles, and with the

increase of iteration, the number of particles undergoing mutation should be gradually reduced. According to the variation operation requirements, the variation probability of particle swarm after each update is set as follows [36]:

$$mp = 1 - \frac{P_{it}}{\max_{it}}, \quad (33)$$

where mp is the mutation probability, P_{it} is the current iterations, and \max_{it} is the maximum number of iterations. In reference to the nonuniform mutation operator in the GA, a random variable *rand* between 0 and 1 is assigned to each particle. If the random variable of particle *i* is less than the probability of variation, then random nonuniform variation operation is carried out on the *D*-dimensional particle position:

$$x_{id} = \begin{cases} x_{id} + \lambda \times v_{id} \times (1 - \text{rand}_i), & \text{rand}_i < 0.5, \\ x_{id} - \lambda \times v_{id} \times (1 - \text{rand}_i), & \text{rand}_i \geq 0.5. \end{cases} \quad (34)$$

In equation (34), λ is the system random parameter ($\lambda > 1$). During the variation operation, if the result is greater than the threshold set by the system, the variation result is set at the boundary of the threshold range.

In addition, to balance the global and local search capability of basic PSO, adding inertia weight is necessary [37], that is, the influence of inertia weight coefficient is considered when updating the velocity of particles. Therefore, the new velocity updating formula of particles is as follows:

$$v_{id}(t+1) = \omega v_{id}(t) + c_1 r_1 (p_{id}(t) - x_{id}(t)) + c_2 r_2 (g_{id}(t) - x_{id}(t)). \quad (35)$$

Combined with the basic PSO algorithm and MOPSO, Figure 3 describes the procedure of the IMOPSO algorithm. The steps of the MOPSO algorithm considering GV are as follows:

- (1) Initialization: set the particle swarm size, parameter coefficient, threshold, maximum number of iterations, and initial velocity and initial position of each particle.
- (2) Use equations (33) and (34) to carry out variation on particle swarm.
- (3) Calculate the fitness value of each particle.
- (4) Construct the set of noninferior solutions of particle swarm according to the construction algorithm of noninferior solutions.
- (5) Update the *pbest* of each particle according to Pareto dominance concept.
- (6) Update the external archive set according to the saving algorithm of noninferior solution.
- (7) Calculate the crowding distance of particles in the external archive. If the number of particles entering the external archive reaches the upper limit of the external archive size, the particles beyond the upper limit of the external archive size are removed in ascending crowding distance order.

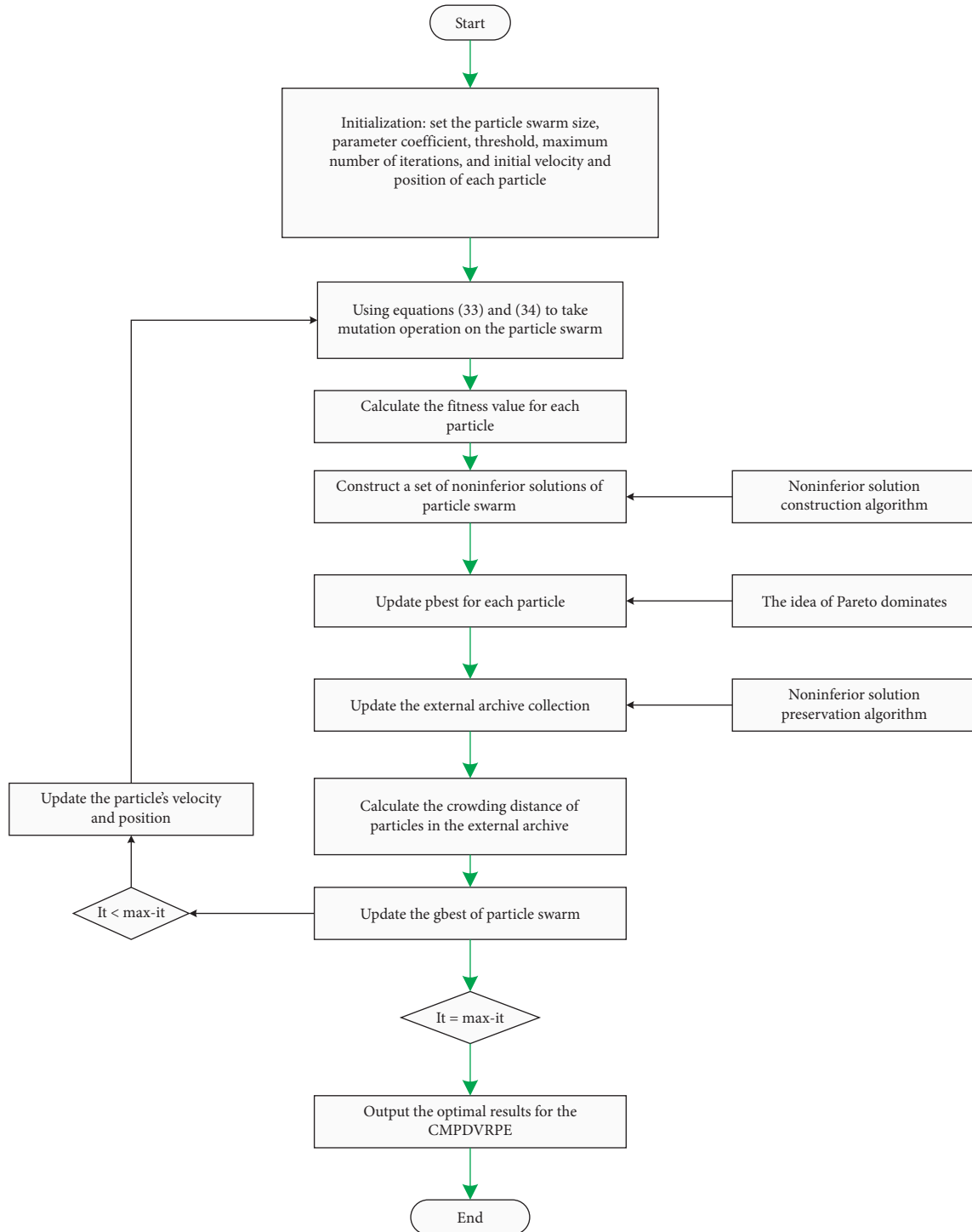


FIGURE 3: Flowchart of the IMOPSO algorithm.

- (8) Update the *gbest* of particle swarm. In the external archive, the front-end particles in descending order of crowding distance are randomly selected as the *gbest*.
- (9) Update the particle velocity and position according to equations (31) and (32), and return to step (2). When the maximum number of iterations is reached, the loop is terminated.

5. Case Study

5.1. Small-Scale Example. The quality of the proposed heuristic algorithm in solving the problem of multidepot vehicle routing with emergency effects is further demonstrated by a small example analysis. In this case, the petrol distribution network consists of two PDs and 31 PSs in the region. Under noncooperation, PD *P* is responsible for P1,

P2, . . . , P16 and other 16 PSs petrol distribution, while PD Q is responsible for Q1, Q2, . . . , Q15 and other 15 PSs petrol distribution. With cooperation according to the customer clustering and the distance between each PS and the PD, the PSs distributed by the two PDs are first repartitioned. In addition, distribution routes are blocked under emergency control. Then, the two PDs can share the petrol distribution trucks. The customers and routes of the distribution truck can be decided according to the demand TW, demand characteristics (including petrol products and quantity demand), and transportation distance and detour route of each petrol station in one distribution task, as shown in Figure 2.

For the convenience of calculation, the following assumption is made for this example: the demand of petrol product of PSs is divided into three categories, namely, nos. 92, 95, and 98. The distribution trucks have three types: single compartment with a capacity of 2,000 gallons, double compartment with a capacity of 1,500 gallons, and three compartments with a capacity of 1,500 gallons. Each time unit represents 10 minutes, and the transportation cost per unit time is \$50 for a single-compartment truck, \$70 for a double-compartment truck, and \$80 for a three-compartment truck. The fixed cost of single-compartment truck, double-compartment truck, and three-compartment truck is \$20, \$30, and \$40, respectively. In addition, considering the customer demand TW, the penalty cost of the distribution truck arriving early per unit time is \$10, and the penalty cost of the distribution truck arriving late per unit time is \$15. The single assignment cost of the distribution truck is \$20. For example, the vehicle route $P \rightarrow Q4 \rightarrow P7 \rightarrow P6 \rightarrow P$ uses a three-compartment vehicle, the entire route vehicle needs to run 11 time units, transportation cost is \$880, fixed cost is \$40, and the vehicle assignment cost is \$20. According to (5), the total cost of the route is \$1,160.

Table 4 shows that compared with the condition of noncooperation, the cooperative multidepot petrol distribution network has a significant decrease in the delivery time, number of distribution trucks, transportation cost, and total cost. Total delivery time under the cooperative condition dropped to 1080 minutes, which was 52% lower than that under the noncooperative condition. With cooperation, the number of trucks required for distribution and use of single- and double-compartment trucks considerably decreased whereas the use of three-compartment trucks increased to a certain extent. Overall, the number of needed distribution trucks declined from 31 to 14, fixed cost declined from \$1470 to \$760, and transportation cost declined from \$15,180 to \$7,800. In the case of joint distribution, the integrated use of trucks and the reasonable arrangement of vehicle routes need consideration, resulting in a penalty cost of \$350 for trucks arriving early or being late. In general, with cooperation, the total cost of dual depots petrol distribution network is \$8,910, which is significantly reduced by 46% compared with the noncooperative condition. In addition, IMOPSO performed 30 random operations, with the optimal result on the 23rd. The results show that considering TS and route optimization, the petrol distribution network can achieve significant cost savings, considerably reduce the

total delivery time, and significantly reduce the number of distribution trucks. Table 4 also reveals two interesting phenomena. First, the cooperative distribution network considerably reduced the use of single- and double-compartment trucks and increased the use of three-compartment trucks. This finding indicates that the use of distribution trucks is coordinated through the integration of customer requirements, and multiple PSs can be served by sending one distribution truck at a time. Second, the penalty cost has increased because the joint distribution comprehensively considers the customer TW and truck route arrangement and the detour of trucks under emergency road blocking. In certain cases, trucks arrive early or late, but the overall delivery time is reduced and the benefits are optimized. Of course, attention should also be paid to the impact of early or late arrival on customer satisfaction.

5.2. Large-Scale Example. In this section, a numerical experiment is applied to a large-scale multidepot petrol distribution network in Chongqing, China. The urban petrol distribution network in Chongqing municipality, which is directly under the jurisdiction of western China, is selected as the experimental object to demonstrate the effectiveness of IMOPSO in solving the vehicle routing optimization for the emergency joint distribution of multidepot. In this case, the petrol distribution network consists of five PDs (PD1, PD2, . . . , PD5) and 86 PSs (PS1, PS2, . . . , PS86). Figure 4 shows the distribution of all PDs and PSs, and each PS has a fixed demand TW. Specifically, PD1 serves the PSs represented by the circle, PD2 serves the PSs represented by the rectangle, PD3 serves the PSs represented by the triangle, PD4 serves the PSs represented by the cross, and PD5 serves the PSs represented by the hexagon. Table 5 shows PSs initially served by different PDs.

As mentioned in the previous Section 3.2, the optimization objective is to minimize the total cost and time of the distribution network through the cooperation of different PDs, customer clustering, TW coordination, integration of distribution trucks, and vehicle route optimization under emergency road blocking. In this numerical experiment, a petrol tanker with a loading capacity of 5,000 gallons was selected, and the distribution trucks were single-compartment $k1$, double-compartment $k2$, and three-compartment $k3$. Relevant parameter values of the optimization model and its algorithm are adopted from the literature [11, 23, 33] as follows: $f_o = 8$, $f_{k1} = 5$, $f_{k2} = 6$, $f_{k3} = 7$, $P_F = 6$, $Q^o = 5000$, $Q^{k1} = 2000$, $Q^{k2} = 1500$, $Q^{k3} = 1500$, $\mu_e = 3$, $\mu_d = 5$, $M_o = 5000$, $M_{k1} = 3700$, $M_{k2} = 4100$, $M_{k3} = 4500$, $FI_1 = 1300$, $FI_2 = 1300$, $FI_3 = 1500$, $FI_4 = 1000$, $FI_5 = 1200$, population *pop-size* = 500, learning factor $c_1 = c_2 = 2$, maximum iteration number $\max-it = 100$, and inertia weight $iw = 0.9$. In addition, the service time of PD is from 6:00 to 24:00. Table 6 shows the service TW of PS while Table 7 shows the demand for different petrol products of each station in the working period.

In this study, a working period can be regarded as a working day. Based on the participation of different cooperation subjects, five PDs can have $2^5 - 1$ different

TABLE 4: Comparison of relative indexes of multidepot petrol distribution network in a small-scale example.

Condition	Total delivery time (minutes)	Number of trucks required for distribution			Fixed cost (USD)	Transportation cost (USD)	Penalty cost (USD)	Total cost (USD)
		Single-compartment	Double-compartment	Three-compartment				
Noncooperative	2240	12	15	4	1470	15180	—	16650
Cooperative	1080	2	4	8	760	7800	350	8910

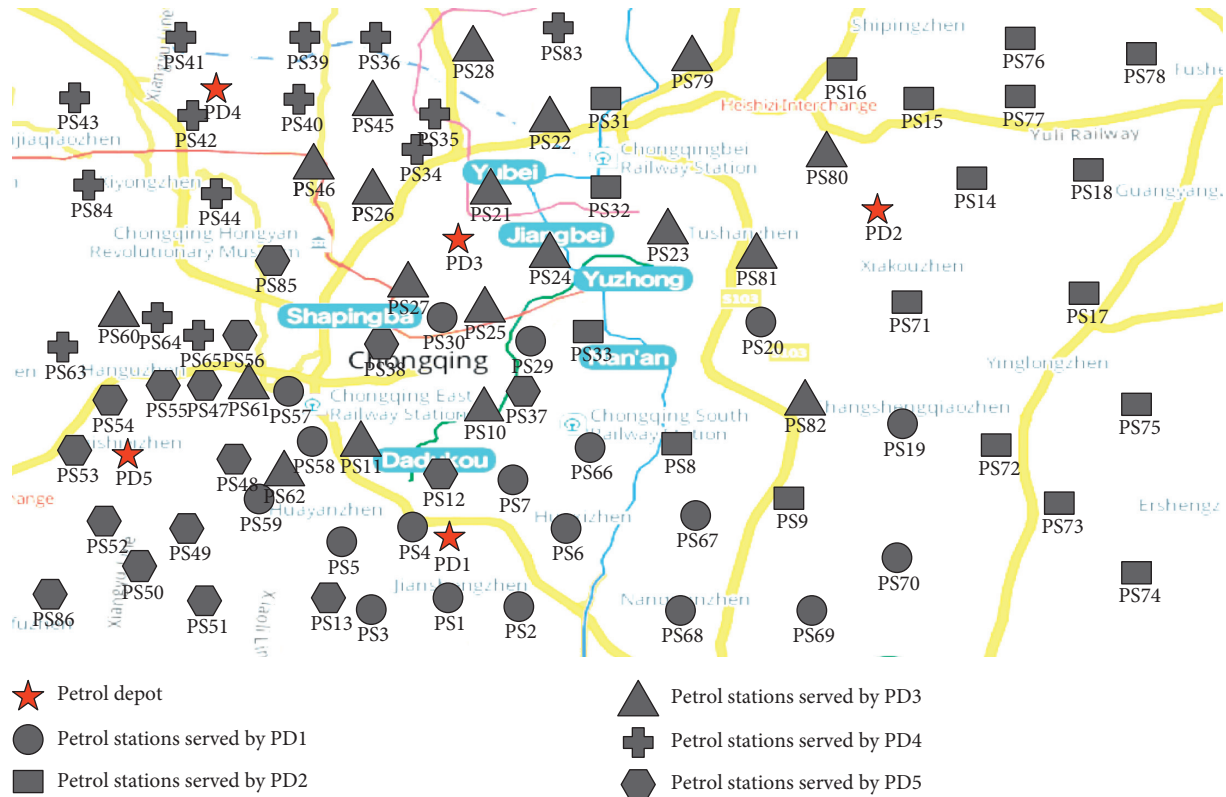


FIGURE 4: Distribution network diagram of multidepot and multistation.

TABLE 5: PSs served by different PDs before optimization.

PD	PS
PD1	PS1 PS2 PS3 PS4 PS5 PS6 PS7 PS19 PS20 PS29 PS30 PS57 PS58 PS59 PS66 PS67 PS68 PS69 PS70
PD2	PS8 PS9 PS14 PS15 PS16 PS17 PS18 PS31 PS32 PS33 PS71 PS72 PS73 PS74 PS75 PS76 PS77 PS78
PD3	PS10 PS11 PS21 PS22 PS23 PS24 PS25 PS26 PS27 PS28 PS45 PS46 PS60 PS61 PS62 PS79 PS80 PS81 PS82
PD4	PS34 PS35 PS36 PS39 PS40 PS41 PS42 PS43 PS44 PS63 PS64 PS65 PS83 PS84
PD5	PS12 PS13 PS37 PS38 PS47 PS48 PS49 PS50 PS51 PS52 PS53 PS54 PS55 PS56 PS85 PS86

cooperation alliances. First, the PSs that are responsible for distribution in each PD are reallocated through a clustering algorithm, and then the assignment and route optimization of distribution trucks are calculated using the IMOPSO algorithm. Thus, the optimized distribution cost, delivery time, and the number of different distribution trucks used per time in a working period are obtained. For the convenience of comparison and analysis, Table 8 and Figure 5 show the cost optimization results of the different cooperative alliances.

Figure 5 shows that the total operating cost of all alliances decreased compared with that of individual PD. In particular, when all PDs are willing to cooperate and a grand alliance can be formed, the reduction in operating costs is significant even if local truck detours are caused by emergency road blocking. Compared with the initial network for the entire petrol distribution, the cost decreased by 65.59%. Therefore, cooperation can benefit the operation costs reduction of multidepot petrol emergency distribution network.

TABLE 6: TW demand of PS.

PS	Demand TW	PS	Demand TW	PS	Demand TW
PS1	[10, 16]	PS30	[7, 13]	PS59	[19, 24]
PS2	[8, 14]	PS31	[13, 18]	PS60	[17, 23]
PS3	[11, 17]	PS32	[10, 16]	PS61	[12, 17]
PS4	[16, 22]	PS33	[17, 23]	PS62	[9, 14]
PS5	[7, 13]	PS34	[8, 14]	PS63	[14, 19]
PS6	[14, 20]	PS35	[12, 17]	PS64	[13, 18]
PS7	[12, 18]	PS36	[15, 21]	PS65	[10, 15]
PS8	[10, 15]	PS37	[9, 14]	PS66	[7, 12]
PS9	[6, 12]	PS38	[16, 22]	PS67	[18, 23]
PS10	[15, 21]	PS39	[11, 17]	PS68	[6, 11]
PS11	[17, 23]	PS40	[14, 20]	PS69	[11, 16]
PS12	[9, 15]	PS41	[6, 11]	PS70	[10, 15]
PS13	[12, 17]	PS42	[18, 24]	PS71	[16, 21]
PS14	[18, 24]	PS43	[10, 16]	PS72	[15, 20]
PS15	[8, 13]	PS44	[8, 13]	PS73	[8, 13]
PS16	[16, 21]	PS45	[15, 21]	PS74	[10, 16]
PS17	[10, 16]	PS46	[12, 18]	PS75	[12, 17]
PS18	[15, 20]	PS47	[7, 12]	PS76	[19, 24]
PS19	[11, 17]	PS48	[19, 24]	PS77	[14, 19]
PS20	[17, 23]	PS49	[9, 15]	PS78	[9, 15]
PS21	[7, 12]	PS50	[14, 20]	PS79	[11, 17]
PS22	[14, 19]	PS51	[8, 14]	PS80	[16, 22]
PS23	[9, 15]	PS52	[18, 23]	PS81	[13, 19]
PS24	[17, 22]	PS53	[11, 17]	PS82	[7, 13]
PS25	[15, 21]	PS54	[17, 23]	PS83	[15, 21]
PS26	[11, 16]	PS55	[10, 16]	PS84	[10, 16]
PS27	[13, 19]	PS56	[12, 18]	PS85	[8, 14]
PS28	[19, 24]	PS57	[16, 21]	PS86	[15, 20]
PS29	[18, 23]	PS58	[7, 13]		

Table 9 and Figure 6 show that the total delivery time of all alliances decreased compared with that of individual PD. In particular, when all PDs are willing to cooperate and a grand alliance can be formed, the total delivery time savings are significant even though several PSs have longer delivery times due to detours. Compared with the initial network for the entire petrol distribution, the delivery time decreased by 56.59%. Therefore, the optimization of vehicle route can benefit the saving of delivery time in multidepot petrol emergency distribution network.

Table 10 shows the changes in distribution truck usage before and after optimization in different cooperative alliances, mainly including the change of demand truck type and corresponding quantity. Specifically, distribution trucks are shared through cooperation between PDs. Based on the service TW of different PSs and the quantity of petrol required, the usage and route arrangement of different truck types are reasonably planned. As a result, usage considerably decreased for single-compartment trucks (k_1), decreased to a certain extent for double-compartment trucks (k_2), and significantly increased for three-compartment trucks (k_3). For example, for the grand alliance {PD1 PD2 PD3 PD4 PD5}, usage of single-compartment trucks (k_1) significantly decreased from 27 trucks to 6 trucks per time, that of double-compartment trucks (k_2) decreased from 36 to 17 trucks per time, while that of three-compartment trucks (k_3) increased from 27 to 35 trucks per time. The change in the number of trucks is mainly due to the change of petrol distribution

TABLE 7: PS demand for different petrol types during a working period.

PS	Petrol demand (gallons)		
	92	95	98
PS1	1309	691	—
PS2	2781	933	422
PS3	857	334	182
PS4	1289	—	157
PS5	2387	491	806
PS6	2576	327	969
PS7	2891	383	262
PS8	1989	—	—
PS9	1467	1028	946
PS10	1510	1351	721
PS11	1016	1258	730
PS12	1010	879	376
PS13	1696	411	607
PS14	1557	1066	312
PS15	2335	1194	690
PS16	632	1137	691
PS17	1635	816	228
PS18	2372	288	993
PS19	694	658	949
PS20	2481	452	—
PS21	1570	1064	829
PS22	1736	752	—
PS23	1949	925	577
PS24	2774	1298	182
PS25	1783	1126	277
PS26	2935	907	667
PS27	2830	—	971
PS28	875	1383	214
PS29	1791	—	597
PS30	1967	794	154
PS31	2058	520	930
PS32	2024	346	—
PS33	770	297	225
PS34	927	322	651
PS35	2955	1060	727
PS36	515	1246	924
PS37	1684	941	474
PS38	1326	539	972
PS39	1672	839	694
PS40	574	959	686
PS41	680	—	493
PS42	982	478	—
PS43	1485	1345	261
PS44	1609	282	237
PS45	1931	1387	690
PS46	1887	1223	221
PS47	2260	1082	348
PS48	528	456	194
PS49	1753	354	—
PS50	2558	410	549
PS51	2782	1264	1000
PS52	507	1096	953
PS53	2366	1117	533
PS54	885	—	845
PS55	639	292	—
PS56	513	—	656
PS57	667	—	678
PS58	2700	507	456

TABLE 7: Continued.

PS	Petrol demand (gallons)		
	92	95	98
PS59	919	1330	—
PS60	962	1372	645
PS61	1105	830	—
PS62	997	1199	468
PS63	2431	874	967
PS64	646	787	663
PS65	2449	—	439
PS66	732	1186	865
PS67	2892	1191	386
PS68	2473	711	783
PS69	1801	740	464
PS70	2396	—	871
PS71	2428	879	223
PS72	1852	631	685
PS73	1917	1357	436
PS74	756	970	334
PS75	2244	926	674
PS76	1300	361	—
PS77	1028	717	942
PS78	577	563	—
PS79	791	1209	547
PS80	2832	266	892
PS81	640	1301	912
PS82	2084	683	387
PS83	522	—	619
PS84	1108	1202	430
PS85	833	837	919
PS86	2447	915	273

from one-to-one assignment to the one-to-many vehicle route optimization between the PD and the PS to coordinate the station TW and the demand for petrol products. Thus, the use of single- and double-compartment trucks decreased and that of three-compartment trucks increased.

Figures 7 and 8 compare the use of distribution trucks k_1 and k_2 before and after optimization. After optimization, usage of both k_1 and k_2 decreased to a certain extent, while that of k_1 decreased more. Due to the realization of the coordination between the service TW of the PS and petrol demand, in most cases, a distribution truck from the PD has to serve multiple PSs, and thus, the use of single-compartment trucks decreased.

Figure 9 shows that, relative to the decreased usage of optimized distribution trucks k_1 and k_2 , the use of distribution truck k_3 increased after optimization. This result is mainly due to two reasons, the demand of PSs for three types of petrol and the vast majority of distribution trucks needed to serve multiple PSs at a time.

A large petrol distribution network consisting of five PDs and 86 PSs is relatively complex. Therefore, for the optimized truck distribution routes, the distribution truck route network formed by PD3 is taken as an example, as shown in Table 11. Before cooperation, the PD was responsible for one-to-one distribution of petrol products to PSs and was only responsible for the distribution of PSs operated by itself. After cooperation, PD3 reduces the distribution of long-distance PSs through clustering, such as PS61 and PS62, and

TABLE 8: Comparison between initial and optimized network over one working period (unit: USD).

Alliance	Initial cost	Optimized cost	Cost saving
{PD1}	7558	4489	3069
{PD2}	7413	4785	2628
{PD3}	8437	5312	3125
{PD4}	6725	4153	2572
{PD5}	7264	4547	2717
{PD1 PD2}	14,475	7528	6947
{PD1 PD3}	14,993	8536	6457
{PD1 PD4}	13,135	6171	6964
{PD1 PD5}	13,587	7612	5975
{PD2 PD3}	14,486	8083	6403
{PD2 PD4}	13,270	7345	5925
{PD2 PD5}	13,964	7956	6008
{PD3 PD4}	13,440	6692	6748
{PD3 PD5}	14,175	7953	6222
{PD4 PD5}	12,766	6975	5791
{PD1 PD2 PD3}	21,405	9567	11,838
{PD1 PD2 PD4}	19,313	7646	11,667
{PD1 PD2 PD5}	20,725	8734	11,991
{PD1 PD3 PD4}	19,694	7508	12,186
{PD1 PD3 PD5}	20,216	8407	11,809
{PD1 PD4 PD5}	20,583	8505	12,078
{PD2 PD3 PD4}	19,997	8156	11,841
{PD2 PD3 PD5}	21,034	9445	11,589
{PD2 PD4 PD5}	19,172	7105	12,067
{PD3 PD4 PD5}	20,895	9057	11,838
{PD1 PD2 PD3 PD4}	26,763	11,302	15,461
{PD1 PD2 PD3 PD5}	27,442	10,608	16,834
{PD1 PD2 PD4 PD5}	27,136	10,715	16,421
{PD1 PD3 PD4 PD5}	25,724	9556	16,168
{PD2 PD3 PD4 PD5}	26,625	10,234	16,391
{PD1 PD2 PD3 PD4 PD5}	33,176	11,415	21,761

increases the distribution of PS31, PS32, and other PSs near the PD. Second, in most cases, a distribution truck serves multiple PSs at once. For example, in the vehicle route PD3 \rightarrow PS21 \rightarrow PS22 \rightarrow PS31 \rightarrow PD3, a three-compartment truck starts from PD3 in the PD and serves PS21, PS22, and PS31 at one time. In addition, considering possible road emergency blocking, detour routes for distribution trucks should be designed. In the vehicle route PD3 \rightarrow PS33 \rightarrow PS29 \rightarrow PS25 \rightarrow PS29 \rightarrow PD3, if the road from PD3 to PS29 is blocked or closed due to emergency, then the distribution truck needs to detour PS29 back to PD3.

In the above example, the applications of several commonly used heuristic algorithms are compared to verify the effectiveness of the proposed IMOPSO algorithm. Table 12 compares ant colony algorithm (ACO) [38, 39], non-dominated sorting genetic algorithm (NSGA-II) [40, 41], and IMOPSO algorithm. These three methods are used 20 times for computation of the example to compare the operation costs, numbers of distribution trucks, and the distribution time. Results show that, on average, IMOPSO obtained the lowest operating cost, and while the three algorithms obtained similar total usage of the distribution

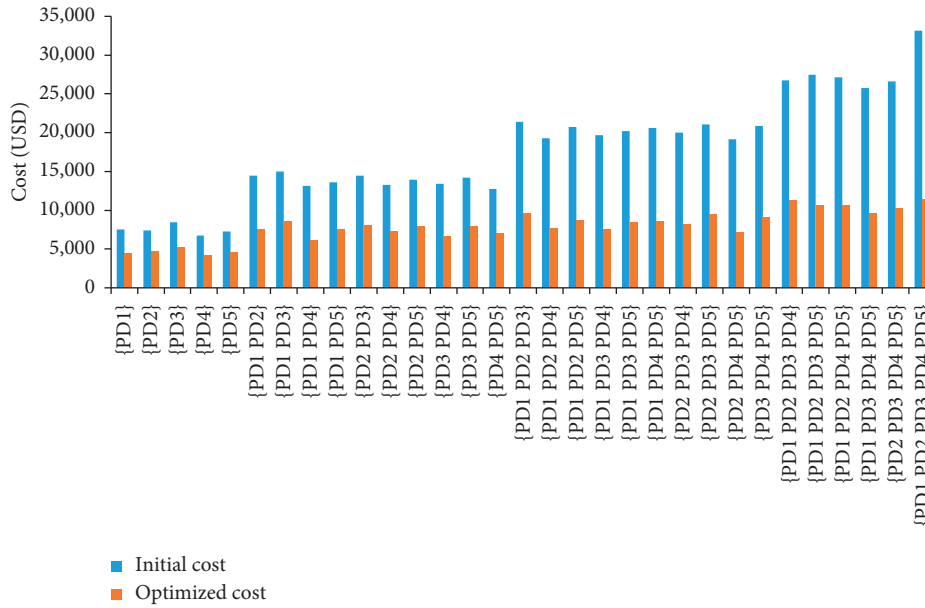


FIGURE 5: Comparison between initial and optimized networks cost solutions.

TABLE 9: Comparison between initial delivery time and optimized delivery time (unit: minutes).

Alliance	Initial delivery time	Optimized delivery time	Time saving
{PD1}	1148	1148	—
{PD2}	1176	1176	—
{PD3}	1134	1134	—
{PD4}	952	952	—
{PD5}	1079	1079	—
{PD1 PD2}	2,324	1157	1167
{PD1 PD3}	2,282	1136	1146
{PD1 PD4}	2,100	1043	1057
{PD1 PD5}	2,227	1105	1122
{PD2 PD3}	2,310	1134	1176
{PD2 PD4}	2,128	1032	1096
{PD2 PD5}	2,255	1116	1139
{PD3 PD4}	2,086	1025	1061
{PD3 PD5}	2,213	1084	1129
{PD4 PD5}	2,031	1007	1024
{PD1 PD2 PD3}	3,472	1528	1,944
{PD1 PD2 PD4}	3,276	1473	1,803
{PD1 PD2 PD5}	3,403	1495	1,908
{PD1 PD3 PD4}	3,234	1466	1,768
{PD1 PD3 PD5}	3,361	1484	1,877
{PD1 PD4 PD5}	3,179	1452	1,727
{PD2 PD3 PD4}	3,262	1479	1,783
{PD2 PD3 PD5}	3,389	1495	1,894
{PD2 PD4 PD5}	3,207	1449	1,758
{PD3 PD4 PD5}	3,165	1446	1,719
{PD1 PD2 PD3 PD4}	4,410	2,113	2,297
{PD1 PD2 PD3 PD5}	4,551	2,167	2,384
{PD1 PD2 PD4 PD5}	4,355	2,108	2,247
{PD1 PD3 PD4 PD5}	4,313	2094	2,219
{PD2 PD3 PD4 PD5}	4,341	2,010	2,331
{PD1 PD2 PD3 PD4 PD5}	5,503	2,389	3,114

trucks, IMOPS showed less usage for single- and double-compartment trucks, but more of three-compartment trucks. This result is consistent with the optimization goals,

that is, to coordinate the service TW and petrol product demand of different PSs and strengthen the sharing of distribution trucks. From the point of distribution time, the

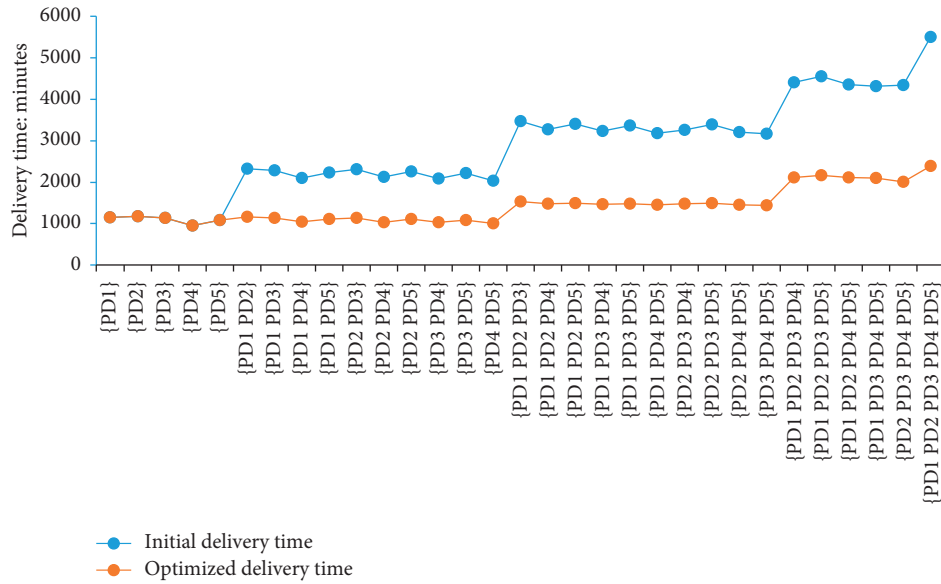


FIGURE 6: Comparison between initial and optimized network delivery time solutions.

TABLE 10: Comparison of truck usage between initial and optimized networks (trucks/time).

Alliance	Initial truck usage			Truck usage after optimization		
	k1	k2	k3	k1	k2	k3
{PD1}	6	8	6	6	8	6
{PD2}	6	8	5	6	8	5
{PD3}	6	7	7	6	7	7
{PD4}	5	6	4	5	6	4
{PD5}	5	7	5	5	7	5
{PD1 PD2}	12	16	11	2	8	15
{PD1 PD3}	12	15	13	2	8	16
{PD1 PD4}	11	14	10	3	7	12
{PD1 PD5}	11	15	11	2	8	14
{PD2 PD3}	12	15	12	2	8	15
{PD2 PD4}	10	14	9	3	7	11
{PD2 PD5}	11	15	10	2	8	13
{PD3 PD4}	11	13	11	3	6	12
{PD3 PD5}	11	14	12	2	8	15
{PD4 PD5}	10	13	9	3	7	12
{PD1 PD2 PD3}	18	23	18	3	12	24
{PD1 PD2 PD4}	16	22	15	2	11	21
{PD1 PD2 PD5}	17	23	16	3	12	22
{PD1 PD3 PD4}	17	21	17	2	11	23
{PD1 PD3 PD5}	17	22	18	4	12	24
{PD1 PD4 PD5}	16	21	15	3	11	21
{PD2 PD3 PD4}	17	21	16	2	11	22
{PD2 PD3 PD5}	17	22	17	3	12	23
{PD2 PD4 PD5}	15	21	14	3	10	20
{PD3 PD4 PD5}	16	20	16	2	11	21
{PD1 PD2 PD3 PD4}	22	29	22	4	14	28
{PD1 PD2 PD3 PD5}	23	30	23	5	16	30
{PD1 PD2 PD4 PD5}	16	29	20	4	14	26
{PD1 PD3 PD4 PD5}	22	28	22	5	15	29
{PD2 PD3 PD4 PD5}	21	28	21	5	14	28
{PD1 PD2 PD3 PD4 PD5}	27	36	27	6	17	35



FIGURE 7: Comparison between initial and optimized networks k1 usage solutions.

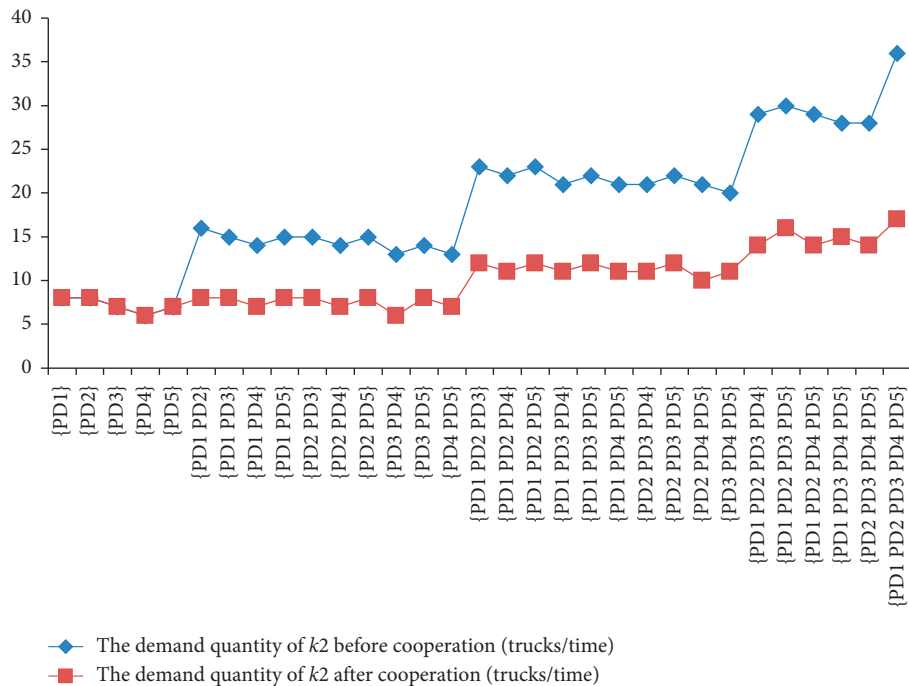


FIGURE 8: Comparison between initial and optimized networks k2 usage solutions.

average distribution time calculated by ACO is the shortest, but only outperforms IMOPSO by 50 minutes, an acceptable slight disadvantage in operational management studies, especially in large distribution networks. Thus, IMOPSO can be considered effective and feasible in addressing the vehicle routing issues in multidrop cooperative emergency distribution of petrol products.

5.3. *Implication.* The optimization of coordinated PS replenishment vehicle route based on regional partitioning and reasonable resource sharing promotes the sustainable development of petrol distribution and emergency energy supply system. Through the optimization of CMPDVRPE, the petrol distribution service area is reasonably divided, long-distance and cross-traffic are reduced, and the

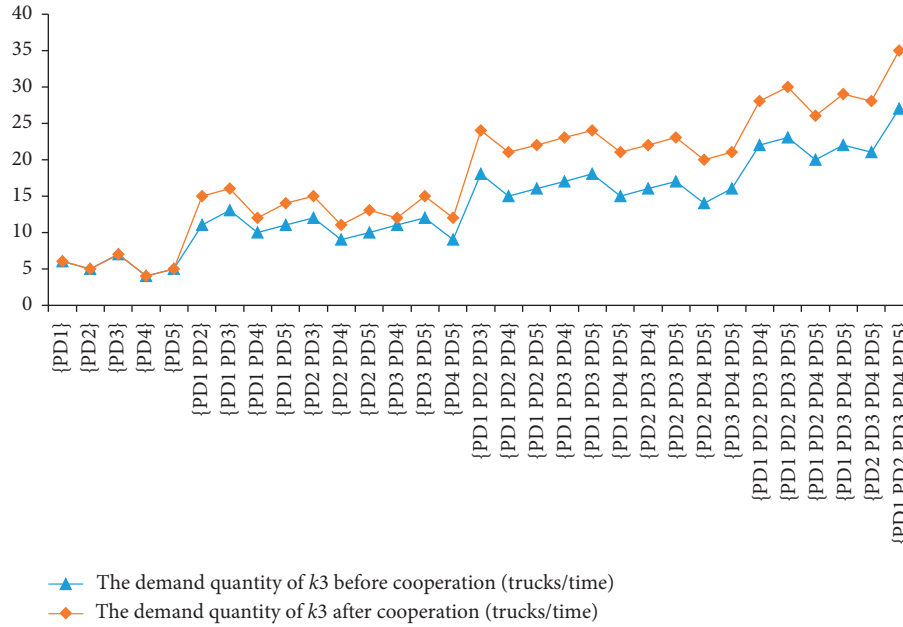


FIGURE 9: Comparison between initial and optimized networks k3 usage solutions.

TABLE 11: Distribution truck route arrangements of PD3 after optimization.

PD	The distribution truck route network
	PD3 → PS21 → PS22 → PS31 → PD3; PD3 → PS32 → PS24 → PD3;
PD3	PD3 → PS33 → PS29 → PS25 → PS29* → PD3; PD3 → PS30 → PS38 → PS27 → PD3; PD3 → PS85 → PS26 → PD3; PD3 → PS34 → PS35 → PS28 → PS35* → PD3; PD3 → PS83 → PD3

*The petrol station passed by vehicles on a detour.

TABLE 12: Comparison of algorithm performances.

Sequence	IMOPSO			ACO			NSGA-II								
	Cost (USD)	Trucks (trucks/time)		Cost (USD)	Trucks (trucks/time)		Cost (USD)	Trucks (trucks/time)		Distribution time (minutes)					
		Distribution time (minutes)	k1 k2 k3		Distribution time (minutes)	k1 k2 k3		Distribution time (minutes)	k1 k2 k3						
1	11,415	6	17	35	1980	13,248	8	20	33	2170	12,532	7	19	34	2060
2	15,324	6	15	37	1550	15,023	8	18	31	1380	14,473	6	18	32	1610
3	11,122	6	18	33	980	19,108	9	18	34	2220	12,914	7	17	32	2010
4	11,184	6	16	35	1690	18,197	8	21	32	1450	11,403	8	19	33	1650
5	10,707	6	16	36	1760	14,280	8	20	31	2130	14,627	8	17	34	2420
6	12,750	6	17	36	1980	12,556	9	19	34	2230	18,158	7	18	33	1980
7	12,566	8	15	32	2250	14,320	9	20	32	2180	16,232	8	17	33	2120
8	17,355	5	15	38	1760	16,886	7	20	32	1430	14,654	6	18	33	2410
9	12,229	6	18	35	1970	19,672	8	18	31	1300	12,434	6	18	34	1940
10	13,338	8	16	34	1820	12,780	9	20	33	2410	12,516	6	19	33	1630
11	14,820	8	15	34	1730	16,830	7	20	31	930	12,721	8	17	34	2310
12	14,842	8	17	32	2230	14,019	8	19	33	1690	17,029	7	17	34	1970
13	15,520	7	15	34	2270	14,210	9	19	34	2190	14,591	7	17	33	2090
14	14,670	5	18	33	1900	18,683	9	21	34	860	13,717	8	17	32	900
15	16,051	6	17	34	1950	17,252	8	19	32	2310	12,716	8	19	32	2010
16	15,862	7	18	36	860	17,760	8	19	32	2340	12,336	7	17	34	1680
17	12,312	6	17	36	1830	12,856	7	18	34	1570	15,641	8	18	34	1980
18	12,322	8	16	37	2060	17,903	8	19	34	880	17,947	7	19	33	2410
19	13,454	8	16	33	1610	15,404	7	20	31	2610	18,621	6	17	33	2530
20	13,254	6	15	33	2110	14,422	8	20	31	950	15,297	8	17	32	2420
Average	13,555	7	16	35	1810	15,770	8	19	32	1760	14,528	7	18	33	2010

distribution time is shortened. Thus, costs are minimized and additional benefits are provided to each PD. Effective vehicle routing arrangement and sharing matching strategy between vehicles and PSs are the important characteristics of this network. These improvements greatly enhance energy and social resources, cost savings, and emergency response capabilities for PD operators and transportation management.

Cooperation among logistics facilities plays an important role in optimizing the distribution in cases of emergency [42–44]. Further integration of transportation resource sharing and optimization of vehicle routing can further save on costs. In addition, traffic management policies that encourage joint distribution are also a sign of political will to achieve sustainable development in administrative areas [31, 32]. As one of the major development factors, petrol distribution activities can be further organized under the coordination of vehicle routes, reducing the number of petrol distribution trucks. Therefore, encouraging the formation of grand coalitions is a relevant method that can benefit not only PDs, but also society as a whole.

6. Conclusions

This study proposes an effective method to solve the CMPDVRPE optimization, which improves the cooperation of PDs and the efficient distribution vehicle routing optimization in emergencies. Through the cooperation between PDs, regional petrol joint distribution, optimization of distribution, and resource sharing can be formed. In the optimization, PS clustering mechanism, road blocking, and TS mechanism are considered. Comparison of the data before and after the cooperation shows that the total operating cost, total delivery time, and the total number of delivery vehicles are significantly decreased.

The optimization model considers customer clustering, multicompartment TS, roadblocks, and TWC, thereby reducing the overall transport distance and the number of trucks used. Taking the regional petrol distribution network in Chongqing as an example, the application of the model and method is evaluated. A heuristic algorithm IMOPSO is proposed, and a case study of different scales of petrol distribution networks was carried out. The operating cost, delivery time, and the number of different types of trucks are compared before and after optimization.

In summary, the optimization of petrol emergency distribution vehicle routing is consistent with reality. The proposed optimization method is superior to the existing research in this field. On the basis of the analysis, the following conclusions are drawn. (1) Through customer clustering, multicompartment TS, vehicle routing optimization, and TWC, the regional petrol distribution network can considerably reduce the delivery time, number of distribution trucks required, and the total operating cost of the petrol distribution network. (2) Optimizing the PSs for each PD and sharing trucks when the TW demand allows can reduce traffic pressure in urban areas and its negative impact on the energy supply system and contribute to the sustainable development of urban traffic. (3) Timely and

efficient supply of petrol is guaranteed through optimization of vehicle routing of petrol emergency distribution.

The results of this study point to interesting research directions for the future. The following views can be considered. (1) This study only examines the cooperation between PD and PS in the secondary distribution of petrol. Thus, the cooperation between the two sides can extend to the transport energy supply chain. (2) Consistent with most existing joint distribution literature, this study assumes a constant transportation speed of petrol distribution trucks. Future research can consider real-time urban traffic speed analysis to obtain more realistic results. (3) From the perspective of vehicle-road interaction, the influence of road geometry on the selection of multicompartment vehicle types can be considered in the future. (4) In the future, a dynamic CMPDVRPE model can be established by considering the spatiotemporal change of roadblocks or congestion.

Data Availability

The service time window and demand quantity data used to support the findings of this study are available from the corresponding companies and administrative departments.

Conflicts of Interest

The authors declare that they have no conflicts of interest.

Acknowledgments

This research was supported by the Social Science Foundation of Chongqing of China (Grant nos. 2020BS62, 2020TBWT-ZD02, 2019YBGL049, and 2020YBGL85), the Special Project of Technology Foresight and System Innovation of Chongqing of China (Grant no. cstc2020jsyj-zdxwtB0003), the National Natural Science Foundation of China (Grant no. 71871035), Humanity and Social Science Foundation of Ministry of Education of China (Grant nos. 18YJC630189 and 17YJA630079), and Humanity and Social Sciences Research Project of Chongqing Education Commission (Grant no. 20SKGH232).

References

- [1] F. Cornillier, F. Boctor, and J. Renaud, "Heuristics for the multi-depot petrol station replenishment problem with time windows," *European Journal of Operational Research*, vol. 220, no. 2, pp. 361–369, 2012.
- [2] L. Bruggen, R. Gruson, and M. Salomon, "Reconsidering the distribution structure of gasoline products for a large oil company," *European Journal of Operational Research*, vol. 81, no. 3, pp. 460–473, 1995.
- [3] Y. Wang, X. Ma, Z. Li, Y. Liu, M. Xu, and Y. Wang, "Profit distribution in collaborative multiple centers vehicle routing problem," *Journal of Cleaner Production*, vol. 144, pp. 203–219, 2017.
- [4] Y. Wang, Y. Yuan, X. Guan, M. Xu, and Y. Liu, "Collaborative two-echelon multicenter vehicle routing optimization based on state-space-time network representation," *Journal of Cleaner Production*, vol. 258, pp. 1–26, 2020.

- [5] F. Cornillier, F. F. Boctor, G. Laporte, and J. Renaud, "A heuristic for the multi-period petrol station replenishment problem," *European Journal of Operational Research*, vol. 191, no. 2, pp. 295–305, 2008.
- [6] F. Cornillier, G. Laporte, F. F. Boctor, and J. Renaud, "The petrol station replenishment problem with time windows," *Computers & Operations Research*, vol. 36, no. 3, pp. 919–935, 2009.
- [7] F. F. Boctor, J. Renaud, and F. Cornillier, "Trip packing in petrol stations replenishment," *Omega*, vol. 39, no. 1, pp. 86–98, 2011.
- [8] D. Popović, M. Vidović, and G. Radivojević, "Variable neighborhood search heuristic for the inventory routing problem in fuel delivery," *Expert Systems with Applications*, vol. 39, no. 18, pp. 13390–13398, 2012.
- [9] M. Vidović, D. Popović, and B. Ratković, "Mixed integer and heuristics model for the inventory routing problem in fuel delivery," *International Journal of Production Economics*, vol. 147, pp. 593–604, 2014.
- [10] B. Wang, Y. Liang, M. Yuan, H. Zhang, and Q. Liao, "A metaheuristic method for the multireturn-to-depot petrol truck routing problem with time windows," *Petroleum Science*, vol. 16, no. 3, pp. 701–712, 2019.
- [11] L. Wang, J. Kinable, and T. Woensel, "The fuel replenishment problem: a split delivery multi-compartment vehicle routing problem with multiple trips," *Computers and Operations Research*, vol. 118, pp. 1–16, 2020.
- [12] S.-H. Huang, "Solving the multi-compartment capacitated location routing problem with pickup-delivery routes and stochastic demands," *Computers & Industrial Engineering*, vol. 87, pp. 104–113, 2015.
- [13] U. Derigs, J. Gottlieb, J. Kalkoff, M. Piesche, F. Rothlauf, and U. Vogel, "Vehicle routing with compartments: applications, modelling and heuristics," *OR Spectrum*, vol. 33, no. 4, pp. 885–914, 2011.
- [14] R. Lahyani, L. C. Coelho, M. Khemakhem, G. Laporte, and F. Semet, "A multi-compartment vehicle routing problem arising in the collection of olive oil in Tunisia," *Omega*, vol. 51, pp. 1–10, 2015.
- [15] L. C. Coelho and G. Laporte, "Classification, models and exact algorithms for multi-compartment delivery problems," *European Journal of Operational Research*, vol. 242, no. 3, pp. 854–864, 2015.
- [16] M. Ostermeier and A. Hübner, "Vehicle selection for a multi-compartment vehicle routing problem," *European Journal of Operational Research*, vol. 269, no. 2, pp. 682–694, 2018.
- [17] M. Qi, W.-H. Lin, N. Li, and L. Miao, "A spatiotemporal partitioning approach for large-scale vehicle routing problems with time windows," *Transportation Research Part E: Logistics and Transportation Review*, vol. 48, no. 1, pp. 248–257, 2012.
- [18] F. Moreira, D. Pereira da Silva, L. Guimarães, P. Amorim, and B. Almada-Lobo, "The time window assignment vehicle routing problem with product dependent deliveries," *Transportation Research Part E: Logistics and Transportation Review*, vol. 116, pp. 163–183, 2018.
- [19] S. Martins, M. Ostermeier, P. Amorim, A. Hübner, and B. Almada-Lobo, "Product-oriented time window assignment for a multi-compartment vehicle routing problem," *European Journal of Operational Research*, vol. 276, no. 3, pp. 893–909, 2019.
- [20] R. Eshtehad, E. Demir, and Y. Huang, "Solving the vehicle routing problem with multi-compartment vehicles for city logistics," *Computers and Operations Research*, vol. 115, pp. 1–16, 2020.
- [21] X. Wang, H. Zhan, and J. Zhang, "Research of oil product secondary distribution optimization based on collaborative distribution," *Procedia Computer Science*, vol. 60, pp. 1367–1376, 2015.
- [22] Y. Wang, Y. Yuan, K. Assogba et al., "Design and profit allocation in two-echelon heterogeneous cooperative logistics network optimization," *Journal of Advanced Transportation*, vol. 2018, Article ID 4607493, 20 pages, 2018.
- [23] Y. Wang, S. Zhang, X. Guan et al., "Collaborative multi-depot logistics network design with time window assignment," *Expert Systems with Applications*, vol. 140, pp. 1–24, 2020.
- [24] J.-B. Sheu, "An emergency logistics distribution approach for quick response to urgent relief demand in disasters," *Transportation Research Part E: Logistics and Transportation Review*, vol. 43, no. 6, pp. 687–709, 2007.
- [25] Q. Zhang and S. Xiong, "Routing optimization of emergency grain distribution vehicles using the immune ant colony optimization algorithm," *Applied Soft Computing*, vol. 71, pp. 917–925, 2018.
- [26] D. Huizing, G. Schäfer, R. D. van der Mei, and S. Bhulai, "The median routing problem for simultaneous planning of emergency response and non-emergency jobs," *European Journal of Operational Research*, vol. 285, no. 2, pp. 712–727, 2020.
- [27] R. J. Kuo, F. E. Zulvia, and K. Suryadi, "Hybrid particle swarm optimization with genetic algorithm for solving capacitated vehicle routing problem with fuzzy demand—a case study on garbage collection system," *Applied Mathematics and Computation*, vol. 219, no. 5, pp. 2574–2588, 2012.
- [28] Y. Wang, X. Ma, M. Xu, Y. Liu, and Y. Wang, "Two-echelon logistics distribution region partitioning problem based on a hybrid particle swarm optimization-genetic algorithm," *Expert Systems with Applications*, vol. 42, no. 12, pp. 5019–5031, 2015.
- [29] H. Zhou, M. Song, and W. Pedrycz, "A comparative study of improved GA and PSO in solving multiple traveling salesmen problem," *Applied Soft Computing*, vol. 64, pp. 564–580, 2018.
- [30] K. Govindan, A. Jafarian, R. Khodaverdi, and K. Devika, "Two-echelon multiple-vehicle location-routing problem with time windows for optimization of sustainable supply chain network of perishable food," *International Journal of Production Economics*, vol. 152, pp. 9–28, 2014.
- [31] Y. Wang, S. Peng, X. Zhou, M. Mahmoudi, and L. Zhen, "Green logistics location-routing problem with eco-packages," *Transportation Research Part E: Logistics and Transportation Review*, vol. 143, pp. 1–33, 2020.
- [32] C. Xu, P. Liu, W. Wang, and Z. Li, "Identification of freeway crash-prone traffic conditions for traffic flow at different levels of service," *Transportation Research Part A: Policy and Practice*, vol. 69, pp. 58–70, 2014.
- [33] G. Xu, M. Xu, Y. Wang, Y. Liu, and Q. Lv, "Collaborative multidepot petrol station replenishment problem with multicompartments and time window assignment," *Journal of Advanced Transportation*, vol. 2020, Article ID 8843397, 22 pages, 2020.
- [34] J. Kennedy and R. Eberhart, "Particle swarm optimization," in *Proceedings of the International Conference on Neural Networks (ICNN'95)*, vol. 4, pp. 1942–1948, Perth, WA, Australia, November 1995.
- [35] C. Coello and M. Lechuga, "MOPSO: a proposal for multiple objective particle swarm optimization," in *Proceedings of the 2002 Congress on Evolutionary Computation*, pp. 1051–1056, Honolulu, HI, USA, May 2002.
- [36] K. Deb, S. Agrawal, A. Pratap, and T. Meyarivan, "A fast elitist non-dominated sorting genetic algorithm for multi-objective

- optimization: NSGA-II,” in *Proceeding of Parallel Problem Solving from Nature VI Conference*, pp. 849–858, Paris, France, September 2000.
- [37] Y. Shi and R. Eberhart, “A modified particle swarm optimizer,” in *Proceedings of the IEEE International Conference on Evolutionary Computation*, pp. 69–73, Piscataway, NJ, USA, May 1998.
- [38] Y.-H. Huang, C. A. Blazquez, S.-H. Huang, G. Paredes-Belmar, and G. Latorre-Núñez, “Solving the feeder vehicle routing problem using ant colony optimization,” *Computers & Industrial Engineering*, vol. 127, pp. 520–535, 2019.
- [39] Y. Li, H. Soleimani, and M. Zohal, “An improved ant colony optimization algorithm for the multi-depot green vehicle routing problem with multiple objectives,” *Journal of Cleaner Production*, vol. 227, pp. 1161–1172, 2019.
- [40] A. Martínez-Puras and J. Pacheco, “MOAMP-Tabu search and NSGA-II for a real bi-objective scheduling-routing problem,” *Knowledge-Based Systems*, vol. 112, pp. 92–104, 2016.
- [41] A. Rauniyar, R. Nath, and P. K. Muhuri, “Multi-factorial evolutionary algorithm based novel solution approach for multi-objective pollution-routing problem,” *Computers & Industrial Engineering*, vol. 130, pp. 757–771, 2019.
- [42] J.-B. Sheu and C. Pan, “A method for designing centralized emergency supply network to respond to large-scale natural disasters,” *Transportation Research Part B: Methodological*, vol. 67, pp. 284–305, 2014.
- [43] Y. Huang, “Modeling and simulation method of the emergency response systems based on OODA,” *Knowledge-Based Systems*, vol. 89, pp. 527–540, 2015.
- [44] Y. Liu, Y. Wang, M. Xu, and G. Xu, “Emergency alternative evaluation using extended trapezoidal intuitionistic fuzzy thermodynamic approach with prospect theory,” *International Journal of Fuzzy Systems*, vol. 21, no. 6, pp. 1801–1817, 2019.

Research Article

A Multistage Dynamic Emergency Decision-Making Method considering the Satisfaction under Uncertainty Information

Yong Liu 

Laboratory of Management Simulation, Chongqing Jiaotong University, Chongqing 400074, China

Correspondence should be addressed to Yong Liu; liuevery@gmail.com

Received 25 February 2021; Revised 24 March 2021; Accepted 29 March 2021; Published 15 April 2021

Academic Editor: Zheng Wang

Copyright © 2021 Yong Liu. This is an open access article distributed under the Creative Commons Attribution License, which permits unrestricted use, distribution, and reproduction in any medium, provided the original work is properly cited.

Emergency decision-making (EDM) is of paramount importance, especially when the emergency occurs. The evolution nature of the emergency, such as multistage, uncertainty, dynamic, and information updating, has been playing a key role in the dynamic emergency decision-making process. However, most existing studies ignored the aforementioned nature. Our approach accounts for the dynamics inherent to a real emergency decision-making process and presents a multistage dynamic emergency decision-making (MSDEDM) procedure of a dynamic programming model based on decision-makers' psychological reference satisfactory degree. Firstly, interval-valued trapezoidal intuitionistic fuzzy numbers (IVTrIFNs) are used to depict the relevant fuzziness and uncertainty of information. Secondly, by considering the dynamic evolution process of emergency and the decision-makers' psychological reference expectation effect, the principle of MSDEDM approach is presented. Based on the analysis, the dynamic model on the new psychological reference satisfactory parameter formula is presented to obtain the optimal satisfaction and weight of each stage. Then, the value utility function based on the DMs' risk attitude is proposed to obtain the comprehensive value of each emergency alternative for each stage and achieve the ranking results of each stage. Furthermore, a case study involving the transportation emergency decision-making problem demonstrates that the proposed method can achieve selection of the optimal alternatives for each stage, as well as adjustment of the alternatives for neighbouring stages. Finally, the comparative analysis and sensitivity analysis for the results are used to further verify the feasibility and practicability of the proposed method.

1. Introduction

Emergencies cause heavy casualties and huge economic losses, such as the appearance and spread of COVID-19 in 2019, explosion accident in Tianjin port in 2015, Wenchuan earthquake in 2008, and SARS in 2003. To minimize these losses as far as possible, the effective emergency decision and response measures must be taken immediately. However, due to the complexity and uncertainty of the decision environment as well as the dynamic nature of the events, it is very difficult to effectively determine the measures for response. It is a typical emergency decision-making (EDM) problem, which has always been a hot research topic of modern decision science. The general objective of EDM is to estimate desirable alternatives on the basis of a set of evaluation criteria by decision-makers (DMs), and its major

task is to integrally and effectively depict the decision-making environment in some representation, assess alternatives on the criteria with a mathematical modeling procedure, and provide the optimal alternative to the emergency response [1, 2]. How to determine and take the effective emergency decision and response measures immediately when the emergency occurs is very important [3, 4].

Over the years, considerable prominent works have been conducted to enrich the fields. Yu and Lai proposed a distance-based multicriteria decision-making method for group emergency decision support [5]. Taking the EDM as a problem of risk analysis, Liu et al. and Wang et al. presented an EDM approach considering the DMs' decision behaviors based on prospect theory [6, 7]. Wang et al. focused on regret theory, which means that the DMs tend to generate an expected regret for decision based on past experiences and

established a decision-making method for emergency response of rainstorm disaster [8]. Xu et al. considered DMs' trust relations and preference risks and developed consensus-based EDM approach [9]. For another solution, Ren et al. introduced the concept of decision information quality and firstly developed a thermodynamic method for EDM [10]. Zhang et al. enumerated all possible situations by the dynamic evolution information of emergency and proposed a linear programming selection model to determine the optimal alternative for each situation [11]. Then, Zhang et al. researched another approach to solve the EDM problem based on game theory, where the different situations were regarded as the strategies between emergencies and DMs [12]. With the emerging information technologies, data mining method was introduced to analyse public attribute preferences for emergency risk decision-making [13]. These methods have done great work and will be useful to EDM. However, for the emergency evolution characteristics consisting of multistage, uncertainty, dynamic, and information updating, the abovementioned decision-making method has some limitations in practical application, such as the description of complex and uncertain decision information, the adjustment mechanism of the alternative between two neighbouring stages, the dynamic nature, and decision information updating. With respect to these limitations, the key to solve the EDM problems is to design a multistage dynamic emergency decision-making (MSDEDM) approach, considering not only comprehensively describing and quantifying the decision environment of uncertainty but also dynamically determining the optimal alternative for the response in time.

The assessment information, obtained from the emergency, is the basis for scientific emergency decision-making [14, 15]. On the one hand, it can reflect the evolution state of the emergency. On the other hand, it can help DMs to judge the events and form the reliable preference assessment. Due to the decision-making environment of variable events, time limitations, and psychological pressure, researchers have found that it is difficult to determine the preference assessment value on the alternative accurately and timely. Furthermore, the processing of their decision is often uncertain and indecisive. In particular, compared with the single-stage decision-making, the complexity and uncertainty of the dynamic emergency decision-making are significantly increased. Therefore, it is necessary to develop more powerful and flexible tools in order to handle these limitations in real-world application. To overcome the issues, fuzzy-based methods aiming at quantifying the individuals' judgment on the alternatives in forms of fuzzy numbers are widely applied in EDM. For example, Li et al. developed an integrated consensus model based on the fuzzy context to solve the EDM problems [16]. Wang et al. and Farhadinia et al. presented an extended hesitant fuzzy decision-making method based on prospect theory and applied it to EDM studies [17, 18]. Wei developed an operator-based model and procedures to solve decision-making problems, in which the criteria values take the forms of intuitionistic fuzzy numbers (IFNs) and interval-valued IFNs [19]. Liu et al. introduced the concept of trapezoidal intuitionistic

fuzzy numbers (TrIFNs) as a special variant of the IFNs and developed a new approach of ratio ranking TrIFNs to solve emergency alternative assessment problems [20]. Wu and Liu studied the multicriteria decision-making problem, in which the given arguments are expressed with IVTrIFNs [21]. It is worth noting that interval-valued trapezoidal intuitionistic fuzzy numbers (IVTrIFNs), introducing interval number from 0 to 1 to portray the DMs' preference assessment degrees, overcome the difficulty that the degrees of membership, nonmembership, and hesitation cannot be described with crisp numbers in reality. Compared with others, IVTrIFNs have more representational parameters, which can not only describe DMs' preference judgment information more comprehensively and exquisitely but also make the preference judgment results closer to the realistic decision-making environment. IVTrIFNs are advantageous and have been applied in other fields with some success [22–25]. However, few articles studied MSDEDM problems where the assessment information can be depicted in forms of IVTrIFNs. This advantage can thus inspire us to introduce IVTrIFNs into MSDEDM problems.

Considering the dynamic nature of the emergency, the decision-making situation is constantly changing, where the DMs should timely adjust the alternative in response to the continuous development of the emergency. With respect to DMs, the most intuitive feedback of these changing is both the decision situation information changing in stages and updating dynamically. Scholars focus on the dynamic nature of both when studying MSDEDM problems. Recently, a few researchers have involved the changing in stages in the EDM problem. For example, Zheng et al. and Ding et al. proposed a dynamic EDM method for alternatives selection of each status, in which the stage of the change was determined by specific development of events [4, 26]. Cai et al. studied multistage EMD approach, where the stage weights were calculated by relative entropy optimization technology [27]. Wu et al. showed that a single-stage emergency decision-making method is unreasonable for the real application and, on this basis, the changing of the stage weights explored by the GM (1, 1) model [28]. In Xu et al.'s work, Markov technology was introduced to describe the evolution state of the emergency [29]. These studies determined the importance of each stage by some assumption and realized the description of the changing in stages. However, such subjective assumption ignored the real impact of the evolution law on the alternative assessing and ranking, such as the control effectivity of the neighbouring stage caused by the alternative response of the previous stage, the evolution of events, and the updating of DMs' psychological expected information.

Due to the dynamical updating of information, scholars often adopt dynamic methods when studying EDM problem. For example, Hao et al. developed a dynamic weight determination method on fuzzy Bayesian network to solve EDM problem, considering the evolving nature of the events [30]. Yan et al. supposed that the results of disaster information evolution had Markov nature and studied the emergency damage assessment problem [14]. Xu considered DMs' psychological preference and the development events,

initially defined DMs' satisfactory degree of the alternative with TOPSIS (technique for order preference by similarity to ideal solution) and constructed a multiobjective dynamic optimization model based on the distance measure to adjust the alternatives interactively [31]. Gao et al. constructed a dynamic decision-making framework and proposed a reference point approach based on the DMs' expectation level of alternatives for dynamic emergency response decisions [32]. Wang et al. applied prospect theory to EDM, which can depict the dynamic features of events by dynamic reference point method [33]. Although these studies adopted the dynamic methods including the ideal reference point, the psychological expected reference point, and the mechanism of emotion updating and obtained some good results, more subjective assumptions could also lead to the deviation of decision-making results.

To sum up, in view of the emergency evolution characteristics of multistage, uncertainty, dynamic, and information updating, these existing researches still have some limitations in the literature. (a) Researchers have found that it is difficult to depict the emergency of uncertainty and complexity in real applications. There is a gap between the quantification of the assessment environment and reality. The depiction of the EDM environment uncertainty should be closer to the reality. (b) Researchers had significant achievements in EDM approaches of the single stage but ignored the dynamic nature of the emergency evolution. (c) For the dynamic nature, the adjustment mechanism of the alternative between two contiguous stages has not been studied particularly from aspects like information updating.

Thus, the uncertainty of situation, the dynamic nature of events, and the adjustment of alternatives should be involved. Inspired by the studies of Xu [31] and Gao et al. [32], the study focuses on the context of fuzzy decision-making and develops an interval-valued trapezoidal intuitionistic fuzzy approach to solve the dynamic emergency response. Both weights of criteria and DMs are completely unknown, and the DMs' satisfactory degree and the dynamic nature of emergency are considered. The main contributions of this paper are presented as follows. (a) We propose a novel EDM approach to determine the optimal alternative at stages under IVTrIFNs environment, in which we construct the satisfactory degree index to quantify the DMs' psychological behaviors. (b) We construct an improved satisfaction degree model, not only portraying the dynamic changing of DMs' psychological behaviors but also avoiding more subjective presupposition. (c) Due to the dynamic nature of emergency, we conduct a multistage dynamic mechanism to achieve the adjustment of the alternatives.

The remainder of the paper is organized as follows. Section 2 reviews the related concepts and definitions of IVTrIFNs. In Section 3, we describe the proposed MSDEDM approach based on the psychological reference satisfactory degree and present its procedure. Section 4 provides a case study on the highway emergency response to illustrate the practicality of feasibility of the proposed MSDEDM approach. We also make a comparative analysis and sensitivity analysis for the results in Section 4. Section 5 presents some concluding remarks and future studies.

2. Preliminaries

In this section, the basic concepts of IVTrIFNs are briefly reviewed, including definitions, operators, and the method of score functions.

Let X be a fixed set, $A = \langle\langle [a, b, c, d]; [\mu_A^L, \mu_A^H], [v_A^L, v_A^H] \rangle\rangle$ denotes an interval-valued trapezoidal intuitionistic fuzzy number on X , and its membership function and nonmembership function are, respectively, defined as $\mu_A = [\mu_A^L, \mu_A^H]$ and $\nu_A = [v_A^L, v_A^H]$, where $a, b, c, d \in R$, $0 \leq \mu_A, \nu_A \leq 1$, and $\mu_A + \nu_A \leq 1$. Ding and Wang gave some operational laws for IVTrIFNs [23, 34].

Definition 1. Let $x_i = ([a_i, b_i, c_i, d_i]; [\mu_i^L, \mu_i^H], [v_i^L, v_i^H])$, ($i = 1, 2, \dots, n$) be a collection of IVTrIFNs, and its score function $S(x_i)$ which is used to evaluate the degree of score of x_i can be defined as follows:

$$S(x_i) = \frac{(a_i + b_i + c_i + d_i)}{8} (\mu_i^L + \mu_i^H - v_i^L - v_i^H), \quad (1)$$

where $S(x_i) \in [-1, 1]$. Generally, the larger the value of score function $S(x_i)$, the more the degree of score of x_i . In addition, we can define the expected value $E(x_i)$ of x_i as follows [21, 35]:

$$E(x_i) = \frac{1}{8} (a_i + b_i + c_i + d_i) (1 + \mu_i - \nu_i). \quad (2)$$

Under the condition $S(x_i) = S(x_j)$ ($i, j = 1, 2, \dots, n$), we can get the following:

- (a) If $E(x_i) > E(x_j)$, then $x_i > x_j$
- (b) If $E(x_i) = E(x_j)$, then $x_i = x_j$
- (c) If $E(x_i) < E(x_j)$, then $x_i < x_j$

Definition 2. Let $x_i = ([a_i, b_i, c_i, d_i]; [\mu_i^L, \mu_i^H], [v_i^L, v_i^H])$, ($i = 1, 2, \dots, n$) be a collection of IVTrIFNs and IVTrIFWA operator is a mapping: $f_\omega^x: \Omega^n \rightarrow \Omega$, if

$$\text{IVTrIFWA}(x_1, x_2, \dots, x_n) = \bigoplus_{i=1}^n w_i x_i = \left(\left[\begin{array}{c} \sum_{i=1}^n w_i a_i, \sum_{i=1}^n w_i b_i \\ \sum_{i=1}^n w_i c_i, \sum_{i=1}^n w_i d_i \end{array} \right]; \left[\begin{array}{c} \left[1 - \prod_{i=1}^n (1 - \mu_i^L)^{w_i}, 1 - \prod_{i=1}^n (1 - \mu_i^H)^{w_i} \right] \\ \left[\prod_{i=1}^n (v_i^L)^{w_i}, \prod_{i=1}^n (v_i^H)^{w_i} \right] \end{array} \right] \right). \quad (3)$$

Thus, IVTrIFWA is referred to as interval-valued trapezoidal intuitionistic fuzzy weighted averaging operator of dimension n , where $w = (w_1, w_2, \dots, w_n)^T$ is the weight vector of x_i ($i = 1, 2, \dots, n$), with $w_i \in [0, 1]$ and $\sum_{i=1}^n w_i = 1$.

Definition 3 (see [21]). Let $x_i = ([a_i, b_i, c_i, d_i]; [\mu_i^L, \mu_i^H], [v_i^L, v_i^H])$, ($i = 1, 2, \dots, n$) be a collection of IVTrIFNs, for any ordered pair $\langle \alpha, \beta \rangle$, $\alpha, \beta \in [0, 1]$, $0 \leq \alpha + \beta \leq 1$, and then the α cut set and the β cut set can be, respectively, defined as follows:

$$x_{i\alpha} = [L_{x_i}(\alpha), R_{x_i}(\alpha)] = \left[a_i + \frac{\alpha(b_i - a_i)}{\mu_{x_i}}, d_i - \frac{\alpha(d_i - c_i)}{\mu_{x_i}} \right],$$

$$x_i^\beta = [L_{x_i}(\beta), R_{x_i}(\beta)] = \left[\frac{(1 - \beta)b_i + (\beta - v_{x_i})a_i}{1 - v_{x_i}}, \frac{(1 - \beta)c_i + (\beta - v_{x_i})d_i}{1 - v_{x_i}} \right],$$

where $\mu_{x_i} = (\mu_i^L + \mu_i^H)/2 \geq \alpha$ and $v_{x_i} = (v_i^L + v_i^H)/2 \leq \beta$. In addition, we can define the expected value of the α cut set and the β cut set, respectively:

$$E(x_{i\alpha}) = \int_0^{\mu_{x_i}} [\eta L_{x_i}(\alpha) + (1 - \eta)R_{x_i}(\alpha)] d\alpha = \frac{\mu_{x_i}}{2} (\eta(a_i + b_i - c_i - d_i) + c_i + d_i),$$

$$E(x_i^\beta) = \int_{v_{x_i}}^1 [\eta L_{x_i}(\beta) + (1 - \eta)R_{x_i}(\beta)] d\beta = \frac{1 - v_{x_i}}{2} (\eta(a_i + b_i - c_i - d_i) + c_i + d_i).$$

Then the comprehensive risk expected score function $\text{RES}(x_i)$ can be obtained as follows:

$$\text{RES}(x_i) = \frac{1}{2} (\text{EV}(x_{i\alpha}) + \text{EV}(x_i^\beta)) = \frac{\eta(a_i + b_i) + (1 - \eta)(c_i + d_i)}{4} \left(1 + \frac{\mu_i^L + \mu_i^H}{2} - \frac{v_i^L + v_i^H}{2} \right),$$

where $\eta \in [0, 1]$ is an indicator of the DMs' risk attitudinal factor; when η approaches 1, the risk attitude is optimistic; adversely, it is pessimistic. Specifically, $\eta = 0.5$ indicates that the attitude of DMs is neutral, and equation (6) simplifies to equation (2), which is similar to the expected value $E(x_i)$ of x_i . Therefore, we can use $\text{RES}(x_i)$ function to convert the interval-valued trapezoidal intuitionistic fuzzy decision information into a representative crisp value and make a sensitivity analysis for the impact of the ranking based on η , with consideration of the DMs risk attitude.

3. A Multistage Dynamic Emergency Decision-Making Method

Emergency activities fully reflect the emergency decision-making characteristics of uncertainty, multistage, dynamic, and information updating. When an emergency breaks out, the managers should always strive to effectively control the development of the emergency situation. They make a scientific study and decision on the situation in the first time and dynamically adjust the emergency plan at the necessary stage according to the development trend of the emergency.

Therefore, the key to solve the problem is how to adjust the response plan dynamically according to the stage of the situation. With respect to the characteristics, we propose a novel dynamic method to make emergency decision on their uncertain opinions.

3.1. Problem Definition. In this section, we introduce the investigated emergency response process. When an emergency breaks out, the managers quickly obtain the limited relevant state information through various ways, such as casualties and property losses, traffic conditions, weather and environment, the rescue force, and emergency supplies. Then, they make a rough analysis of the emergency according to the abovementioned information and give the preference degree values of each alternative on the set of the evaluation criteria. Finally, the comprehensive quantification and ranking of each alternative are carried out. In particular, the preference degree values are based on the maximum satisfaction of each decision-maker for the selected emergency alternative performance.

However, such emergency response process ignores the question of multistage dynamic evolution of emergencies,

which should be involved. For the first stage, the selected emergency alternative is used to respond to the emergency and also plays a role in the control of emergency. Meanwhile, the emergency is also changing. The decision-makers obtain more and more information about the emergency, and the expected satisfaction of the psychological reference of the emergency alternative performance will also change accordingly. For the next stage, the emergency continues to evolve. The decision-makers give new preference degree values of each alternative on the set of the evaluation criteria. After evaluation, if the new satisfaction of the alternative at the moment reaches the last satisfaction of the moment, the emergency plan will not be adjusted; otherwise, the optimal response plan will be selected by recalculation. For the following stages of emergency development, the above-mentioned judgment method is used to determine the new response alternative until the emergency is effectively controlled. The multistage dynamic emergency decision-making framework is illustrated in Figure 1.

With regard to the basic framework of multiattribute decision-making problem, the relevant variable parameters involved in the multistage dynamic emergency decision-making method are presented in Table 1.

3.2. Dynamic Adjustment Method Based on the Satisfaction Information Updating

Definition 4 (see [34]). Let $x_i = ([a_i, b_i, c_i, d_i]; [\mu_i^L, \mu_i^H], [v_i^L, v_i^H])$, ($i = 1, 2, \dots, n$) be a collection of IVTrIFNs, and the positive and negative ideal points are, respectively, as follows:

$$\begin{aligned} x^+ &= ([\max a_i, \max b_i, \max c_i, \max d_i]; [1, 1], [0, 0]), \\ x^- &= ([\min a_i, \min b_i, \min c_i, \min d_i]; [0, 0], [1, 1]). \end{aligned} \quad (7)$$

Xu defined a decision satisfaction index based on TOPSIS method [31]. It can be defined as

$$\phi(x_i) = \frac{d(x_i, x^-)}{d(x_i, x^+) + d(x_i, x^-)}, \quad (8)$$

where $d(x_i, x^+)$ and $d(x_i, x^-)$, respectively, indicate the Hamming distances between x_i and ideal points. On the basis of equation (8), we introduce decision-maker's risk preference index θ and construct a satisfaction function, which can be expressed by

$$\phi(x_i) = \frac{\theta d(x_i, x^-)}{\theta d(x_i, x^+) + (1 - \theta)d(x_i, x^-)}, \quad (9)$$

where $\theta \in [0, 1]$. If $\theta > 0.5$, the decision-maker's risk preference is positive and optimistic. If $\theta < 0.5$, the decision-maker's risk preference is passive and pessimistic. Also, when $\theta = 0.5$, it is neutral, and equation (9) can be simplified as equation (8).

Since the satisfaction index has advantages on objectively describing the decision-maker's expected satisfactory degree of psychological reference, it has been widely used in the

research of multiattribute decision-making problems. However, in practical decision-making problems, it is difficult to determine the risk preference index of decision-makers. Previous studies generally assume that decision-makers' risk appetite is neutral. In order to overcome this shortcoming, we construct a new satisfaction index calculation method.

Definition 5. Let $x_i = ([a_i, b_i, c_i, d_i]; [\mu_i^L, \mu_i^H], [v_i^L, v_i^H])$, ($i = 1, 2, \dots, n$) be a collection of IVTrIFNs, let \bar{x} be the weighted average of x_i , and let $d(x_i, \bar{x})$ be the Hamming distance between x_i and \bar{x} . The satisfaction index of x_i can be calculated by

$$\phi(x_i) = \frac{E(x_i)}{1 + V(x_i)} = \frac{\sum_{k=1}^l w_i^k E(x_i^k)}{1 + \sum_{k=1}^l w_i^k d(x_i^k, \bar{x}_i)}, \quad (10)$$

where $\phi(x_i) \in [0, 1]$, and we determine \bar{x} using the IVTrIFWA operator. $E(x_i)$ and $V(x_i)$ are the expected value and the weighted average deviation value, respectively. The higher $E(x_i)$ is, the higher x_i is, which means that a more satisfactory degree on the selected alternative can be obtained by DMs. The smaller $V(x_i)$ is, the smaller the difference in preferences is, which shows that a higher consensus degree on the selected alternative can be obtained by DMs, as well as the higher the satisfaction is. Otherwise, the smaller $E(x_i)$, the higher $V(x_i)$ and the lower the satisfaction index. Based on the principle of maximum satisfactory degree, we construct a programming model as follows.

$$\begin{aligned} \max \quad & \sum_{i=1}^m \tau(x_{ij}^{pk}) \\ & \phi(x_{ij}^{pk}(w^{pk})) \geq \tau(x_{ij}^{pk}) \\ \text{s.t.} \quad & \sum_{k=1}^l w^{pk} = 1, \quad 0 \leq w^{pk} \leq 1 \\ & i = 1, 2, \dots, m; \quad j = 1, 2, \dots, n; \\ & k = 1, 2, \dots, l; \quad p = 1, 2, \dots, q. \end{aligned} \quad (11)$$

Then, at state T^p , the maximum satisfaction degree $\tau^*(x_{ij}^{pk})$ on the selected alternative and the corresponding weight $w^{*pk} = (w^{*p1}, w^{*p2}, \dots, w^{*pl})$ are calculated by equation (11). We determine the ranking and optimal alternative A_i .

Apparently, the DMs' psychological reference satisfactory degree on the performance of the selected alternative is not completely fixed and can be influenced by the dynamic development of the events. With the implementation of the selected A_i , the emergency will be in control. For the coming stage T^{p+1} , the DMs obtain new certain information of the emergency and make new decision if necessary. Using $\tau^*(x_{ij}^{pk})$ as a decision reference, if $\tau^*(x_{ij}^{(p+1)k}) \geq \tau^*(x_{ij}^{pk})$, then the current emergency alternative A_i is not adjusted and continues to be implemented; otherwise, the new satisfactory expectation degree will be recalculated, and the optimal alternative will be dynamically selected until the

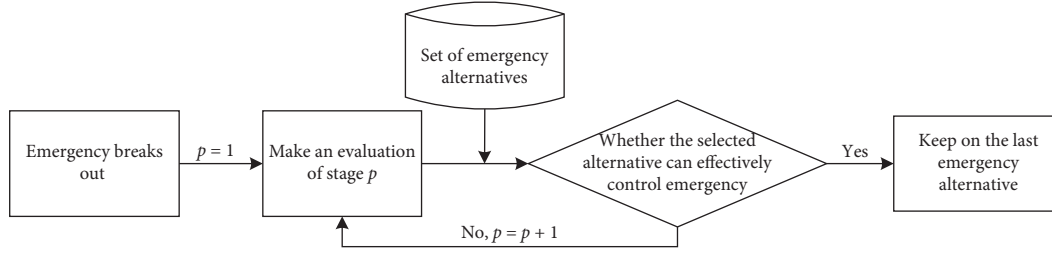


FIGURE 1: Schematic of the multistage dynamic emergency decision-making framework.

TABLE 1: Mathematical notations and definitions.

Symbols	Definitions
$T^p (p = 1, 2, \dots, q)$	Set of stages in the evolution of an emergency scenario
$E^k (k = 1, 2, \dots, l)$	Set of experts involved in emergency decision-making
$w^{pk} (k = 1, 2, \dots, l)$	Weight of E^k , with $\sum_{k=1}^l w^{pk} = 1$ and $0 \leq w^{pk} \leq 1$
$A_i (i = 1, 2, \dots, m)$	Set of emergency response alternatives
$C_j (j = 1, 2, \dots, n)$	Set of evaluation criteria for selection of alternatives
$w_j^{pk} (k = 1, 2, \dots, l)$	Weight of corresponding criterion, with $\sum_{j=1}^n w_j^{pk} = 1$ and $w_j^{pk} \geq 0$
$X^{pk} (p = 1, 2, \dots, q; k = 1, 2, \dots, l)$	Set of preference degree values of each alternative on each criterion by each expert

emergency is effectively controlled. Considering the dynamic of the decision-making process, we construct a dynamic programming model as follows.

$$\begin{aligned}
 & \max \sum_{i=1}^m \tau(x_{ij}^{(p+1)k}) \\
 & \phi(x_{ij}^{(p+1)k}(w^{(p+1)k})) \geq \tau(x_{ij}^{(p+1)k}) \geq \tau^*(x_{ij}^{pk}) \\
 & \text{s.t.} \quad \sum_{k=1}^l w^{(p+1)k} = 1, 0 \leq w^{(p+1)k} \leq 1 \\
 & \quad i = 1, 2, \dots, m; j = 1, 2, \dots, n; \\
 & \quad k = 1, 2, \dots, l; p = 1, 2, \dots, q.
 \end{aligned} \tag{12}$$

3.3. Dynamic Emergency Decision-Making Procedures. In this section, we introduce our proposed approach of the multistage dynamic emergency decision-making. Firstly, the preference degree value of decision-makers is described in the form of interval trapezoidal intuitionistic fuzzy number. On this basis, the entropy weight method is used to calculate the experts' weight in each stage, and the preference degree value on emergency alternative is aggregated to rank and select the optimal alternation. Then, considering the dynamic evolution of the emergency situation, the driving force, which causes the decision-makers to timely adjust emergency response plan, is mainly on whether the stage of emergency plan for emergency performance meets the psychological expected reference satisfaction of decision-makers. For this aspect, we construct the dynamic decision-making model under the influence of decision-makers' psychological reference satisfaction. Also, the experts' weights and the optimal satisfaction of each evolutionary stage are calculated. Finally, the comprehensive value of each emergency decision scheme in each evolutionary stage is calculated to obtain the ranking of alternative decision

schemes in each evolutionary stage. According to Gao et al. [32], the detailed procedure is illustrated in Figure 2.

In summary, the steps of the multistage dynamic emergency decision-making method can be detailed as follows:

Step 1. Let the DMs $E^k (k = 1, 2, \dots, l)$ assess the performance of the emergency alternatives $A_i (i = 1, 2, \dots, m)$ on the criteria $C_j (j = 1, 2, \dots, n)$, and determine the normalized preference matrix of each alternative in stage T^p , which can be expressed by $X^{pk} = (x_{ij}^{pk})_{m \times n}$, where $x_{ij}^{pk} = ([a_{ij}^{pk}, b_{ij}^{pk}, c_{ij}^{pk}, d_{ij}^{pk}]; [\mu_{ij}^{pkL}, \mu_{ij}^{pkH}], [v_{ij}^{pkL}, v_{ij}^{pkH}])$, $p = 1, 2, \dots, q; k = 1, 2, \dots, l$.

Step 2. Based on the normalized preference matrix X^{pk} , derive the weights w_j^{pk} of criteria in stage $T^p (p = 1, 2, \dots, q)$ by the entropy method [20, 25], which can be calculated by

$$w_j^{pk} = \frac{(1 - H_j^{pk})}{(n - \sum_{j=1}^n [-(\ln m)^{-1} \sum_{i=1}^m f_{ij}^{pk} \ln f_{ij}^{pk}])}. \tag{13}$$

where $f_{ij}^{pk} = (E(x_{ij}^{pk}) / \sum_{i=1}^m E(x_{ij}^{pk}))$, and if $f_{ij} = 0$, then $f_{ij} \ln f_{ij} = 0$.

Step 3. Aggregate the DMs' preference values by IVTrIFWA operator, and calculate the comprehensive preference values on each alternative of each DM at stage T^p . The comprehensive preference matrix can be expressed by

$$Y^{pk} = (y_i^{pk})_{m \times l} = \text{IVTrIFWA}(x_{ij}^{pk}) = \bigoplus_{j=1}^n w_j^{pk} x_{ij}^{pk}. \tag{14}$$

Moreover, calculate the expected matrix of Y^{pk} by equation (2) as follows:

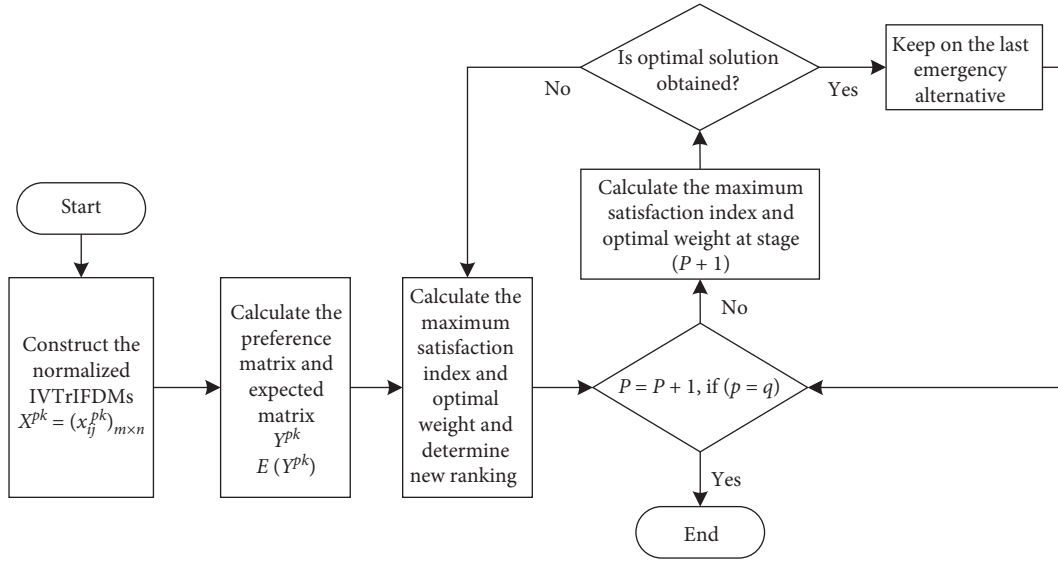


FIGURE 2: Flowchart of the proposed dynamic emergency decision-making methodology.

$$E(Y^{pk}) = (E(y_i^{pk}))_{m \times l}, \quad (i = 1, 2, \dots, m; k = 1, 2, \dots, l). \quad (15)$$

Step 4. At the current stage T^p , determine the maximum satisfactory degree $\tau^*(x_{ij}^{pk})$ on the alternative A_i and the corresponding weight $w^{*pk} = (w^{*p1}, w^{*p2}, \dots, w^{*pl})$ calculated by equation (11).

Step 5. Obtain the comprehensive preference values EV_i^p by IVTrIFWA operator, and determine the ranking of alternatives according to equation (6). Thus, the optimal alternative is A_i^{*p} at stage T^p .

Step 6. As the emergency evolves, for the next stage T^{p+1} , let the DMs reassess the performance of the emergency alternatives based on the criteria, and determine the new preference matrix of each alternative. Then, calculate the maximum satisfactory degree $\tau^*(x_{ij}^{(p+1)k})$ on the alternative A_i^{p+1} by equation (12). By comparing $\tau^*(x_{ij}^{(p+1)k})$ and $\tau^*(x_{ij}^{pk})$, we can get the following:

- If $\tau^*(x_{ij}^{(p+1)k}) \geq \tau^*(x_{ij}^{pk})$, then continue to implement the alternative A_i , and move to Step 7.
- If $\tau^*(x_{ij}^{(p+1)k}) < \tau^*(x_{ij}^{pk})$, then move to Step 4. Recalculate the new satisfactory expectation degree $\tau^*(x_{ij}^{(p+1)k})$ and the optimal weight $w^{*(p+1)k} = (w^{*(p+1)1}, w^{*(p+1)2}, \dots, w^{*(p+1)l})$, and determine the new optimal alternative A_i^{*p+1} at stage T^{p+1} .

Step 7. When $p = q$, it indicates that the emergency is completely under control; namely, the emergency decision-making process is over.

4. Illustrative Example

In this section, the decision-making problem of a transportation emergency is introduced as a case to verify the effectiveness and practicability of the multistage dynamic approach.

4.1. Implementation and Results. A highway section in a mountainous area is experiencing a sudden landslide and mudflow caused by a heavy rainfall. The related highway department is responsible for the emergency alternative decision-making and response. Shortly after the emergency, they firstly organize the relevant experts to study and judge the emergency and quickly launch the emergency alternative. There are our experts E^k ($k = 1, 2, 3, 4$) from related professional fields, and three emergency alternatives A_i ($i = 1, 2, 3$) for the event are developed as follows:

A_1 : do not close lanes, and keep traffic moving in time-phased sharing. Meanwhile, start the rescue work immediately by small machinery and equipment.

A_2 : close side road, and keep traffic moving in the other lane. Meanwhile, start the rescue work immediately by medium-sized machinery and equipment.

A_3 : close all lanes, and stop the traffic except emergency vehicles. Meanwhile, start the rescue work immediately by heavy machinery and equipment.

Fully considering the changes in the weather, suppose that there are three different stages of emergency evolution, namely, T^p ($p = 1, 2, 3$). They can be described as follows:

T^1 : 06:00–10:00 am, it is likely to suffer small-to-moderate rain. Then, with the increasing unstable and uncertain factors, the emergency is also easy to be out of control, and the adverse trends might have a big effect on the rescue progress.

T^2 : 10:00–14:00 pm, it is likely to suffer moderate-to-heavy rain. Then, there is a high probability of worsening the emergency, and the difficulty of managing such emergency is ever increasing.

T^3 : 14:00–18:00 pm, extreme weather is gradually abating and would benefit the subsequent rescue work.

For each alternative, five benefit-oriented evaluation criteria $C_j (j = 1, 2, 3, 4, 5)$ are considered by the experts, including the emergency alternative of responsibility, completeness, operability, timeliness, and economy. With the development of emergency, experts need to determine the optimal alternative for the emergency at each stage. Considering the uncertainty of dynamic situation, experts describe the cognitive preferences of each alternative using IVTrIFNs linguistic variables. Table 2 lists the mapping of the IVTrIFNs linguistic variables.

Step 1. Each expert assesses the performance of each alternative on each evaluation criterion, as given in Table 3.

Step 2. Determine the weights w_j^{pk} of criteria in stage $T^p (p = 1, 2, \dots, q)$ by equation (13). Table 4 summarizes the results.

Step 3. The IVTrIFWA operator is used to aggregate the DMs' preference values of stage T^p and yield the comprehensive preference values Y^{pk} . Then calculate the expected preference value $E(Y^{pk})$ and the weighted average deviation value $V(Y^{pk})$, as shown in Tables 5 and 6, respectively.

Step 4. According to stage T^p , construct a programming model based on equation (11) as follows.

$$\max \sum_{k=1}^3 \tau(x_{ij}^{1k})$$

$$\frac{0.227w^{11} + 0.492w^{12} + 0.354w^{13}}{1 + 0.134w^{11} + 0.158w^{12} + 0.008w^{13}} \geq \tau(x_{ij}^{11})$$

$$\frac{0.499w^{11} + 0.521w^{12} + 0.556w^{13}}{1 + 0.034w^{11} + 0.006w^{12} + 0.04w^{13}} \geq \tau(x_{ij}^{12}) \quad (16)$$

s.t.

$$\frac{0.192w^{11} + 0.202w^{12} + 0.311w^{13}}{1 + 0.041w^{11} + 0.031w^{12} + 0.008w^{13}} \geq \tau(x_{ij}^{13})$$

$$w^{11} + w^{12} + w^{13} = 1; w^{13} \geq w^{12} \geq w^{11} \geq 0.3.$$

Consequently, according to the model of stage T^1 , we can obtain the most satisfactory degree and the optimal weight as follows: $\tau^*(x_{ij}^{1k}) = (0.326, 0.514, 0.237)$ and $w^{*1k} = (0.3, 0.3, 0.4)$.

Step 5. Using equation (3), the comprehensive preference values of each alternative EV_i^1 are calculated as

$$EV_1^1 = ([0.447, 0.547, 0.647, 0.747]; [0.484, 0.593], [0.290, 0.407]),$$

$$EV_2^1 = ([0.593, 0.693, 0.793, 0.893]; [0.605, 0.710], [0.180, 0.290]),$$

$$EV_3^1 = ([0.363, 0.463, 0.563, 0.663]; [0.368, 0.469], [0.429, 0.531]). \quad (17)$$

Suppose that the experts involved in the assessment have a neutral attitude to face uncertain risk, namely, $\eta = 0.5$. Then, using equation (6), the comprehensive risk expected

TABLE 2: Mapping of IVTrIFNs linguistic variables.

Linguistic terms	Linguistic values of TrIFNs
Absolutely low (AL)	([0.0, 0.0, 0.1, 0.2]; [0.0, 0.0],[1.0, 1.0])
Low (L)	([0.1, 0.2, 0.3, 0.4]; [0.1, 0.2],[0.7, 0.8])
Fairly low (FL)	([0.3, 0.4, 0.5, 0.6]; [0.3, 0.4],[0.5, 0.6])
Medium (M)	([0.4, 0.5, 0.6, 0.7]; [0.4, 0.5],[0.4, 0.5])
Fairly high (FH)	([0.5, 0.6, 0.7, 0.8]; [0.5, 0.6],[0.3, 0.4])
High (H)	([0.7, 0.8, 0.9, 1.0]; [0.7, 0.8],[0.1, 0.2])
Absolutely high (AH)	([0.8, 0.9, 1.0, 1.0]; [1.0, 1.0],[0.0, 0.0])

TABLE 3: Evaluating decision matrix X^{pk} given by expert E^k at stage T^p .

E^k	C_j	T^1			T^2			T^3		
		A_1	A_2	A_3	A_1	A_2	A_3	A_1	A_2	A_3
E^1	C_1	M	FH	FL	M	M	H	FH	H	AH
	C_2	L	FH	FL	FL	FH	AH	H	H	AH
	C_3	M	FH	FL	M	H	AH	FH	AH	AH
	C_4	H	H	M	H	H	FH	FH	FH	H
	C_5	FH	H	FL	H	FH	H	M	FH	H
E^2	C_1	FH	H	M	FH	H	H	H	H	AH
	C_2	H	FH	FL	M	FH	H	FH	FH	H
	C_3	M	H	FL	H	H	AH	M	FH	H
	C_4	FH	H	M	M	FH	H	H	H	H
	C_5	M	FH	FL	FH	H	H	H	AH	H
E^3	C_1	H	FH	M	H	FH	H	AH	AH	AH
	C_2	FH	H	FH	FH	H	H	H	H	H
	C_3	FH	H	M	H	FH	H	FH	FH	H
	C_4	FH	FH	FL	M	H	FH	M	H	AH
	C_5	L	FH	M	FH	H	M	H	FH	H

TABLE 4: Weights w_j^{pk} of criteria at stage T^p .

C_j	T^1			T^2			T^3		
	E^1	E^2	E^3	E^1	E^2	E^3	E^1	E^2	E^3
C_1	0.088	0.169	0.138	0.221	0.258	0.220	0.235	0.017	0.081
C_2	0.460	0.460	0.421	0.429	0.255	0.088	0.047	0.269	0.046
C_3	0.088	0.191	0.138	0.220	0.046	0.102	0.267	0.349	0.352
C_4	0.130	0.077	0.117	0.065	0.345	0.295	0.157	0.062	0.383
C_5	0.234	0.103	0.186	0.065	0.096	0.295	0.294	0.303	0.138

TABLE 5: Expected preference value $E(Y^{pk})$ at stage T^p .

E^k	T^1			T^2			T^3		
	A_1	A_2	A_3	A_1	A_2	A_3	A_1	A_2	A_3
E^1	0.227	0.499	0.192	0.284	0.450	0.886	0.370	0.780	0.891
E^2	0.492	0.521	0.202	0.334	0.510	0.853	0.463	0.749	0.851
E^3	0.354	0.556	0.311	0.452	0.590	0.478	0.671	0.758	0.885

TABLE 6: Weighted average deviation value $V(Y^{pk})$ at stage T^p .

E^k	T^1			T^2			T^3		
	A_1	A_2	A_3	A_1	A_2	A_3	A_1	A_2	A_3
E^1	0.134	0.034	0.041	0.079	0.086	0.072	0.554	0.018	0.015
E^2	0.158	0.006	0.031	0.034	0.011	0.040	0.429	0.013	0.024
E^3	0.008	0.040	0.080	0.117	0.094	0.561	0.007	0.007	0.009

score $RES(x_i)$ is obtained as follows: $RES(EV_1^1) = 0.355$, $RES(EV_2^1) = 0.528$, $RES(EV_3^1) = 0.241$, and $RES(EV_2^1) > RES(EV_1^1) > RES(EV_3^1)$. Thus, at the first stage T^1 , the optimal ranking of the response alternatives is $A_2 > A_1 > A_3$; namely, the emergency alternative A_2 can be selected as the most suitable response.

Step 6. In the second stage T^2 , on the basis of the last satisfactory degree $\tau^*(x_{ij}^{1k})$, a new programming model based on equation (12) is obtained as follows.

$$\begin{aligned} & \max \sum_{k=1}^3 \tau(x_{ij}^{2k}) \\ & \frac{0.284w^{21} + 0.334w^{22} + 0.452w^{23}}{1 + 0.079w^{21} + 0.034w^{22} + 0.117w^{23}} \geq \tau(x_{ij}^{21}) \geq \tau^*(x_{ij}^{11}) = 0.326 \\ & \text{s.t.} \quad \frac{0.45w^{21} + 0.51w^{22} + 0.59w^{23}}{1 + 0.086w^{21} + 0.011w^{22} + 0.094w^{23}} \geq \tau(x_{ij}^{22}) \geq \tau^*(x_{ij}^{12}) = 0.514 \\ & \quad \frac{0.886w^{21} + 0.853w^{22} + 0.478w^{23}}{1 + 0.072w^{21} + 0.04w^{22} + 0.561w^{23}} \geq \tau(x_{ij}^{23}) \geq \tau^*(x_{ij}^{13}) = 0.237 \\ & \quad w^{21} + w^{22} + w^{23} = 1; w^{23} \geq w^{22} \geq w^{21} \geq 0.3. \end{aligned} \quad (18)$$

Clearly, the above model is unsolvable under the current constraints, which indicates that the previous stage is no longer suitable for managing the current emergency. The current emergency alternative needs to be reassessed and adjusted; meanwhile, the new satisfactory expectation degree can be updated. Consequently, according to equation (11), a new programming model is obtained as follows.

$$\begin{aligned} & \max \sum_{k=1}^3 \tau(x_{ij}^{2k}) \\ & \frac{0.284w^{21} + 0.334w^{22} + 0.452w^{23}}{1 + 0.079w^{21} + 0.034w^{22} + 0.117w^{23}} \geq \tau(x_{ij}^{21}) \\ & \text{s.t.} \quad \frac{0.45w^{21} + 0.51w^{22} + 0.59w^{23}}{1 + 0.086w^{21} + 0.011w^{22} + 0.094w^{23}} \geq \tau(x_{ij}^{22}) \quad (19) \\ & \quad \frac{0.886w^{21} + 0.853w^{22} + 0.478w^{23}}{1 + 0.072w^{21} + 0.04w^{22} + 0.561w^{23}} \geq \tau(x_{ij}^{23}) \\ & \quad w^{21} + w^{22} + w^{23} = 1; w^{23} \geq w^{22} \geq w^{21} \geq 0.3. \end{aligned}$$

Through solving the model, the most satisfactory degree is $\tau^*(x_{ij}^{2k}) = (0.331, 0.486, 0.604)$, and the optimal weight is $w^{*2k} = (0.333, 0.333, 0.334)$, respectively. By equation (3), the comprehensive preference values of each alternative EV_i^2 are obtained as follows:

$$\begin{aligned} EV_1^2 &= ([0.460, 0.560, 0.660, 0.760]; [0.477, 0.583], [0.306, 0.417]), \\ EV_2^2 &= ([0.583, 0.683, 0.783, 0.883]; [0.598, 0.703], [0.186, 0.297]), \\ EV_3^2 &= ([0.670, 0.770, 0.870, 0.946]; [1.000, 1.000], [0.000, 0.000]). \end{aligned} \quad (20)$$

Similarly, let $\eta = 0.5$, and determine the comprehensive risk expected score $RES(EV_i^2)$ as follows: $RES(EV_1^2) = 0.356$, $RES(EV_2^2) = 0.517$, $RES(EV_3^2) = 0.814$, and $RES(EV_3^2) > RES(EV_2^2) > RES(EV_1^2)$. Thus, the optimal ranking of the response alternatives is $A_3 > A_2 > A_1$, which indicates that the emergency alternative A_3 is the best for the emergency response at present.

Step 7. For the coming stage T^3 , a new programming model is constructed using equation (12) as follows.

$$\begin{aligned} & \max \sum_{k=1}^3 \tau(x_{ij}^{3k}) \\ & \frac{0.37w^{31} + 0.463w^{32} + 0.671w^{33}}{1 + 0.554w^{31} + 0.429w^{32} + 0.007w^{33}} \geq \tau(x_{ij}^{31}) \geq \tau^*(x_{ij}^{21}) = 0.331 \\ & \text{s.t.} \quad \frac{0.78w^{31} + 0.749w^{32} + 0.758w^{33}}{1 + 0.018w^{31} + 0.013w^{32} + 0.007w^{33}} \geq \tau(x_{ij}^{32}) \geq \tau^*(x_{ij}^{22}) = 0.486 \\ & \quad \frac{0.891w^{31} + 0.851w^{32} + 0.885w^{33}}{1 + 0.015w^{31} + 0.024w^{32} + 0.009w^{33}} \geq \tau(x_{ij}^{33}) \geq \tau^*(x_{ij}^{23}) = 0.604 \\ & \quad w^{31} + w^{32} + w^{33} = 1; w^{33} \geq w^{32} \geq w^{31} \geq 0.3. \end{aligned} \quad (21)$$

Obviously, the model has an optimal solution, which is obtained as follows: $w^{*3k} = (0.3, 0.3, 0.4)$ and $\tau^*(x_{ij}^{3k}) = (0.399, 0.753, 0.863)$. The results show that the previous alternative has played a good role in managing the emergency and should continue to be implemented, namely, $A_3 > A_2 > A_1$. Meanwhile, the comprehensive risk expected score $RES(EV_i^3)$ is calculated as follows: $RES(EV_1^3) = 0.665$, $RES(EV_2^3) = 0.762$, $RES(EV_3^3) = 0.877$, and $RES(EV_3^3) > RES(EV_2^3) > RES(EV_1^3)$, which indicates the effectiveness and reliability of the model at stage T^3 .

In conclusion, for the multistage dynamic emergency decision-making problem, the ranking order of the three stages is $A_2 \Rightarrow A_3 \Rightarrow A_3$.

4.2. Results Analysis and Discussion. From the above-mentioned example, we can see that the severe weather not only is the key emergency instigator but also affects the emergency response procedure, and thus the weather changes should be involved in the dynamic assessment of the alternative. The three alternatives A_i ($i = 1, 2, 3$), showing a progressive nature for emergency response, have different

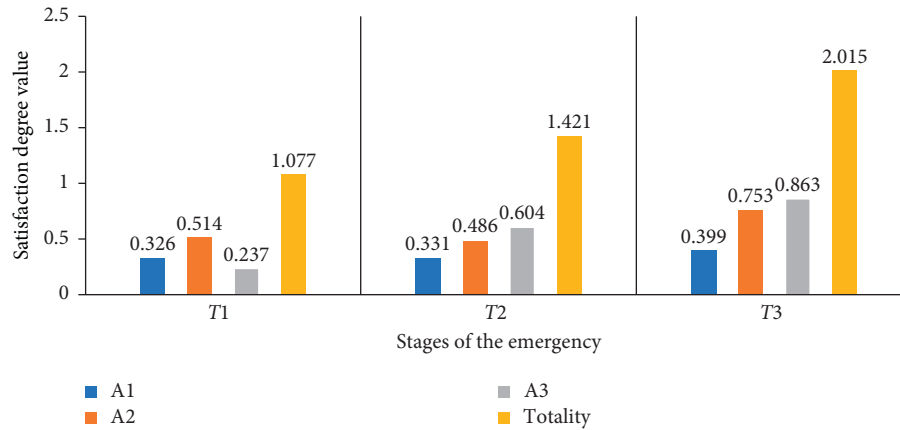


FIGURE 3: Satisfaction degree value of each alternative at each stage.

focus according to the development of the event. It is reasonable for the experts to evaluate the emergency and make multistage decisions to select optimal alternative with respect to the developments. The optimal alternative of each stage can be obtained using the proposed method of dynamic multistage emergency decision-making, and the results are shown in Figures 3 and 4.

Figure 3 presents the satisfactory degree value of each alternative at each stage, showing the preference information updating of the DMs. Obviously, with the emergency development and the selected alternative implementation, the satisfactory degree index of each expert is increasing and getting close to one until the events are effectively controlled. It is indicated from the results, obtained by using the proposed dynamic method based on the satisfactory degree index, that the dynamic emergency decision-making processing involving the changes of DMs' psychological reference on the uncertainties is also reasonable.

Figure 4 shows the comprehensive value of each alternative and the optimal alternative ranking at each stage determined using the proposed dynamic approach. In the first state T^1 , the traffic emergency occurs. Although there is limited and uncertain information for the experts from the events, they still evaluate the situation and select the optimal alternative A_2 . For the implementation of response A_2 , the emergency is evolving according to the internal and external factors and continues to change. For the coming stage T^2 , more explicit information obtained through the various information channels can influence the expectation of the experts' psychological reference satisfaction degree to be continually updated. Then, the decision-making results show that A_2 is unable to control the emergency effectively, and the alternative is adjusted to A_3 . Next, it happened to stage T^3 , and the new satisfactory degree of A_3 reaches an acceptable level, namely, A_3 plays a role in responding to the current emergency. There is no need to adjust alternative A_3 at this stage. Therefore, on account of the multistage, uncertainty, dynamic, and information updating in reality, it is practical that the emergency decision-making involves the updating process of the DMs' psychological reference satisfaction and the dynamic adjustment mechanism of the emergency response.

In addition, to further verify the stability of the proposed MSDEDM method, we conduct the sensitivity analysis of the DMs' risk attitudinal factor $\eta \in [0, 1]$. Table 7 shows the results of the comprehensive risk expected score function $RES(x_i)$, indicating the influence on the choice of the emergency alternatives. For the variable $\eta \in [0, 1]$, we obtain the variation features of $RES(x_i)$ at each stage, as shown in Figures 5 to 7.

Depending on the kinds of figures, we can determine that the risk expected score function $RES(x_i)$ decreases with the increase in value of η . However, as the risk attitudinal variable increases from 0 to 1, the obtained alternative rankings at each stage are changed. The ranking of the first stage T^1 is $A_2 > A_1 > A_3$, and thus alternative A_2 is always the optimal one and is selected as the response. For the second stage T^2 , the alternative ranking is $A_3 > A_2 > A_1$, and A_2 is adjusted to A_3 . According to the coming stage T^3 , after calculation by the proposed model, the obtained ranking is $A_3 > A_2 > A_1$, and alternative A_3 is always the optimal one and is selected as the response similar to the last stage T^2 . Thus, the sensitivity analysis shows that the alternative assessment value can change as the risk attitudinal variable η changes at each stage, which should be involved in the decision-making problems. Meanwhile, although the comprehensive value of each alternative is remarkably correlated linearly with the DMs' risk attitudinal factor, the ranking results are not affected by the factor, which further indicates the strong stability of the proposed approach.

Therefore, considering the emergency situations of the multistage, uncertainty, dynamic, and information updating in reality, the proposed MSDEDM approach has the following application advantages: (a) The study introduced IVTrIFNs that have more parameters than others into the multistage dynamic emergency decision-making process, to develop a novel approach for exquisitely describing the heterogeneous preference assessment information of the experts with respect to the uncertainty. This means that the obtained assessment information by IVTrIFNs can be closer to reality and let the results be more accurate in the situations of fuzziness and uncertainty. It is especially well suited for the dynamic emergency decision-making with the characteristics of uncertain information, time limitations,

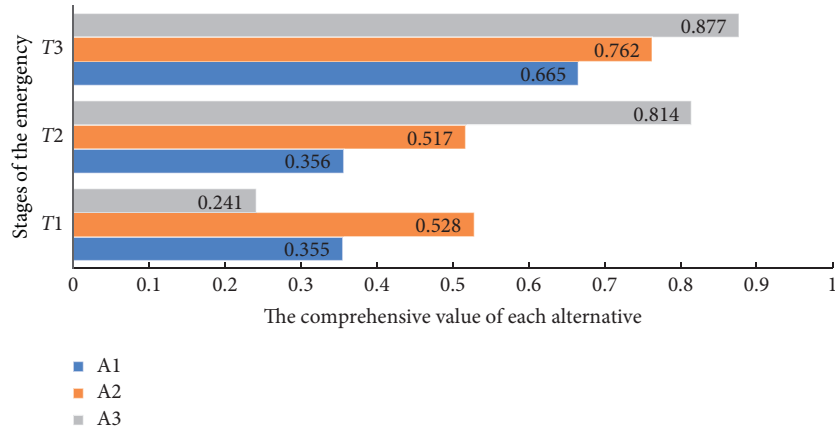


FIGURE 4: Comprehensive value of each alternative at each stage.

TABLE 7: Results of the comprehensive risk expected score function $RES(x_i)$.

T^p	A_i	$RES(V_i^p)$
T^1	A_1	$RES(V_1^1) = -0.119\eta + 0.415$
	A_2	$RES(V_2^1) = -0.142\eta + 0.599$
	A_3	$RES(V_3^1) = -0.094\eta + 0.288$
T^2	A_1	$RES(V_1^2) = -0.117\eta + 0.415$
	A_2	$RES(V_2^2) = -0.141\eta + 0.587$
	A_3	$RES(V_3^2) = -0.188\eta + 0.908$
T^3	A_1	$RES(V_1^3) = -0.198\eta + 0.764$
	A_2	$RES(V_2^3) = -0.190\eta + 0.857$
	A_3	$RES(V_3^3) = -0.182\eta + 0.968$

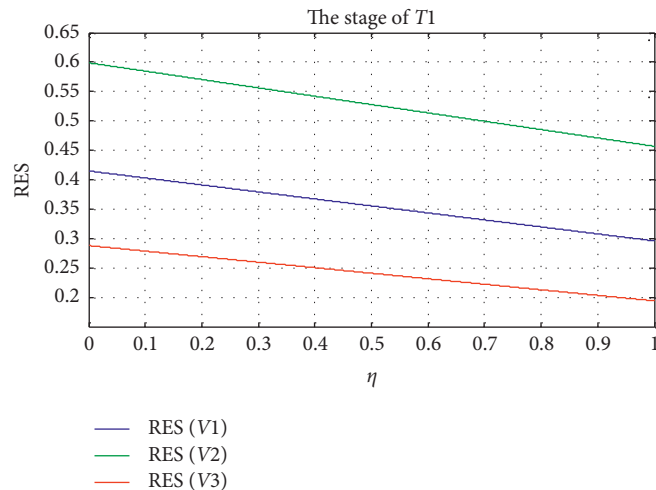


FIGURE 5: $RES(x_i)$ of stage T^1 .

and psychological pressure. Therefore, under these decision-making characteristics, the proposed solution can be applied to enhance the flexibility of decision-making results. (b) Considering the evolution of the emergency, we present a dynamic programming model based on the psychological reference satisfactory degree, to effectively generate and adjust the alternative of each stage. It is better for the dynamic emergency response and not only considers both the

dynamic nature of the events and DMs' heterogeneous preference but also generates the optimal adjustment alternation of each evolution stage. (c) With the DMs' risk preference behavior, we introduced the comprehensive risk expected score function to indicate the influence of the DMs' risk attitude and quantify the effect of the risk preference behavior. It can enhance the reliability of decision-making results.

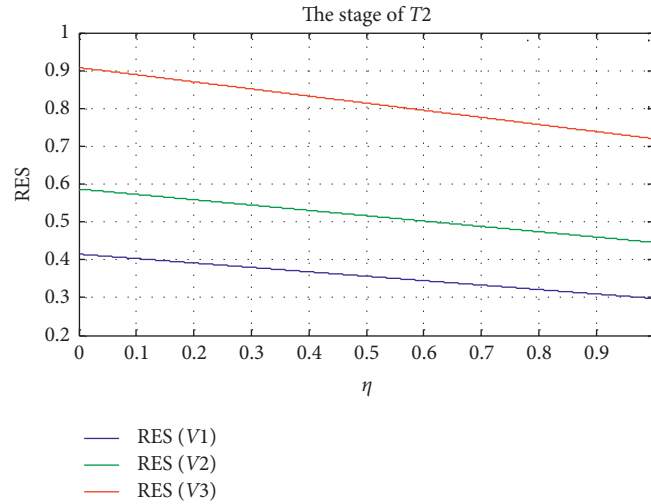


FIGURE 6: RES(x_i) of stage T^2 .

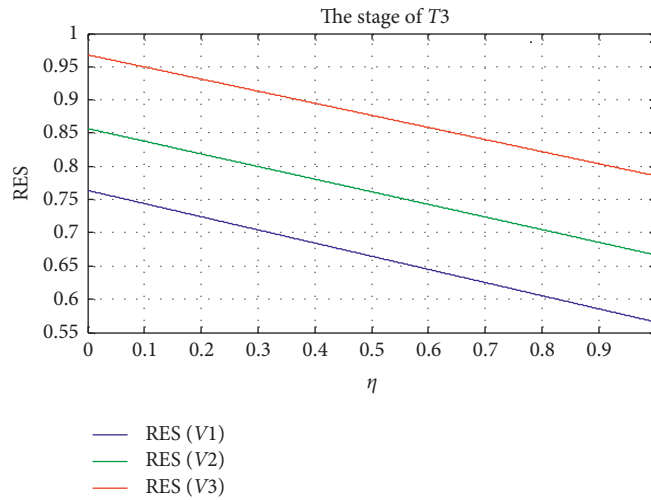


FIGURE 7: RES(x_i) of stage T^3 .

5. Concluding Remarks

Considering the emergency characteristic of the multistage, uncertainty, dynamic, and information updating in reality, we propose a novel MSDEDM approach with interval-valued trapezoidal intuitionistic fuzzy operational laws, psychological reference satisfaction theory, and dynamic programming model. With the emergency developing and decision information updating, we extend the single-stage emergency decision model to the multistage dynamic emergency decision model. Firstly, interval-valued trapezoidal intuitionistic fuzzy theory and method are applied to construct the decision-making framework under uncertainty environment. Then, a dynamic programming model is obtained based on the psychological reference satisfactory degree to effectively generate and adjust the alternative of each stage. Based on the programming model, the dynamic updating and adjusting mechanism of the emergency response are proposed. Besides, a sensitivity analysis based on the DMs' risk preference behaviors is conducted to reveal the reliability and effectiveness

of the proposed MSDEDM approach. Finally, a practical MSDEDM example of highway emergency is given to illustrate the effectiveness and practicability of the proposed dynamic fuzzy approach. Remarkably, the application implies that the fuzzy theory can well handle the uncertainty of real world in practice and have wide application prospect in other related fields, such as public transport [36–38], logistics network [39–41], and traffic management [42]. The method of the dynamic decision-making procedure would be a useful reference to the similar decision-making researches.

In the future, the proposed MSDEDM method can be applied to the hybrid depiction of the heterogeneous preference assessment information. DMs' new heterogeneous preference behaviors could be also involved, such as loss aversion, anchoring, disappointment, regret theory, and prospect theory. Moreover, the current emerging technology, including big data, data mining, and deep learning, provides a good direction for the development of EDM methods [43]. We strongly suggest integrating the mentioned technology with EDM to provide better measures.

Data Availability

The data used to support the findings of this study are available from the corresponding author upon request.

Conflicts of Interest

The author declares that there are no conflicts of interest regarding the publication of this paper.

Acknowledgments

This work was supported by the Social Science Foundation of Chongqing of China (nos. 2020BS62 and 2020TBWT-ZD02), the Special Project of Technology Foresight and System Innovation of Chongqing of China (no. cstc2020jsy-zdxwtB0003), the Research Start-up Funding of Chongqing Jiaotong University (no. 21JDKJC-A021), and the Team Building Project for Graduate Tutors in Chongqing (no. JDDSTD2019008).

References

- [1] L. Zhou, X. Wu, Z. Xu, and H. Fujita, "Emergency decision making for natural disasters: an overview," *International Journal of Disaster Risk Reduction*, vol. 27, pp. 567–576, 2018.
- [2] A. Hafezalkotob, A. Hafezalkotob, H. Liao, and F. Herrera, "An overview of MULTIMOORA for multi-criteria decision-making: theory, developments, applications, and challenges," *Information Fusion*, vol. 51, pp. 145–177, 2019.
- [3] Q. Ding, Y. Wang, and M. Goh, "TODIM dynamic emergency decision-making method based on hybrid weighted distance under probabilistic hesitant fuzzy information," *International Journal of Fuzzy Systems*, 2021.
- [4] J. Zheng, Y. Wang, K. Zhang, and J. Liang, "A dynamic emergency decision-making method based on group decision making with uncertainty information," *International Journal of Disaster Risk Science*, vol. 11, no. 5, pp. 667–679, 2020.
- [5] L. Yu and K. Lai, "A distance-based group decision-making methodology for multi-person multi-criteria emergency decision support," *Decision Support Systems*, vol. 51, no. 2, pp. 307–315, 2011.
- [6] Y. Liu, Z. Fan, and Y. Zhang, "Risk decision analysis in emergency response: a method based on cumulative prospect theory," *Computers & Operations Research*, vol. 42, no. 2, pp. 75–82, 2014.
- [7] L. Wang, Y. Wang, and L. Martínez, "A group decision method based on prospect theory for emergency situations," *Information Sciences*, vol. 418–419, pp. 119–135, 2017.
- [8] Y. Wang, Y. Liang, and H. Sun, "A regret theory-based decision-making method for urban rail transit in emergency response of rainstorm disaster," *Journal of Advanced Transportation*, vol. 2020, Article ID 3235429, 12 pages, 2020.
- [9] X. Xu, Q. Zhang, and X. Chen, "Consensus-based non-cooperative behaviors management in large-group emergency decision-making considering experts' trust relations and preference risks," *Knowledge-Based Systems*, vol. 190, p. 10, 2020.
- [10] P. Ren, Z. Xu, and Z. Hao, "Hesitant fuzzy thermodynamic method for emergency decision making based on prospect theory," *IEEE Transactions on Cybernetics*, vol. 47, no. 9, pp. 2531–2543, 2017.
- [11] Z. Zhang, L. Wang, and Y. Wang, "An emergency decision making method based on prospect theory for different emergency situations," *International Journal of Disaster Risk Science*, vol. 9, no. 3, pp. 407–420, 2018.
- [12] Z. Zhang, L. Wang, and Y. Wang, "An emergency decision making method for different situation response based on game theory and prospect theory," *Symmetry*, vol. 10, no. 10, p. 476, 2018.
- [13] X. Xu, X. Yin, and X. Chen, "A large-group emergency risk decision method based on data mining of public attribute preferences," *Knowledge-Based Systems*, vol. 163, pp. 495–509, 2019.
- [14] Z. Yan, H. Zhao, F. Wang et al., "Rapid assessment of building collapse based on sequential dynamic fusion of multi-source disaster information from news media," *International Journal of Disaster Risk Reduction*, vol. 51, 2020.
- [15] J. Gao, Z. Xu, Z. Liang, and H. Liao, "Expected consistency-based emergency decision making with incomplete probabilistic linguistic preference relations," *Knowledge-Based Systems*, vol. 176, pp. 15–28, 2019.
- [16] X. Li, H. Liao, and Z. Wen, "A consensus model to manage the non-cooperative behaviors of individuals in uncertain group decision making problems during the COVID-19 outbreak," *Applied Soft Computing*, vol. 99, 2021.
- [17] Z. Wang, H. Nie, and H. Zhao, "An extended GEDM method with heterogeneous reference points of decision makers and a new hesitant fuzzy distance formula," *Computers & Industrial Engineering*, vol. 146, 2020.
- [18] B. Farhadinia and Z. Xu, "An extended hesitant group decision-making technique based on the prospect theory for emergency situations," *Iranian Journal of Fuzzy Systems*, vol. 17, no. 3, pp. 51–68, 2020.
- [19] G. Wei, "Some induced geometric aggregation operators with intuitionistic fuzzy information and their application to group decision making," *Applied Soft Computing*, vol. 10, no. 2, pp. 423–431, 2010.
- [20] Y. Liu, Y. Wang, M. Xu, and G. Xu, "Emergency alternative evaluation using extended trapezoidal intuitionistic fuzzy thermodynamic approach with prospect theory," *International Journal of Fuzzy Systems*, vol. 21, no. 6, pp. 1801–1817, 2019.
- [21] J. Wu and Y. Liu, "An approach for multiple attribute group decision making problems with interval-valued intuitionistic trapezoidal fuzzy numbers," *Computers & Industrial Engineering*, vol. 66, no. 2, pp. 311–324, 2013.
- [22] G. Wei, "Approaches to interval intuitionistic trapezoidal fuzzy multiple attribute decision making with incomplete weight information," *International Journal of Fuzzy Systems*, vol. 17, no. 3, pp. 484–489, 2015.
- [23] A. Liu, Y. Xiao, H. Lu et al., "A fuzzy three-stage multi-attribute decision-making approach based on customer needs for sustainable supplier selection," *Journal of Cleaner Production*, vol. 239, pp. 1–16, 2019.
- [24] V. L. G. Nayagam, S. Jeevaraj, and P. Dhanasekaran, "An improved ranking method for comparing trapezoidal intuitionistic fuzzy numbers and its applications to multicriteria decision making," *Neural Computing and Applications*, vol. 30, no. 2, pp. 671–682, 2018.
- [25] S. Wan, J. Xu, and J. Dong, "Aggregating decision information into interval-valued intuitionistic fuzzy numbers for heterogeneous multi-attribute group decision making," *Knowledge-Based Systems*, vol. 113, pp. 155–170, 2016.
- [26] X. Ding, H. Liu, and H. Shi, "A dynamic approach for emergency decision making based on prospect theory with

- interval-valued Pythagorean fuzzy linguistic variables,” *Computers & Industrial Engineering*, vol. 131, pp. 57–65, 2019.
- [27] C. Cai, X. Xu, P. Wang, and X. Chen, “A multi-stage conflict style large group emergency decision-making method,” *Soft Computing*, vol. 21, no. 19, pp. 5765–5778, 2017.
- [28] J. Wu, X. Liu, Z. Wang, and S. Zhang, “Dynamic emergency decision-making method with probabilistic hesitant fuzzy information based on GM (1, 1) and TOPSIS,” *IEEE Access*, vol. 7, pp. 7054–7066, 2019.
- [29] X. Xu, B. Pan, and Y. Yang, “Large-group risk dynamic emergency decision method based on the dual influence of preference transfer and risk preference,” *Soft Computing*, vol. 22, no. 22, pp. 7479–7490, 2018.
- [30] Z. Hao, Z. Xu, H. Zhao, and H. Fujita, “A dynamic weight determination approach based on the intuitionistic fuzzy bayesian network and its application to emergency decision making,” *IEEE Transactions on Fuzzy Systems*, vol. 26, no. 4, pp. 1893–1907, 2018.
- [31] Z. Xu, “Intuitionistic fuzzy multiattribute decision making: an interactive method,” *IEEE Transactions on Fuzzy Systems*, vol. 20, no. 3, pp. 514–525, 2012.
- [32] J. Gao, Z. Xu, and H. Liao, “A dynamic reference point method for emergency response under hesitant probabilistic fuzzy environment,” *International Journal of Fuzzy Systems*, vol. 19, no. 5, pp. 1261–1278, 2017.
- [33] L. Wang, Z. Zhang, and Y. Wang, “A prospect theory-based interval dynamic reference point method for emergency decision making,” *Expert Systems with Applications*, vol. 42, no. 23, pp. 9379–9388, 2015.
- [34] Q. Ding and Y. Wang, “An improved aggregation operators-based method for multiple attribute group decision making using interval-valued trapezoidal intuitionistic fuzzy sets,” *Journal of Intelligent & Fuzzy Systems*, vol. 37, no. 1, pp. 965–980, 2019.
- [35] J. Wang and Z. Zhang, “Aggregation operators on intuitionistic trapezoidal fuzzy number and its application to multi-criteria decision making problems,” *Journal of Systems Engineering and Electronics*, vol. 20, no. 2, pp. 321–326, 2009.
- [36] J. Tang, Y. Yang, W. Hao et al., “A data-driven timetable optimization of urban bus line based on multi-objective genetic algorithm,” *IEEE Transactions on Intelligent Transportation Systems*, vol. 22, no. 4, pp. 2417–2429, 2020.
- [37] J. Tang, Y. Yang, and Y. Qi, “A hybrid algorithm for Urban transit schedule optimization,” *Physica A: Statistical Mechanics and Its Applications*, vol. 512, pp. 745–755, 2018.
- [38] W. Wang, D. Wang, H. Sun, and J. Wu, “Public transit service operation strategy under indifference thresholds-based bimodal equilibrium,” *Journal of Advanced Transportation*, vol. 50, no. 6, pp. 1124–1138, 2016.
- [39] Y. Wang, X. Ma, Z. Li, Y. Liu, M. Xu, and Y. Wang, “Profit distribution in collaborative multiple centers vehicle routing problem,” *Journal of Cleaner Production*, vol. 144, pp. 203–219, 2017.
- [40] Y. Wang, S. Peng, X. Zhou, M. Mahmoudi, and L. Zhen, “Green logistics location-routing problem with eco-packages,” *Transportation Research Part E: Logistics and Transportation Review*, vol. 143, p. 102118, 2020.
- [41] Y. Wang, Y. Yuan, X. Guan et al., “Collaborative two-echelon multicenter vehicle routing optimization based on state-space-time network representation,” *Journal of Cleaner Production*, vol. 258, p. 120590, 2020.
- [42] Y. Zou, B. Lin, X. Yang et al., “Application of the bayesian model averaging in analyzing freeway traffic incident clearance time for emergency management,” *Journal of Advanced Transportation*, vol. 2021, Article ID 6671983, 9 pages, 2021.
- [43] M. Tang and H. Liao, “From conventional group decision making to large-scale group decision making: what are the challenges and how to meet them in big data era? A state-of-the-art survey,” *Omega*, vol. 100, p. 102141, 2021.

Research Article

An Optimization Model for Tramp Ship Scheduling considering Time Window and Seaport Operation Delay Factors

Ang Yang , Yu Cao , Kang Chen , Qingcheng Zeng, and Zigen Chen

School of Maritime Economics and Management, Dalian Maritime University, Dalian 116026, China

Correspondence should be addressed to Kang Chen; chenkang@dlnu.edu.cn

Received 14 November 2020; Revised 20 February 2021; Accepted 3 March 2021; Published 23 March 2021

Academic Editor: Yong Wang

Copyright © 2021 Ang Yang et al. This is an open access article distributed under the Creative Commons Attribution License, which permits unrestricted use, distribution, and reproduction in any medium, provided the original work is properly cited.

The quantity of electrical coal transported through the tramp shipping network is increasing due to the high demands. This trend has increased the scheduling difficulty combined with the underdevelopment of the private thermal power plant port. The high coal consumption and low port storage capacity requires the scheduling of the tramp ship to be on a strict time window to ensure the continuous operation of the thermal power plant. The low port unloading capacity often leads to the port congestion and delay of the unloading operation. This paper develops a mixed-integer-programming model for the optimization of the tramp ship scheduling to reduce the total operation cost, including the transportation cost and the unloading waiting cost, and the branch-and-price algorithm is adopted to solve this large-scale model. The model and algorithm are tested with historical operation data from the thermal power plant in the southern coastal areas of China. The optimized scheme significantly reduces the total operation cost by reducing the unloading waiting time and the number of active vessels in certain periods. The results also demonstrate the algorithm improvement in the aspects of the optimization quality and efficiency comparing with the heuristic solution.

1. Introduction

The supply of electric coal (coal used to generate electricity) in the southern coastal areas of China follows the basic pattern of transporting coal from north to south [1]. Electric coal is mainly transported through waterways from the main producing regions of northern China to the numerous thermal power plants located in the southern coastal areas [2]. In this vast and complex supply system, large-scale power generation companies (who typically operate approximately 10–20 power plants) play the role of transport organizers. These companies are responsible for not only organizing the electric coal transport fleet through the international ship charter market but also setting the scheduling and operation plan of the fleet. Specifically, these companies make decisions regarding the electric coal transportation plan, ship routing, and scheduling. In the past, the experience and subjective judgment of decision makers (heads of the transportation departments of the power generation companies) have been the primary basis

for formulating the electric coal transportation plan [3]. Due to the limited amount of transport and the small size of the fleet, this practice did not present severe flaws at the time and was able to ensure that transportation plans based on the human experience achieved a delicate balance between efficiency and cost.

However, in recent years, the electric coal transportation system has undergone a disruptive change with further increases in the amount of thermal power generation. To meet the growing electricity demand, since 2010, the Chinese government has stepped up efforts to build thermal power units in the southern coastal areas. In turn, the volume of coal and the size of coal transportation fleets have also increased rapidly. In 2010, the company transported only 30,000 tons of electric coal per day and used only five vessels every day on average [4]. In contrast, in 2016, this company transported approximately 70,000 tons per day and used over 20 vessels every day [4].

With the rapid growth of transportation needs, several characteristics of the near-sea electric coal transportation

have drawn the attention of many researchers. The electric coal transportation is strictly based on pre-made plans, which includes the loading and unloading task, fleet management, and fleet scheduling. Because of the high consumption volume and the low storage capacity of the small thermal power plant port, the transportation tasks have a high requirement on the time sensitivity to ensure the continuous supply of the electrical coal for the thermal plant. The fleets consist of different types and number of ships with different transportation capacities and often supported with the renting of the additional vessel for temporary high capacity demands [5, 6]. In electric coal transportation systems, the operating capacity of these ports is typically extremely limited because unloading ports are mainly constructed and operated by thermal power plants. These ports can only provide unloading services for one ship at a time, often resulting in long queues of ships waiting to be unloaded (i.e., the port congestion problem). Lastly, the railway has always been one of the essential modes of transportation in the southern Chinese coastal electric coal transportation system [7]. Since the Chinese railway is the dominant transportation mode, the establishment of the modern integrated transportation hubs has also enabled the land-and-water coordinated transport [8, 9].

Three factors should be considered for the formulation of the electric coal transportation plan (referred to as the electric coal ship-scheduling problem, ECSSP). The first factor is the time-window constraints of electric coal transportation. Since the storage capacity of the unloading port is quite limited compared to the electric coal consumption, even the minor delay of the transportation could cause the shutdown of the powerplant, which in turn leads to economic and social loss. Thus, it is crucial for the shipment to be completed within their time windows. The second factor is the congestion of the unloading port. The congestion could cause port operation delays, which could not be neglected due to the short voyage duration and high operation frequency [10]. Because of the strict time window and the interdependent scheduling for the whole transportation operation, the delay could have a chain reaction effect, which would decrease the effectiveness of the entire transportation network. The third factor is the synergy between water transportation and railway transportation. The complementarity and cooperation of the railway with waterway transportation are necessary guarantees to ensure the stability of electric coal transportation.

The abovementioned three factors make the current ECSSP highly complex. Decision makers should not only consider the constraint of the shipping time windows on scheduling and the ship unloading processes but also the reasonable cooperative application of water transportation and railway transportation. Thus, it is more complicated than the traditional tramp ship routing and scheduling problem and deserves further study [11]. Therefore, how to design a reasonable electric coal transportation plan has become a significant issue for major power generation companies [3].

Based on the unique characteristics of the electric coal transportation system in the southern coastal areas of China,

this paper addresses the ECSSP under the background of hard time-window constraints, unloading port congestion, and synergy between water transportation and railway transportation. The main contributions of this paper are as follows: (1) A new tramp ship routing and scheduling optimization method considering port congestion is proposed. (2) A mixed-integer-programming model is developed to optimize the shipping routing, the corresponding scheduling, and the share rate for water and railway transportation simultaneously (e.g., the beginning time point of the transportation task and the necessary waiting times at unloading ports). (3) A new algorithm based on branch-and-price is designed, which can solve ECSSP efficiently.

This paper is organized as follows. In Section 2, we review the relevant literature, clarify the field of ECSSP research, and analyze the difference and connection between the ECSSP and the corresponding classic problems. In Section 3, a detailed description of ECSSP is provided. A mixed-integer-programming model is developed in Section 4. The algorithm of this model is designed in Section . In Section 6, the model and the algorithm are tested with historical data. The performance of the algorithm is presented, and the practical value of the model and algorithm is discussed based. Conclusions are provided in Section 7.

2. Literature Review

According to Ronen's definition, the ECSSP belongs to the tramp ship routing and scheduling problem (TRSP) [12]. Systematic reviews of the literature on the TRSP have been provided by Christiansen et al. [11, 13], Ronen [12, 14], Lane, et al. [15], and Meng, et al. [16]. Christiansen and Fagerholt [17] noted that approximately 40% of the TRSP models use the set partitioning (SP) model framework, which can characterize the TRSP effectively. The core idea of the SP model framework is to translate the TRSP into a classic set partitioning problem by assuming that all the feasible ship-scheduling plans are preknown. A feasible prerequisite for this framework is that decision makers must be able to provide an estimation of the feasible ship-scheduling plans set in advance.

For the TRSP, the early representative studies include the following research. Brown et al. [18] conducted a thorough study of the crude oil transportation problem. In this study, carriers must ship crude oil from the Middle East to Europe and North America with hard time-window constraints. For a known fleet, the decision maker must design a crude oil transport scheduling for each vessel. In response to this problem, Brown et al. [18] constructed an integer-programming model based on the SP framework. Due to the relatively small size of the problem, the feasible ship-scheduling plans set can be obtained by enumeration, which means that the model can be solved efficiently. Therefore, we refer to this kind of method the enumeration SP algorithm (ESPA). Bausch et al. [19] and Perakis and Bremer [20] also used the ESPA to solve the TRSP in their respective studies. Christiansen and Fagerholt [17] discussed an extension of the TRSP where decision makers must consider the impact

of port nonoperating periods and climatic conditions on the ship-scheduling plan and also built a model based on SP and solved it using the ESPA.

For the port congestion problem, while many studies indicate it is a significant and complex issue, only limited solutions are proposed. Jafari [21] studied the causes of the lag and halt in port operation, including document incompleteness, shortage of ship and truck, the unpreparedness of goods owners, and labor issues. These factors could have significant effects on port operation efficiency. Rahman et al. [22] also study the factors that caused the port operation delay and found that a variety of aspects of ports, ships, cargo owners, and environmental uncertainty all contribute to the port congestion. Their research suggested that the subfactor of foul weather and tide prediction is the most significant factor for port operation delay, which is also the main impact factor for the fleet scheduling problem. For electrical coal transportation, the unloading port for the corresponding thermal power plant is relatively small and only has 1 or 2 berths with low port storage capacity. Once something unexpected happens, subsequent ships can only wait for the available berths for the loading and unloading operations. Thus, the port congestion could cause a significant delay for the following operation. To solve this complex issue, several studies have attempted to provide effective solutions. For example, Kavirathna et al. [23] proposed the vessel transportation policy for the terminals' cooperative management to increase the overall efficiency of the port. The berth scheduling problem is also studied to achieve the minimized total port operation delay [24, 25]. The problem of port operation delay can also be regarded as the unbalanced distribution of logistic resources in time and space. Some scholars adopted the method of state-space-time (SST) network to promote the collaboration of the logistic network and optimize the distribution of logistic resources in time and space. Wang et al. [26] adopted the state-space-time (SST) network to solve the problem of collaborative two-echelon multicenter vehicle routing optimization. By promoting collaboration among service providers in the logistics network, logistic costs are reduced, transportation efficiency is improved, and transportation emissions are reduced [26]. The green logistics route planning problem with ecopackages could also be optimized by identifying the best location strategy with the state-space-time (SST) network [27]. While those methods show great potential, they are not suitable for the Chinese electric coal transportation issues for the relatively small unloading ports with only limited unloading capacity. Therefore, from the perspective of fleet management, introducing the operation delay time into the TRSP could be an innovative solution for the port congestion issue.

In recent years, scholars have reached a consensus on the modeling of the TRSP [11], and the standard TRSP model has been proposed. However, because the fleet sizes mentioned by these TRSP issues are continuously expanding and the demands for transport are diversified, it has become increasingly difficult to enumerate all feasible ship-scheduling plans. The traditional ESPA-based enumeration method is no longer

applicable, and how to solve the TRSP efficiently has become the research focus. According to the standard TRSP model, Brønmo et al. [28] proposed a multistage local search heuristic algorithm and compared the advantages and disadvantages of the new algorithm through four examples. This study proved that the new algorithm could effectively solve the large-scale TRSP within a feasible timeframe. Kobayashi and Kubo [29] proposed a column generation solution algorithm (CGSPA) for the standard TRSP model, in which the shortest path algorithm considering the constraints of time windows were incorporated. Fagerholt et al. [30] studied a variant of the TRSP in which there is a particular mechanism for addressing a shortage in transport capacity. This mechanism allows decision makers to address the shortage of fleet capacity by temporarily renting vessels. However, the chartered vessels must complete at least two transport missions before releasing. For this problem, they proposed an integer-programming model and a tabu search algorithm (denoted as TSPA) based on the work of Korsvik et al. [31]. Norstad et al. [32] considered the factor of ship speed while studying the TRSP and proposed a local heuristic search algorithm (named multistart) to solve this problem. Hemmati et al. [10] proposed a two-phase hybrid heuristic algorithm for the maritime inventory and routing problem that can also be used to solve the TRSP. Wang et al. [33] also adopted the integer-programming-model-based approach for searching the reasonable solutions for each vehicle in the distribution center network, which provides the best sequential transportation coalition and efficient model performance. Similar studies include the work of Sopot and Gribkovskaia [34], Gansterer et al. [35], and Cuesta et al. [36].

A comprehensive analysis of the existing relevant literature illustrates that the majority of studies assume that the ships in the fleet do not affect each other during the transportation task. However, in the ECSSP proposed in this paper, the operational statuses of each ship are interrelated. Due to the operation delay caused by port congestion, the deviation of the transportation plan of any ship may have unexpected effects on the transport of other ships. Therefore, the problem proposed in this paper represents a special type of TRSP, in which the scheduling plans of the vehicles (ships) interfere with and affect each other. Solving the ECSSP could enrich the research on the routing and scheduling optimization method with the consideration of the port congestion. The mixed-integer-programming model proposed in this research considered characteristics such as the shipping routing, related scheduling, and land-and-water coordinated transport and achieved simultaneous optimization. This paper also proposed a branch-and-price-based algorithm for the effective solving of ECSSP, which would be beneficial to solve other complex models.

3. Problem Description

The China Southern Coastal Electric Coal Transportation System (CSTS) studied in this paper is a complex transportation system involving multiple links, multiple constraints, and multiple transportation modes. The system consists of the electric coal supply port (referred to as the loading port), electric coal unloading port (referred to as the

unloading port), water transport subsystem, and rail transport subsystem. Electric coal must be shipped from the loading port to reach a specific unloading port by the waterway or rail subsystem. The CSTS has five unique features that cannot be ignored.

First, while the spatial distribution of loading ports is concentrated, the spatial distribution of the unloading ports is scattered; thus, the water transport network is star shaped. As shown in Figure 1, in the CSTS, the loading ports are densely distributed in a small area (Supply Port Group) in the western region of the Bohai Sea. These ports typically have sufficient transport capacity with the major coal-producing regions and, thus, have a steady coal supply capacity. In addition, due to the dense distribution of loading ports, the western Bohai Sea region has an extremely high port service capacity and can meet the demand for electric coal loading operations of any volume at almost any time. In contrast, because most of the unloading ports are built near power plants, they are widely clustered in the coastal areas of South China. In terms of the network structure, if we abstractly view the supply port group as a virtual loading port, then the network can be considered as a star-shaped transport network, with the center as the virtual loading port and the peripheral nodes as the unloading ports.

Second, electric coal transportation has strict time and capacity requirements. In practice, due to the limitation of coal storage capacity, thermal power plants must regularly replenish coal inventories and prepare a detailed task list of electric coal purchases and transportation in advance. The task list provides details of each transport mission, including the type of coal to be transported, the volume of coal, the loading port, the unloading port, and the time window for loading and unloading. The time window is the time duration between the earliest possible loading time and the latest possible unloading time of the ship loading and unloading operation according to the berth operation schedule and ship operation schedule. Because the implementation status of the task list directly determines whether the relevant thermal power plants can operate stably, decision makers often demand that the electric coal transportation system strictly fulfills the listed transportation tasks, even without cost considerations. Therefore, the electric coal transport system must be able to provide adequate capacity to ensure that the electric coal is shipped and delivered within the prescribed time window.

Third, electric coal transportation ships have been switched between the status of commissioning and storage. In the CSTS, decision makers usually need to manage a self-owned fleet of 20 to 30 ships of various types. In order to reduce the operating costs of the fleet, decision makers must implement temporary decommissioning of some vessels and choose when to use them again based on the demand for electric coal transportation. Therefore, in ECSSP, decision makers must not only consider the ship's scheduling plan but also must plan the operation status (commissioning and decommissioning) of each ship. Because different types of ships have significantly different decommissioning costs and

operating costs, how to formulate an appropriate operation plan based on the needs of electric coal transportation has also become an important issue.

Fourth, the transportation pattern of single demand, single mode, and single voyage is adopted. This transportation pattern is the standard ship-scheduling rules for thermal coal transportation in production and transportation practice with significant advantages. Since 3%–8% cargo loss will occur for the transportation mode of the multiple bulk cargo, the adopted transportation could efficiently reduce the cargo loss for the frequent electric coal transportations in the network. Besides, transporting multiple cargoes in a single voyage or transporting the cargoes to multiple unloading nodes could bring significant difficulties for the statistical management of the company. Thus, the transportation pattern of single demand, single mode, and single voyage is adopted in the Coastal Electric Coal Transportation System (CSTS). In the CSTS, this pattern is adopted to facilitate the settlement of freight, avoid mutual pollution between different types of coal, and reduce unnecessary coal losses due to transport. In this pattern, only one mode of transportation can be used for certain transportation tasks. The transportation task cannot be split in any way, and a ship can complete at most one transportation task in a single voyage. This pattern forces decision makers to make a careful choice between water transportation and rail transportation when setting up a fleet to match the ship's capacity with transportation demands. How to make efficient use of the transportation resources of the system has become one of the critical issues that decision makers must solve on the premise of ensuring that transportation tasks are completed on time.

Fifth, the factors involved in transport organization are complex. This feature is mainly reflected in the following two interactive relationships: the interaction between rail transportation and waterway transportation. The interaction relationship selected for this paper is because of the following reasons. Even though the waterway transportation has the advantage of lower transportation batch cost, thermal coal transportation should consider other factors rather than a simple economic factor. The supply of thermal coal must guarantee the continuous operation of thermal power plants as the premise. However, the disruption of the coal transportation could cause the shutdown of the thermal power plant due to the low port storage capacity of the thermal coal port and the high coal consumption rate. As discussed above, the electoral coal transportation by waterway could suffer from the port congestion issue, whereas rail transportation can ignore uncertain factors such as the port congestion. Thus, it is necessary to consider the combination of water transportation and other transportation modes to complete the thermal coal transportation to ensure that thermal coal can be supplied to thermal power plants in time. In the CSTS, the water transportation subsystem is designed, managed, and operated by the power generation group (i.e., the decision maker). Decision makers will form a fleet in advance according to the electricity production plan and then formulate and implement a dispatch plan for electric coal ships based on the transportation

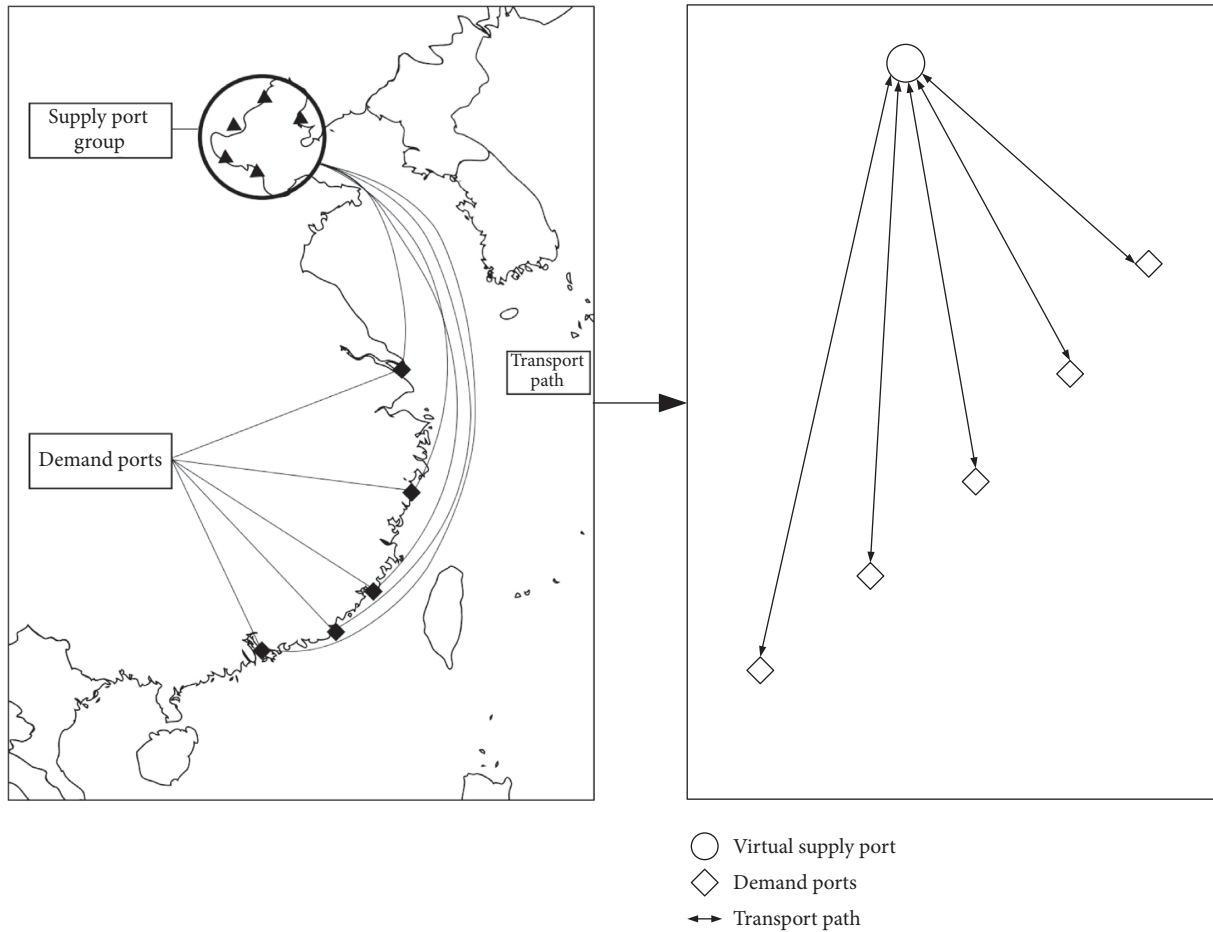


FIGURE 1: Distribution of electric coal loading and unloading ports and topology of the transportation network.

task list and the operational capabilities of each port. The railway transportation subsystem is operated by the government department of railway transportation. The decision makers obtain the necessary transportation services through purchase. The advantages of the waterway transportation subsystem are large transportation capacity and low unit transportation cost; however, the transportation organization is very complicated due to the impact of the port congestion. The advantage of the railway transportation subsystem is that the transportation capacity is abundant, and the transportation process is reliable. The decision maker does not need to consider the transportation scheduling problem, nor is it affected by the factors of port congestion, but the transportation cost is high. Therefore, how to make full use of the complementary advantages of the two transportation modes to improve transportation efficiency and reduce transportation costs is another crucial issue that decision makers must consider.

The interactions between ship-scheduling plans amplify the impact of port congestion. In the traditional TRSP problem, the scheduling process of a single ship is relatively independent, and the operation of each ship does not affect the others. However, in the electric coal ship-scheduling problem, the port congestion has a chain reaction effect on the operation processes of all ships in the plan period, which

causes difficulty in the electrical coal supply for the subsequent thermal power plant. For example, when ship A encounters congestion in port i , this congestion may delay its arrival at subsequent port j , which in turn affects ships B and C that use port j as the unloading port. The impact of congestion in a certain port, with the unloading port as a medium, creates a continuous and complex chain reaction causing more significant operation delays throughout the fleet and planning period and ultimately disrupts the scheduling of every ship within the system. Under this mechanism, the improper scheduling of any one vessel may disrupt the operation of the entire system through the amplification of a chain reaction. Therefore, the scheduling problem of ECSSP with the consideration of operation delay is far more complicated than that of the traditional TRSP problem. Decision makers must not only focus on the conventional decision-making problems, such as the matching of ships and transportation tasks and the order of ships to complete transportation tasks, but also accurately consider when each task should begin, when it is completed, and the waiting period at each port, thus reducing unnecessary economic losses.

Based on the abovementioned facts, we present the following description of the ECSSP proposed in this paper. Given are (1) the planning period, (2) the task list of electric

coal transportation (including transportation volume, loading and unloading port, and loading and unloading time window), and (3) the information regarding renting ships (e.g., daily rent, earliest available time, dead weight, and average speed). Assumptions: there is only one hub-type loading port in the system, and the loading and unloading capacity of the port is sufficient for the transportation needs, and it is the starting point for all of the electric coal transportation tasks; there are several unloading ports in the system, each port has several berths, and berthing and unloading operations are arranged in accordance with the principle of first-come first-serve; electric coal transportation tasks can use either waterway or railway transportation; electric coal transportation adopts the pattern of a single-demand, single-mode, single-batch mode; all ships are activated at the beginning of the planning period, and the decision makers can choose the opportunity to switch (enable or store) according to their needs. However, since this switching requires a long preparation time and complicated procedures, it is assumed that the operating status of each ship can only be switched at most two times during the observation period. Decision making: to achieve the goal of the lowest total cost of the transportation system, the following decisions are required: choosing the transportation method for each transportation task; assigning transportation tasks to each ship; determining the task-execution sequence, the best start and end time; and switching the ship's operating status between active and inactive.

4. Model Formulation

4.1. Water Voyage and Land Voyage. To facilitate the reader's understanding, we first introduce the concepts of water voyage and land voyage. Water voyage refers to the procedure by which a ship departs from a loading port, arrives at a designated unloading port, and then returns to the loading port (assuming that the ship must return to the loading port to be on standby after transportation). The water voyage can be further divided into delivery subvoyage and return subvoyage. The former refers to the process of the ship's departure from the loading port to the unloading port, and the latter refers to the process of returning the ship from the unloading port to the loading port. Land voyage refers to the process by which electric coal is transported by the railway system.

Both water voyage and land voyage are derived from the electric coal transportation task. Assume that an electric coal transportation task refers to electric coal being shipped from the port a in period t_1 - t_2 and arriving at the port b in period t_3 - t_4 , where the transportation volume is d tons. Then, the water voyage derived from this task is the process of the loading of d tons of electric coal at the port a in period t_1 - t_2 , then starting the delivery, arriving at the port b in period t_3 - t_4 , and finally, returning to port a after unloading. The land voyage for this task is d tons of coal are loaded from the port a in period t_1 - t_2 and arrive at the port b in period t_3 - t_4 . To simplify the problem, we set the following terms for the land voyage: (1) for any transportation task, the electric coal transportation can always be delivered on time by land voyage and that land voyage is always feasible; however, the

cost is higher; (2) because of the single-demand, single-mode, single-voyage mode of transportation, water and land voyages derived from the same transportation are mutually exclusive, and decision makers can choose only one way to fulfill the transportation task. From now on, we shall refer to the water and land voyages derived from the same transportation task as a complementary voyage. For the ease of reading, the sets, parameters, and variables that appear multiple times in this article are listed in Table 1.

It should be noted that this article additionally defines two virtual water voyages, which are, respectively, denoted as 0 and \bar{e} . Voyage 0 means that the ship starts to carry out water transportation tasks from an inactive status, while voyage \bar{e} means that the ship no longer performs any water transportation tasks and enters the storage state. For example, if ship A performs voyage 0 at time t_1 and voyage \bar{e} at time t_2 , it means that ship A switched from the storage state to the operating state at time t_1 and from the operating state to the storage state at t_2 . For voyage 0 and voyage \bar{e} , the values of t_i^l , t_i^{us} , T_i^l , and T_i^u are all 0, and the value of t_i^e and t_i^{uc} is the length of the observation period.

4.2. Feasible Single-Vessel Scheduling Plan. The concept of a single-vessel scheduling plan can be defined based on the concept of a water voyage. The single-ship-scheduling plan is the work plan and the schedule of the electric coal transportation ship, which determines the operation timing, operation order, and specific water voyage nodes. Let vector $((\alpha_{vp}), (y_{ip}), (t_{ip}^s), (T_{ip}^{wl}), (T_{ip}^{wu}))$ represent a known single-ship-scheduling plan p . Whether the design of a single-ship-scheduling plan p is reasonable depends mainly on whether the key parameters satisfy the following constraints:

Constraint group 1: the constraints of the task selection and the sequencing of the water voyage.

Equations (1)–(4) provide the first set of constraints that ensure that the single-ship-scheduling plan is feasible, which mainly describes the conditions that a feasible plan p should meet in the selection and sequencing of the water voyage. x_{ijp} is a binary variable; if the ship in the single-ship-scheduling plan p starts water transportation task j immediately after it finishes task i , it takes a value of 1; otherwise, it is 0. Equations (1) and (2) ensure that the designs for voyage 0 and voyage \bar{e} are satisfied, which means the plan p starts at virtual node 0 and ends at the virtual node \bar{e} . Equation (3) is used to ensure that any water voyage i has presequence and postsequence voyages if it is to be carried out. The algebraic relationship between y_{ip} and x_{ijp} is defined in equation (4).

$$\sum_{j \in I} x_{0jp} = 1, \quad (1)$$

$$\sum_{j \in I} x_{j\bar{e}p} = 1, \quad (2)$$

$$\sum_{j \in I} x_{ijp} = \sum_{j \in I} x_{jip}, \quad \forall i \in I, \quad (3)$$

TABLE 1: Notation and primary parameters.

Sets:	
I	The set of known water voyages, each element of which is denoted as i ; denote $0 \in I$, $\bar{e} \in I(0$ and \bar{e} as virtual nodes, the meaning will be explained in the following section)
G	The set of unloading ports, each element is denoted as g
V	All ships that can be rented, each element is denoted as v
P	The set of single-ship-scheduling plan, each element is denoted as p
Q	The set of fleet-scheduling plan, each element is denoted as q , $Q \subseteq P$
Parameters:	
t_i^{ls}	The earliest loading time of the water voyage i
t_i^{le}	The latest loading time of the water voyage i
t_i^{us}	The earliest unloading time of the water voyage i
t_i^{ue}	The latest unloading time of the water voyage i
t_{ip}^s	The starting time of the single scheduling plan p in the water voyage i
t_i	Any specific time of the ship during the water voyage i
T_{ip}^{wl}	The waiting duration of the loading operation in the single scheduling plan p for the water voyage i
T_{ip}^{wu}	The waiting duration of the unloading operation in the single scheduling plan p for the water voyage i
T_i^{r1}	The voyage duration of forward subvoyage in water voyage i (days)
T_i^{r2}	The voyage duration of return subvoyage in water voyage i (days)
T_i^l	The net loading time period of the water voyage i (do not include the loading time due to port congestion, days)
T_i^u	The net unloading time period of the water voyage i (do not include the unloading time due to port congestion, days)
w_v	The transportation capacity of ship v
b_g	The number of berths in port g
d_i	The task volume of the water voyage i
Decision variables:	
α_{vp}	If the single-ship-scheduling scheme p is executed by ship v , it is 1; otherwise, it is 0
β_{ig}	If the port g is an unloading port in waterway voyage i , it is 1; otherwise, it is 0
γ_i	If the task of corresponding electric coal transportation is undertaken by the complementary railway land plan in waterway voyage i , it is 1; otherwise, it is 0
x_p	If the feasible single-ship-scheduling plan $p \in P$ is selected in the subset Q , it is 1; otherwise, it is 0
x_{ijp}	For the single-ship-scheduling plan p , if the ship starts water transportation task j immediately after it finishes task i , it is 1; otherwise, it is 0
y_{ip}	If the single-ship-scheduling scheme p is executed by water voyage i , it is 1; otherwise, it is 0
y_{ipv}	If the plan p uses the ship v to perform the water voyage i , it is 1; otherwise, it is 0
z_{ipt}	For the corresponding ship of the plan p at the time point t (day t), if it is currently performing water voyage i and in unloading status, it is 1; otherwise, it is 0

$$y_{ip} = \sum_{j \in I} x_{ijp}, \quad \forall i \in I. \quad (4)$$

Constraint group 2: the constraints on the time point when the water voyage is undertaken.

The relationship between the three variables t_{ip}^s , T_{ip}^{wl} , and T_{ip}^{wu} and the key time nodes of the water transportation task is shown in Figure 2. For example, in the

plan p , if the first water voyage executed is i , and then, the t_{ip}^s is the starting time of the water voyage i . Since the execution order of the task is depicted by x_{ijp} , the values of t_{ip}^s and x_{ijp} are tightly related. In addition, to ensure that the single-ship-scheduling plan is feasible, the values of t_{ip}^s , T_{ip}^{wl} , and T_{ip}^{wu} should also meet the loading and unloading time-window constraints related to the water transportation task.

$$t_{jp}^s \geq t_{ip}^s + T_{ip}^{wl} + T_i^l + T_i^{r1} + T_{ip}^{wu} + T_i^u + T_i^{r2} + M(1 - x_{ijp}), \quad \forall i, j \in I, \quad (5)$$

$$t_{0p}^s \geq \sum_{v \in V} t_v^0 \alpha_{vp}, \quad (6)$$

$$y_{ip} t_i^{ls} \leq t_{ip}^s + T_{ip}^{wl} \leq y_{ip} t_i^{le}, \quad \forall i \in I, \quad (7)$$

$$y_{ip} t_i^{us} + (1 - y_{ip})(T_i^{r1} + T_i^l) \leq t_{ip}^s + T_{ip}^{wl} + T_i^{r1} + T_i^l + T_{ip}^{wu} \leq y_{ip} t_i^{ue} + (1 - y_{ip})(T_i^{r1} + T_i^l), \quad \forall i \in I, \quad (8)$$

$$z_{ipt} \leq T_{ip}^{wu}, \quad \forall i \in I, \quad (9)$$

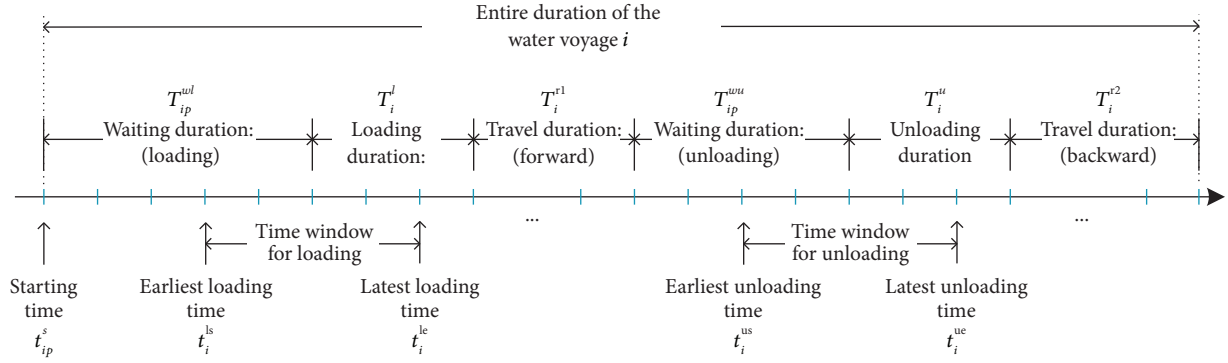


FIGURE 2: Relationship between the definitions of the water voyage time variables.

$$t_i \geq t_{ip}^s + T_{ip}^{wl} + T_i^{r1} + T_i^l + T_{ip}^{wu} - M(1 - z_{ipt}), \quad \forall i \in I, \quad (10)$$

$$t_i \leq t_{ip}^s + T_{ip}^{wl} + T_i^{r1} + T_i^l + T_{ip}^{wu} + T_i^u + M(1 - z_{ipt}), \quad \forall i \in I, \quad (11)$$

$$\sum z_{ipt} \geq y_{ip} T_i^u, \quad \forall i \in I. \quad (12)$$

Based on the abovementioned analysis, the second set of constraints that ensure the feasibility of the single-ship-scheduling plan is shown in equations (5)–(11), where M represents a maximal positive number. The binary variable z_{ipt} represents whether the corresponding ship of the plan p is performing water voyage i and at unloading status at the time point t (dayt); if so, then, z_{ipt} takes a value of 1; otherwise, it is 0. Equations (5) and (6) depict the algebraic relationship between t_{ip}^s and x_{ijp} ensuring the start time of a water voyage is the end time of its preceding voyage, where t_v^0 represents the initial time for the ship v to be operational. Equations (7) and (8) ensure that the settings of T_{ip}^{wl} , T_{ip}^{wu} , and t_{ip}^s satisfy the time-window constraints of the relevant water voyage. Equation (9) requires that the value of z_{ipt} is 0; when $y_{ip} = 0$, namely, if the plan p does not implement the water voyage, the ship used in the plan shall not be in the unloading state of the water voyage at any time. Equations (10) and (11) determine the logical relation between T_{ip}^{wl} , T_{ip}^{wu} , and z_{ipt} at time t_i . Equation (12) makes sure that the time for ship docked in the port is not less than the port unloading time used in the plan p .

Constraint group 3: constraints on ship selection considering the single-vessel scheduling.

Equations (13)–(15) are the third group of constraints, which mainly describe the conditions that the feasible plan p should meet in choosing the vessels. Among them, w_v indicates the transportation capacity of the ship v ; the variable y_{ipv} indicates whether the plan p uses the ship v to perform the water voyage i ; if it is, it is taken as 1; otherwise, it is taken as 0; d_i represents the task volume of the water voyage i . Equation (13) is used to ensure that plan p uses only one vessel. Equation (14) is used to ensure that the capacity of the vessel is larger than the transportation demand. Equation (15) is the

mathematical relationship among y_{ipv} , y_{ip} , and α_{vp} ; that is, when y_{ip} and α_{vp} are both equal to 1, y_{ipv} is taken as 1; otherwise, it is 0.

It should be noted that, in order to reduce the complexity of solving the model and construct a linear programming optimization model, this article linearizes equation (15) to obtain equation (15a). The apostrophe in the equation label indicates it is the linearization version of the equation without the apostrophe. In the following, we define a plan p that satisfies equation (1)–(15) as a feasible single-ship-scheduling plan. The complete set of such feasible plans is denoted as P .

$$\sum_{v \in V} \alpha_{vp} = 1, \quad (13)$$

$$\sum_{v \in V} w_v y_{ipv} \geq d_i y_{ip}, \quad \forall i \in I, \quad (14)$$

$$y_{ipv} = y_{ip} \cdot \alpha_{vp}, \quad \forall i \in I, v \in V, \quad (15)$$

$$\frac{1}{2}(y_{ip} + \alpha_{vp}) - \frac{1}{2} \leq y_{ipv} \leq \frac{1}{2}(y_{ip} + \alpha_{vp}), \quad \forall i \in I, v \in V. \quad (15a)$$

4.3. Feasible Fleet Scheduling Plan

As mentioned at the end of Sections 1 and 2, there will be an interactive relationship between different single-ship feasible plans when they are implemented. The fourth set of constraints will be constructed for the impact between different single-ship feasible solutions. Constraint group 4: constraints on the interactive relationship between multiple single-ship plans.

In the present study, we define a subset $Q(Q \subseteq P)$ as the fleet scheduling plan. The elements of the subset Q are a single-ship plan and should satisfy the following two conditions. (1) the single-ship single-task constraint: in Q , a ship can only carry out a single-ship-scheduling plan once during the planning period. (2) The exclusivity constraint of port operation: the number of unloading ships should not exceed the number of berths designed in the port at the same time.

Based on the abovementioned analysis, we propose the feasible conditions for the subset Q shown in equations (16) and (17). Among them, the variable x_p represents whether the feasible single-ship-scheduling plan $p \in P$ is selected in the subset Q ; if it is, x_p is taken as 1;

otherwise, x_p is 0. The indicator variable β_{ig} indicates whether the port is an unloading port in the waterway voyage i . If it is, it is taken as 1; otherwise, it is taken as 0. b_g represents the number of berths in the ports g . Equation (16) ensures that each ship can only be operated once with a single-ship-scheduling plan, which means parts of the fleets are allowed to not participate in the plan. Equations (16a) and (16b) are the linearization versions of equation (16) for the same constraint. Equation (17) ensures that the number of unloading ships does not exceed the number of berths designed in the port at the same time. Equations (17a) and (17b) are the linearization versions of equation (17) for the same constraint.

$$\sum_{p \in P} \alpha_{vp} x_p \leq 1, \quad \forall v \in V, \quad (16)$$

$$\frac{1}{2}(\alpha_{vp} + x_p) - \frac{1}{2} \leq u_{vp} \leq \frac{1}{2}(\alpha_{vp} + x_p), \quad \forall v \in V, p \in P, \quad (16a)$$

$$\sum_{p \in P} u_{vp} \leq 1, \quad \forall v \in V, \quad (16b)$$

$$\sum_{i \in I} \sum_{p \in P} \beta_{ig} z_{ipt} x_p \leq b_g, \quad \forall g \in G, \quad (17)$$

$$\frac{1}{2}(z_{ipt} + x_p) - \frac{1}{2} \leq m_{ipt} \leq \frac{1}{2}(z_{ipt} + x_p), \quad \forall i \in I, p \in P, \quad (17a)$$

$$\sum_{i \in I} \sum_{p \in P} \beta_{ig} m_{ipt} \leq b_g, \quad \forall g \in G. \quad (17b)$$

4.4. Electric Coal Fleet Transportation Plan Optimization Model

Based on the abovementioned constraints, the scheduling process of waterway transportation has been fully characterized. The last set of constraints is introduced for the constraints of the choice of waterway and rail transportation.

Constraint group 5: constraints on the choice of waterway and rail transportation.

According to the assumptions, any water transportation voyage can be replaced by a complementary railway land voyage, so the decision maker can choose either of them. The fifth set of constraints contains only equation (18). Equations (18a) and (18b) are the linearization versions of equation (18) for the same constraint. It shows that if any feasible single-vessel solution for the waterway voyage i is not selected for set Q , ($y_{ip} x_p = 0$), the task of corresponding electric coal transportation must be undertaken by the complementary railway land plan (γ_i must be 1).

$$\sum_{p \in P} y_{ip} x_p + \gamma_i \geq 1, \quad \forall i \in I, \quad (18)$$

$$\sum_{p \in P} q_{ip} + \gamma_i \geq 1, \quad \forall i \in I, \quad (18a)$$

$$\frac{1}{2}(y_{ip} + x_p) - \frac{1}{2} \leq q_{ip} \leq \frac{1}{2}(y_{ip} + x_p), \quad \forall i \in I, p \in P. \quad (18b)$$

Based on the definitions of constraint 1–5, we can provide a complete mathematical model (denoted as ECSSM). The model is also improved from the common SPP model. Let c_p^{op} represent the operating costs of the plan p ; c_i^a represents the cost of the land voyage associated with the water voyage i ; c_v^r represents the daily rent of ship v (which equals to the difference between the daily operating cost when the ship v is activated and the daily management cost when ship v is sealed). Equation (19) is the objective function of the model to minimize the total system transportation cost, which equals to the sum of the cost of water voyage and railway land. Equation (20) is used to calculate c_p^{op} . In

particular, similar to SPP, in this model, the feasible single-ship-scheduling plan P and water voyage I are considered as known, and the decision variables of the model are x_p and γ_i .

ECSSM:

$$\min \sum_{p \in P} c_p^{\text{op}} x_p + \sum_{i \in I} c_i^a \gamma_i, \quad (19)$$

s.t. equation (1) ~ (18).

$$c_p^{\text{op}} = \sum_{v \in V} (t_{ep}^s - t_{0p}^s) c_v^r \alpha_{vp}, \quad \forall p \in P. \quad (20)$$

The ECSSM is a large-scale linear integer-programming model. The ECSSM takes into full consideration the synergetic transportation of sea and rail, the time-window constraints of transportation tasks, and the congestion in the port. It can adequately describe the characteristics of the electrical coal transportation in the southern coastal areas of China. However, the ECSSM still have some limitation for the wide application of coastal waterway transportations. With the consideration of the electric coal transportation's operational practice in the Chinese coast area, the transportation pattern of single vessel, single mission, and single voyage is adopted for the tramp ship schedule. Although this assumption is suitable for the scope of this study, it also limits the application of the ECSSM for the applications with other characteristics, such as multiple-voyage or multiple types of cargoes. Furthermore, the ECSSM also adopts the assumption of fixed vessel speed, which is a common assumption for the waterway transportation with the consideration of the economical speed. However, since the thermal power plant could not risk the shutdown, the tramp ship would consider changing the vessel speed to deliver the electric coal in time for extreme situations. Therefore, adopting the assumption of fixed speed ignores the other possible measure to mitigate the damage caused by the operation delay. Although the ECSSM has such limitations; these limitations only become significant in the other cases with distinct differences as well as the extreme application cases. For the purpose of studying the electric coal transportation in the Chinese coastal area, the ECSSM could accurately describe the characteristics of transportation and suitable for further study.

The crux of the model's solvability lies in the size of the single-ship-scheduling plan set P . However, the plan set P involves the setting and combination of many factors such as waterway voyage selection, waterway voyage sequencing, waterway operation time node, and waiting time. In reality, the size of the plan set P is extremely large, and the enumeration algorithm cannot meet the needs of practical application. Thus, we must design a targeted solution to solve the ECSSM efficiently.

5. Algorithm Design

The ECSSM is a large-scale mixed-integer optimization model. At present, there are three methods for solving

such models. One is the traditional calculation method based on branch and bound. This method has low efficiency and is powerless for many complicated problems. The second is the heuristic algorithm based on the evolutionary framework. The efficiency of this kind of algorithm is relatively high, but it cannot ensure that the global optimal solution is obtained, and the algorithm has poor robustness and unstable calculation results. The third is the branch-and-price algorithm (B&P) which has been widely adopted in recent years. Because of the high computational efficiency of the branch-and-price algorithm and the theoretically accurate solution of large-scale models, it has become an ideal tool for solving large-scale mixed-integer optimization. Therefore, this paper adopts the branch-and-price algorithm to solve the above-mentioned model.

The core of the branch-and-price algorithm is column generation. The idea of column generation evolved from the original Dantzig-Wolfe decomposition idea. It decomposes the original model into two models, called the master model (MM) and submodel (SM). The decision variables in the main model are only a subset of all variables in the original model. The role of the submodel is to continuously introduce new variables into the main model until the optimal solution of the original model is obtained. The objective function of the submodel is the reduce cost of the introduced variable.

The flow of the branch-and-price algorithm can be briefly described as follows: (1) Construct an initial solution and solve the main model. In theory, any feasible solution satisfying all constraints can be taken as the initial solution. In addition, by solving the main model, the dual price of each constraint in the model is also obtained. (2) Solve the submodel and obtain the reduce cost of the variable to be introduced, that is, the objective function of the submodel. If the reduce cost is negative, the variable (called column in the main model) is added to the main model. (3) Solve the main model and submodel repeatedly until the reduce cost of the submodel is nonnegative. In theory, the optimal solution of the main model at this time is the optimal solution of the original model. The abovementioned process is shown in Figure 3.

5.1. Main Model and Submodel

5.1.1. Mathematical Expression of the Main Model. The mathematical expression of the main model (denoted as MM) is shown in equations (21)–(25). Among them, \bar{P} represents the currently known feasible set of single-ship plan; the rest of the symbols are the same as before. The structure of this model is similar to that of the ECSSM; the difference is that the MM uses \bar{P} to replace the original full set P of feasible solutions of the single-ship plan. Since \bar{P} is known, the variables of this model are x_p and γ_i . Since $\bar{P} \subseteq P$, the optimal solution of the MM should theoretically be the upper bound of the ECSSM. The scale of \bar{P} is much smaller than that of P , so we use Gurobi to solve the model.

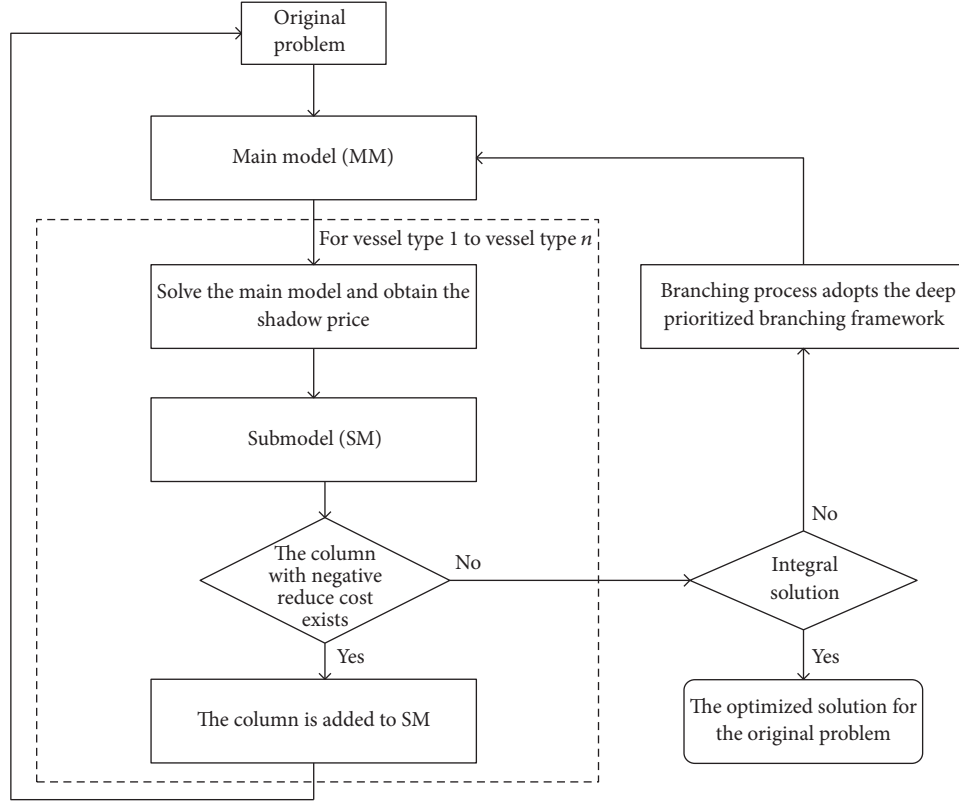


FIGURE 3: Diagram of branch-and-price algorithm.

ECSSM-MM:

$$\min \sum_{p \in \tilde{P}} \tilde{c}_p^s x_p + \sum_{i \in I} \tilde{c}_i^t \gamma_i, \quad (21)$$

$$\text{s.t. } \tilde{c}_p^s = \sum_{v \in V} (t_{ep}^s - t_{0p}^s) c_v^r s_{vp}, \quad \forall p \in \tilde{P}, \quad (22)$$

$$\sum_{p \in \tilde{P}} u_{vp} \leq 1, \quad \forall v \in V, \quad (23)$$

$$\sum_{i \in I} \sum_{p \in \tilde{P}} \delta_{il} m_{ipt} \leq n_l^b, \quad \forall t \in T, l \in L, \quad (24)$$

$$\sum_{p \in \tilde{P}} q_{ip} + \gamma_i \geq 1, \quad \forall i \in I. \quad (25)$$

5.1.2. *Mathematical Expressions of Submodels.* The submodel (denoted as SM) is as shown in equations (26)–(41). \tilde{P} represents the new feasible single-ship-scheduling plan (i.e., a new column) to be generated. $\pi_v^{(23)}$, $\pi_{lt}^{(24)}$, and $\pi_i^{(25)}$ represent the shadow price from equations (23)–(25) of the MM, and the rest of the symbols are the same as before. Equation (26) is the objective function of the SM, which means whether the single-ship feasible plan has a further probability for improvement. If the value of equation (26) is negative, \tilde{P} needs to be further optimized. Equations (27)–(41) are the constraint conditions for the SM. They are the corresponding equations of equations (1)–(15). The difference is that the \tilde{P} is used to replace the p in original equations, which means the main characterization object of the SM is \tilde{P} .

ECSSM-SM:

$$\min \sum_{v \in V} (t_{ep}^s - t_{0p}^s) c_v^r s_{vp} - \sum_{v \in V} \pi_v^{(23)} s_{vp} - \sum_{l \in L, t \in T} \pi_{lt}^{(24)} b_{ipt} - \sum_{i \in I} \pi_i^{(25)} a_{ip}, \quad (26)$$

$$\text{s.t. } \sum_{j \in I} \tilde{x}_{0jp} = 1, \quad (27)$$

$$\sum_{i \in I} \tilde{x}_{iep} = 1, \quad (28)$$

$$\sum_{j \in I} \tilde{x}_{ij\tilde{p}} = \sum_{j \in I} \tilde{x}_{j\tilde{p}}, \quad \forall i \in I, \quad (29)$$

$$a_{i\tilde{p}} = \sum_{j \in I} \tilde{x}_{ij\tilde{p}}, \quad \forall i \in I, \quad (30)$$

$$t_{j\tilde{p}}^s \geq t_{i\tilde{p}}^s + t_{i\tilde{p}}^{w1} + t_i^{h1} + t_i^{r1} + t_{i\tilde{p}}^{w2} + t_i^{h2} + t_i^{r2} + M(1 - \tilde{x}_{ij\tilde{p}}), \quad \forall i, j \in I, \quad (31)$$

$$t_{0\tilde{p}}^s \geq \sum_{v \in V} t_v^0 \times s_{v\tilde{p}}, \quad (32)$$

$$a_{i\tilde{p}}^{ls} t_i^s \leq t_{i\tilde{p}}^s + t_{i\tilde{p}}^{w1} \leq a_{i\tilde{p}}^{le} t_i^e, \quad \forall i \in I, \quad (33)$$

$$a_{i\tilde{p}}^{ds} t_i^{ds} + (1 - a_{i\tilde{p}})(t_i^{r1} + t_i^{h1}) \leq t_{i\tilde{p}}^s + t_{i\tilde{p}}^{w1} + t_i^{r1} + t_i^{h1} + t_{i\tilde{p}}^{w2} \leq a_{i\tilde{p}}^{de} t_i^{de} + (1 - a_{i\tilde{p}})(t_i^{r1} + t_i^{h1}), \quad \forall i \in I, \quad (34)$$

$$b_{i\tilde{p}t} \leq a_{i\tilde{p}}, \quad \forall i \in I, \quad (35)$$

$$t \geq t_{i\tilde{p}}^s + t_{i\tilde{p}}^{w1} + t_i^{r1} + t_i^{h1} + t_{i\tilde{p}}^{w2} - M(1 - b_{i\tilde{p}t}), \quad \forall i \in I, t \in T, \quad (36)$$

$$t \leq t_{i\tilde{p}}^s + t_{i\tilde{p}}^{w1} + t_i^{r1} + t_i^{h1} + t_{i\tilde{p}}^{w2} + t_i^{h2} + M(1 - b_{i\tilde{p}t}), \quad \forall i \in I, t \in T, \quad (37)$$

$$\sum_{t \in T} b_{i\tilde{p}t} \geq a_{i\tilde{p}} t_i^{h2}, \quad \forall i \in I, \quad (38)$$

$$\sum_{v \in V} s_{v\tilde{p}} = 1, \quad (39)$$

$$\sum_{v \in V} w_v \tilde{a}_{i\tilde{p}v} \geq D_i a_{i\tilde{p}}, \quad \forall i \in I, \quad (40)$$

$$\tilde{a}_{i\tilde{p}v} = a_{i\tilde{p}} \cdot s_{v\tilde{p}}, \quad \forall i \in I, v \in V. \quad (41)$$

In the submodel, each waterway voyage i is abstracted as a transportation node and the executing order of the voyage is regarded as the transportation between the node. Virtual nodes 0 and \tilde{e} are added additionally. Then, the subproblem in this section will be converted to an elemental shortest path problem with resource constraint (ESPPRC). Therefore, it can be solved using the common multidimensional labeling method. In this ESPPRC, the total cost of the whole route equals to the total costs of all nodes (water voyages) of the route.

5.2. Design of Multidimensional Labeling. Multidimensional labeling requires labeling for each transportation node. The label L_i used in this article contains a set of operational data for a v -type shuttle tanker from the port to the node $\text{pos}(L_i^v)$. The labels in this chapter include three different types of information related to the problem attributes. (1) Voyage execution time $t(L_i^v)$: it indicates the time required to reach the resident nodes of the tag following the waterway voyage sequence indicated by the tag. (2)

Voyage operation cost $c(L_i^v)$: it represents the total operation cost of the ship when it reaches the resident node of the tag. (3) Resident node $\text{pos}(L_i^v)$: it indicates the current node of waterway voyage i where the ship extends. In particular, the $c(L_i^v)$ of initial label L_0^v specification is 0.

Based on such definition, the updates principle of the labels is as follows: (1) $t(L_j^v) = t(L_i^v) + t_j$; (2) $c(L_j^v) = c(L_i^v) + c_j + \sum_{z \in Z, t \in T, k \in K} \pi_{zt(L_i^v)}^{(24)} b_{jkt(L_i^v)} + \pi_j^{(25)}$, where t_j represents the operation time for the water voyage j . It should be noted that the decision variables of the original problem include the waiting time in the water voyage, so there will be multiple possibilities for the time and cost of completing the water voyage i and the water voyage j in sequence. In this chapter, the waiting time is measured in days, and the discrete processing is conducted for various situations, corresponding to the different transportation routes between the two nodes.

After defining the update rule, the domination rule is defined. For the same ship type v , when the resident node of the labels L_1^v and L_2^v are the same FPSO, namely,

$\text{pos}(L_1^v) = \text{pos}(L_2^v)$, if the following conditions are met, the label L_2^v is dominated by the label L_1^v . The specific conditions are (1) less time consumption $t(L_1^v) \leq t(L_2^v)$; (2) less operation cost $c(L_1^v) \leq c(L_2^v)$.

6. Numerical Experiments

6.1. Experimental Design. At present, there are only two feasible algorithms for the ECSSP other than the CGSPA; one is the ESPA, and the other is a heuristic algorithm based on experience (denoted by PHA). Practice rule-based heuristic algorithm is the heuristic algorithm based on the operation rules derived from the practical transportation operation. The practical rules enable the PHA to effectively optimize the transportation task volume and maintain the advantage in enhancing computing efficiency by reducing computational time [37]. The heuristic algorithm is proved to be effective in solving the complex transportation network optimization problem involving multiple network nodes and multiple vehicles [37]. Thus, PHA is a suitable algorithm for the computing efficiency comparison.

In the first phase of our experiment, we demonstrate the advantages of the CGSPA by analyzing the performance of the CGSPA, ESPA, and PHA in terms of computational accuracy and efficiency. In the second stage of this experiment, we perform an optimization calculation for a real historical instance and analyze the results.

We use the transport demand and fleet data of a Chinese thermal power generation group in May and June 2015 (totaling 60 days) as data. Please refer to Table 2 for further details. The ports involved in the experiment are shown in Figure 4. The loading port is the Tianjin Port (#1). The unloading ports include the Shajiao North Port (#2) and Shajiao South Port (#3), Zhuhai Port (#4), Jinwan Port (#5), HuiLai Port (#6), Shanwei Port (#7), Shaoguan Port (#8), Maoming Port (#9), Xinsha Port (#10), Haichang Port (#11), Zhanjiang Port (#12), Pinghai Port (#13), Zhongyue Port (#14), Yangjiang Port (#15), and Luoding Port (#16). We assume that 30 vessels can be rented, including three vessels of 20,000 tons, ten vessels of 20,000 to 60,000 tons, and 17 vessels of 60,000 to 90,000 tons. Please refer to Table 3 for further details regarding each ship (e.g., daily rent, available time, and detailed transportation capacity). In the first stage of the experiment, based on the abovementioned data, we randomly generate test data for the comparative calculation. In the second phase of the experiment, we directly use the abovementioned data for the optimization calculation.

6.2. Algorithm Efficiency. The calculation process of the ESPA is relatively simple. First, we obtain the set P by enumeration, and then, we use Gurobi to solve the ECSSM model. In theory, the ESPA algorithm can solve the ECSSP accurately and is an ideal reference to evaluate the accuracy of the CGSPA. The calculation process of the PHA is relatively complex. This algorithm is the primary method used by power generation companies to solve the ECSSP. A summary of the PHA calculations is provided in Table 4, where Step 2.1 is the heart of the algorithm. Step 2.1 is used to

estimate whether the ship v' can complete the task i_k on time. For details, please refer to Table 5.

To compare the performance of the CGSPA, ESPA, and PHA, we generate 15 sets of test data based on the data given in Section 6.1. For convenience, we characterize these sets by the number of unloading ports (P), the number of vessels that can be rented (S), the length of the planning period (D), and the number of tasks (T). For example, if a dataset has five unloading ports, four ships, a planning period of 30 days, and ten tasks, this set is named P5S4D30T10. We use C++ to program all the algorithms and use a PC which has an Intel I5-6500 CPU and 16 GB DDR4-2138 memory to run them. The integer program solver used by the CGSPA and ESPA is Gurobi 7.5.

Table 6 shows the calculation results and efficiency comparison of the three algorithms for each test. CDPT represents the total computation time of the CGSPA for solving the submodel, CGUT represents the total computation time of the algorithm calling Gurobi to solve the main model, and CGT represents the computation time of the entire calculations. ENT represents the time consumed by the ESPA to enumerate set P , EGUT represents the total time that the ESPA spends using Gurobi to solve the ECSSM, and EGT represents the total time that the ESPA takes to complete the calculations. %CGSPA–ESPA and %CGSPA–PHA present the gaps corresponding to the relative difference between the solution values of the CGSPA and ESPA and between the CGSPA and PHA, respectively. OM represents that the relevant calculation is aborted because the memory capacity of the computer is exceeded.

As shown in Table 6, the CGSPA is far superior to the ESPA in terms of computational efficiency. For example, in the small-sized example P4S7T10D30, the CGSPA obtained the optimal solution in 54.71 s, whereas the ESPA took 5.02 s. In the mid-size example P11S17T30D30, because of the size of set P , the ESPA did not obtain an optimization result in an acceptable time (3 h), whereas the CGSPA completed the calculation in only 176.1 s. In terms of accuracy, the CGSPA is far superior to PHA. For example, in the mid-sized example P9S13T20D40, the result of the CGSPA was 17.6% more accurate than the PHA result, whereas in the larger example P11S17T30D40, the CGSPA's result was 19.2% more accurate than the PHA result. The abovementioned results illustrate that compared with the existing algorithms, the CGSPA has notable advantages in terms of computation time and calculation accuracy.

In addition, to test the robustness of the CGSPA, we perform multiple calculations by adjusting the rentable ship set. The results are shown in Table 7, where NUM of P' represents the total number of P' (the number of the columns) created by the CGSPA during the calculation. The number of rentable vessels is not positively related to the total time spent by the CGSPA. For example, P6S9T20D40 (7 ships) has a shorter computation time than P6S7T15D40 (9 ships). Further analysis indicates that the efficiency of the submodel solution and the total amount of P' generated are the key factors determining the efficiency of the CGSPA. The results shown in Table 7 illustrate that the CGSPA has better robustness and can still solve the problem after specific parameters are changed.

TABLE 2: The transport demand and fleet data of a Chinese thermal power generation group from May to June 2015.

Id	Ship name	Earliest available time (days)	Earliest release time (days)	Dead weight (tons)	Daily rent (Yuan)
0	Yuedian 1	9	40	6.9	2771
1	Yuedian 3	14	40	6.7	2713
2	Yuedian 4	0	40	7	2799
3	Yuedian 6	19	30	7.5	2943
4	Yuedian 7	10	40	7.5	2943
5	Yuedian 51	6	40	5.7	2426
6	Yuedian 54	17	40	5.7	2426
7	Yuedian 56	25	40	5.8	2454
8	Yuedian 57	15	30	5.8	2454
9	Yuedian 59	25	40	5.8	2454
10	Yuedian 103	34	50	8.7	3288
11	New Guangzhou	1	30	6.5	2656
12	New Jinghai	3	30	6.9	2771
13	New Ningjiang	5	40	4.7	2138
14	Yuqi Sea	3	30	6.4	2627
15	Yulin Sea	9	30	7.5	2943
16	Guangzhu	7	40	8.8	3317
17	Guangyue	10	40	6.9	2771
18	Guangqian	16	30	7.5	2943
19	Taihang 6	11	40	6.7	2713
20	Yuedian 52	38	0	5.7	2426
21	Yuedian 53	35	0	5.7	2426
22	Yuedian 58	21	0	5.6	2397
23	Yuedian 101	3	0	8.6	3259
24	Yuedian 102	17	0	8.6	3259
25	New Dajiang	25	0	4.2	1995
26	Guangzhong	48	0	6.6	2684
27	Enyao	9	0	2.2	1391
28	Entend 1	14	0	2	1333
29	Entend 2	44	0	2	1305

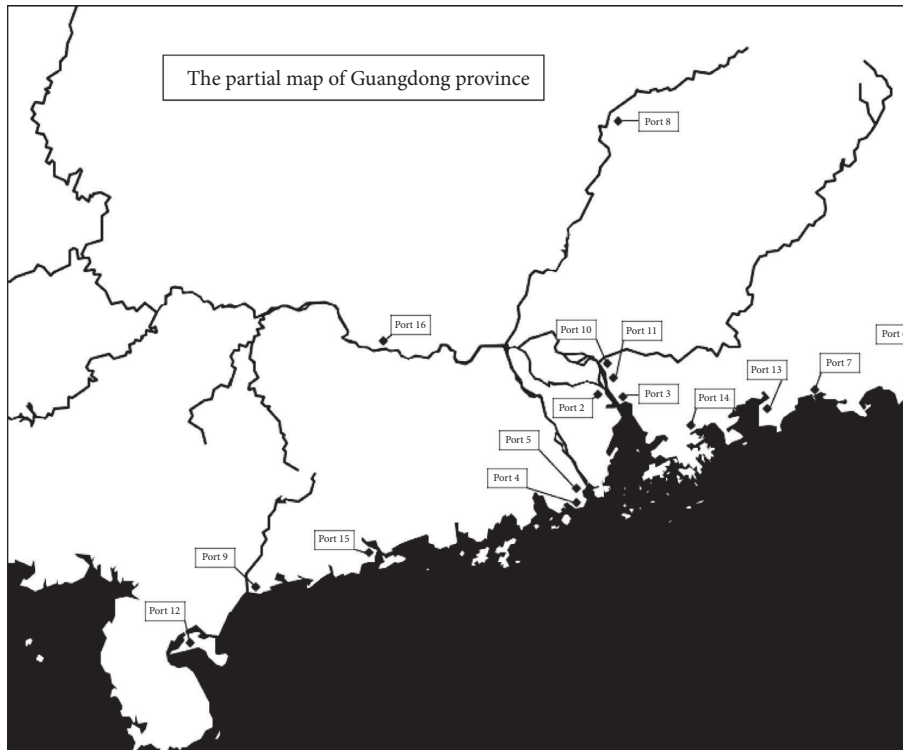


FIGURE 4: Geographical distribution of unloading ports.

TABLE 3: The operational details of unloading ports.

Id	Plant name	Min stock (tons)	Max stock (tons)	Consume rate (tons/day)	Current stock (tons)	Unload speed (tons/day)
0	Sha A	5.88	25	0.84	15.03	1.7
1	Sha C	9.24	60	1.32	21.55	1.7
2	Huangpu	3.71	20	0.53	7.47	2.4
3	Zhuhai	6.65	33	0.95	19.792	2
4	Jinwan	3.71	40	0.53	9.45	2
5	Shanwei	13.37	39	1.91	23.833	3
6	Huilai	6.51	50	0.93	40.2	3
7	Maoming	2.24	15	0.32	9.655	1.5
8	Zhanjiang	4.83	43	0.69	28.2	2
9	Yunhe	4.62	29	0.66	10.49	2
10	Pinghai	9.87	36	1.41	26.636	2
11	Zhongyue	6.23	32	0.89	19.89	2
12	Shaoguan	3.22	26	0.46	20.72	2.4
13	Yunfu	1.89	26	0.27	16.08	2
14	Luoding	1.54	15	0.22	2.86	2.2

TABLE 4: A summary of the PHA calculation process.

PHA calculation process
Step 0: according to the lower bound of the unloading time window, sort the water voyages and obtain an ordered set $\bar{I} = \{i_k\}$, where $i_k \in I$, k represents the number of the water voyage in \bar{I} , and for any k , $td_{i_k}^e \leq td_{i_{k+1}}^e$
Step 1: select the ship v' with the highest shipping capacity among the currently available ship set V and obtain the currently available time point t' of the ship
Step 2: if $\bar{I} \neq \emptyset$ and $V \neq \emptyset$, then let $k = 1$; else, go to step 3
Step 2.1: if the transportation volume of the task i_k is no less than 60% of the capacity of v' , the ship v' may complete the task as required (see Table 5); then, delete i_k in \bar{I} , update the ship available time point t' , and record that ship v' performs task i_k ; else, let $k = k + 1$
Step 2.2: if $k > \bar{I} $, or $t' > T $, then remove v' from ship set V and return step 2.1
Step 3: the calculation is completed

TABLE 5: Procedure for determining whether vessel v can process mission i at time t .

Step 1: if the transportation loading of i_k is larger than the ship capacity of vessel type v , then go to step false
Step 2: if $t \leq t_{i_k}^{ls}$, then $t_{i_k}^{wl} = t_{i_k}^{ls} - t$, $t = t_{i_k}^{ls}$ (calculating the waiting time at the loading port)
Step 3: if $t > t_{i_k}^{le}$, then go to step false
Step 4: if $t + t_{i_k}^l + t_{i_k}^{r1} > t_{i_k}^{ue}$, then go to step false
Step 5: if $\left\{ t' \mid \sum_{t''=t'}^{t'+t_{i_k}^{ul}} b_{g_k t''} = 0, t' \leq t_{i_k}^{ue}, t' \geq t + t_{i_k}^l + t_{i_k}^{r1} \right\} = \emptyset$, then go to step false
Step true: take $t' = \min_{t'} \left\{ \sum_{t''=t'}^{t'+t_{i_k}^{ul}} b_{g_k t''} = 0, t' \leq t_{i_k}^{ue}, t' \geq t + t_{i_k}^l + t_{i_k}^{r1} \right\}$ as the time of unloading
$t_{i_k}^{uu} = t' - (t + t_{i_k}^l + t_{i_k}^{r1})$
For all $t'' \in [t', t' + t_{i_k}^{ul}]$, execute $b_{g_k t''} = 1$
$t = t' + t_{i_k}^{r2}$
Return true
Step false: $t = t - t_{i_k}^{wl}$, return false
(Return value: true, possible; false, and impossible)

6.3. *Scenario Analysis.* In the second phase of the experiment, we use the model and algorithm proposed in this paper to solve a real historical instance and compare the optimal solution with the actual electric coal transportation plan used by power generation enterprises. This issue considers all the rentable vessels given in Table 2, all the tasks given in Table 3, and all the ports given are in Section 6.1 with a 70-day planning horizon. The relevant rental fee of August and September in 2016 is set as the average relevant ship rental rate. The railway rates are taken from the China

Railway Corporation announced at the same time as the tariffs.

Comparisons of the key parameters of the electric coal transportation optimization plan and the actual transportation plan are shown in Table 8 and Figures 4–6, where OPR represents the optimized plan, RPR represents the actual transportation plan, NUM represents the number of vessels used, GRT represents the total renting duration of the vessels in days, GWT represents the total waiting time of the vessels in days, RTU represents the ratio of GRT to GWT,

TABLE 6: CGSPA performance analysis.

Test classes	CGSPA			ESPA			PHA	% CGSPA-ESPA	% CGSPA-PHA
	CDPT(s)	CGUT(s)	CGT(s)	ENT(s)	EGUT(s)	EGT(s)	PGT(s)		
P2S2T4D20	0.042	0.007	0.05	0.09	0.53	0.62	0.10	0	-2.5
P2S3T6D20	0.126	0.011	0.14	0.70	3.26	3.96	0.13	0	-4.3
P4S6T10D20	0.224	0.025	0.25	1.12	7.78	8.90	0.19	0	-4.0
P8S9T15D30	3.78	2.71	6.49	38.31	OM	—	0.27	—	-11.2
P9S11T20D30	35.43	19.25	54.69	1437	OM	—	0.44	—	-15.0
P11S13T25D30	128.8	27.9	156.7	1839	OM	—	1.09	—	-16.8
P2S3T7D40	0.031	0.007	0.04	0.78	2.34	3.12	0.13	0	-5.2
P3S6T10D40	1.68	0.143	1.82	3.07	12.32	15.39	0.20	0	-6.9
P6S9T15D40	3.31	1.82	5.13	45.73	OM	—	0.30	—	-15.3
P6S11T20D40	49.83	21.51	71.34	1643	OM	—	0.42	—	-15.6
P9S13T25D40	61.97	26.16	88.13	—	—	—	0.54	—	-16.1
P11S17T35D40	209.7	41.9	251.6	—	—	—	1.45	—	-18.9

TABLE 7: CGSPA reliability analysis.

Test classes	CDPT(s)	NUM of P'(s)	CGUT(s)	CGT(s)
P6S6T15D45	2.08	974	0.783	2.30
P6S7T15D45	8.48	5035	0.709	8.72
P6S8T20D45	6.25	4192	0.790	7.33
P6S9T20D45	4.89	1647	0.97	6.19
P6S20T20D45	10.41	1952	1.02	11.58

TABLE 8: Key feature comparison between the optimized and actual plans.

Ship type	Dead Weight(t)	NUM	OPR					RPR					% OPR-RPR	
			GRT (days)	GWT (days)	RTW (days)	AW (tons)	RW	NUM	GRT (days)	GWT (days)	RTW (days)	AW (tons)		RW
Small	<2w	1	64	19	0.30	1.75	0.92	2	82	24	0.29	1.86	0.93	
Medium	2w-6w	10	324	1	0.01	5.28	0.95	10	387	60	0.16	5.29	0.97	-22.60%
Large	6w-9w	14	605	3	0.01	6.96	0.96	17	814	173	0.21	6.94	0.96	

AW represents the average volume of transportation tasks undertaken by the vessels of the relevant type, RW represents the average utilization rate of the relevant vessels (i.e., the average ratio of the volume of completed traffic to the capacity of the relevant vessels), and % OPR-RPR represents the relative standard deviation of the optimized plan and actual plan in total transportation costs. As shown in Table 6, the performance of the optimized plan in terms of capacity allocation is highly similar to that of the actual plan. Both use all the available ships and reach a high level of utilization (both exceeding 90%). There was not a significant waste of capacity in either plan. However, the optimization plan is significantly better than the actual plan in terms of the time of use of the ships, with the effect being particularly evident for large electric coal transportation ships. Specifically, in the practical plan, the waiting time for large ships in the port accounts for more than 21% of the total renting duration, compared with only 0.01% in the optimized plan.

To further analyze the advantages of the optimized plan in reducing the waiting time of the vessels, Figure 5 compares the number of waiting ships on each observation point (day) between the optimized plan and the actual plan. The waiting time of ships during the planning period is

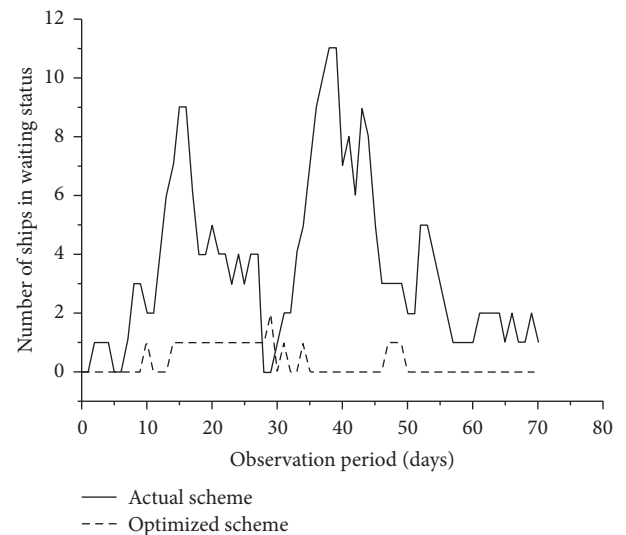


FIGURE 5: Comparative analysis of ships in waiting status.

significantly reduced in the optimized plan, with a daily average number of waiting ships of only 0.30 compared to 2.98 in the actual plan. The abovementioned analysis

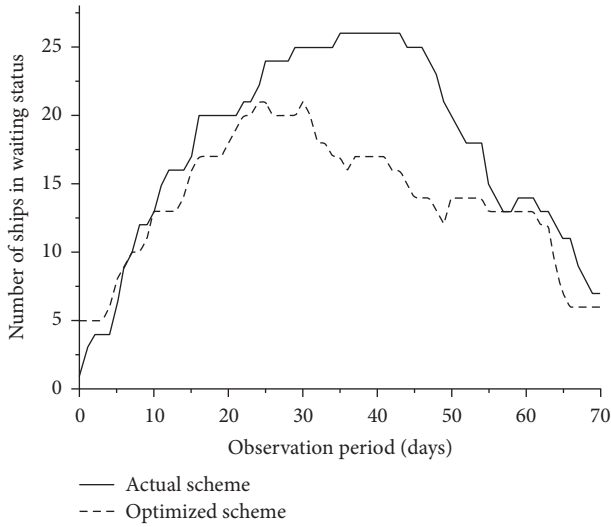


FIGURE 6: Comparative analysis of ships in waiting status.

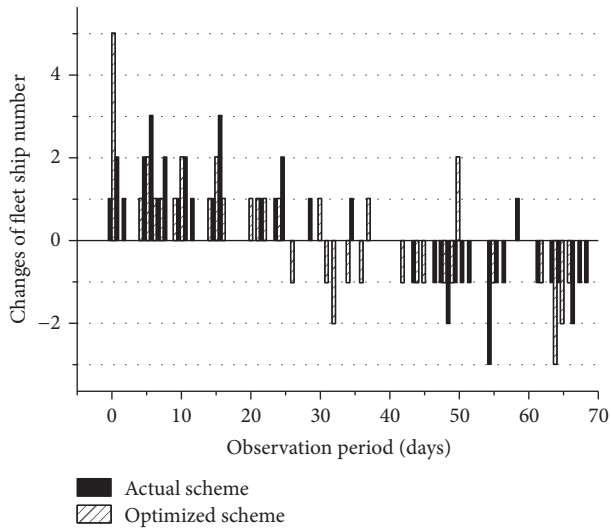


FIGURE 7: Comparative analysis of ships in waiting status.

illustrates that the optimized plan can effectively reduce the waiting time of the vessels at the unloading port while ensuring that the transportation tasks are completed as required, thus reducing the fleet operation and rental costs.

Figures 6 and 7 compare the differences between the optimized and actual plans in terms of fleet size, the time point to start renting a ship, and the time point to stop renting it. As shown in the figure, during phase A of the observation period (from day 0 to day 25), the overall size of the fleet used by both programs was controlled at a scale of 20–25 ships. The options for the two plans at the point of chartering are also similar. However, significant differences were observed during phase B of the observation period (day 25 to day 70). Due to the rationalization of the transportation assignment by the optimized plan, many vessels were allowed to be released on day 25, whereas in the actual plan, releasing was not started until day 45, when a large number of vessels were suspended. As a result, the average

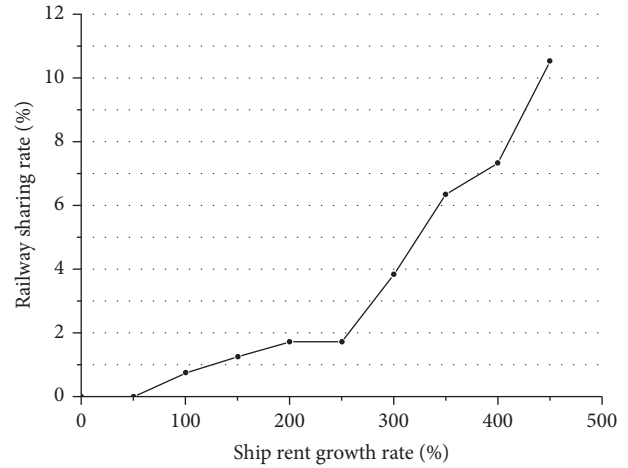


FIGURE 8: Relationship between ship rent growth and the railway freight sharing rate.

fleet size of the optimized plan in phase B was only 14.30, compared to that of 19.65 in the actual plan. The smaller average fleet size combined with the lesser average vessel chartering time makes the optimized plan far superior to the actual plan in terms of electric coal transportation costs, with an approximate 22.60% reduction (% OPR-RPR).

Neither the actual plan nor the optimized plan has applied rail transportation. In other words, water transportation is highly competitive in the actual cases covered in this paper. To determine the advantages of the competitiveness of water transportation, we use the model and algorithm proposed in this paper to study the impact of the floating rent of vessels on the competitiveness of water transportation. The results of the analysis are shown in Figure 8. Railway transportation begins to be employed when the daily rent increases by 50%. The railway transportation share rate increases to 3.82% and 10.52% when the daily rent increases by 300% and 450%, respectively. This result illustrates that, in the cases discussed in this experiment, the water transportation system is highly competitive and will not fundamentally change the condition that the electric coal transportation is dominated by water transportation even though the rents of ships have risen substantially.

7. Conclusions

In this paper, a new mathematic model for the ECSSP is developed with the consideration of the synergetic transportation of sea and rail, the time-window constraints of transportation tasks, and the congestion in the port. The model can be used to optimize fleet scheduling planning while considering the multiple transportation plan constraints. A precise algorithm is designed based on the architecture of the branch-and-price algorithm to effectively solve relatively large-scale optimization. The reliability of the model and algorithm is demonstrated through algorithm analysis and a practical case in the southern coastal areas of China. Results indicate that the proposed model and algorithm can effectively solve the ECSSP for the increasing

transformation need in the coastal areas of Southern China. The total transportation cost is significantly reduced by reducing the total waiting time and the active vessels throughout the transportation task.

There are still issues that need further study. For example, in the transportation process, we assume that the transport system adopts the pattern of a single-vessel, single-mission, single-voyage system. Although this mode of transportation is a convention for the transportation of coal in China, it may lead to wasted shipping capacity in many cases. Therefore, how to optimize electric coal transportation under the condition of allowing multiple ships to participate in a set of voyage tasks is an interesting and challenging issue. Meanwhile, the ship's speed is assumed to be fixed, whereas a ship can adjust the speed in practice. Further studies should investigate the transportation of coal considering the variable speed.

Data Availability

The transport demand and fleet data used to support the findings of this study are included within the article.

Conflicts of Interest

The authors declare no conflicts of interest.

Acknowledgments

This work was supported by the Fundamental Research Funds for the Central Universities (No. 3132020227); the Department of Science and Technology of Liaoning Province (No. 2020JH2/10100042).

References

- [1] Z. Tan, K. Chen, L. Ju, P. Liu, and C. Zhang, "Issues and solutions of China's generation resource utilization based on sustainable development," *Journal of Modern Power Systems and Clean Energy*, vol. 4, no. 2, pp. 147–160, 2016.
- [2] J. Wang, R. Feng, and N. Meng, "Analysis on supply capability in seaborne-coal supply logistics system," in *Proceedings of the 2008 IEEE International Conference on Service Operations and Logistics, and Informatics*, pp. 3047–3051, Washington, DC, USA, December 2008.
- [3] J. Chen, L. Jing, and J. Liang, "Design and implementation of coastal thermal coal transportation management and decision support system," *Coal Technology*, vol. 21, 2011.
- [4] C. Wang and C. Ducruet, "Transport corridors and regional balance in China: the case of coal trade and logistics," *Journal of Transport Geography*, vol. 40, pp. 3–16, 2014.
- [5] Q. Zeng and Z. Yang, "Model integrating fleet design and ship routing problems for coal shipping," in *Proceedings of International Conference on Computational Science*, pp. 1000–1003, Pune, India, August 2019.
- [6] B.-H. Lin, H.-S. Lee, and C.-C. Chung, "The construction and implication of group scale efficiency evaluation model for bulk shipping corporations," *Mathematics*, vol. 8, no. 5, p. 702, 2020.
- [7] I. Cera, *Coal Rush: The Future of China's Coal Markets*, IHS CERA, Cambridge, MA, USA, 2013.
- [8] B. Rioux, P. Galkin, F. Murphy, and A. Pierru, "Economic impacts of debottlenecking congestion in the Chinese coal supply chain," *Energy Economics*, vol. 60, pp. 387–399, 2016.
- [9] V. Reis, J. Fabian Meier, G. Pace, and R. Palacin, "Rail and multi-modal transport," *Research in Transportation Economics*, vol. 41, no. 1, pp. 17–30, 2013.
- [10] A. Hemmati, L. M. Hvattum, M. Christiansen, and G. Laporte, "An iterative two-phase hybrid matheuristic for a multi-product short sea inventory-routing problem," *European Journal of Operational Research*, vol. 252, no. 3, pp. 775–788, 2016.
- [11] M. Christiansen, K. Fagerholt, B. Nygreen, and D. Ronen, "Ship routing and scheduling in the new millennium," *European Journal of Operational Research*, vol. 228, no. 3, pp. 467–483, 2013.
- [12] D. Ronen, "Cargo ships routing and scheduling: survey of models and problems," *European Journal of Operational Research*, vol. 12, no. 2, pp. 119–126, 1983.
- [13] M. Christiansen, K. Fagerholt, and D. Ronen, "Ship routing and scheduling: status and perspectives," *Transportation Science*, vol. 38, no. 1, pp. 1–18, 2004.
- [14] D. Ronen, "Ship scheduling: the last decade," *European Journal of Operational Research*, vol. 71, no. 3, pp. 325–333, 1993.
- [15] D. E. Lane, T. D. Heaven, and D. Uyeno, "Planning and scheduling for efficiency in liner shipping," *Maritime Policy & Management*, vol. 14, no. 2, pp. 109–125, 1987.
- [16] Q. Meng, S. Wang, H. Andersson, and K. Thun, "Containership routing and scheduling in liner shipping: overview and future research directions," *Transportation Science*, vol. 23, 2013.
- [17] M. Christiansen and K. Fagerholt, "Robust ship scheduling with multiple time windows," *Naval Research Logistics*, vol. 49, no. 6, pp. 611–625, 2002.
- [18] G. G. Brown, G. W. Graves, and D. Ronen, "Scheduling ocean transportation of crude oil," *Management Science*, vol. 33, no. 3, pp. 335–346, 1987.
- [19] D. O. Bausch, G. G. Brown, and D. Ronen, "Scheduling short-term marine transport of bulk products," *Maritime Policy & Management*, vol. 25, no. 4, pp. 335–348, 1998.
- [20] A. N. Perakis and W. M. Bremer, "An operational tanker scheduling optimization system: background, current practice and model formulation," *Maritime Policy & Management*, vol. 19, no. 3, pp. 177–187, 1992.
- [21] H. Jafari, "Measuring the performance of dry bulk cargo loading and unloading operation: latakia case study," *Journal of Business and Management Sciences*, vol. 1, pp. 77–82, 2013.
- [22] N. S. F. A. Rahman, M. K. Othman, I. A. Sanusi, A. M. Arof, and A. Ismail, "Evaluation of delay factors on dry bulk cargo operation in Malaysia: a case study of kemaman port," *The Asian Journal of Shipping and Logistics*, vol. 35, no. 3, pp. 127–137, 2019.
- [23] C. A. Kavirathna, T. Kawasaki, S. Hanaoka, and Y. M. Bandara, "Cooperation with a vessel transfer policy for cooperation among container terminals in a single port," *Transport Policy*, vol. 89, pp. 1–12, 2020.
- [24] M. A. Dulebenets, "An adaptive island evolutionary algorithm for the berth scheduling problem," *Memetic Computing*, vol. 12, no. 1, pp. 51–72, 2019.
- [25] H.-P. Hsu and C.-N. Wang, "Resources planning for container terminal in a maritime supply chain using multiple particle swarms optimization (MPSO)," *Mathematics*, vol. 8, no. 5, p. 764, 2020.

- [26] Y. Wang, Y. Yuan, X. Guan et al., “Collaborative two-echelon multicenter vehicle routing optimization based on state-space-time network representation,” *Journal of Cleaner Production*, vol. 258, Article ID 120590, 2020.
- [27] Y. Wang, S. Peng, X. Zhou, M. Mahmoudi, and L. Zhen, “Green logistics location-routing problem with eco-packages,” *Transportation Research Part E: Logistics and Transportation Review*, vol. 143, Article ID 102118, 2020.
- [28] G. Bronmo, M. Christiansen, K. Fagerholt, and B. Nygreen, “A multi-start local search heuristic for ship scheduling—a computational study,” *Computers & Operations Research*, vol. 34, no. 3, pp. 900–917, 2007.
- [29] K. Kobayashi and M. Kubo, “Optimization of oil tanker schedules by decomposition, column generation, and time-space network techniques,” *Japan Journal of Industrial and Applied Mathematics*, vol. 27, no. 1, pp. 161–173, 2010.
- [30] K. Fagerholt, L. M. Hvattum, T. A. V. Johnsen, and J. E. Korsvik, “Routing and scheduling in project shipping,” *Annals of Operations Research*, vol. 207, no. 1, pp. 67–81, 2013.
- [31] J. E. Korsvik, K. Fagerholt, and G. Laporte, “A tabu search heuristic for ship routing and scheduling,” *Journal of the Operational Research Society*, vol. 61, no. 4, pp. 594–603, 2010.
- [32] I. Norstad, K. Fagerholt, and G. Laporte, “Tramp ship routing and scheduling with speed optimization,” *Transportation Research Part C: Emerging Technologies*, vol. 19, no. 5, pp. 853–865, 2011.
- [33] Y. Wang, X. Ma, Z. Li, Y. Liu, M. Xu, and Y. Wang, “Profit distribution in collaborative multiple centers vehicle routing problem,” *Journal of Cleaner Production*, vol. 144, pp. 203–219, 2017.
- [34] E. Sopot and I. Gribkovskaia, “Routing of supply vessels to with deliveries and pickups of multiple commodities,” *Procedia Computer Science*, vol. 31, pp. 910–917, 2014.
- [35] M. Gansterer, M. Küçüktepe, and R. F. Hartl, “The multi-vehicle profitable pickup and delivery problem,” *OR Spectrum*, vol. 39, no. 1, pp. 303–319, 2017.
- [36] E. F. Cuesta, H. Andersson, K. Fagerholt, and G. Laporte, “Vessel routing with pickups and deliveries: an application to the supply of offshore oil platforms,” *Computers & Operations Research*, vol. 79, pp. 140–147, 2017.
- [37] Y. Kim, K. Gotoh, and M. Toyosada, “Automatic two-dimensional layout using a rule-based heuristic algorithm,” *Journal of Marine Science and Technology*, vol. 8, no. 1, pp. 37–46, 2003.

Research Article

Application of the Bayesian Model Averaging in Analyzing Freeway Traffic Incident Clearance Time for Emergency Management

Yajie Zou,¹ Bo Lin ,¹ Xiaoxue Yang,¹ Lingtao Wu,² Malik Muneeb Abid,³ and Jinjun Tang ⁴

¹Key Laboratory of Road and Traffic Engineering of Ministry of Education, Tongji University, Shanghai 201804, China

²Texas A&M Transportation Institute, Texas A&M University System, 3135, TAMU, College Station, TX 77843-3135, USA

³Department of Civil Engineering, College of Engineering and Technology, University of Sargodha, Sargodha, Pakistan

⁴The School of Traffic & Transportation Engineering, Central South University, Changsha 410075, China

Correspondence should be addressed to Jinjun Tang; jinjuntang@csu.edu.cn

Received 11 December 2020; Revised 31 January 2021; Accepted 1 March 2021; Published 11 March 2021

Academic Editor: Yong Wang

Copyright © 2021 Yajie Zou et al. This is an open access article distributed under the Creative Commons Attribution License, which permits unrestricted use, distribution, and reproduction in any medium, provided the original work is properly cited.

Identifying the influential factors in incident duration is important for traffic management agency to mitigate the impact of traffic incidents on freeway operation. Previous studies have proposed a variety of approaches to determine the significant factors for traffic incident clearance time. These methods commonly select a single “true” model among a majority of alternative models based on some model selection criteria. However, the conventional methods generally neglect the uncertainty related to the choice of models. This paper proposes a Bayesian Model Averaging (BMA) model to account for model uncertainty by averaging all plausible models using posterior probability as the weight. The BMA model is used to analyze the 2,584 freeway incident records obtained from I-5 corridor in Seattle, WA, USA. The results show that the BMA approach has the capability of interpreting the causal relationship between explanatory variables and clearance time. In addition, the BMA approach can provide better prediction performance than the Cox proportional hazards model and the accelerated failure time models. Overall, the findings in this study can be useful for traffic emergency management agency to apply an alternative methodology for predicting traffic incident clearance time when model uncertainty is considered.

1. Introduction

Improving the efficiency of the traffic incident management is a common measure to alleviate traffic congestion [1–3]. Although the definition and components of traffic incident duration vary in different studies, clearance time is regarded as the most uncontrollable component [4]. As a phase of incident duration, it depends on the unique factors of each individual incident [5]. Thus, understanding the effects of influential factors and accurate incident clearance time prediction are essential to evaluate traffic incident management strategy [6].

A variety of approaches have been utilized to predict incident clearance time and analyze the effects of influential factors during the past several decades. In general, these approaches can be classified into statistical methods [7] and machine learning methods [8, 9]. Statistical methods

generally can explain the mechanism between independent and dependent variables based on the rigorous mathematical formula [10, 11]. From a methodological perspective, regression analysis and hazard-based methods are the two main statistical methods to analyze incident duration data. Regression methods were widely used for incident duration prediction in previous studies, such as linear regression [12, 13]. To overcome the simple linear assumption between incident clearance time and explanatory variables, researchers proposed the hazard-based duration models (HBDM) to predict the incident duration precisely and explore the influence of significant factors on the incident duration, such as the Cox Proportional Hazards (PH) model and the Accelerated Failure Time (AFT) model [14]. Nam and Mannering [5] applied different distributions in HBDMs to analyze incident duration based on 681 incidents from Washington State’s incident response team program.

Lee and Fazio [15] used a proportional hazard-based Cox-regression model to analyze the effect of explanatory variables on response time and clearance time, respectively. Li and Shang [16] selected the best-fit model from 17 candidate different AFT models with different distributions according to the Bayesian Information Criterion (BIC) values, to investigate the effective factors of each incident and predict the time of each incident phase. Ghosh et al. [17] pointed out that the AFT model with a generalized F distribution outperformed other five parametric hazard-based duration models when analyzing the incident clearance time data collected in Michigan. Haule et al. [18] investigated the effects of significant factors on incident clearance time and selected the best-fit model from three AFT models with different distributions in terms of the Akaike information criterion (AIC).

Recently, large quantities of alternative methods have been introduced under the framework of the HBDMs in recent years. For example, a 2-component log-logistic finite mixture model was used by Zou et al. [19] to analyze the incident clearance time data obtained from the Washington Incident Tracking System (WITS), and the model could be better in accounting for the heterogeneities compared to the standard survival model. Different from conventional conditional-mean HBDMs, the quantile regression (QR) model can estimate the changing influence of explanatory variables on incident clearance time as each quantile of the incident duration distribution varied [20, 21]. And a copula-based approach was proposed to accommodate the correlation between incident clearance and other phases of incident duration, and the results showed that the copula models outperformed the log-normal AFT model in predicting the clearance time [22, 23].

Compared with the statistical methods, machine learning approaches can be employed to overcome complex nonlinear relationships between incident clearance time and explanatory variables without prior assumptions about input data [24, 25]. In the previous studies, K-Nearest Neighbor algorithm (KNN) and Bayesian networks were used to predict the incident clearance time [26–28]. Besides, decision trees (DT) models can specify the relative importance of different explanatory variables associated with response variables and are widely used to analyze the traffic incident duration [29]. Nevertheless, the structure of the decision tree highly depends on the data, resulting in instability. To overcome the imbalanced traffic incident duration data problem of the single-tree-based method, Ma et al. [30] found that the gradient boosting decision tree model has a superior performance in model interpretation and prediction accuracy to conventional DT models [31]. Also based on traditional DT models, the extreme gradient boosting machine algorithm was applied to analyze and predict the clearance time data [32, 33]. However, the machine learning models are usually not capable of interpreting the mechanism between estimator and explanatory variables.

Overall, the hazard-based models and the tree-based models are two commonly used statistical and machine learning models in traffic accident duration analysis. However, these aforementioned approaches generally failed

to take account of the model uncertainty (e.g., the AFT models with Gamma, Weibull, or log-logistic model) [34]. In other words, traditional methods typically assumed that the model to be estimated is the “true” model and then made tests among a majority of alternative “true” model according to some criteria like BIC [35]. Consequently, it is important to consider the uncertainty between candidate models, especially when these model are considered reasonable in spite of difference in predictions [36]. Otherwise, the resulting model estimates may be biased and lead to erroneous inference in the analysis of incident clearance time. The Bayesian Model Averaging (BMA) proposed by Draper [37] provided a statistical theoretical basis for solving the model uncertainty problem in econometric modeling. This approach combines and averages all plausible models considered (models with various combinations of influential variables) through setting different prior probability distributions [38] and has been widely used in various fields, such as water main failures prediction [39], firm default prediction [40], and chemical engineering [41].

The objective of this research is to apply the BMA method to account for both model and parameter uncertainty when modeling the incident clearance time. To examine the proposed approach, 2,584 freeway incident records obtained from I-5 corridor in Seattle are analyzed. Estimation and prediction results from the proposed BMA model and conventional HBDMs are then compared and analyzed.

2. Methodology

This section describes the general features of the BMA, two conventional HBDMs and Occam’s Window Method. The last method is one of the sampling techniques used in the model space.

2.1. Bayesian Model Averaging. BMA uses posterior probability as the weight to average all plausible models considered. Thus, let $M = \{M_1, \dots, M_K\}$ denote the set of all models and let y denote the future observed value of the incident clearance time using new input data. Then, in accordance with the law of total probability, the probability density function (PDF) of y under the observed dataset D is

$$p(y|D) = \sum_{k=1}^K p(y|M_k, D)p(M_k|D), \quad (1)$$

where $p(y|M_k, D)$ is the mean of the posterior distribution of y based on candidate model M_k , which is the output of BMA approach. And $p(M_k|D)$ is the probability of the correct prediction model M_k , which is also referred to as the posterior model probability (PMP). And in model space M , $\sum_{k=1}^K p(M_k|D) = 1$. The PMP is given by Bayes’ rule:

$$p(M_k|D) = \frac{p(M_k)p(D|M_k)}{\sum_{l=1}^K p(M_l)p(D|M_l)}, \quad (2)$$

where

$$p(D|M_k) = \int p(D|\theta_k, M_k)p(\theta_k|M_k)d\theta_k, \quad (3)$$

is the marginal model likelihood for the given model M_k and θ_k is the vector of parameters of the model M_k . Additionally, $p(\theta_k|M_k)$ and $p(D|\theta_k, M_k)$ are the prior density of θ_k and the likelihood given the model M_k , respectively. $p(M_k)$ refers to the prior probability that M_k is considered as the “true” model. The posterior mean and variance of y are presented as follows:

$$E[y|D] = \sum_{k=1}^K E[y|D, M_k]p(M_k|D),$$

$$\text{Var}[y|D] = \sum_{k=1}^K (\text{Var}[y|D, M_k] + E[y|D, M_k]^2)p(M_k|D) - E[y|D]^2. \quad (4)$$

Based on the previous work, the size of model space makes the summation of (1) impractical. In order to solve this problem, Occam’s window method is used to select an appropriate collection of candidate models from the model space and will be introduced in the following section.

2.2. Occam’s Window Method. Occam’s window approach was proposed by Madigan and Raftery [42] to reduce the number of models with low posterior probability in the model space M . Two basic principles were conducted to eliminate models that predict far less well than their competitors.

First, if the PMP for the model M_k in the model space M is calculated far lower than the model that provides the highest PMP, model M_k is discarded from the model space M . Those models failing to satisfying the formula

$$A' = \left\{ M_k: \frac{\max_l \{p(M_l|D)\}}{p(M_k|D)} \leq C \right\} \quad (5)$$

should be excluded from equation (1). The $\max_l \{p(M_l|D)\}$ refers to the model with the highest PMP, and the value of C equals 20 since it is determined by the data analyst.

Second, if the PMPs of complex models are lower than their simpler submodels using Occam’s razor method, these models should be discarded from model space M belonging to

$$B = \left\{ M_k: \exists M_l \in M, M_l \subset M_k, \frac{p(M_l|D)}{p(M_k|D)} > 1 \right\}. \quad (6)$$

Therefore, formula (1) can be expressed as

$$p(y|D) = \sum_{M_k \in A} p(y|M_k, D)p(M_k|D), \quad (7)$$

where $A = A' \setminus B \in M$.

Additionally, the leaps and bounds algorithm is applied to implement the above principles as the search strategy. Interested readers can see the companion paper for more details about this algorithm [43].

2.3. Cox Proportional Hazards (PH) Model. The Cox proportional hazard (PH) model is one of the most commonly used semiparametric survival analysis models. This model is used for investigating the relationship between survival time of respondents and predictor variables [44] and is given as follows:

$$h(t, X) = h_0(t) \exp\left(\sum_{i=1}^p \beta_i X_i\right), \quad (8)$$

where t is the survival time, $X = (X_1, X_2, \dots, X_p)$ represents a vector of explanatory variables, β are the coefficients to be estimated, which measure the impact of the p -covariates, $h(t, X)$ is the hazard function, $h_0(t)$ is an unknown baseline hazard, that is, the value of the hazard if all the X_i are equal to zero, and equation (8) can also be written as

$$\log\left(\frac{h(t, X)}{h_0(t)}\right) = \sum_{i=1}^p \beta_i X_i, \quad (9)$$

where $(h(t, X)/h_0(t))$ is defined as hazard ratios (HR), in which any two individuals are constant over time according to the assumption of the Cox PH model.

2.4. Accelerated Failure Time (AFT) Model. Based on the hazard function, the AFT model assumes that the log of the survival times is affected linearly by the covariates of X and can be clearly written as

$$\ln(t) = \xi_i X_i + \varepsilon, \quad (10)$$

where ξ are the coefficients to be estimated, and ε is an error term. There are kinds of different parametric distributions (e.g., Weibull, log-normal, and log-logistic models), which can be used for the AFT model.

For comparison purposes, the incident data were also analyzed using the Cox PH model and the log-logistic AFT model. In the previous study, it is suggested that the log-logistic AFT model outperformed the other two AFT models (with Weibull or log-normal distribution) in terms of the goodness-of-fit statistics and predictive performance. Therefore, the two conventional HBDMs were finally selected as the benchmark models in this study.

2.5. Data Description. In this study, the incident data obtained from the I-5 corridor between Boeing Access Road and the Seattle Central Business District were retrieved from the WITS, which is used to manage the incident log data. The reason for choosing this site is the heavy traffic demand and frequent incident-induced traffic congestion events. Additionally, in previous studies, Tang et al. [32] used the data source to analyze the influence of explanatory variables and examine the prediction performance of the proposed model. And Hou et al. [45] analyzed the time-varying effects of significant variables based on this dataset. A total of 2,584 valid incidents from 1 January to 31 December 2009 were selected from the WITS dataset including 15 categorical

candidate explanatory variables. Additionally, in this dataset, the mean and median of the incident clearance time were 13.58 minutes and 9 minutes. The minimum and maximum values were 1 minutes and 382 minutes, respectively. And the standard deviation was 17.35 minutes. The key information of candidate variables is presented in Table 1.

3. Results and Discussion

This section describes the modeling results for the BMA approach, Cox PH model, and the log-logistic AFT model. In terms of the model averaging strategies, it is assumed that all possible combinations of 15 candidate explanatory variables are equally likely a priori. As previously mentioned, Occam's window method is implemented to exclude complex models that perform far less well than their simpler competitors and discard them from the model space. The results show that the BMA approach and two benchmark models differ in interpreting the explanatory variables based on the same dataset, and the former can provide better prediction performance. All statistical analyses were conducted using statistical software R.

Table 2 lists the posterior means, standard deviations, and posterior effect probabilities $P(\beta \neq 0|D)$ for the coefficients related to different explanatory variables by using the proposed method. The posterior effect probability $P(\beta \neq 0|D)$ equals the sum of the posterior probabilities for all the selected models containing that explanatory variable. For example, the posterior effect probabilities associated with the explanatory variable single lane blocked have 7.8% of its mass at zero. Unlike other statistical models, it can be observed that the variable "single lane blocked" is not included in all the selected models, although it has a significant impact on incident clearance time. 20 different models with the highest PMP were finally selected by Occam's window approach, among which five optimal models ($PMP > 0.05$) shown in Table 2 account for 59.69% of the total posterior probability. Additionally, the estimated coefficients for some variables (i.e., advised WSP, disabled vehicle, debris, heavy truck, weekends, winter, weather, and incident on HOV lane) are not listed in Table 2 because the p values are larger than the significance level (0.05). It is found that model 1 with the largest PMP can account for 22.8% of the total posterior probability, which means that there exists quite a bit model uncertainty.

As shown, the model averaging results of the predictors for incident clearance time generate interesting interpretations. The posterior effect probabilities of seven explanatory variables equal 100%. This result demonstrates that, for response time, traffic control, collision, multiple lane blocked, total closure, injury involved, and summer, all the selected models with the highest PMP contain these explanatory variables, and thus they are the main factors affecting the duration of traffic incident clearance. The positive coefficient in the results of the proposed model indicates that the hazard is higher, and the clearance time decreases with higher values of that variable.

It is clear that summer results in shorter clearance time, which means that the incident clearance time varies with the month of year and gets shorter in summer than other seasons, and for the remaining variables, they all result in longer clearance time.

As the BMA results in Table 2 indicate, we can see that response time shows a weak effect on incident clearance time, the coefficient of which implies that more time is required to prepare for incident response in congested traffic periods. The estimated coefficient -0.527 of traffic control on clearance time deserves attention to improve the measures undertaken by traffic incident management like incident response team (IRT) on directing upstream traffic around the incident.

Among the considered incident types, collision is the only one significant variable affecting the clearance time. And the involvement of fire and injury shows positive effect on incident clearance time. These results demonstrate that both fire and collision involvement can result in longer clearance time or smaller hazard rates and are generally the main factors causing traffic congestion.

Four types of lane closure except all travel lanes blocked all have a significant impact on incident clearance time. This is caused by the increasing operational complexity of the recovery process around the incident. On closer inspection, of all significant variables, total closure has the strongest impact on incident clearance time, which indicates that longer clearance time is generally associated with total closed lanes. To further explain the BMA model, the estimated survival probabilities are plotted in Figure 1.

Meanwhile, Tables 3 and 4 list parameter estimation results of the Cox PH model and the log-logistic AFT model for comparison purposes, respectively. The estimated coefficients for some variables are not listed in Tables 3 and 4 because the p values are larger than the significance level (0.05). It is noted that, in the Cox model, the sign of the regression coefficient (coef) is opposite to that of the AFT model. The positive coefficient in the results of the Cox PH model indicates that the hazard is higher, and thus the clearance time decreases with higher values of that variable. Note that, different from the results of the BMA, all types of incident are significant in terms of p values in the Cox PH model. Moreover, three lane closure types (single lane blocked, multiple lane blocked, and total closure), response time, traffic control, injury involved, fire involved, and work zone involved all result in longer clearance time or smaller hazard rates. Debris, abandoned vehicle, night, and summer all result in shorter incident clearance time or larger hazard rates. These findings are consistent with the previous study using quantile regression.

In the log-logistic AFT model, night is found statistically significant compared with the BMA model. And disabled vehicle, debris, and abandoned vehicle all result in longer clearance time in both survival models, while these variables are not statistically significant in the BMA model. The reason is that when model uncertainty is considered, their posterior effect probabilities from BMA are significantly lower than

TABLE 1: The key information for valid incidents affected by candidate explanatory variables.

Category	Variable	Value set
Incident	Incident type	(Disabled vehicle, debris, abandoned vehicle, collision and others ^a (=0))
	Lane closure type	(Single lane blocked, multiple lanes blocked, all travel lanes blocked and total closure)
	Injury involved	(0, 1)
	Fire involved	(0, 1)
	Work zone involved	(0, 1)
Temporal	Heavy truck involved	(0, 1)
	Time of the day	(Daytime (=0), night (22:00–6:00) (=1))
	Day of the week	(Weekday (=0), weekend (Sat, Sun) (=1))
Geographic	Month of the year	(Summer (Jun, Jul, Aug), winter (Dec, Jan, Feb) and other seasons (=0))
Environmental	Incident on Hov lane ^b	(0, 1)
Traffic	Weather	(Rainy, snowy and other type (=0))
	Peak hours (6:00–9:00, 15:00–18:00)	(0, 1)
Operational	Response time	R+
	Traffic control	(0, 1)
	Washington state patrol (WSP) involved	(0, 1)

^aOthers refer to car fires, police activity, and medical emergency on the road, etc. ^bHov lane refers to the vehicle lane with high-occupancy.

TABLE 2: Selected models with the highest posterior probabilities using BMA.

Variable	$P(\beta \neq 0 D)$	EV ^a	SD ^b	Model1	Model2	Model3	Model4	Model5
Response time	100.0	-0.092	0.004	-0.091	-0.094	-0.091	-0.092	-0.092
Traffic control	100.0	-0.527	0.062	-0.536	-0.509	-0.533	-0.502	-0.533
Collision	100.0	-0.737	0.211	-0.866	-0.780	-0.877	-0.380	-0.868
Single lane blocked	92.2	-0.182	0.078	-0.173	-0.217	-0.176	-0.216	-0.182
Multiple lane blocked	100.0	-0.619	0.111	-0.608	-0.670	-0.586	-0.639	-0.623
Total closure	100.0	-1.491	0.357	-1.501	-1.531	-1.536	-1.444	-1.523
Injury involved	100.0	-0.485	0.123	-0.486	-0.484	-0.475	-0.500	-0.484
Fire involved	92.6	-1.061	0.455	-1.248	-1.177	-1.143	-8.969	-1.257
Summer	100.0	0.170	0.045	0.176	0.171	0.173	0.163	0.173
nVar ^c				11	12	10	12	12
BIC				-1488	-1486	-1486	-1486	-1485
PMP				0.228	0.117	0.106	0.086	0.060

^aEV is posterior means. ^bSD means the standard deviation. ^cnVar refers to the number of variables in the M_k model.

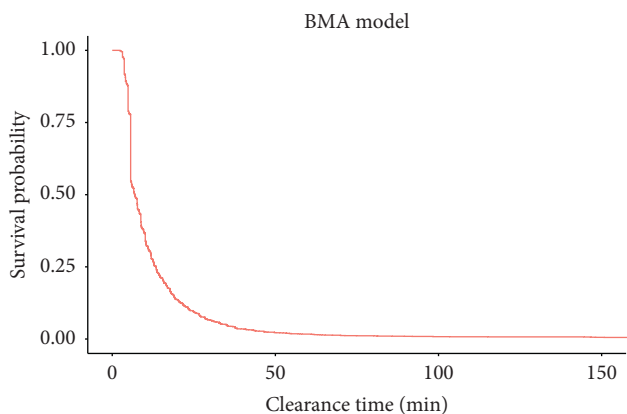


FIGURE 1: Estimated survival probability for the BMA model.

other variables. To further explain the Cox PH model, the log-logistic AFT model, the estimated survival probabilities are plotted in Figures 2 and 3.

The estimated coefficients from the Cox PH, the log-logistic AFT, and BMA models can give macroscopic and

valuable insights for incident duration time. For all travel lanes blocked, the estimated coefficient -0.796 of the Cox PH model and the coefficient 0.615 of the log-logistic AFT model indicate a strong impact on clearance time, while the posterior effect probability in the BMA model equals 8.2% , which means that this variable is actually a less significant determinant of incident clearance time. Furthermore, the contributing factors resulting in longer clearance time can be identified, and thus traffic emergency management agency can improve their management planning and response strategies. As shown in Tables 2–4, the variables “total closure” and “fire involved” have a stronger positive impact on incident clearance time. Thus, when closing all lanes and fire involved traffic incidents are considered, more attention should be given to prevent further severe incidents.

More importantly, the posterior effect probability in the BMA model can overcome the overstatement of the evidence for an effect. The p values for the coefficients indicate whether these relationships are statistically significant. In general, the p values for the predictors for the single model are used as a measure of interpreting the effect on incident

TABLE 3: The estimated parameters for the Cox PH model^a.

Variable	Cox PH model			
	Coef ^b	SE	z-statistic	p value
Response time	-0.098	0.004	-25.840	<2e-16
Traffic control	-0.531	0.056	-9.540	<2e-16
Disabled vehicle	-0.268	0.115	-2.340	0.019
Debris	0.465	0.132	3.520	0.000
Abandoned vehicle	0.272	0.128	2.130	0.034
Collision	-0.636	0.125	-5.070	0.000
Single lane blocked	-0.291	0.060	-4.890	0.000
Multiple lane blocked	-0.736	0.103	-7.120	0.000
Total closure	-1.631	0.357	-4.570	0.000
Injury involved	-0.450	0.123	-3.670	0.000
Fire involved	-1.118	0.342	-3.270	0.001
Work zone involved	-0.459	0.184	-2.490	0.013
Night	0.447	0.123	3.640	0.000
Summer	0.171	0.048	3.540	0.000

^aLikelihood ratio test (LR): 1767, and $p < 2e-16$. ^bCoef means Coefficient.

TABLE 4: The estimated parameters for the log-logistic AFT model.

Variable	Log-logistic AFT model			
	Coef	SE	z-statistic	p value
(Intercept)	1.635	0.076	21.570	<2e-16
Response time	0.072	0.002	39.970	<2e-16
Traffic control	0.220	0.030	7.470	0.000
Disabled vehicle	0.131	0.066	1.990	0.046
Debris	-0.282	0.073	-3.830	0.000
Abandoned vehicle	-0.293	0.074	-3.970	0.000
Collision	0.417	0.071	5.850	0.000
Single lane blocked	0.239	0.033	7.310	0.000
Multiple lane blocked	0.467	0.059	7.930	0.000
All travel lanes blocked	0.615	0.232	2.650	0.008
Total closure	0.633	0.176	3.600	0.000
Injury involved	0.418	0.072	5.830	0.000
Fire involved	0.731	0.200	3.650	0.000
Night	-0.310	0.071	-4.380	0.000
Summer	-0.055	0.026	-2.080	0.038

clearance time. However, p values generally overstate the evidence for an effect [46].

Turning to the model results, Table 5 shows the posterior effect probabilities and p values of several variables. For a few variables (i.e., response time, traffic control, collision, multiple lane blocked, total closure, injury involved, and summer), the p values from Cox PH model and the posterior effect probability $P(\beta \neq 0|D)$ from the BMA model all indicate that there is a highly significant effect ($p < 0.05$ and $P(\beta \neq 0|D) = 100\%$) on the clearance time. However, the BMA model and Cox PH model show the different conclusions for the variables in Table 5. The p values from the Cox PH model overstate the evidence for the effects. For night, debris, and work zone involved, they are considered highly significant in terms of p values ($p < 0.01$), while the posterior effect probabilities from the BMA model suggest that the evidence for an effect is not strong. Additionally, disabled vehicle, abandoned vehicle, and all travel lanes blocked are less significant determinant of incident clearance

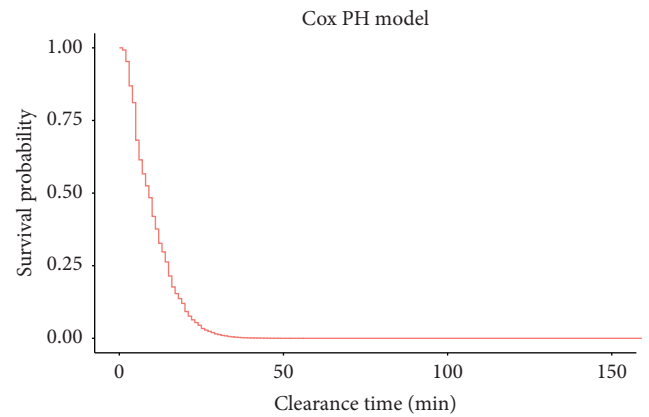


FIGURE 2: Estimated survival probability for the Cox PH model.

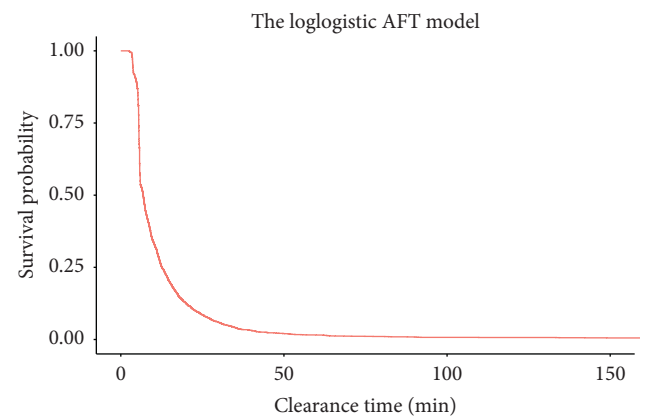


FIGURE 3: Estimated survival probability for the log-logistic AFT model.

time for p values ($p < 0.1$), but the posterior effect probabilities provide weak evidence for the effect on incident clearance time. And for the last variable incident on HOV lane, both approaches show extremely low certainty evidence for an effect. Thus, the Cox PH model overstates the evidence for the effect on explanatory variables compared with the posterior effect probabilities ($P(\beta \neq 0|D) < 78\%$) for the BMA model according to the results in Table 5.

Furthermore, when rejecting the null hypothesis of “no effect,” p values used by the Cox PH model cannot distinguish between two scenarios, which are as follows: (a) there are few data to detect the effect on explanatory variables, and (b) the data provide evidence for the null hypothesis. However, the posterior effect probability in BMA can overcome the overstatement of the evidence for an effect resulting from the above issues. For instance, all travel lanes blocked and incidents on HOV lane are found to be a less significant determinant of incident clearance time for p values and posterior effect probabilities. And for all travel lanes blocked, $P(\beta \neq 0|D)$ equals 8.2%, which is exactly described in scenario (a), whereas the $P(\beta \neq 0|D) = 1.2\%$ of incident on HOV lane indicates the evidence for the null hypothesis of “no effect.” The latter can be approximated as the posterior probability with the effect small enough,

TABLE 5: A comparison of some posterior effect probabilities from BMA and p values from the Cox PH model.

Variable	$P(\beta \neq 0 D)$ (%) (BMA)	p value (Cox PH)
Night	74.3	0.000
Debris	44.6	0.000
Work zone involved	15	$3.9e-07$
Disabled vehicle	77.7	0.019
Abandoned vehicle	23.7	0.034
All travel lanes blocked	8.2	0.059
Incident on Hov lane	1.2	0.106

namely, $P(|\beta| < \epsilon)$, when ϵ is less than half of a standard error [47].

3.1. Comparison of the Prediction Performance. As mentioned before, BMA can improve the prediction performance than any other single candidate model due to the overlook of model uncertainty for single selected models. The incident duration data were also applied to analyze the importance of each explanatory variable contributing to response variables by using two traditional survival analysis models. It is noted that the predicted values of Cox PH model are relative to the sample observations. Thus, we applied the nonparametric step-function (NPSF) approach to predict expected durations [48]. To further demonstrate the prediction performance of BMA, the Mean Absolute Error (MAE), the Root Mean Square Error (RMSE), and the mean absolute percentage error (MAPE) were used to measure the discrepancy between BMA and Cox PH model on assessing the accuracy. These performance indexes were calculated as $MAE = (1/n) \sum_{i=1}^n |O_i - P_i|$, $RMSE = (1/n) \sqrt{\sum_{i=1}^n (O_i - P_i)^2}$ and $MAPE = (1/n) \sum_{i=1}^n |(O_i - P_i)/O_i| \times 100\%$, where O_i and P_i are the observed value and the predicted value of clearance time for incident i , respectively. Smaller MAE, RMSE, and MAPE values indicate a better prediction performance.

In this study, 2,584 incident records were randomly divided into two subsets, one of which was used as training subdataset for the application of BMA and benchmark models, and the other is used as testing subdataset to measure prediction performance. The number of sections used to build and test the model was 1500 and 1084, respectively. To make the results more credible, training and testing subdataset varied according to ten random seeds selected.

Table 6 reports the mean of the prediction performance indexes from the BMA and Cox PH model, as well as the log-logistic AFT model. Bold values are the smallest MAE, RMSE, and MAPE values among three models. As shown in Table 6, multiple random experiments in this study indicate that the proposed BMA model results in better prediction performance in contrast with two traditional survival models in terms of three performance indexes. Thus, it can be concluded that the BMA model can improve the prediction performance for the conventional survival model.

TABLE 6: Performance index values for the Cox PH, log-logistic AFT model and BMA models.

Performance index	Cox PH	Log-logistic AFT model	BMA
MAE	6.051	6.325	5.968
RMSE	15.677	19.272	15.654
MAPE	48.791%	48.728%	48.320%

4. Conclusions

This study has applied Bayesian Model Averaging (BMA) for incident clearance time analysis and prediction. The BMA approach was compared with the Cox Proportional Hazards model and Accelerated Failure Time model (with the log-logistic distribution) in analyzing the 2,584 freeway incident records obtained from I-5 corridor in Seattle. The main conclusions are summarized as follows: (1) Response time, traffic control, collision, multiple lane blocked, total closure, injury involved, and summer are the main factors affecting the duration of traffic incident clearance. (2) The modeling results from three considered models show discrepancy in estimated coefficients, such as response time, traffic control, and night. (3) Compared to the Cox PH and the log-logistic AFT model, the posterior effect probabilities for BMA can overcome the overstatement of the evidence for the effect on explanatory variables in contrast with p values for a single model. (4) The prediction performance of BMA is better than the two classical survival models when predicting the traffic incident clearance time.

For future work, BMA can be applied to explain the effect of explanatory variables on incident clearance time or other phases of incident duration. Markov chain Monte Carlo model composition should be conducted to make a comparison with Occam's window method. Additionally, BMA can be extended to identify outliers in the clearance time data in terms of posterior model probabilities.

Data Availability

The data used to support the findings of this study are available from the corresponding author upon request.

Conflicts of Interest

The authors declare that they have no conflicts of interest.

Acknowledgments

This research was sponsored jointly by the National Key Research and Development Program of China (grant no. 2018YFE0102800), the Shanghai Science and Technology Committee (grant no. 19210745700) and the Fundamental Research Funds for the Central Universities (grant no. 22120210009).

References

- [1] A. M. S. Alkaabi, D. Dissanayake, and R. Bird, "Analyzing clearance time of urban traffic accidents in Abu Dhabi, United Arab Emirates, with hazard-based duration modeling

- method,” *Transportation Research Record: Journal of the Transportation Research Board*, vol. 2229, no. 1, pp. 46–54, 2011.
- [2] H. Zhou and Z. Tian, “Modeling analysis of incident and roadway clearance time,” *Procedia—Social and Behavioral Sciences*, vol. 43, pp. 349–355, 2012.
 - [3] Y. Zou, Y. Zhang, and K. Cheng, “Exploring the impact of climate and extreme weather on fatal traffic accidents,” *Sustainability*, vol. 13, no. 1, p. 390, 2021.
 - [4] B. Ghosh, M. T. Asif, J. Dauwels, U. Fastenrath, and H. Guo, “Dynamic prediction of the incident duration using adaptive feature set,” *IEEE Transactions on Intelligent Transportation Systems*, vol. 20, no. 11, pp. 4019–4031, 2019.
 - [5] D. Nam and F. Mannering, “An exploratory hazard-based analysis of highway incident duration,” *Transportation Research Part A: Policy and Practice*, vol. 34, no. 2, pp. 85–102, 2000.
 - [6] R. Li, F. C. Pereira, and M. E. Ben-Akiva, “Overview of traffic incident duration analysis and prediction,” *European Transport Research Review*, vol. 10, no. 2, 2018.
 - [7] Y. Wang, X. Ma, Z. Li, Y. Liu, M. Xu, and Y. Wang, “Profit distribution in collaborative multiple centers vehicle routing problem,” *Journal of Cleaner Production*, vol. 144, pp. 203–219, 2017.
 - [8] J. Tang, L. Zheng, C. Han et al., “Statistical and machine-learning methods for clearance time prediction of road incidents: a methodology review,” *Analytic Methods in Accident Research*, vol. 27, Article ID 100123, 2020.
 - [9] X. Yang, Y. Zou, J. Tang, J. Liang, and M. Ijaz, “Evaluation of short-term freeway speed prediction based on periodic analysis using statistical models and machine learning models,” *Journal of Advanced Transportation*, vol. 2020, Article ID 9628957, 16 pages, 2020.
 - [10] Y. Wang, S. Peng, X. Zhou, M. Mahmoudi, and L. Zhen, “Green logistics location-routing problem with eco-packages,” *Transportation Research Part E: Logistics and Transportation Review*, vol. 143, Article ID 102118, 2020.
 - [11] Y. Wang, Y. Yuan, X. Guan et al., “Collaborative two-echelon multicenter vehicle routing optimization based on state-space-time network representation,” *Journal of Cleaner Production*, vol. 258, Article ID 120590, 2020.
 - [12] A. Khattak, X. Wang, and H. Zhang, “Incident management integration tool: dynamically predicting incident durations, secondary incident occurrence and incident delays,” *IET Intelligent Transport Systems*, vol. 6, no. 2, p. 204, 2012.
 - [13] J. Hong, R. Tamakloe, D. Park, and Y. Choi, “Estimating incident duration considering the unobserved heterogeneity of risk factors for trucks transporting HAZMAT on expressways,” *Transportation Research Record: Journal of the Transportation Research Board*, vol. 2673, no. 2, pp. 232–242, 2019.
 - [14] R. Li, M. Guo, and H. Lu, “Analysis of the different duration stages of accidents with hazard-based model,” *International Journal of Intelligent Transportation Systems Research*, vol. 15, no. 1, pp. 7–16, 2017.
 - [15] J.-T. Lee and J. Fazio, “Influential factors in freeway crash response and clearance times by emergency management services in peak periods,” *Traffic Injury Prevention*, vol. 6, no. 4, pp. 331–339, 2005.
 - [16] R. Li and P. Shang, “Incident duration modeling using flexible parametric hazard-based models,” *Computational Intelligence and Neuroscience*, vol. 2014, Article ID 723427, 10 pages, 2014.
 - [17] I. Ghosh, P. T. Savolainen, and T. J. Gates, “Examination of factors affecting freeway incident clearance times: a comparison of the generalized F model and several alternative nested models,” *Journal of Advanced Transportation*, vol. 48, no. 6, pp. 471–485, 2014.
 - [18] H. J. Haule, T. Sando, R. Lentz, C.-H. Chuan, and P. Alluri, “Evaluating the impact and clearance duration of freeway incidents,” *International Journal of Transportation Science and Technology*, vol. 8, no. 1, pp. 13–24, 2019.
 - [19] Y. Zou, K. Henrickson, D. Lord, Y. Wang, and K. Xu, “Application of finite mixture models for analysing freeway incident clearance time,” *Transportmetrica A: Transport Science*, vol. 12, no. 2, pp. 99–115, 2016.
 - [20] A. J. Khattak, J. Liu, B. Wali, X. Li, and M. Ng, “Modeling traffic incident duration using quantile regression,” *Transportation Research Record: Journal of the Transportation Research Board*, vol. 2554, no. 1, pp. 139–148, 2016.
 - [21] Y. Zou, J. Tang, L. Wu, K. Henrickson, and Y. Wang, “Quantile analysis of factors influencing the time taken to clear road traffic incidents,” *Proceedings of the Institution of Civil Engineers—Transport*, vol. 170, pp. 1–9, 2017.
 - [22] Y. Zou, X. Ye, K. Henrickson, J. Tang, and Y. Wang, “Jointly analyzing freeway traffic incident clearance and response time using a copula-based approach,” *Transportation Research Part C: Emerging Technologies*, vol. 86, pp. 171–182, 2018.
 - [23] H. Laman, S. Yasmin, and N. Eluru, “Joint modeling of traffic incident duration components (reporting, response, and clearance time): a copula-based approach,” *Transportation Research Record: Journal of the Transportation Research Board*, vol. 2672, no. 30, pp. 76–89, 2018.
 - [24] Q. Shang, D. Tan, S. Gao, and L. Feng, “A hybrid method for traffic incident duration prediction using BOA-optimized random forest combined with neighborhood components analysis,” *Journal of Advanced Transportation*, vol. 2019, Article ID 4202735, 11 pages, 2019.
 - [25] L. Li, X. Sheng, B. Du, Y. Wang, and B. Ran, “A deep fusion model based on restricted Boltzmann machines for traffic accident duration prediction,” *Engineering Applications of Artificial Intelligence*, vol. 93, Article ID 103686, 2020.
 - [26] S.-b. Lee, D. H. Han, and Y.-I. Lee, “Development of freeway traffic incident clearance time prediction model by accident level,” *Journal of Korean Society of Transportation*, vol. 33, no. 5, pp. 497–507, 2015.
 - [27] K. Ozbay and N. Noyan, “Estimation of incident clearance times using Bayesian networks approach,” *Accident Analysis & Prevention*, vol. 38, no. 3, pp. 542–555, 2006.
 - [28] S. Wang, R. Li, and M. Guo, “Application of nonparametric regression in predicting traffic incident duration,” *Transport*, vol. 33, no. 1, pp. 22–31, 2015.
 - [29] J. Weng, L. Feng, G. Du, and H. Xiong, “Maximum likelihood regression tree with two-variable splitting scheme for subway incident delay,” *Transportmetrica A: Transport Science*, vol. 15, no. 2, pp. 1061–1080, 2019.
 - [30] X. Ma, C. Ding, S. Luan, Y. Wang, and Y. Wang, “Prioritizing influential factors for freeway incident clearance time prediction using the gradient boosting decision trees method,” *IEEE Transactions on Intelligent Transportation Systems*, vol. 18, no. 9, pp. 2303–2310, 2017.
 - [31] C. Zhan, A. Gan, and M. Hadi, “Prediction of lane clearance time of freeway incidents using the M5P tree algorithm,” *IEEE Transactions on Intelligent Transportation Systems*, vol. 12, no. 4, pp. 1549–1557, 2011.
 - [32] J. Tang, L. Zheng, C. Han, F. Liu, and J. Cai, “Traffic incident clearance time prediction and influencing factor analysis using extreme gradient boosting model,” *Journal of Advanced Transportation*, vol. 2020, Article ID 6401082, 12 pages, 2020.

- [33] A.-S. Mihaita, Z. Liu, C. Cai, and M.-A. Rizoiu, "Arterial incident duration prediction using a bi-level framework of extreme gradient-tree boosting," 2019, <https://arxiv.org/abs/1905.12254>.
- [34] Y. Zou, D. Lord, Y. Zhang, and Y. Peng, "Application of the bayesian model averaging in predicting motor vehicle crashes," in *Proceedings of the Transportation Research Board 91st Annual Meeting*, Washington, DC, USA, 2012.
- [35] G. Blattenberger, R. Fowles, and P. D. Loeb, "Determinants of motor vehicle crash fatalities using Bayesian model selection methods," *Research in Transportation Economics*, vol. 43, no. 1, pp. 112–122, 2013.
- [36] G. Li and J. Shi, "Application of Bayesian model averaging in modeling long-term wind speed distributions," *Renewable Energy*, vol. 35, no. 6, pp. 1192–1202, 2010.
- [37] D. Draper, "Assessment and propagation of model uncertainty," *Journal of the Royal Statistical Society: Series B (Methodological)*, vol. 57, no. 1, pp. 45–70, 1995.
- [38] A. E. Raftery, D. Madigan, and J. A. Hoeting, "Bayesian model averaging for linear regression models," *Journal of the American Statistical Association*, vol. 92, no. 437, pp. 179–191, 1997.
- [39] G. Kabir, S. Tesfamariam, and R. Sadiq, "Predicting water main failures using Bayesian model averaging and survival modelling approach," *Reliability Engineering & System Safety*, vol. 142, pp. 498–514, 2015.
- [40] J. Traczynski, "Firm default prediction: a Bayesian model-averaging approach," *Journal of Financial and Quantitative Analysis*, vol. 52, no. 3, pp. 1211–1245, 2017.
- [41] A. Tran, M. Pont, A. Aguirre, H. Durand, M. Crose, and P. D. Christofides, "Bayesian model averaging for estimating the spatial temperature distribution in a steam methane reforming furnace," *Chemical Engineering Research and Design*, vol. 131, pp. 465–487, 2018.
- [42] D. Madigan and A. E. Raftery, "Model selection and accounting for model uncertainty in graphical models using Occam's window," *Journal of the American Statistical Association*, vol. 89, no. 428, pp. 1535–1546, 1994.
- [43] A. E. Raftery, "Bayesian model selection in social research," *Sociological Methodology*, vol. 25, pp. 111–163, 1995.
- [44] D. G. Kleinbaum and M. Klein, *Survival Analysis*, Springer, Berlin, Germany, 2010.
- [45] L. Hou, Y. Lao, Y. Wang, Z. Zhang, Y. Zhang, and Z. Li, "Time-varying effects of influential factors on incident clearance time using a non-proportional hazard-based model," *Transportation Research Part A: Policy and Practice*, vol. 63, pp. 12–24, 2014.
- [46] J. A. Hoeting, D. Madigan, A. E. Raftery, and C. T. Volinsky, "Bayesian model averaging: a tutorial," *Statistical Science*, vol. 14, no. 4, pp. 382–401, 1999.
- [47] J. O. Berger and M. Delampady, "Testing precise hypotheses," *Statistical Science*, vol. 2, no. 3, pp. 317–335, 1987.
- [48] J. Kropko and J. J. Harden, "Beyond the hazard ratio: generating expected durations from the cox proportional hazards model," *British Journal of Political Science*, vol. 50, no. 1, pp. 303–320, 2017.

Research Article

An Improved Fuzzy Trajectory Clustering Method for Exploring Urban Travel Patterns

Fang Liu ¹, Wei Bi ², Wei Hao ¹, Fan Gao ² and Jinjun Tang ²

¹School of Traffic and Transportation Engineering, Changsha University of Science and Technology, Changsha 410114, China

²Smart Transportation Key Laboratory of Hunan Province, School of Traffic and Transportation Engineering, Central South University, Changsha 410075, China

Correspondence should be addressed to Wei Bi; biweibw@csu.edu.cn

Received 15 December 2020; Revised 14 January 2021; Accepted 25 January 2021; Published 4 February 2021

Academic Editor: Yong Wang

Copyright © 2021 Fang Liu et al. This is an open access article distributed under the Creative Commons Attribution License, which permits unrestricted use, distribution, and reproduction in any medium, provided the original work is properly cited.

Exploring urban travel patterns can analyze the mobility regularity of residents to provide guidance for urban traffic planning and emergency decision. Clustering methods have been widely applied to explore the hidden information from large-scale trajectory data on travel patterns exploring. How to implement soft constraints in the clustering method and evaluate the effectiveness quantitatively is still a challenge. In this study, we propose an improved trajectory clustering method based on fuzzy density-based spatial clustering of applications with noise (TC-FDBSCAN) to conduct classification on trajectory data. Firstly, we define the trajectory distance which considers the influence of different attributes and determines the corresponding weight coefficients to measure the similarity among trajectories. Secondly, membership degrees and membership functions are designed in the fuzzy clustering method as the extension of the classical DBSCAN method. Finally, trajectory data collected in Shenzhen city, China, are divided into two types (workdays and weekends) and then implemented in the experiment to explore different travel patterns. Moreover, three indices including Silhouette Coefficient, Davies–Bouldin index, and Calinski–Harabasz index are used to evaluate the effectiveness among the proposed method and other traditional clustering methods. The results also demonstrate the advantage of the proposed method.

1. Introduction

Travel patterns can be explored by analyzing the travel characteristics of moving objects (vehicles and humans), which reflects peoples' travel regularity, traffic congestion regularity, and social activity pattern. Travel patterns have been applied in many areas, for instance, providing the decision information for urban planning and emergency [1–4], analyzing and optimizing the path to provide personalized travel recommendations for residents [5–8], vehicles dispatching [9, 10], and station optimization and selection [11]. These applications can prove insights for urban construction and development.

Nowadays, more and more researchers and scholars explore urban travel patterns using large-scale trajectory data, which contain huge hidden information about travel feature and regularity. Several approaches have been used for

this application. (1) Clustering methods: trajectory clustering has been gaining increasing interest in recent years, and it generally requires two components, similarity measurement and clustering algorithm [12–15]. (2) Spatial statistics: Ni et al. [16] employed a spatial econometric model for travel flow analysis to explore factors that influence travel demand; Zhang et al. [17] proposed a Bayesian hierarchical approach for modeling the destination choice behavior considering the unavailable factors and spatio-temporal correlations; Kamruzzaman et al. [18] estimated the effects of urban form and spatial biases on residential mobility. (3) Deep learning: especially nonparametric deep learning methods have proven to give more accurate predictions in urban traffic forecast [19, 20]. (4) Classical traffic theory models: some classical models have been used in travel patterns analysis. For instance, using combined Markov chain and multinomial logit model [21] to improve the

accuracy of travel destination prediction and using traffic assignment models [22] for O-D matrix estimation.

In the abovementioned methods, the clustering method is an unsupervised learning process that classifies datasets on the basis of similarity. By defining a reasonable similarity criterion, the clustering method can effectively excavate hidden information from massive trajectory data and thus reveal travel patterns. Some researchers adopt traditional clustering methods for travel patterns analysis, such as C -means [23], shared nearest neighbor clustering [24], DBSCAN [25, 26], hierarchical clustering method [27, 28], and optics algorithm [29, 30]. Besides, there are also some researchers who propose several modified clustering methods to obtain better clustering results: a modified bee colony optimization (MBCO) [31] is proposed which introduces the approach based on probability selection; a hybrid model-fused k -means and fuzzy c -means clustering with the modified cluster centroid (FKMFCM-MCC) [32]; Wang et al. [33] presented a modified find density peaks (MFDP) algorithm to transform the high-dimensional points into two-dimensional, and it expressed good potential for application.

The literatures mentioned above have provided practical applications of travel patterns analysis, and several classical or modified clustering methods have been proved that they can achieve good clustering results to explore residents' travel patterns. However, there are also some limitations need to be improved in trajectory clustering for travel patterns analysis. Firstly, as for similarity measurements, lots of literatures only consider the spatial attribute of trajectories, and fewer literatures consider the multiattributes (such as temporal, directional, and other characteristics) of trajectories, ignoring other attributes will cause inaccurate results and unreasonable travel patterns. Besides, many researchers who consider multiattributes do not assign weights to different attributes. The configuration and discussion of weights is necessary because different attributes have different influences on trajectory clustering. Secondly, trajectory data have the attribute of faint borders and overlapping borders; thus, the efficient algorithm which has soft constrains is required to handle such dataset, while lots of researchers consider the ideology of hard divided clustering. Finally, many works pay attention on improving clustering algorithm to reduce computational complexity and obtain better results, and there are lacks in using multiple indices to the quantitative evaluation of results.

Fuzzy clustering methods have the ability to identify clusters with variable density distributions and partially overlapping borders [34]. In fuzzy clustering methods, the framework of the fuzzy set theory is defined with the aim to make up for the shortage of crisp clustering algorithms. Generally, the clustering methods realize soft constraints by introducing weight entropy, membership function, or fuzzy distance function. Currently, the fuzzy clustering methods have been applied in many areas, such as predictive models: Seresht et al. [35] proposed a fuzzy clustering algorithm and assign weights to the fuzzy inference systems to improve the accuracy of predictive models; virus research: Mahmoudi et al. [36] used fuzzy clustering technique to compare the

spread of COVID-19 in many countries; image segmentation: Wu and Chen [37] proposed a novel fuzzy clustering method to improve the robustness of the exiting picture clustering. Moreover, some internal evaluation indices are adopted for trajectory data which are unlabeled in clustering results analysis: silhouette coefficient [38, 39]; Davies–Bouldin index [40]; Calinski–Harabasz index [41]; Q-Measure [42]; Dunn's index [39, 43].

The main contributions of this paper include the following several aspects. Firstly, an improved fuzzy clustering method based on DBSCAN is proposed to cluster taxi trajectory data, in which fuzzy theory is introduced to defining membership functions. It is different from traditional DBSCAN algorithm and can effectively deal with taxi trajectory data which have the attributes of faint borders and overlapping borders. The greatest advantage of the proposed method is introducing the theory of soft constrain, which can divide trajectories into reasonable clusters. While traditional DBSCAN uses hard constrain, when a trajectory may belong to either cluster 1 or cluster 2, the algorithm divides it into first cluster, and this is unreasonable. Secondly, we define the trajectory distance considering the combination of spatial, temporal, and directional attributes to measure the similarity between trajectories. Besides, the weights of different attributes are optimized in trajectory distance function to obtain better results. Finally, several internal evaluation indices are used in model comparison, and the results show the effectiveness and advantage of the proposed method comparing with other classical clustering methods.

The remainder of this paper is organized as follows. Section 2 introduces the framework and theory of the proposed method. In Section 3, data description and case results' analysis of Shenzhen city are introduced. In Section 4, the evaluation among compared approaches is conducted, and the results are then discussed. In Section 5, we summarize the conclusion of this paper.

2. Methodology

2.1. Framework. The proposed method for taxi trajectory clustering in this paper is shown in Figure 1 as a framework. The framework mainly contains three aspects: (1) after preprocessing the initial trajectory data, the trajectory distance can be calculated with the combination of spatial, temporal, and directional distance using the weight coefficients; (2) the TC-FDBSCAN is adopted to cluster trajectories, which need to determine the weight coefficients and other algorithm parameters; (3) three indices are used to evaluate the clustering results.

2.2. Multicharacteristics Similarity Measurement. A trajectory is denoted by TR in this paper. $TR = \{(p_1, t_1), (p_2, t_2), \dots, (p_k, t_k)\}$, where $p_k = (p_k^x, p_k^y)$ denotes the location (abscissa p_k^x and ordinate p_k^y , the longitude and latitude, are converted to plane coordinates) of track point k , and t_k denotes the recording time of track point k . Next, we introduce measurements of multicharacteristics similarity

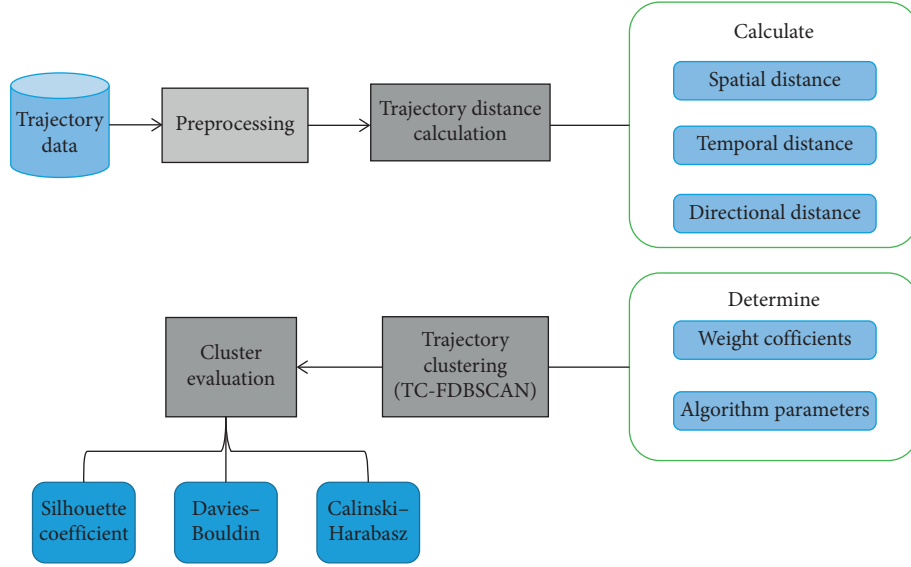


FIGURE 1: Framework of the trajectory clustering method.

between two trajectories TR_A and TR_B , where $TR_A = \{(p_{A1}, t_{A1}), (p_{A2}, t_{A2}), \dots, (p_{Ai}, t_{Ai})\}$ and $TR_B = \{(p_{B1}, t_{B1}), (p_{B2}, t_{B2}), \dots, (p_{Bj}, t_{Bj})\}$.

2.2.1. Spatial Distance between Trajectories. Determining a rule to calculate the spatial distance of track points between trajectories is the key to measure the spatial similarity of trajectories. Hausdorff distance is a common distance measurement method for two points and can be introduced

$$\begin{aligned}
 h(TR_A, TR_B) &= \frac{1}{n_i} \sum_{p_{Ai} \in TR_A} \left\{ \min_{p_{Bj} \in TR_B} (\text{dist}(p_{Ai}, p_{Bj})) \right\}, \\
 h(TR_B, TR_A) &= \frac{1}{n_j} \sum_{p_{Bj} \in TR_B} \left\{ \min_{p_{Ai} \in TR_A} (\text{dist}(p_{Bj}, p_{Ai})) \right\}, \\
 H(TR_A, TR_B) &= \max(h(TR_A, TR_B), h(TR_B, TR_A)),
 \end{aligned} \tag{1}$$

where n_i denotes the number of track points in TR_A , n_j denotes the number of points in TR_B , $\text{dist}(p_{Ai}, p_{Bj})$ is the Euclidean distance between points p_{Ai} and p_{Bj} , and $H(TR_A, TR_B)$ is an absolute Hausdorff distance, which denotes the spatial distance between two trajectories.

into trajectory dataset. Figure 2 shows the Hausdorff distance between two trajectories.

Traditional Hausdorff distance calculates the Max-Min distance, which can only measure the dispersion of the distance between trajectories. And, it is susceptible to local shapes of trajectories. In order to improve its robustness to local effects, a modified Hausdorff distance is defined as follows:

2.2.2. Temporal Distance between Trajectories. The trajectory is represented as an interval, which is related to time of starting points and time of ending points. Considering the influence of trajectory duration, the temporal distance between two trajectories is defined as follows:

$$\text{Tem}(TR_A, TR_B) = \begin{cases} 1, & T_A \cap T_B = \emptyset, \\ \frac{|t_{A1} - t_{B1}| + |t_{Ai} - t_{Bj}|}{(t_{Ai} - t_{A1}) + (t_{Bj} - t_{B1})}, & T_A \cap T_B \neq \emptyset, \end{cases} \tag{2}$$

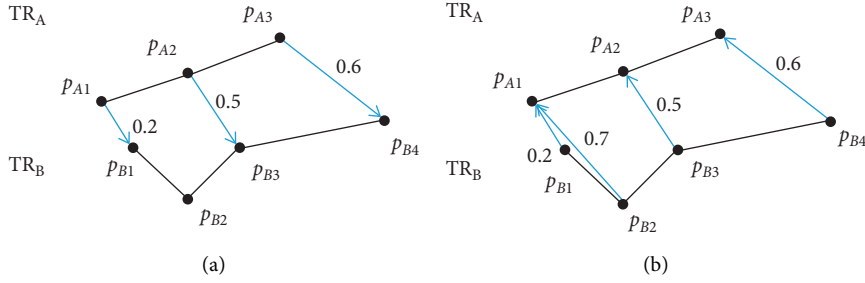


FIGURE 2: Hausdorff distance between two trajectories.

where $T_A = \{t_{A1}, t_{A2}, \dots, t_{Ai}\}$ and $T_B = \{t_{B1}, t_{B2}, \dots, t_{Bj}\}$.

Only if the starting time and ending time of two trajectories are the same ($t_{A1} = t_{B1}$, $t_{Ai} = t_{Bj}$), the temporal distance is 0, which means two trajectories are completely similar in temporal characteristic. When two trajectories are separated in temporal characteristic, they are not completely similar and have a temporal distance $\text{Tem}(\text{TR}_A, \text{TR}_B)$ between 0 and 1.

2.2.3. Directional Distance between Trajectories. Linear directional mean is commonly used to describe the trend or average direction of a set of lines. On the basis of linear directional mean, for trajectory TR_A , treating each trajectory segment (which consists of two consecutive points in TR_A) as a line, its average direction is defined as follows:

$$\gamma_{\text{TR}_A} = \arctan \left| \frac{\sum_{k=1}^{n_i-1} \sin \theta'_{Ak}}{\sum_{k=1}^{n_i-1} \cos \theta'_{Ak}} \right|,$$

$$\gamma'_{\text{TR}_A} = \begin{cases} \gamma_{\text{TR}_A}, & \sum_{k=1}^{n_i-1} \cos \theta'_{Ak} > 0, \sum_{k=1}^{n_i-1} \sin \theta'_{Ak} \geq 0, \\ 180^\circ - \gamma_{\text{TR}_A}, & \sum_{k=1}^{n_i-1} \cos \theta'_{Ak} < 0, \sum_{k=1}^{n_i-1} \sin \theta'_{Ak} \geq 0, \\ 180^\circ + \gamma_{\text{TR}_A}, & \sum_{k=1}^{n_i-1} \cos \theta'_{Ak} < 0, \sum_{k=1}^{n_i-1} \sin \theta'_{Ak} \leq 0, \\ 360^\circ - \gamma_{\text{TR}_A}, & \sum_{k=1}^{n_i-1} \cos \theta'_{Ak} > 0, \sum_{k=1}^{n_i-1} \sin \theta'_{Ak} \leq 0, \end{cases}$$

$$\theta_{Ak} = \arctan \left| \frac{p_{Ak+1}^y - p_{Ak}^y}{p_{Ak+1}^x - p_{Ak}^x} \right|,$$

$$\theta'_{Ak} = \begin{cases} \theta_{Ak}, & p_{Ak+1}^x - p_{Ak}^x > 0, p_{Ak+1}^y - p_{Ak}^y \geq 0, \\ 180^\circ - \theta_{Ak}, & p_{Ak+1}^x - p_{Ak}^x < 0, p_{Ak+1}^y - p_{Ak}^y \geq 0, \\ 180^\circ + \theta_{Ak}, & p_{Ak+1}^x - p_{Ak}^x < 0, p_{Ak+1}^y - p_{Ak}^y \leq 0, \\ 360^\circ - \theta_{Ak}, & p_{Ak+1}^x - p_{Ak}^x > 0, p_{Ak+1}^y - p_{Ak}^y \leq 0, \end{cases} \quad (3)$$

where θ'_{Ak} is the real direction of trajectory segment $\{(p_{Ak}, t_{Ak}), (p_{Ak+1}, t_{Ak+1})\}$, which represents the angle rotated counterclockwise due east, $\theta'_{Ak} \in [0^\circ, 360^\circ]$.

The angle of linear directional mean between two trajectories is defined as follows:

$$\gamma(\text{TR}_A, \text{TR}_B) = |\gamma_{\text{TR}_A}' - \gamma_{\text{TR}_B}'|. \quad (4)$$

2.2.4. Trajectory Distance. Firstly, the spatial and directional distance need to be Min-Max normalized and converted to the dimensionless value, while the temporal distance does not need to be normalized because its value is between 0 and 1; then, the corresponding distance can be defined as follows:

$$\text{SDist}(\text{TR}_A, \text{TR}_B) = \frac{H(\text{TR}_A, \text{TR}_B) - \min\{H\}}{\max\{H\} - \min\{H\}},$$

$$\text{TDist}(\text{TR}_A, \text{TR}_B) = \text{Tem}(\text{TR}_A, \text{TR}_B), \quad (5)$$

$$\text{DDist}(\text{TR}_A, \text{TR}_B) = \frac{\gamma(\text{TR}_A, \text{TR}_B) - \min\{\gamma\}}{\max\{\gamma\} - \min\{\gamma\}},$$

where H and γ are the set of spatial and directional distance between all pairs of trajectories, respectively.

In combination with spatial, temporal, and directional distance, the trajectory distance is defined considering the influence of weights:

$$\begin{aligned} \text{TRDist}(\text{TR}_A, \text{TR}_B) &= \alpha \cdot \text{SDist}(\text{TR}_A, \text{TR}_B) \\ &\quad + \beta \cdot \text{TDist}(\text{TR}_A, \text{TR}_B) \\ &\quad + \omega \cdot \text{DDist}(\text{TR}_A, \text{TR}_B), \\ \alpha + \beta + \omega &= 1, \quad \alpha \geq 0, \beta \geq 0, \omega \geq 0, \end{aligned} \quad (6)$$

where α , β , and ω are weight coefficients.

2.3. Trajectory Clustering Method TC-FDBSCAN. In this section, based on the classical DBSCAN method, an improved TC-FDBSCAN (trajectory clustering method based on fuzzy density-based spatial clustering of applications with noise) method is proposed in trajectory data clustering. In this method, membership functions are introduced to achieve fuzziness and parameters MinTRs (minimum trajectories in neighborhood) and ε (radius of neighborhood)

in classical DBSCAN are replaced by MinTRs_{\min} (minimum value of minimum trajectories in neighborhood), MinTRs_{\max} (maximum value of minimum trajectories in neighborhood), ε_{\min} (minimum radius), and ε_{\max} (maximum radius).

Several extended definitions of the modified method are described in detail as follows.

Definition 1. Neighborhood: the region within a definite radius of a trajectory.

Definition 2. Core trajectory: the number of trajectories in the neighborhood of a trajectory is greater than a definite value.

$$\mu_{\varepsilon}(\text{TR}, \text{TR}_l) = \begin{cases} 1, & |\text{TRDist}(\text{TR}, \text{TR}_l)| \leq \varepsilon_{\min}, \\ \frac{\varepsilon_{\max} - |\text{TRDist}(\text{TR}, \text{TR}_l)|}{\varepsilon_{\max} - \varepsilon_{\min}}, & \varepsilon_{\min} < |\text{TRDist}(\text{TR}, \text{TR}_l)| < \varepsilon_{\max}, \\ 0, & |\text{TRDist}(\text{TR}, \text{TR}_l)| > \varepsilon_{\max}. \end{cases} \quad (8)$$

This membership function considers the fuzzies of neighborhood, which causes a trajectory having a specified membership degree in the fuzzy neighborhood of another trajectory.

$$\mu_{\text{MinTRs}}(\text{den}(\text{TR})) = \begin{cases} 1, & \text{den}(\text{TR}) \geq \text{MinTRs}_{\max}, \\ \frac{\text{den}(\text{TR}) - \text{MinTRs}_{\min}}{\text{MinTRs}_{\max} - \text{MinTRs}_{\min}}, & \text{MinTRs}_{\min} < \text{den}(\text{TR}) < \text{MinTRs}_{\max}, \\ 0, & \text{den}(\text{TR}) \leq \text{MinTRs}_{\min}. \end{cases} \quad (9)$$

This membership function considers the fuzzies of core trajectory, which causes the number of trajectories in the fuzzy neighborhood having a specified membership degree.

Definition 6. Core membership degree: if $\mu_{\text{MinTRs}}(\text{den}(\text{TR})) > 0$, then trajectory TR is a fuzzy core trajectory, and it

$$\text{fuzzyborder}(\text{TR}) = \min_{\text{TR}_l \in \text{neighborcore}(\text{TR})} (\min(\mu_{\text{MinTRs}}(\text{den}(\text{TR}_l)), \mu_{\varepsilon}(\text{TR}, \text{TR}_l))), \quad (10)$$

where $\text{neighborcore}(\text{TR}) = \{\text{TR}_l, \mu_{\text{MinTRs}}(\text{den}(\text{TR}_l)) > 0 \text{ and } \mu_{\varepsilon}(\text{TR}, \text{TR}_l) > 0\}$.

The trajectory will be a noise trajectory if it is not a fuzzy core trajectory or fuzzy border trajectory.

Definition 3. The local density of a trajectory:

$$\text{den}(\text{TR}) = \sum_{\text{TR}_l \in \text{neighbor}(\text{TR}, \varepsilon_{\max})} \mu_{\varepsilon}(\text{TR}, \text{TR}_l), \quad (7)$$

where $\text{neighbor}(\text{TR}, \varepsilon_{\max}) = \{\text{TR}_l, |\text{TRDist}(\text{TR}, \text{TR}_l)| < \varepsilon_{\max}\}$ and $\text{den}(\text{TR})$ denotes the number of trajectories in neighborhood with membership degree $\mu_{\varepsilon}(\text{TR}, \text{TR}_l)$.

Definition 4. ε membership function:

Definition 5. MinTRs membership function:

belongs to a cluster with core membership degree $\text{fuzzycore}(\text{TR}) = \mu_{\text{MinTRs}}(\text{den}(\text{TR}))$.

Definition 7. Border membership degree: if $\mu_{\text{MinTRs}}(\text{den}(\text{TR})) = 0$, then trajectory TR should be a border or noise trajectory. Then, TR can be a fuzzy border trajectory which belongs to a cluster with border membership degree:

Definition 8. Directly density-reachable: if trajectory TR_j is in the fuzzy neighborhood of trajectory TR_i and TR_i is a fuzzy core trajectory, then TR_j is directly density-reachable to TR_i .

Definition 9. Density-reachable: if each TR_n is directly density-reachable to TR_{n-1} under the condition of TR_n and TR_{n-1} are in the $\{TR_i, \dots, TR_{n-1}, TR_n, \dots, TR_j\}$, then TR_j is density-reachable to TR_i .

Definition 10. Density-connected: if TR_k is density-reachable to both TR_i and TR_j , then TR_i and TR_j are density-connected.

The aim of the TC-FDBSCAN is to divide the regions with high density into clusters, which are the largest sets of density-connected trajectories. The major difference from classical DBSCAN is that a trajectory is determined to be a core trajectory or border trajectory considering membership degree, which means the possibility of this trajectory to belong to clusters.

The process is demonstrated as follows which is similar with classical DBSCAN:

- (1) Randomly select a trajectory to visit. If it is a fuzzy core trajectory, then add it into a new cluster with membership degree computed by equation (11) and add other trajectories in its fuzzy neighborhood into an alternate set.
- (2) Visit other trajectories in the alternate set; if the trajectories satisfy the fuzzy core trajectory condition, then add them into the original cluster with membership degree computed by equation (11) and add the trajectories in their fuzzy neighborhood; if they do not satisfy the fuzzy core trajectory condition, then add them into original cluster as fuzzy border trajectories with membership degree computed by equation (12).
- (3) Repeat step (2) until all trajectories in the alternate set have been visited.
- (4) Repeat step (1) to step (3) until all trajectories in the dataset have been visited.

There is a simple approach to allow users to determine two percentages, per_{\min} and per_{\max} . And, then, use $per_{\min} \cdot \max\{\text{TRDist}\}$ and $per_{\max} \cdot \max\{\text{TRDist}\}$ to determine the values of ε_{\min} and ε_{\max} , where $\max\{\text{TRDist}\}$ denotes the

maximum distance between all pairs of trajectories. For MinTRs_{\min} and MinTRs_{\max} , a curve can be drawn, in which the x -coordinate is ε and y -coordinate is the number of trajectories in the set where the distance between each other is equal to ε . This curve is not monotonically decreasing; then, the corresponding y -coordinate values in the first two bends can be selected as MinTRs_{\min} and MinTRs_{\max} .

2.4. Cluster Evaluation Indices. In the relevant studies of cluster evaluation, as the experimental data is labeled and which cluster the sample belongs to is known in advance, so the method based on accuracy such as Purity, Rand Index, and Accuracy can be used. While the trajectory data is unlabeled, there is no external information that can be used to verify the authenticity of the clustering results. Then, several internal evaluation indices which consider the geometric structure of data are required to evaluate the effect of clustering results.

Silhouette coefficient (SC) [36]:

$$SC = \frac{1}{n_C} \sum_{i=1}^{n_C} \frac{b_i - a_i}{\max(a_i, b_i)}, \quad (11)$$

$$b_i = \min_{h=1,2,\dots,n_C, h \neq i} \left(\frac{1}{n_{C_h}} \sum_{TR_h \in C_h} \text{TRDist}(TR_i, TR_{C_h}) \right), \quad (12)$$

$$a_i = \frac{1}{n_{C_i}} \left(\sum_{TR_i \in C_i} \text{TRDist}(TR_i, TR_{C_i}) \right), \quad (13)$$

where n_C is the number of clusters, C_i denotes the i th cluster, n_{C_i} denotes the number of trajectories in C_i , and TR_{C_i} denotes the center of C_i . The larger value of SC indicates better clustering results.

Davies–Bouldin index (DB) [44]:

$$DB = \frac{1}{n_C} \sum_{i=1}^{n_C} \max_{h=1,2,\dots,n_C, i \neq h} \frac{(1/n_{C_i})(\sum_{TR_i \in C_i} \text{TRDist}(TR_i, TR_{C_i})) + (1/n_{C_h})(\sum_{TR_h \in C_h} \text{TRDist}(TR_h, TR_{C_h}))}{\text{TRDist}(TR_{C_i}, TR_{C_h})}, \quad (14)$$

where C_h denotes the h th cluster, n_{C_h} denotes the number of trajectories in C_h , and TR_{C_h} denotes the center of C_h . The smaller value of DB indicates better clustering results.

Calinski–Harabasz index (CH) [45]:

$$CH = \sum_{i=1}^{n_C} \left(\frac{n_{C_i} \text{TRDist}^2(TR_{C_i}, TR_{C_i}) / (n_C - 1)}{\sum_{i=1}^{n_C} \sum_{TR_i \in C_i} (\text{TRDist}^2(TR_i, TR_{C_i}) / (n_{TR} - n_C))} \right), \quad (15)$$

where n_{TR} denotes the number of all trajectories in dataset and TR_C denotes the center of dataset. The larger value of CH indicates better clustering results.

3. Case Study

3.1. Data Description. The research area of the experiments is Shenzhen City, China. Shenzhen city consists of eight administrative districts (Futian, Luohu, Nanshan, Yantian,

Baoan, Longgang, Longhua, Pingshan, and Guangming) and one functional district (Dapeng), which are located between 113°46' E to 114°37' E and 22°27' N to 22°52' N. In this study, taxi trajectory data is used in experiment, and it is composed of a series of sample points collected by vehicular GPS equipment.

Each sample point includes the information of the license plate, location (latitude and longitude), recording time, and instantaneous speed and state (0 represents vacant and 1 represents occupied). We use the data collected by 1000 taxis during one week in May, 2019, and we divide them into two groups to conduct experiment separately, which are weekdays (from May 13th to May 17th) and weekends (from May 18th to May 19th). In order to reduce the influence of abnormal points on clustering results, the original data is preprocessed firstly, which mainly includes eliminating the outliers (latitude and longitude are 0 or out of right range and the state is neither 0 or 1) and interpolating the missing points (recording time interval discontinuity). Finally, 2,499,880 original points during the workdays generate 82,144 passenger-occupied trajectories (49,456 trajectories are valid), and 107,186 original points during the weekends generate 34,384 passenger-occupied trajectories (22,774 trajectories are valid).

The travel time and travel distance of trajectories on workdays and weekends can be calculated, respectively, as shown in Figure 3. The percentage represents the ratio of the number of trajectories in the interval to all trajectories. It can be concluded that both on workdays and weekends, most passengers prefer to take taxi in a short (0 to 5 km) or medium (5 to 15 km) travel distance and takes no more than 20 minutes. Few passengers take more than 1 hour by taxi.

3.2. Parameter Configuration. In the proposed method, the parameters including α , β , ω , ε_{\min} , ε_{\max} , MinTRs_{\min} , and MinTRs_{\max} are needed to be determined to obtain reasonable clustering results. In parameter configuration and comparison, we adjust parameters and select the reasonable parameter combination according to the Silhouette Coefficient (SC) of the clustering results. Firstly, set up several combinations of weight coefficients to compare the clustering results, and the trajectory distance TRDist can be calculated meanwhile. Secondly, determine two percentages $\text{per}_{\min} = 40\%$ and $\text{per}_{\max} = 60\%$ according to the approach mentioned in Section 2.3; then, ε_{\min} and ε_{\max} can be determined according to the value of $\max\{\text{TRDist}\}$. In this part, $\max\{\text{TRDist}\}$ is equal to 1 in these combinations, so we select $\varepsilon_{\min} = 0.4$ and $\varepsilon_{\max} = 0.6$. Thirdly, the statistical curve is drawn to select MinTRs_{\min} and MinTRs_{\max} as mentioned in Section 2.3. For workday data, $\text{MinTRs}_{\min} = 1876$ and $\text{MinTRs}_{\max} = 2353$, which are shown in Figure 4(b). While, for weekend data, $\text{MinTRs}_{\min} = 782$ and $\text{MinTRs}_{\max} = 986$, which are shown in Figure 5(b). Finally, the optimal parameter combination is determined in the condition that the value of SC is largest in all combinations.

Next, the process of parameter configuration for workday data and weekend data are demonstrated as follows, respectively. Totally, we compare twenty combinations

of weight coefficients, and the detailed results including the SC, the number of clusters, and the number of noise trajectories of each clustering result are shown in Tables 1 and 2. We can observe the points which have largest value of SC from Figures 4(a) and 5(a). These points reflect that the clustering results under the corresponding weight combination are the best result for the case study. And, the best results are highlighted in bold in Tables 1 and 2.

Finally, for workday data, we select $\alpha = 0.5$, $\beta = 0.3$, $\omega = 0.2$, $\varepsilon_{\min} = 0.4$, $\varepsilon_{\max} = 0.6$, $\text{MinTRs}_{\min} = 1876$, and $\text{MinTRs}_{\max} = 2353$, while, for weekend data, we select $\alpha = 0.4$, $\beta = 0.4$, $\omega = 0.2$, $\varepsilon_{\min} = 0.4$, $\varepsilon_{\max} = 0.6$, $\text{MinTRs}_{\min} = 782$, and $\text{MinTRs}_{\max} = 986$.

3.3. Clustering Results. Based on the selected parameters, we then adopt the proposed method to cluster taxi trajectory data in Shenzhen city. Figure 6 shows travel patterns of taxi trajectory data collected on workday and weekend. Tables 3 and 4 show the detailed temporal and directional information of each cluster. The value of main direction represents the angle of rotation counterclockwise in terms of east.

We can conclude some findings comparing the final results between workday and weekend data. Several common phenomena are observed as follows. (1) Most of the trajectories in final clusters are located in arterial roads of city and are concentrated in the downtown area. (2) Some main commuter roads are both detected in clusters (for example, Beijing-Hong Kong-Macau expressway and Binhe avenue are two main roads where most trajectories of clusters located in, which can be observed in Figure 6(a) Cluster 5 and Figure 6(b) Cluster 1). (3) Some clusters do not show obvious characteristics on temporal attribute, while they are prominent on spatial and directional attributes (for example, the main travel time periods of Cluster 4 and Cluster 5 in Figure 6(a) do not have a concentrate pattern, while Cluster 4 concentrates on Guangming district, the travel trend is the southeast, and Cluster 5 concentrates on Futian district, the travel trend is towards the east). (4) Clusters which have opposite direction are found in the workday and weekend results, respectively (for example, in Figure 6(a) and Table 3, Cluster 3 and Cluster 4 have opposite direction, since the main direction of Cluster 3 is 138.26° and the main direction of Cluster 4 is 319.35°). It shows that the proposed method can effectively cluster trajectories which have different trends of directions.

There are also obvious differences between workday and weekend. Firstly, the clustering results of weekend data is better than workday data according to the value of SC (workday: 0.6382 and weekend: 0.6418). Secondly, on weekend, the range of clusters are more widespread, and residents tend to travel to the suburb (for example, in Figure 6(b), Cluster 2 and Cluster 3 reflect the larger travel range, the trajectories travel on roads including Pingshan avenue and Pingkui road are added to the final cluster). Thirdly, in contrast to workday, the trajectories of clusters reflect travel in night on weekend (for example, in Figure 6(b) and Table 4, the trajectories in Cluster 4 concentrate on night periods, which during 22:00 to 0:30).

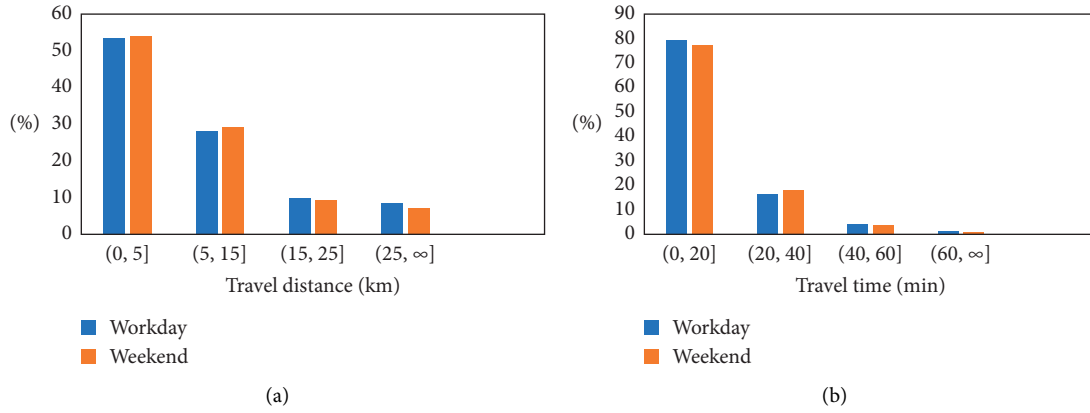


FIGURE 3: The statistical characteristics of trajectories on workdays and weekends: (a) the proportion of trajectories in different travel distance intervals and (b) the proportion of trajectories in different travel time intervals.

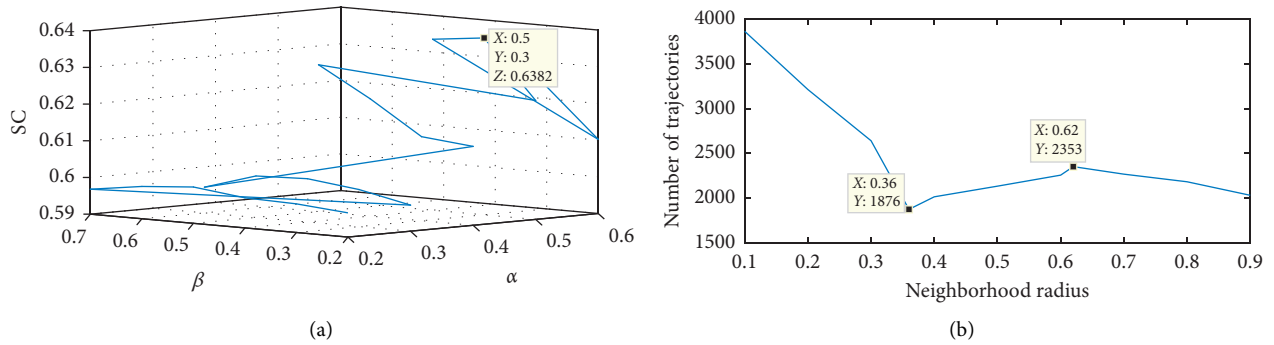


FIGURE 4: Parameter configuration for the data collected on workday: (a) the SC under different combinations of weight coefficients and (b) the curve used to determine MinTR_{\min} and MinTR_{\max} .

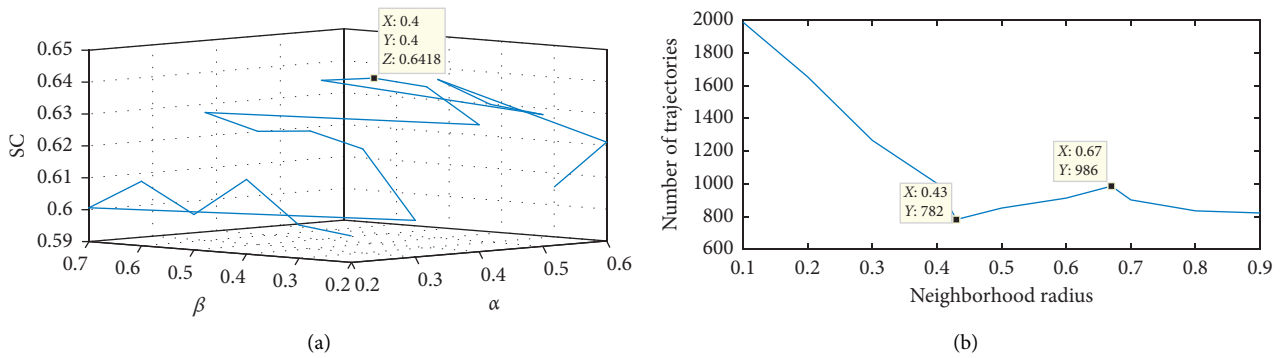


FIGURE 5: Parameter configuration for the data collected on weekend: (a) the SC under different combinations of weight coefficients and (b) the curve used to determine MinTR_{\min} and MinTR_{\max} .

TABLE 1: Comparison of different parameter combinations for workday data.

α	β	ω	SC	The number of clusters	The number of noise trajectories
0.2	0.2	0.6	0.5966	4	16351
0.2	0.3	0.5	0.5978	4	15970
0.2	0.4	0.4	0.5982	5	11369
0.2	0.5	0.3	0.5999	5	12158
0.2	0.6	0.2	0.5988	5	14223
0.2	0.7	0.1	0.5968	5	10196
0.3	0.2	0.5	0.5971	5	9945

TABLE 1: Continued.

α	β	ω	SC	The number of clusters	The number of noise trajectories
0.3	0.3	0.4	0.6001	5	12454
0.3	0.4	0.3	0.6018	5	13112
0.3	0.5	0.2	0.6013	5	10898
0.3	0.6	0.1	0.5970	4	15668
0.4	0.2	0.4	0.6115	4	16011
0.4	0.3	0.3	0.6129	5	12447
0.4	0.4	0.2	0.6220	5	12098
0.4	0.5	0.1	0.6300	6	10256
0.5	0.2	0.3	0.6224	6	9963
0.5	0.3	0.2	0.6382	6	10891
0.5	0.4	0.1	0.6366	5	11025
0.6	0.2	0.2	0.6102	7	8861
0.6	0.3	0.1	0.6233	5	10258

TABLE 2: Comparison of different parameter combinations for weekend data.

α	β	ω	SC	The number of clusters	The number of noise trajectories
0.2	0.2	0.6	0.5983	6	5999
0.2	0.3	0.5	0.6004	6	5766
0.2	0.4	0.4	0.6134	6	5988
0.2	0.5	0.3	0.6011	8	5365
0.2	0.6	0.2	0.6102	7	5531
0.2	0.7	0.1	0.6006	7	5688
0.3	0.2	0.5	0.6015	5	6012
0.3	0.3	0.4	0.6226	7	5764
0.3	0.4	0.3	0.6269	7	5841
0.3	0.5	0.2	0.6255	8	5499
0.3	0.6	0.1	0.6301	8	5501
0.4	0.2	0.4	0.6298	7	5223
0.4	0.3	0.3	0.6404	9	4913
0.4	0.4	0.2	0.6418	8	5423
0.4	0.5	0.1	0.6398	9	4826
0.5	0.2	0.3	0.6313	9	5012
0.5	0.3	0.2	0.6332	10	4788
0.5	0.4	0.1	0.6397	8	4978
0.6	0.2	0.2	0.6210	8	4814
0.6	0.3	0.1	0.6356	7	5112

Finally, the number of clusters on weekend is more than weekend and the direction of clusters are more various on weekend which are shown in Figures 6(a) and 6(b).

4. Discussion

In order to verify the effectiveness of the proposed method, we compare it with other commonly used clustering methods in this section. The case data is 10,000 trajectories randomly selected from the original data (from May 13th to May 19th). Three internal evaluation indices such as Silhouette Coefficient, Davies–Bouldin index, and Calinski–Harabasz index as mentioned in Section 2.4 are adopted to evaluate the clustering results.

4.1. Comparative Approaches

4.1.1. Hard C-Means (HCM). HCM or K-means clustering algorithm is an iterative solution of the cluster analysis algorithm. In this method, the data is divided into C groups, which

are randomly selected from C objects as the initial clustering centers. Then, for each object, calculate the distance between every seed clustering center to each object from its nearest cluster center. The clustering centers and the objects assigned to them represent a cluster. Since each sample has been assigned, the clustering center of the cluster is recalculated according to the existing objects in the cluster. This process is repeated until a termination condition is met. The termination condition can be that no (or minimum number) objects are reassigned to different clusters, no (or minimum number) cluster centers change again, and the error sum of squares is locally minimum.

4.1.2. Fuzzy C-Means (FCM). Fuzzy C-means clustering is a kind of clustering algorithm which uses membership degree to determine the degree of each object belonging to a certain cluster. It is an improvement of the earlier HCM clustering method. FCM divides the original data into C fuzzy groups and finds the clustering center of each group in order to minimize the value function of the nonsimilarity index. The main difference between FCM and HCM is FCM applying

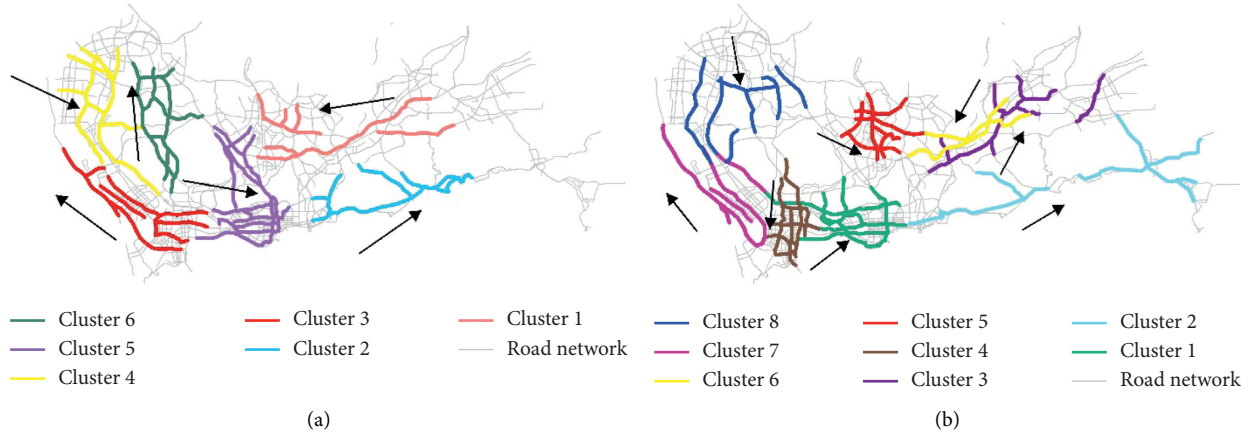


FIGURE 6: Clustering results: (a) workday and (b) weekend.

TABLE 3: Detailed information of each cluster on workday.

Cluster	Main travel time periods	Main direction (angle)
Cluster 1	7:00 to 9:00	189.29°
Cluster 2	16:30 to 19:00	44.38°
Cluster 3	All day	138.26°
Cluster 4	All day	319.35°
Cluster 5	All day	332.17°
Cluster 6	7:00 to 9:00; 16:00 to 20:00	94.32°

TABLE 4: Detailed information of each cluster on weekend.

Cluster	Main travel time periods	Main direction (angle)
Cluster 1	All day	46.18°
Cluster 2	All day	42.06°
Cluster 3	9:00 to 11:00	57.92°
Cluster 4	22:00 to 0:30	264.32°
Cluster 5	20:00 to 22:30	331.23°
Cluster 6	16:00 to 19:00	227.36°
Cluster 7	All day	124.06°
Cluster 8	All day	274.34°

fuzzy division so that each given trajectory is determined by the membership degree between 0 and 1. In accordance with the introduction of fuzzy division, the membership matrix has normalization provisions so that the sum of membership degrees of a dataset is always equal to 1.

4.1.3. Agglomerative Nesting Algorithm (AGNES). Agglomerative nesting algorithm adopts a bottom-up strategy. Each object is initially treated as a cluster, and these clusters are then merged step by step according to some criteria. The distance between two clusters can be determined by the similarity of the closest data in the two different clusters. The merging process of clustering is repeated until all objects meet the number of clusters.

4.1.4. DBSCAN. DBSCAN is a density-based clustering algorithm, which generally assumes that clusters can be determined by the density of the sample distribution. Samples of the same cluster are closely related to each other, and there must be

other samples of the same cluster not far away from any sample of the cluster. A cluster is obtained by grouping closely related samples together. The final result of all clusters is obtained by dividing all groups of closely related samples into different clusters. The definitions of DBSCAN algorithm are similar to the descriptions in Section 2.3 without membership constraint.

4.1.5. Shared Nearest Neighbor Clustering (SNNC). The shared nearest neighbor clustering algorithm was proposed by Jarvis and Patrick, where a link is created between a pair of points p and q , if and only if p and q have each other in their closest k -nearest neighbor [46]. This algorithm is an extension of the DBSCAN. The basic idea of SNNC is based on determining the core points around which clusters with various sizes and shapes are built, without worrying about determining their number [47]. Counting the number of points shared between two points p and q in their k -nearest neighbor list based on the distance metric allows us to determine the similarity between them. The greater the number of shared points, the higher the similarity between p and q .

4.2. Results' Discussion. In order to apply these approaches to the case study in comparison analysis, the distance in HCM, FCM, AGNES, DBSCAN, and SNNC is calculated by the trajectory distance as mentioned in our method. The weight coefficients are determined, so the trajectory distance is described by $TRDist = 0.4 \times SDist(TR_A, TR_B) + 0.3 \times TDist(TR_A, TR_B) + 0.3 \times DDist(TR_A, TR_B)$. The detailed results are shown in Table 5.

Table 5 and Figure 7 show the effectiveness evaluation of different clustering approaches, and we can observe their

TABLE 5: Comparison of different clustering approaches for case data.

Serial number	Approach	Main parameters	SC
1	HCM	The number of clusters: 8	0.563
2	FCM	The number of clusters: 8 Fuzzy degree parameter: 2	0.591
3	AGNES	The number of clusters: 8	0.545
4	DBSCAN	Linkage distance: 0.45 ϵ : 0.45; MinTRs: 350	0.620
5	SNNC	\	0.633
6	TC-FDBSCAN	MinTRs _{min} : 300; MinTRs _{max} : 500; ϵ_{min} : 0.36; ϵ_{max} : 0.54	0.652

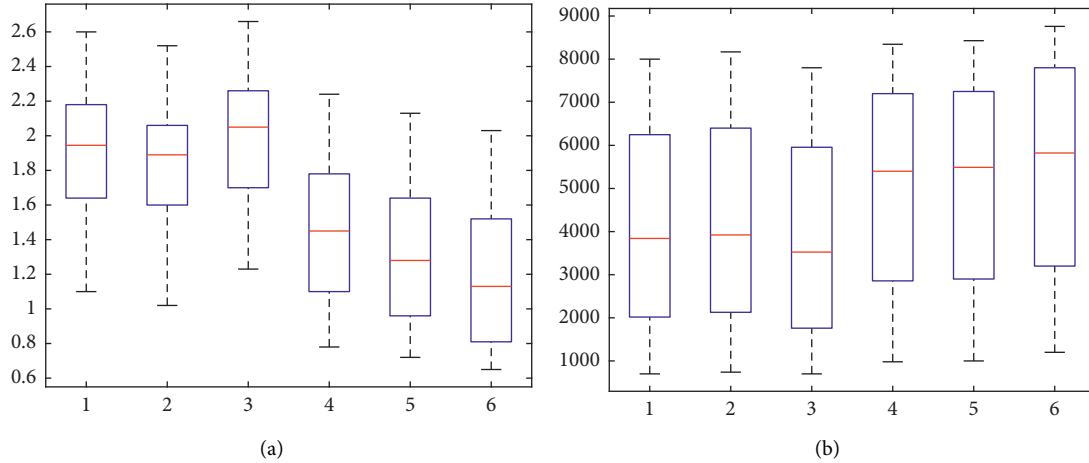


FIGURE 7: Boxplot diagram of the clustering evaluation for case data. (a) DB index. (b) CH index.

ability in analyzing unlabeled data samples. The values of SC show that the proposed TC-FDBSCAN model produces better clustering results than other methods, while AGNES produces worse clustering results than others. In Figure 7, the DB index and CH index describe the similar effect: (1) TC-FDBSCAN is obviously superior to other methods; (2) AGNES is obviously inferior to others; (3) HCM and FCM show the similar results, while FCM is better than HCM; (4) DBSCAN and SNNC show that their clustering performance are close, while SNNC is better than DBSCAN. Overall, the proposed method can find better clustering division and provide high clustering accuracy for large-scale trajectory data in travel pattern analysis.

5. Conclusion

Clustering taxi trajectory based on similarity measurement is a widely applied way to explore urban travel patterns. This study proposes an improved TC-FDBSCAN to uncover urban travel patterns. The taxi trajectory data collected in Shenzhen city is used to evaluate clustering results in the case study. The dataset is divided into two parts, workdays and weekends, which are be used in clustering analysis and model comparison. Some main findings are concluded in following aspects. (1) Both on workdays and weekends, the trajectories in clusters are mainly distributed on the arterial roads. However, clustering results show that, on weekends, the range of residents' travel is wider than that analyzed on

workdays. (2) Introducing the fuzzy theory into traditional DBSCAN algorithm can improve clustering performance according to three evaluation indicators. (3) Different attributes of trajectories have different influences on clustering results according to the values of weight coefficients.

There are still some limitations which need to be improved in future study. On the one hand, other fuzzy clustering methods need to be studied to reduce computational complexity of the algorithm. On the other hand, other fuzzy theory such as weight entropy should be combined in the trajectory clustering method. Moreover, the proposed method is also necessary to be applied in different cities to prove its universality.

Data Availability

The trajectory data used to support the findings of this study are available from the corresponding author upon request.

Conflicts of Interest

The authors declare that there are no conflicts of interest regarding the publication of this paper.

Acknowledgments

This research was funded in part by the Innovation-Driven Project of Central South University (no. 2020CX041),

Natural Science Foundation of Hunan Province (no. 2020JJ4752), National Key R&D Program of China (no. 2020YFB1600400), and Foundation of Central South University (no. 502045002).

References

- [1] Y. Yan, S. Zhang, J. Tang, and X. Wang, "Understanding characteristics in multivariate traffic flow time series from complex network structure," *Physica A: Statistical Mechanics and its Applications*, vol. 477, pp. 149–160, 2017.
- [2] R. A. Acheampong, "Spatial structure, intra-urban commuting patterns and travel mode choice: analyses of relationships in the Kumasi Metropolis, Ghana," *Cities*, vol. 96, Article ID 102432, 2020.
- [3] J. J. Tang, J. Hu, W. Hao, X. Q. Chen, and Y. Qi, "Markov chains based route travel time estimation considering link spatio-temporal correlation," *Physica A*, vol. 545, pp. 1–15, 2020.
- [4] Y. Wang, S. Peng, X. Zhou, M. Mahmoudi, and L. Zhen, "Green logistics location-routing problem with eco-packages," *Transportation Research Part E: Logistics and Transportation Review*, vol. 143, Article ID 102118, 2020.
- [5] Y. Wang, X. Ma, Z. Li, Y. Liu, M. Xu, and Y. Wang, "Profit distribution in collaborative multiple centers vehicle routing problem," *Journal of Cleaner Production*, vol. 144, pp. 203–219, 2017.
- [6] J. Tang, S. Zhang, X. Chen, F. Liu, and Y. Zou, "Taxi trips distribution modeling based on Entropy-Maximizing theory: a case study in Harbin city-China," *Physica A: Statistical Mechanics and its Applications*, vol. 493, pp. 430–443, 2018.
- [7] X. Jiao, Y. Xiao, W. Zheng, H. Wang, and C.-H. Hsu, "A novel next new point-of-interest recommendation system based on simulated user travel decision-making process," *Future Generation Computer Systems*, vol. 100, pp. 982–993, 2019.
- [8] Y. Wang, Y. Yuan, X. Guan et al., "Collaborative two-echelon multicenter vehicle routing optimization based on state-space-time network representation," *Journal of Cleaner Production*, vol. 258, Article ID 120590, 2020.
- [9] L. Dimitriou, E. Kourti, C. Christodoulou, and V. Gkania, "Dynamic estimation of optimal dispatching locations for taxi services in mega-cities based on detailed GPS information," *IFAC (International Federation of Automatic Control) Conference*, vol. 49, no. 3, pp. 197–202, 2016.
- [10] M. Ramezani and M. Nourinejad, "Dynamic modeling and control of taxi services in large-scale urban networks: a macroscopic approach," *Transportation Research Procedia*, vol. 23, pp. 41–60, 2017.
- [11] M. Kabak, M. Erbaş, C. Çetinkaya, and E. Özceylan, "A GIS-based MCDM approach for the evaluation of bike-share stations," *Journal of Cleaner Production*, vol. 201, pp. 49–60, 2018.
- [12] J. Kim and H. S. Mahmassani, "Spatial and temporal characterization of travel patterns in a traffic network using vehicle trajectories," *Transportation Research Part C: Emerging Technologies*, vol. 59, pp. 375–390, 2015.
- [13] P. D'Urso, L. D. Giovanni, and R. Massari, "Robust fuzzy clustering of multivariate time trajectories," *International Journal of Approximate Reasoning*, vol. 99, pp. 12–38, 2018.
- [14] L. Zheng, D. Xia, X. Zhao et al., "Spatio-temporal travel pattern mining using massive taxi trajectory data," *Physica A: Statistical Mechanics and its Applications*, vol. 501, pp. 24–41, 2018.
- [15] J. J. Tang, W. Bi, F. Liu, and W. H. Zhang, "Exploring urban travel patterns using density-based clustering with multi-attributes from large-scaled vehicle trajectories," *Physica A*, vol. 561, pp. 1–18, 2020.
- [16] L. Ni, X. Wang, and X. Chen, "A spatial econometric model for travel flow analysis and real-world applications with massive mobile phone data," *Transportation Research Part C: Emerging Technologies*, vol. 86, pp. 510–526, 2018.
- [17] S. Zhang, X. Liu, J. Tang, S. Cheng, Y. Qi, and Y. Wang, "Spatio-temporal modeling of destination choice behavior through the Bayesian hierarchical approach," *Physica A: Statistical Mechanics and its Applications*, vol. 512, pp. 537–551, 2018.
- [18] M. Kamruzzaman, J. De Vos, G. Currie, B. Giles-Corti, and G. Turrell, "Spatial biases in residential mobility: implications for travel behaviour research," *Travel Behaviour and Society*, vol. 18, pp. 15–28, 2020.
- [19] J. Tang, J. Liang, S. Zhang, H. Huang, and F. Liu, "Inferring driving trajectories based on probabilistic model from large scale taxi GPS data," *Physica A: Statistical Mechanics and its Applications*, vol. 506, pp. 566–577, 2018.
- [20] J. J. Vázquez, J. Arjona, M. Linares, and J. Casanovas-Garcia, "A comparison of deep learning methods for urban traffic forecasting using floating car data," *Transportation Research Procedia*, vol. 47, pp. 195–202, 2020.
- [21] F. Zong, Y. Tian, Y. He, J. Tang, and J. Lv, "Trip destination prediction based on multi-day GPS data," *Physica A: Statistical Mechanics and its Applications*, vol. 515, pp. 258–269, 2019.
- [22] P. Krishnakumari, H. van Lint, T. Djukic, and O. Cats, "A data driven method for OD matrix estimation," *Transportation Research Part C: Emerging Technologies*, vol. 113, pp. 38–56, 2020.
- [23] Z. Chan, L. Collins, and N. Kasabov, "An efficient greedy K-means algorithm for global gene trajectory clustering," *Expert Systems with Applications*, vol. 30, no. 1, pp. 137–141, 2006.
- [24] R. Liu, H. Wang, and X. Yu, "Shared-nearest-neighbor-based clustering by fast search and find of density peaks," *Information Sciences*, vol. 450, pp. 200–226, 2018.
- [25] K. Kailing, H. P. Kriegel, A. Pryakhin, and M. Schubert, "Clustering multi-represented objects with noise," in *Proceedings of the 8th Pacific-Asia Conference on Knowledge Discovery and Data Mining (PAKDD)*, Sydney, Australia, May 2004.
- [26] L. Gong, T. Yamamoto, and T. Morikawa, "Identification of activity stop locations in GPS trajectories by DBSCAN-TE method combined with support vector machines," *Transportation Research Procedia*, vol. 32, pp. 146–154, 2018.
- [27] D. Zhang, K. Lee, and I. Lee, "Hierarchical trajectory clustering for spatio-temporal periodic pattern mining," *Expert Systems with Applications*, vol. 92, pp. 1–11, 2018.
- [28] B. A. Sabarish, R. Karthi, and T. G. Kumar, "Graph similarity-based hierarchical clustering of trajectory data," *Procedia Computer Science*, vol. 171, pp. 32–41, 2020.
- [29] A. L. T. Palma, *A Clustering-Based Approach for Discovering Interesting Places in Trajectories*, Universidade Federal do Rio Grande do Sul, Porto Alegre, Brazil, 2008.
- [30] K. P. Agrawal, S. Garg, S. Sharma, and P. Patel, "Development and validation of OPTICS based spatio-temporal clustering technique," *Information Sciences*, vol. 369, pp. 388–401, 2016.
- [31] P. Das, D. K. Das, and S. Dey, "A modified Bee Colony Optimization (MBCO) and its hybridization with k-means for

- an application to data clustering,” *Applied Soft Computing*, vol. 70, pp. 590–603, 2018.
- [32] T. Wu, Y. Zhou, Y. Xiao, D. Needell, and F. Nie, “Modified fuzzy clustering with segregated cluster centroids,” *Neuro-computing*, vol. 361, pp. 10–18, 2019.
- [33] G. Wang, C. Bu, and Y. Luo, “Modified FDP cluster algorithm and its application in protein conformation clustering analysis,” *Digital Signal Processing*, vol. 92, pp. 97–108, 2019.
- [34] D. Ienco and G. Bordogna, “Fuzzy extensions of the DBScan clustering algorithm,” *Soft Computing*, vol. 22, no. 5, pp. 1719–1730, 2016.
- [35] N. G. Seresht, R. Lourenzutti, and A. R. Fayek, “A fuzzy clustering algorithm for developing predictive models in construction applications,” *Applied Soft Computing*, vol. 96, Article ID 106679, 2020.
- [36] M. R. Mahmoudi, D. Baleanu, Z. Mansor, B. A. Tuan, and K.-H. Pho, “Fuzzy clustering method to compare the spread rate of Covid-19 in the high risks countries,” *Chaos, Solitons & Fractals*, vol. 140, Article ID 110230, 2020.
- [37] C. Wu and Y. Chen, “Adaptive entropy weighted picture fuzzy clustering algorithm with spatial information for image segmentation,” *Applied Soft Computing*, vol. 86, Article ID 105888, 2020.
- [38] P. J. Rousseeuw, “Silhouettes: a graphical aid to the interpretation and validation of cluster analysis,” *Journal of Computational and Applied Mathematics*, vol. 20, pp. 53–65, 1987.
- [39] S. Manochandar, M. Punniyamoorthy, and R. K. Jeyachitra, “Development of new seed with modified validity measures for k-means clustering,” *Computers & Industrial Engineering*, vol. 141, Article ID 106290, 2020.
- [40] F. Liu and Z. Zhang, “Adaptive density trajectory cluster based on time and space distance,” *Physica A: Statistical Mechanics and its Applications*, vol. 484, pp. 41–56, 2017.
- [41] R. M. Alguliyev, R. M. Aliguliyev, and L. V. Sukhostat, “Weighted consensus clustering and its application to Big data,” *Expert Systems with Applications*, vol. 150, Article ID 113294, 2020.
- [42] H. P. Kriegel and M. Pfeifle, “Density-based clustering of uncertain data,” in *Proceedings of the KDD Conference*, Chicago, IL, USA, August 2005.
- [43] S. Barak and T. Mokfi, “Evaluation and selection of clustering methods using a hybrid group MCDM,” *Expert Systems with Applications*, vol. 138, Article ID 112817, 2019.
- [44] D. L. Davies and D. W. Bouldin, “A cluster separation measure,” *IEEE Transactions on Pattern Analysis and Machine Intelligence*, vol. PAMI-1, no. 2, pp. 224–227, 1979.
- [45] T. Calinski and J. Harabasz, “A dendrite method for cluster analysis,” *Communications in Statistics - Simulation and Computation*, vol. 3, no. 1, pp. 1–27, 1974.
- [46] R. A. Jarvis and E. A. Patrick, “Clustering using a similarity measure based on shared near neighbors,” *IEEE Transactions on Computers*, vol. C-22, no. 11, pp. 1025–1034, 1973.
- [47] D. Malchiodi, S. Bassis, and L. Valerio, “Discovering regression data quality through clustering methods,” in *Proceedings of the New Directions in Neural Networks-18th Italian Workshop on Neural Networks*, pp. 76–85, IOS Press, Amsterdam, Netherlands, July 2008.

Research Article

Cooperative Hypercube Queuing Model for Emergency Service Systems

Han Liu ^{1,2}, Hao Yin ³, Yang Zhou ⁴, and Meng Li ¹

¹Department of Civil Engineering, Tsinghua University, Beijing 100084, China

²The Research Institute of Emergency Science, The Central Research Institute, China Coal Technology and Engineering Group (CCTEG), Beijing 100013, China

³SF Technology Co., Ltd., Shenzhen 518000, China

⁴College of Civil Engineering and Architecture, Zhejiang University, Hangzhou 310058, China

Correspondence should be addressed to Meng Li; mengli@tsinghua.edu.cn

Received 11 November 2020; Revised 9 December 2020; Accepted 18 December 2020; Published 8 January 2021

Academic Editor: Yong Wang

Copyright © 2021 Han Liu et al. This is an open access article distributed under the Creative Commons Attribution License, which permits unrestricted use, distribution, and reproduction in any medium, provided the original work is properly cited.

As a useful descriptive tool for emergency service effectiveness, the hypercube queuing model has been applied in systems of many countries, such as the SAMU system in Brazil. However, the traditional hypercube queuing model and its extended forms assume that the service provider performs independent services, lacking a compelling description of the situation where emergency vehicles perform cooperative services (e.g., NEPPHE in China). To this end, we assume that vehicles in the same fleet simultaneously start and end services and propose a cooperative hypercube queuing (CHQ) model that can describe the state of emergency systems which apply multivehicle dispatches. In order to verify the accuracy of the model, we apply Arena simulation software in Wuhan case. The results show that the CHQ model can illustrate cooperative performance effectively. Sensitivity analyses under more general parameters are conducted to reveal insights into the model application.

1. Introduction

The emergency system's rapid response plays a crucial role in the mitigation and control of disasters. Especially for catastrophic events, response delay will bring about irreparable losses to people's lives and property. However, a lot of these incidents require several types of vehicles to respond together to complete the rescue mission [1], which casts a big challenge if the required vehicles have a long way to dispatch. In urban fire rescue, major hazardous chemical fires require the cooperation of water tank fire trucks, foam fire trucks, and biochemical fire trucks; for skyscraper fires, lifting jet trucks are also indispensable vehicles among various fire trucks. For example, the Beirut explosion in 2020 and the fire in the China Central Television Building in 2009 require various fire vehicles in cooperative fleets [2, 3]. The applicable scenarios of cooperative response are not limited to the field of fire rescue but also are widely seen in medical assistance. For example, Covid-2019 has brought about huge losses to people

worldwide [4, 5]. In high-risk areas, frequent emergency medical needs are usually accompanied by social incidents of quarrels and provocations. Therefore, police cars need to clear the way for ambulances, and sometimes they need to be escorted by military armed vehicles to ensure the smooth completion of the mission [6]. As the cooperation-needed disaster scales and diversities continue to develop, capturing a complex cooperative system's emergency performance poses a significant challenge to practitioners and researchers. In particular, according to the system vehicle's configuration with professional functions or purposes, evaluating cooperative service effectiveness is essential for discovering and designing better configuration plans.

In recent decades, deterministic and probabilistic models on the emergency facility location have been studied. The location set covering problem (LSCP) model by Toregas et al. [7] and the maximum coverage location problem (MCLP) introduced by Church and ReVelle [8] are two classic models that regard the emergency system as static and deterministic.

The former model assumes that resources are unlimited and strategically determine the minimum number of facilities for entire demand coverage. The latter assumes that resources are limited and aims to make their full use for maximal demand coverage. Based on these two classic models, researchers have proposed extended models in line with the emergency field's reality. Marianov and ReVelle extended LSCP model to a probabilistic version by adding an availability/busy constraint [9]. Daskin (1983) combined vehicle availability with the MCLP model and proposed the maximum expected coverage location model [10]. Erkut et al. incorporated the survival function (i.e., a monotonically decreasing function of survival rate with response time) into the coverage model and constructed the maximum survival location problem (MSLP) [11]. Gendreau et al. considered the characteristics of different coverage radii of various facilities and proposed the dual-standard coverage model (DSM) [12]. The optimization result of facility locations ensures that at least a certain percentage of demand points are located within the smaller standard radius while locating all demand points within the larger standard radius. Wang et al. proposed a logistics location-routing problem under a cooperation mechanism for the benefit and risk-sharing [13]. Later, a collaborative multiple center vehicle routing (CMCVR) problem based on a state-space-time network was presented by designing a suitable profit distribution mechanism [14, 15]. He et al. proposed a two-stage stochastic programming model for the last mile delivery system [16]. Motivated by China's fire emergency services mechanism, Wang et al. proposed a strategic location model for coordinated rescue facilities by considering the impact of the vehicle number and distance on the progressive coverage level [17]. Yufeng Zhou et al. proposed a hybrid genetic algorithm for facility location and relief material transportation problem on the background of the 5.12 Wenchuan Earthquake [18].

For decades, scholars have also conducted numerous academic researches on spatial queuing theory. The hypercube queuing model, developed by Larson [19], is a useful descriptive tool for emergency system performance analysis. It considers geographical and temporal complexities in a server-to-customer system under consideration and illustrates server state transactions under Markovian equilibriums. Based on Larson's work, Jarvis [20] proposed an approximation model by determining servers' busy probabilities in their specific location. Chelst and Barlach [21] extended a multiple unit dispatches model for hypercube queuing services. Their model avoided the exponential growth of problem complexity and thus did not identify each server's actual state for each type of call. Some extensions of the hypercube model have been applied in SAMU emergency system in Brazil [22–25]. For example, Iannoni and Morabito [25] proposed a hypercube queuing model under multiple dispatches and partial backup policies. However, these models did not allow simultaneous transition of cooperative servers from busy states to available states, which may not provide sufficient insight into the hypercube model application in cooperation scenarios.

To the best of our knowledge, hypercube queuing equilibrium under emergency server cooperation has not

been carefully studied. The impact of the supply/demand relationship under the cooperative preference design has generally been ignored in the hypercube queuing literature. Although the classic hypercube queuing model has been widely used in emergency systems in many countries, it may result in inaccurate operational estimations when applied in severe public health incidents such as the Covid-2019 virus outbreak, where necessary cooperative policies are frequently adopted. In light of this gap, we extend the hypercube model under cooperative service equilibrium. Our model relaxes the traditional assumptions that servers dispatched to the same call are independent with different mean service time by assuming that servers in the same fleet become free simultaneously when they finish a cooperative service. The state probabilities in some traditional models are eliminated, which helps reduce the computational complexity of the model. Moreover, our model adds more necessary states for differentiating cooperative server states among their possible combinations, thus providing more accurate dispatching details. The cooperative hypercube model's validation is conducted under different supply/demand scenarios to provide practical insight.

The remainder of this paper is organized as follows. Section 2 introduces the cooperative rescue mechanism by taking an emergency system in Wuhan as an example. Section 3 develops a novel spatial queuing model under cooperative hypercube equilibrium and conducts the model validation through a simulation method. In Section 4, we conduct parameter sensitivity analysis to explore the model application under various scenarios. Finally, Section 5 provides concluding remarks and future research directions.

2. Cooperative Dispatching Preferences

The emergency service system is typically modelled as a zero-capacity waiting line system [25]. The continuous-time Markov chain in the hypercube queuing model can be described as server-status vertices. In the basic hypercube queuing model, the total number of possible states is 2^N , since each server must be the only one of two states (idle (0) or busy (1)). For example, a four-server system generates 16 possible states according to the hypercube vertices; the state {1010} denotes that the first server and the third server are busy and the other two servers are idle. Based on the aggregation of similar events in adjacent locations, the service area can be divided into subareas named atoms in the literature. Each atom is modelled as a single point (marked as j_1, j_2, \dots) in the atom's central area to indicate where the emergency call occurs. Emergency calls at each geographical atom generate in a Poisson process with mean arrival rates λ_j , independent from other atoms. The service time of server follows a negative exponential distribution. Table 1 shows the dispatching preference lists for a noncooperative system (e.g., SAMU system in Brazil), which can be described by the classic hypercube model. Taking Type 2 calls (calls at Atom 2) as an example, while the SAMU system also applies the double dispatch policy, there are three independent candidates in its preference list. When it comes to a Type 2 call that requires double dispatch, the first and second preferred

TABLE 1: Noncooperative dispatching preference lists.

Atom	Dispatch policy	Type of call	First	Second	Third	Fourth
1	A	1	V1	V3	—	—
2	A or B	2	V2	V1	V3	—
3	A or B or C	3	V4	V2	V3	V1

servers (V2 and V1) are simultaneously dispatched; if any one of the two servers is busy, the third one (V3) would be dispatched as a backup one; moreover, if any two servers of the three candidates are both busy, the only idle one would be dispatched as a single dispatch. If the three candidates are all unavailable, the call is lost. One can observe that SAMU's policy may not be suitable for major disasters, which should be simultaneously coped with by multiple types of servers. See [25] for more details.

However, some severe demand has a chance to be saved if and only if vehicles of all essential types are available. Taking China's emergency system as an example, a high-level hazard demand (e.g., a virus outbreak, nuclear power plants, or explosive energy facility) requires specific combinations of professional emergency vehicles (e.g., advanced ambulance, police vehicles, and fire-fighting turntable ladders) to form a cooperative rescue fleet. The essential responder types in cooperation for serving catastrophic demand are confirmed by the National Emergency Plan for Public Health Emergencies (NEPPHE) [1] of China. It describes incidents' physical or chemical properties, including virus-affected patients and other rescue events, and specifies necessary responders' cooperative service standards. If any type of required vehicle stipulated in the NEPPHE is not available, the specific demand's cooperative mission cannot go through.

Motivated by the cooperative mechanism (e.g., NEPPHE) for coping with major disasters, we extend the classic hypercube queuing model to the cooperative hypercube queuing (CHQ) model. We assume that cooperative servers in the same fleet operated by NEPPHE become free simultaneously when they finish a cooperative service. Call types are classified into three levels according to the incident risks: low-risk calls, medium-risk calls, and high-risk calls. The descriptions of dispatching preference policies are given in Table 2:

- (i) A low-risk call requires a single dispatch of an ambulance. For example, to provide basic emergency care, one ambulance is highly competent at this work.
- (ii) A medium-risk call requires the dispatched fleet, including servers of two types (an ambulance and a police car together). When a medium-risk call arrives, the fleet composed of the nearest ambulance and a police car will serve as the first preferred fleet; if either one is busy, then a further available server of the absent type would be selected to formulate the second preference fleet; otherwise, the call is lost to other systems.

TABLE 2: Cooperative dispatching preference lists for NEPPHE, China.

Atom	Dispatch policy	Type of call	First vehicle	Second vehicle
1	Type A	1	V1	V3
2	Types A & B	2	V1 & V2	V3 & V2
3	Types A & B & C	3	V3&V2&V4	V1&V2&V4

- (iii) A high-risk call requires cooperative servers of three types (an ambulance, a police car, and a fire engine). Calls of this type respond to the highest-level severity. For example, in a terrorist attack or a radioactive material accident, the combinatory fleet of three-type vehicles is necessary for a response. When a high-risk call arrives, the fleet composed of the nearest ambulance, a police car, and a fire engine would be dispatched as the first preferred fleet. If any one of the three nearest vehicles is busy, the further available vehicle, which is the same type as the busy one, would be combined with the other available vehicles for the coordinated response. If there is no suitable vehicle to substitute the busy one, the call is lost.

In this way, the traditional model assumption that servers dispatched to the same call are independent (with different mean service time) is relaxed. The suitable cooperative fleet is assigned to the corresponding call before identifying essential server status.

To capture the inherent mechanism of CHQ model, we apply the model in an emergency system in Wuhan (China) according to the released data from the Health Commission of Hubei Province [26]. Figure 1 shows a real network layout of three atoms and four vehicles (i.e., two ambulances: V1 and V3 with service rates $\mu_1 = 0.86$ and $\mu_3 = 0.73$, respectively; one police car: V2 with service rate $\mu_2 = 1.16$; and one fire engine: V4 with service rate $\mu_4 = 1.37$) hosted in three emergency stations that share the same locations of the atoms. The ambulances V1 and V3 are hosted at emergency stations 1 and 3, respectively. The police car V2 is at emergency station 2, and the fire engine V4 is at emergency station 3. According to the free travel time from each station to each atom (AMAP data), the preference list is as follows:

Type 1 calls with arrival rate $\lambda_1 = 0.13$ require the single-Type A dispatch, and there are two Type-A candidate servers in NEPPHE dispatching preference list (the nearest server V1 as the first preference and the further V3 as the second preference). When a Type 1 call arrives, V1 takes the response; if V1 is already in the busy state, V3 will be dispatched as a backup server, although the further travel distance may cause delay; if both V1 and V3 are busy, the call is lost.

Type 2 calls with arrival rate $\lambda_2 = 0.28$ require the double-type (e.g., one Type A server and one Type B server) dispatch, and there are two candidate fleets (the combinatory fleet of V1 and V2 is prior to that of V3

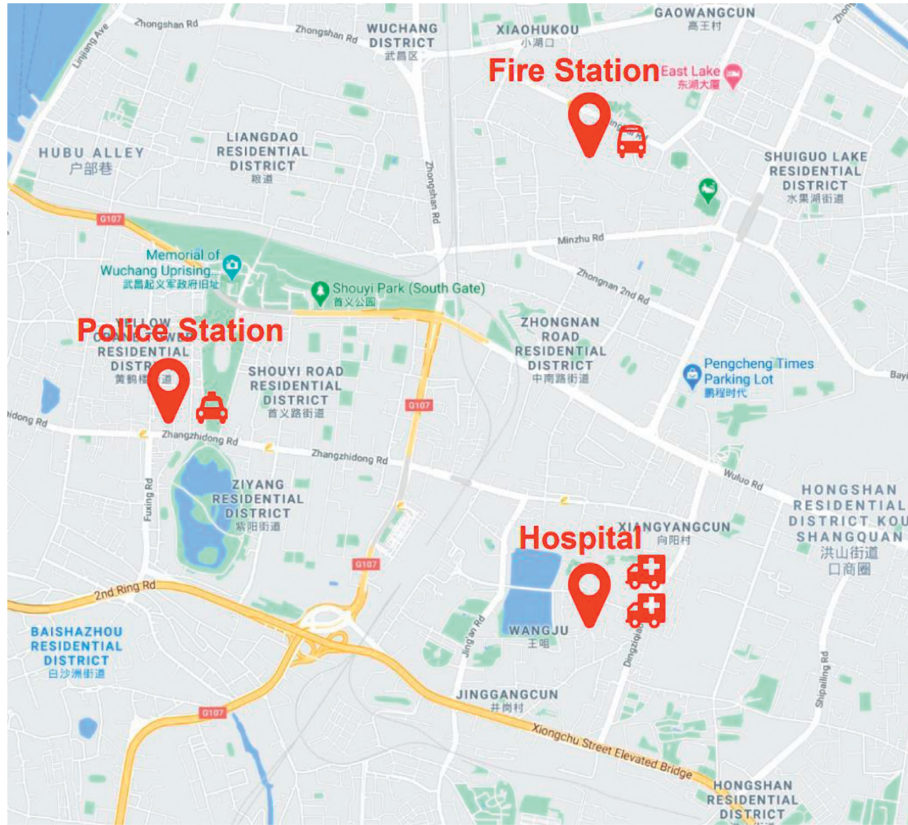


FIGURE 1: A real network with three atoms and four servers in urban areas of Wuhan.

and V2 because the nearer server in a candidate fleet is preferred) in the NEPPHE list.

Type 3 calls with arrival rate $\lambda_3 = 0.09$ require the triple-type (e.g., one Type A server, one Type B server, and one Type C server) dispatch. There are also two candidate fleets, and each fleet contains three essential types of servers in the NEPPHE list. For a Type 3 call, the first fleet of V2 & V3 & V4 is dispatched; if V3 in this fleet is busy, the further Type 1 vehicle (i.e., V1) will be dispatched together with V2 & V4, which may also cause a delay in the cooperative emergency service; if the two candidate fleets are not busy, the call is lost.

Compared to SAMU, NEPPHE attaches great importance to cooperative characteristics in emergency services because essential server absence probably causes task failure. Since emergency response systems in many regions have applied the cooperative dispatch policy, the hypercube queuing model needs further study to accurately describe system performance. A new extension of the classic hypercube model is then proposed in the next section.

3. CHQ Model and Validation

Using the spatial queuing theory and Markovian analysis application, we formulate the CHQ model by a set of flow equilibrium equations. We use B to represent each possible state of the system (e.g., $B = \{1100\}$). P_B is the equilibrium probability of state B . Compared with the basic hypercube queuing model, the total number of possible states in the CHQ model may not be 2^N because the server combination changes the original candidate unit set. On the one hand, some states in partial dispatch policy never exist in the CHQ model and thus should be eliminated. For example, the state $\{0100\}$ is not a candidate unit for dispatch in the CHQ model, since V2 cannot be dispatched alone according to the cooperative preference list (see Table 2). The states such as $\{0001\}$, $\{1010\}$, $\{1001\}$, $\{0101\}$, $\{0011\}$, and $\{1011\}$ are also the states that should be eliminated in the CHQ model.

On the other hand, new states will be added in the CHQ model to identify in which type of calls the server is busy. For example, $\{1110\}^2$ (the first fleet: V1; the second fleet: V2 & V3) and $\{1110\}^1$ (the first fleet: V3; the second fleet: V2 & V1) are substituted for $\{1110\}$. Besides, $\{1111\}^1$ (the first

fleet: V1; the second fleet: V2 & V3 & V4) and $\{1111\}^2$ (the first fleet: V3; the second fleet: V2 & V1 & V4) are substituted for $\{1111\}$. Possible hypercube and queue states for the

example of the CHQ model are shown in Figure 2. The CHQ model with three atoms and four servers is as follows:

$$(\lambda_1 + \lambda_2 + \lambda_3) \cdot P\{0000\} = \mu_1 \cdot P\{1000\} + (\mu_1 + \mu_2) \cdot P\{1100\} + (\mu_2 + \mu_3 + \mu_4) \cdot P\{0111\} + \mu_3 \cdot P\{0010\} + (\mu_2 + \mu_3) \cdot P\{0110\} + (\mu_1 + \mu_2 + \mu_4) \cdot P\{1101\}, \quad (1)$$

$$(\lambda_2 + \lambda_3 + \mu_1) \cdot P\{1000\} = \lambda_1 \cdot P\{0000\} + (\mu_2 + \mu_3) \cdot P\{1110\}^2 + (\mu_2 + \mu_3 + \mu_4) \cdot P\{1111\}^1, \quad (2)$$

$$(\lambda_2 + \lambda_3 + \mu_3) \cdot P\{0010\} = (\mu_1 + \mu_2) \cdot P\{1110\}^1 + (\mu_1 + \mu_2 + \mu_4) \cdot P\{1111\}^2, \quad (3)$$

$$[(\mu_1 + \mu_2) + \lambda_1] \cdot P\{1100\} = \mu_3 \cdot P\{1110\}^1 + \lambda_2 \cdot P\{0000\}, \quad (4)$$

$$[\lambda_1 + (\mu_2 + \mu_3)] \cdot P\{0110\} = \mu_1 \cdot P\{1110\}^2, \quad (5)$$

$$[(\mu_1 + \mu_2 + \mu_4) + \lambda_1] \cdot P\{1101\} = \mu_3 \cdot P\{1111\}^2, \quad (6)$$

$$[(\mu_2 + \mu_3 + \mu_4) + \lambda_1] \cdot P\{0111\} = \lambda_3 \cdot P\{0000\} + \mu_1 \cdot P\{1111\}^1, \quad (7)$$

$$[(\mu_1 + \mu_2) + \mu_3] \cdot P\{1110\}^1 = \lambda_2 \cdot P\{0010\} + \lambda_1 \cdot P\{1100\}, \quad (8)$$

$$[\mu_1 + (\mu_2 + \mu_3)] \cdot P\{1110\}^2 = \lambda_2 \cdot P\{1000\} + \lambda_1 \cdot P\{0110\}, \quad (9)$$

$$[\mu_1 + (\mu_2 + \mu_3 + \mu_4)] \cdot P\{1111\}^1 = \lambda_3 \cdot P\{1000\} + \lambda_1 \cdot P\{0111\}, \quad (10)$$

$$[\mu_3 + (\mu_1 + \mu_2 + \mu_4)] \cdot P\{1111\}^2 = \lambda_3 \cdot P\{0010\} + \lambda_1 \cdot P\{1101\}, \quad (11)$$

$$P\{0000\} + P\{1000\} + \dots + P\{1111\}^2 = 1. \quad (12)$$

Equation (12) ensures that state probabilities' summation should be equal to 1, called equilibrium probability normalization.

To illustrate the proposed hypercube queuing mechanism, we take equation (2), which is the state transaction of the state $\{1000\}$, as an example; that is $(\lambda_2 + \lambda_3 + \mu_1) \cdot P\{1000\} = \lambda_1 \cdot P\{0000\} + (\mu_2 + \mu_3) \cdot P\{1110\}^2 + (\mu_2 + \mu_3 + \mu_4) \cdot P\{1111\}^1$.

On the left side of this equation (outflow rate of state $\{1000\}$), all types of calls generated can be serviced in the system. On the right side, the probabilities of all the possible states that transition into $\{1000\}$ are:

$\{0000\} \rightarrow \{1000\}$: V1 goes into service when a Type 1 call arrives at atom 1

$\{1110\}^2 \rightarrow \{1000\}$: the fleet of V2 & V3 finishes a Type 2 call service, and the two servers become available simultaneously

$\{1111\}^1 \rightarrow \{1000\}$: the fleet of V2 & V3 & V4 finishes a Type 3 call service, and the three servers become available simultaneously

Note that the state $\{1010\}$ cannot be the past state of $\{1000\}$ because it is impossible to release another Type A server V3 when V1 is serving the Type 1 call in the case. There are similar equilibrium probability equations for other states. Performance measures such as system lost probability, server workload, and dispatch frequency probability can be evaluated based on state probabilities calculated in the proposed CHQ model.

The hypercube queuing model often needs to be verified to show its effect in describing the entire service system. Therefore, we used Arena simulation software to calculate the system service performance under different parameter values. The results can be compared with those of the mathematical model to find the matched service system mode of our proposed model.

In the Arena simulation software, we enter these parameters and build logic flow modules to implement the cooperative dispatch policy. We set the warm-up time as 730 days (about two years) and conducted a replication length of 3650 days (about ten years) so that the system is in a stationary state, and the half-width of each variable is correlated. The simulation module design is shown in Figure 3.

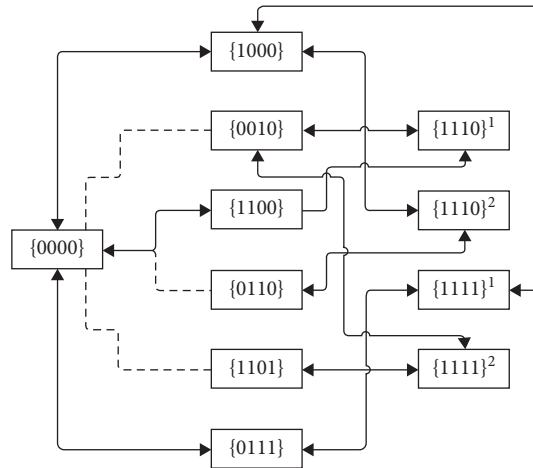


FIGURE 2: Possible hypercube and queue states for the example of the CHQ model.

Status: -1 idle; -2 busy; -4 failure

Call type: 1-am1; 2-am2; 3-am3

Service type: 1-first_choice; 2-second_choice; -1-failure

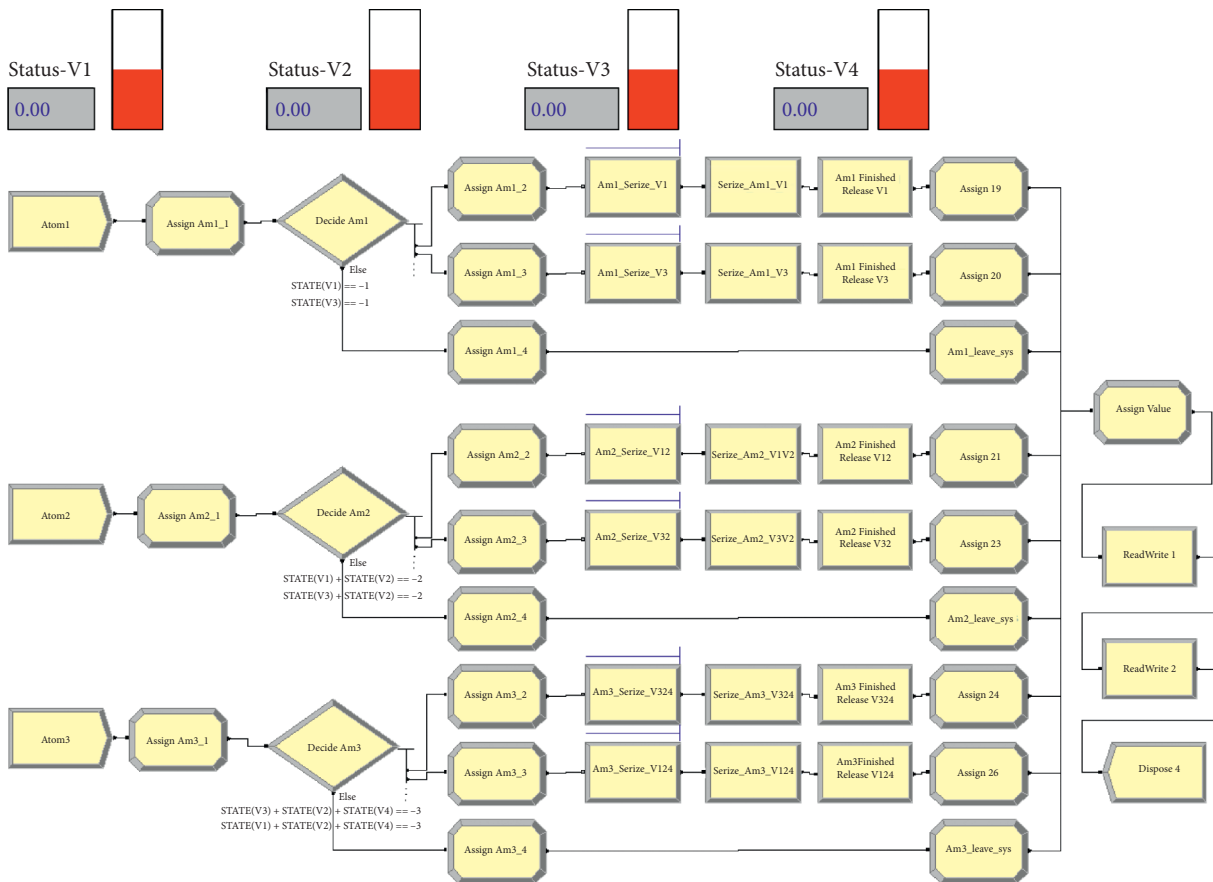


FIGURE 3: The simulation module design of the cooperative response process in the Arena simulation software.

Table 3 shows the system performance results from the CHQ model and the Arena simulation software in Wuhan case study. The call lost probability results indicate that nearly 90% of calls can be served under the cooperative policy in the four-vehicle system. We can observe relatively

small differences in lost probability performance of Type 1, Type 2, and Type 3 (e.g., 0.46%, 2.72%, and 0.42%). The workload statistics show that V1 has the highest probability of being busy. Because V1 is the first response candidate for more frequent calls (e.g., Type 1 and Type 2), since Type 3

TABLE 3: System performance results from the CHQ model and the Arena simulation software in Wuhan case.

System performance	CHQ model	Arena simulation	Difference (%)
Call lost probability			
Type 1	0.005	0.000385	0.46
Type 2	0.08	0.052797	2.72
Type 3	0.026	0.030193	0.42
Workload			
V_1	0.221	0.232246	1.12
V_2	0.143	0.148918	0.59
V_3	0.056	0.07391	1.79
V_4	0.024	0.023217	0.08
Dispatch frequency			
V_1 to j_1	0.203	0.212726	0.97
V_3 to j_1	0.052	0.047627	0.44
V_1 to j_2	0.422	0.436617	1.46
V_2 to j_2	0.48	0.505857	2.59
V_3 to j_2	0.057	0.06924	1.22
V_1 to j_3	0.002	0.004015	0.20
V_2 to j_3	0.154	0.150415	0.36
V_3 to j_3	0.152	0.1464	0.56
V_4 to j_3	0.154	0.150415	0.36

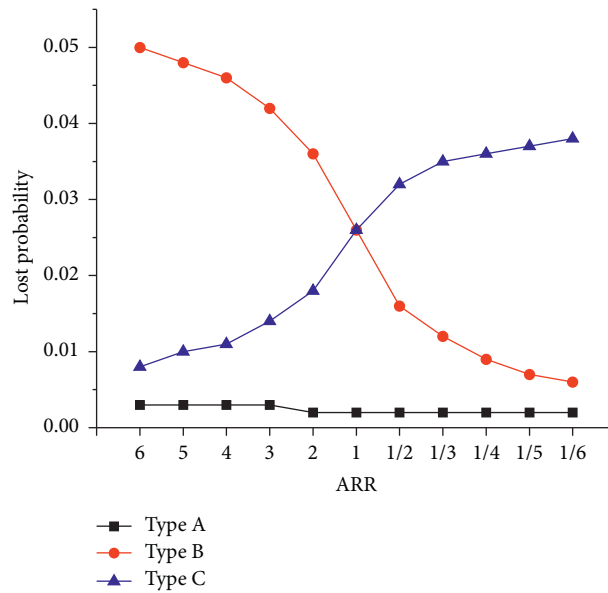


FIGURE 4: Lost probability performance under various ARR.

demand is not as frequent as the other two types of demand, V_4 has the highest idle rate. The workload differences of servers from the two methods are 1.12%, 0.59%, 1.79%, and 0.08%, showing effectiveness in describing system servers' status.

We can also calculate the dispatch frequency statistics under the cooperative policy, such as single-dispatch frequency of V_1 or V_3 to Type 1 calls; double-dispatch frequency of V_1 & V_2 (or V_3 & V_2) to Type 2 calls; triple-dispatch frequency of V_3 & V_2 & V_4 (or V_1 & V_2 & V_4) to Type 3 calls. According to the model results, the dispatch frequency of first choice V_1 (i.e., 0.203) is almost four times that of the second choice V_3 (0.056) in serving Type 1 calls. Regarding Type 2 calls, the dispatch frequency measures of V_1 , V_2 , and V_3 are

0.422, 0.48, and 0.057, respectively. V_2 's dispatch frequency is relatively large because it connects with either V_1 or V_3 . For the triple dispatch to Type 3 calls, the frequency measures of V_2 , V_3 , and V_4 are nearly the same (i.e., 0.154, 0.152, and 0.154). This measure for V_1 is the least because of its non-priority in the preference list and the less frequency of Type 3 calls. The dispatching frequency differences between the CHQ model and the Arena simulation software are from 0.20% to 2.59%.

In the validation, the simulation results are close to those calculated by the CHQ model. Most of the difference values are under 3%. This shows that the model we proposed can accurately describe the server's status and system performances under cooperation conditions. As a result, satisfied

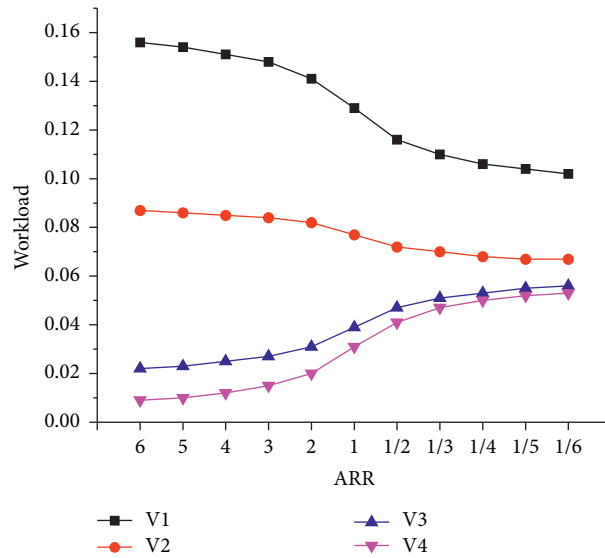


FIGURE 5: Workload performance under various ARR.

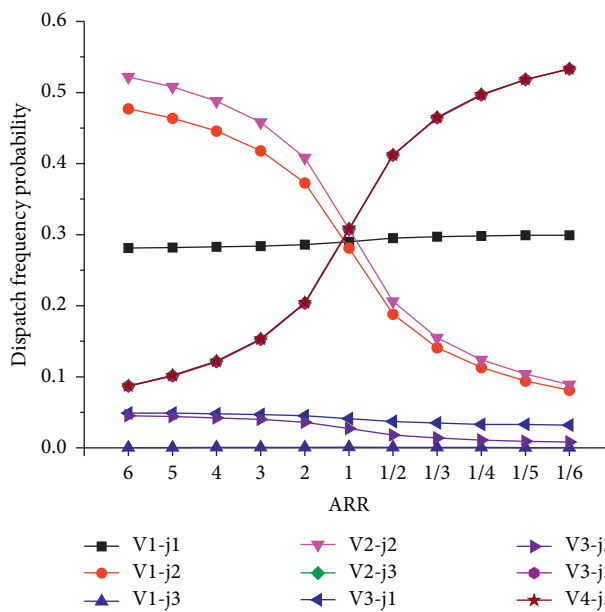


FIGURE 6: Dispatch frequency performance under various ARR.

configurations for engineering guidelines and policy enhancements can be explored through CHQ model application.

4. Sensitivity Analysis

In this section, we conduct additional analysis with homogeneous and heterogeneous demand arrival rates and service rates. The extended hypercube model's potential application can be explored in more circumstances.

4.1. Arrival Rate Value of Different Type Calls. We fix the value of λ_1 , the arrival rate of Type 1 demands, as 0.1 and assume that λ_2 is symmetric to λ_3 with respect to λ_1 . The ratio λ_2/λ_3 is defined as the arrival rate ratio (ARR) of demands that require cooperation responses (i.e., $\lambda_1 = 0.1$, $\lambda_2 = 2(1 + (1/ARR))^{-1}$, and $\lambda_3 = 2(1 + ARR)^{-1}$). The service rate of each vehicle is assumed to be 1. Figures 4–6 show the system performances (e.g., lost probability, server workload, and dispatch frequency) with different ARR (i.e., 1/6, 1/5, 1/4, 1/3, 1/2, 1, 2, 3, 4, 5, and 6). As ARR decreases, the lost probability of Type 1 decreases slightly, while the lost

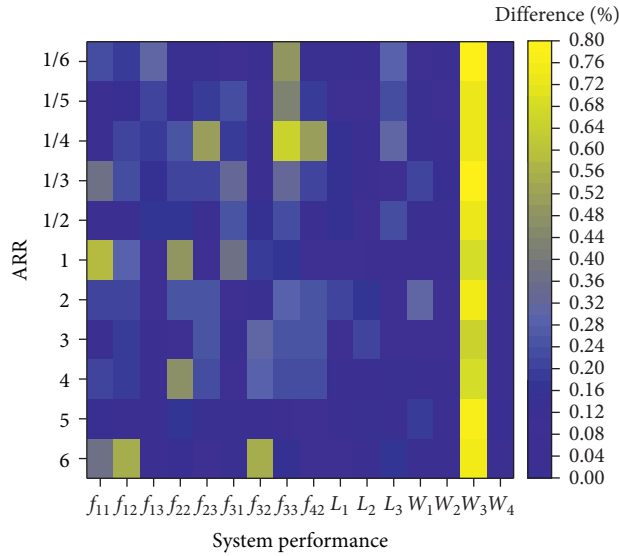


FIGURE 7: System performance difference under various ARR.

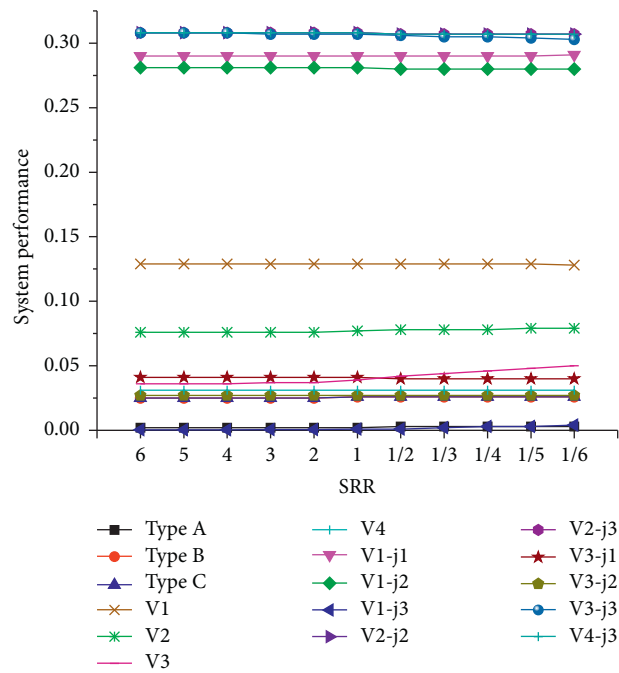


FIGURE 8: System performance under various SRR.

probabilities of Types 2 and 3 show the opposite trend. The centralization degree of vehicle workload probability has gradually strengthened. This is because a smaller ARR parameter leads to more frequent cooperation, promoting vehicles' full utilization.

Regarding dispatch frequency, the probabilities of V1 and V2 to j2 decrease, while the probabilities of V2, V3, and V4 to j3 increase. The dispatch probability of other cooperative vehicles has changed slightly. This shows that the dispatch probabilities of prior vehicles in cooperation are

very sensitive to ARR. Figure 7 illustrates the differences between the CHQ model and the Arena simulation software. The workload difference of V3 remains below 1%, although it is slightly larger than other system performance measures. The proposed model can accurately describe the system performance under a variety of ARR parameters.

4.2. Service Rate Value of Different Servers. The arrival rate of each type of call is assumed to be 0.1. We fix the values of μ_1

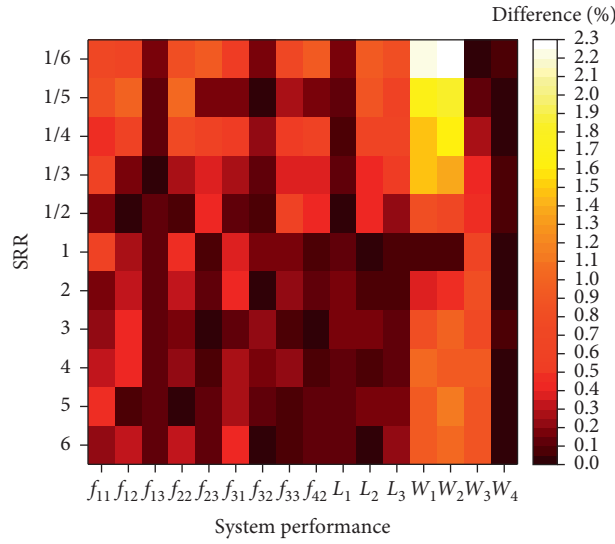


FIGURE 9: System performance difference under various SRR.

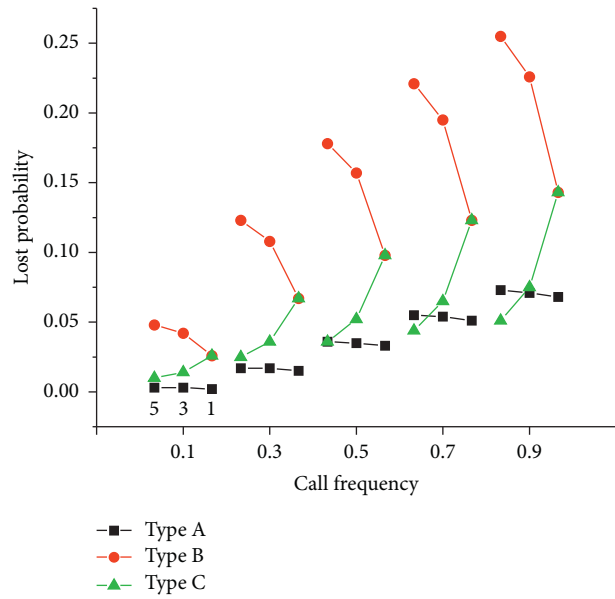


FIGURE 10: Lost probability performance under various call frequencies.

and μ_3 as 1 and assume that μ_2 is symmetric to μ_3 with respect to μ_1 (or μ_3). The ratio μ_2/μ_3 is defined as the service rate ratio (SRR) of necessary vehicles for cooperation responses (i.e., $\mu_1 = \mu_3 = 1$, $\mu_2 = 2(1 + (1/SRR))^{-1}$, and $\mu_3 = 2(1 + SRR)^{-1}$). System performances under different SRR (i.e., 1/6, 1/5, 1/4, 1/3, 1/2, 1, 2, 3, 4, 5, and 6) scenarios are calculated. Figure 8 shows that each system performance measures slight changes, and its sensitivity to SRR is relatively weak. Figure 9 illustrates the differences between the CHQ model and the Arena simulation software. When the SRR value is more considerable, the CHQ model can describe the system performance more accurately.

4.3. Relative Value of Demand/Service Rate. We set the value of λ_1 as 0.1, 0.3, 0.5, 0.7, and 0.9, respectively. For each value of λ_1 , the ARR with the values of 1, 3, and 5 are designed. Lost probability and workload performance under various call frequencies are shown in Figures 10 and 11, respectively. Figure 12 also illustrates the differences between the CHQ model and the Arena simulation software. Note that when the frequency of call increases (e.g., λ_1 is greater than 0.3), the CHQ model's accuracy gradually decreases. Especially when it equals 0.9, the workload difference of V3 can reach more than 10%. This shows that the CHQ model is suitable for cooperative emergency systems with low system

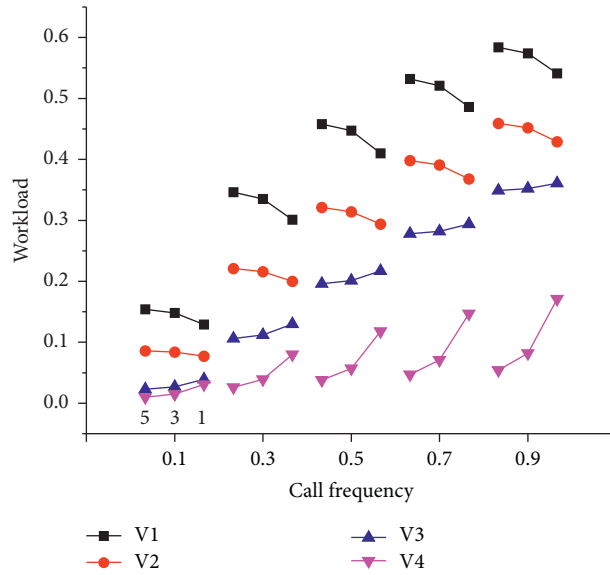


FIGURE 11: Workload performance under various call frequencies.

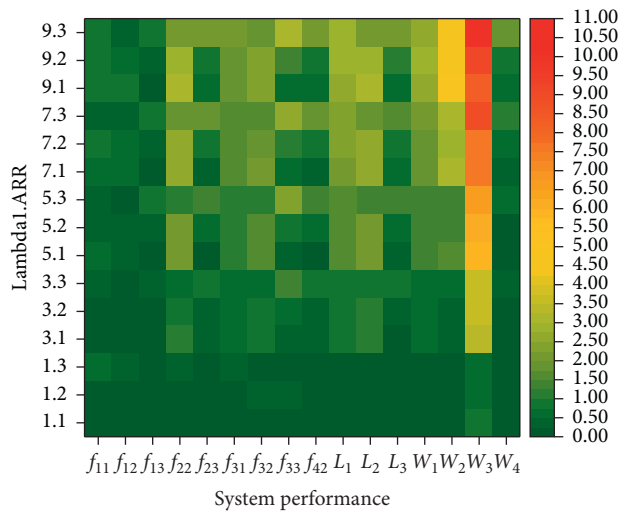


FIGURE 12: System performance difference under various call frequencies.

requirements or strong service capabilities. When the cooperative system’s saturation is large, the accuracy of CHQ’s description for cooperative vehicle workload may decrease.

5. Conclusions

Over the past few decades, the hypercube queuing model has been widely used in engineering practice because it can effectively describe the single-dispatch state of emergency response systems. However, for complex disasters that require cooperative service, the classic hypercube queuing model and its extensions may not provide accurate cooperation performance. To this end, we propose the cooperative hypercube queuing model by assuming that certain types of calls require cooperative service; cooperative servers can become free simultaneously from busy states. We test

the model in an empirical emergency system in which two ambulances, one police car, and one fire engine are combined as response candidates. The validation results by the Arena simulation software show that the CHQ model can accurately describe system performance in the case study. To further verify the potential of model application in general scenarios, we test the model’s accuracy under different ARR, SRR, and call frequency values. We find that ARR values have a significant impact on the dispatch frequency of priority vehicles, and its smaller value can promote the balanced use of vehicles. Compared with ARR, the value of SRR has a small effect on system performance. However, larger values of SRR help to improve the accuracy of the model description. The sensitivity analysis on the call frequency shows that the abrupt increase of call frequency may have a negative impact on the accuracy of the CHQ model.

Cooperative emergency systems with low demand or high service rates may be more suitable for applying the CHQ model. An interesting topic for future research would be the CHQ model calibration for an emergency system with frequent calls and limited-service abilities. Another exciting line of research would be to develop heuristic algorithms for large system applications of the CHQ model.

Data Availability

The data were obtained from AMap (<http://www.amap.com>).

Conflicts of Interest

The authors declare that they have no conflicts of interest.

Acknowledgments

The authors thank Professor Yanfeng Ouyang from the University of Illinois at Urbana-Champaign for his valuable support in this research. This work was supported by the National Key Research and Development Project of China (2019YFF0301300) and the National Natural Science Foundation of China (51828802).

References

- [1] Central People's Government of the People's Republic of China, "National public health emergency response plan," 2006, http://www.gov.cn/yjgl/2006-02/26/content_211654.htm.
- [2] J. Simons and N. Faour, "Mail online: exclusive: female firefighter dubbed "Bride of Beirut" is buried in emotional funeral as her heroic colleagues who broke into doomed warehouse as blaze took hold are named," 2020, <https://www.dailymail.co.uk/news/article-8599961/Hero-firefighters-trying-open-door-doomed-Beirut-warehouse-tragic-photo-named.html>.
- [3] A. Jacobs, "Fire ravages renowned building in Beijing," 2009, <https://www.nytimes.com/2009/02/10/world/asia/10beijing.html>.
- [4] European Centre for Disease Prevention and Control, "Increase in COVID-19 cases in many EU countries," 2020, <https://www.ecdc.europa.eu/en/covid-19-pandemic>.
- [5] Disease Control and Prevention (CDC), "CDC COVID data tracker," 2020, https://covid.cdc.gov/covid-data-tracker/#cases_casesper100klast7days.
- [6] U.S. Department Of Health and Human Services, *COVID-19 and HIPAA: Disclosures to Law Enforcement, Paramedics, Other First Responders and Public Health Authorities*, U.S. Department Of Health and Human Services, Washington, DC, USA, 2020, <https://www.hhs.gov/sites/default/files/covid-19-hipaa-and-first-responders-508.pdf>.
- [7] C. Toregas, R. Swain, C. ReVelle, and L. Bergman, "The location of emergency service facilities," *Operations Research*, vol. 19, no. 6, pp. 1363–1373, 1971.
- [8] R. Church and C. ReVelle, "The maximal covering location problem," *Papers of the Regional Science Association*, Springer, vol. 32, no. 1, pp. 101–118, Berlin, Germany, 1974.
- [9] V. Marianov and C. Revelle, "The queuing probabilistic location set covering problem and some extensions," *Socio-Economic Planning Sciences*, vol. 28, no. 3, pp. 167–178, 1994.
- [10] M. S. Daskin, "A maximum expected covering location model: formulation, properties and heuristic solution," *Transportation Science*, vol. 17, no. 1, pp. 48–70, 1983.
- [11] E. Erkut, A. Ingolfsson, and G. Erdoğan, "Ambulance location for maximum survival," *Naval Research Logistics (NRL)*, vol. 55, no. 1, pp. 42–58, 2008.
- [12] M. Gendreau, G. Laporte, and F. Semet, "The maximal expected coverage relocation problem for emergency vehicles," *Journal of the Operational Research Society*, vol. 57, no. 1, pp. 22–28, 2006.
- [13] Y. Wang, S. Peng, X. Zhou, M. Mahmoudi, and L. Zhen, "Green logistics location-routing problem with eco-packages," *Transportation Research Part E: Logistics and Transportation Review*, vol. 143, p. 102118, 2020.
- [14] Y. Wang, Y. Yuan, X. Guan et al., "Collaborative two-echelon multicenter vehicle routing optimization based on state-space-time network representation," *Journal of Cleaner Production*, vol. 258, p. 120590, 2020.
- [15] Y. Wang, X. Ma, Z. Li, Y. Liu, M. Xu, and Y. Wang, "Profit distribution in collaborative multiple centers vehicle routing problem," *Journal of Cleaner Production*, vol. 144, pp. 203–219, 2017.
- [16] Y. He, M. Qi, F. Zhou, and J. Su, "An effective metaheuristic for the last mile delivery with roaming delivery locations and stochastic travel times," *Computers & Industrial Engineering*, vol. 145, p. 106513, 2020.
- [17] J. Wang, H. Liu, S. An, and N. Cui, "A new partial coverage locating model for cooperative fire services," *Information Sciences*, vol. 373, pp. 527–538, 2016.
- [18] Y. Zhou, B. Zheng, B. Zheng, J. Su, and Y. Li, "The joint location-transportation model based on grey bi-level programming for early post-earthquake relief," *Journal of Industrial & Management Optimization*, vol. 13, no. 5, 2017.
- [19] R. C. Larson, "A hypercube queuing model for facility location and redistricting in urban emergency services," *Computers & Operations Research*, vol. 1, no. 1, pp. 67–95, 1974.
- [20] J. P. Jarvis, "Approximating the equilibrium behavior of multi-server loss systems," *Management Science*, vol. 31, no. 2, pp. 235–239, 1985.
- [21] K. R. Chelst and Z. Barlach, "Multiple unit dispatches in emergency services: models to estimate system performance," *Management Science*, vol. 27, no. 12, pp. 1390–1409, 1981.
- [22] L. F. Rodrigues, R. Morabito, F. Y. Chiyoshi, A. P. Iannoni, and C. Saydam, "Towards hypercube queuing models for dispatch policies with priority in queue and partial backup," *Computers & Operations Research*, vol. 84, pp. 92–105, 2017.
- [23] S. Ansari, S. Yoon, and L. A. Albert, "An approximate hypercube model for public service systems with co-located servers and multiple response," *Transportation Research Part E: Logistics and Transportation Review*, vol. 103, pp. 143–157, 2017.
- [24] F. Y. Chiyoshi and R. Morabito, "A Tabu search algorithm for solving the extended maximal availability location problem," *International Transactions in Operational Research*, vol. 18, no. 6, pp. 663–678, 2011.
- [25] A. P. Iannoni and R. Morabito, "A multiple dispatch and partial backup hypercube queuing model to analyze emergency medical systems on highways," *Transportation Research Part E: Logistics and Transportation Review*, vol. 43, no. 6, pp. 755–771, 2007.
- [26] Health Commission of Hubei Province, "Information released of COVID-19 in Hubei Province," 2020, <http://wjw.hubei.gov.cn/bmdt/ztl/fkxxgzbdgrfyyq/xxfb>.

Research Article

Research on Operation Characteristics and Safety Risk Forecast of Bus Driven by Multisource Forewarning Data

Shejun Deng , Hongru Yu , and Caoye Lu 

College of Civil Science and Engineering, Yangzhou University, YangZhou, JiangSu 225009, China

Correspondence should be addressed to Shejun Deng; yzrx6@163.com

Received 7 November 2020; Revised 2 December 2020; Accepted 8 December 2020; Published 18 December 2020

Academic Editor: Zheng Wang

Copyright © 2020 Shejun Deng et al. This is an open access article distributed under the Creative Commons Attribution License, which permits unrestricted use, distribution, and reproduction in any medium, provided the original work is properly cited.

To prevent and control public transport safety accidents in advance and guide the safety management and decision-making optimization of public transport vehicles, based on the forewarning and other multisource data of public transport vehicles in Zhenjiang, holographic portraits of public transport safety operation characteristics are constructed from the perspectives of time, space, and driver factors, and a prediction model of fatigue driving and driving risk of bus drivers based on BP neural network is constructed. Finally, model checking and virtual simulation experiments are carried out. The result of the research shows that the driver's fatigue risk during the period of 7:00-8:00 am is much higher than other periods. When the bus speed is about 30 km/h, the driver fatigue forewarning events occur the most. Drivers aged 30-34 years have the largest proportion of vehicle abnormal forewarning, drivers aged 40-44 years have the largest proportion of fatigue forewarning events, and drivers with a driving experience of 15-19 years have the largest overall proportion of various forewarning events. When the vehicle speed range is (18, 20) km/h and (42, 45) km/h, the probability of fatigue driving risk and driving risk forewarning increases sharply; and when the vehicle speed is lower than 17 km/h or 41 km/h, the probability of fatigue driving risk and driving risk forewarning, respectively, is almost zero. The probability of fatigue forewarning during low peak hours on rainy days is about 30% lower than that during peak hours. The probability of driving forewarning during flat peak hours is 15% higher than that during low peak hours and about 10% lower than that during peak hours. This paper realized for the first time the use of real forewarning data of buses in the full time, the whole region, and full cycle to carry out research. Related results have important theoretical value and practical significance for scientifically guiding the safety operation and emergency management strategies of buses, improving the service level of bus passenger transportation capacity and safety operation, and promoting the safety, health, and sustainable development of the public transportation industry.

1. Background Introduction

At present, China mainly evaluates the safety of buses based on the incidence of traffic accidents. The evaluation indicators and analysis methods are relatively single, and there is still a lack of accurate control, effective prevention, and emergency management countermeasures. Since 2019, with the integration and system development of BDS, video, radar, and other technologies, buses in some Chinese cities have installed vehicle driving safety forewarning systems, enabling holographic perception, dynamic monitoring, and risk reminders of the bus operation process [1]. By acquiring the historical data of vehicle forewarning of Zhenjiang Public Transport Company in Jiangsu Province of China,

this paper realized for the first time the use of real forewarning data of buses in the full time, the whole region, and full cycle to carry out research. This paper excavates the general rules and main hidden dangers of vehicle forewarning events and carries out objective analysis and situation prediction of bus operation risks [2]. Relevant research conclusions have important practical significance for improving the safe operation of buses, carrying out corresponding optimized dispatching [3] and emergency management, eliminating hidden dangers of bus operation, and improving and promoting the convenience, safety, and sustainable development of public transportation [4].

Many studies believe that the fatigued driver and driver driving state is the most important factor affecting urban

public transport safety, and the driver state is affected by the driver's attributes, external environment, and other aspects. Relevant scholars have researched related factors affecting the safe operation of buses, mainly as shown in Table 1. By studying the related factors that affect the severity of bus collisions [5], it can be seen that the factors such as start inhibition, automatic door opening, bus materials, and internal structure are relatively related to bus safety. Researches on perception and driving behavior [6] have shown that drivers who have experienced accidents are more likely to have collision accidents in the future. By studying the factors affecting road traffic accidents, it is known that the advanced driver assistance assessment system (ADAS) [7] can provide drivers with safety support and help avoid distractions. Besides, the vehicle anticollision forewarning strategy [8, 9] is formulated through the study of the driver's reaction time when a collision occurs. The Palm probability distribution method [10] is used to study road accident risk under different weather conditions. The research results show that the accident risk probability of snow is higher than that of rain. Among them, the greater the precipitation intensity, the higher the relative accident risk probability. Secondly, the logistic regression model [11] is used to study the correlation between the driver's age, gender, vehicle, road environment, and other factors and the severity of traffic accidents. The results show that the road infrastructure conditions and the driver's age have a significant impact on the severity of road traffic accidents. By using a logarithmic linear model [12] to study the impact of time factors on the severity of bus driver collision injuries, the results show that driving in the late night or early morning will increase the risk of serious injury to bus drivers.

Many scholars have researched vehicle safety characteristics and management requirements, mainly as follows. Firstly, utilizing the historical traffic data in the USA from 2005 to 2009, the potential risk factors of public transportation safety accidents are summarized [13], and it is found that the driver is the main factor in the occurrence of public transportation safety accidents. Studies have shown that as the driver's attention changes, there are significant differences in eye movement and gear operation [14]. At the same time, the characteristics of steering wheel operation and the characteristics of vehicle movement are also related to the characteristics of vehicle movement during lane changes [15]. Secondly, algorithms and models are used to analyze the causes and predictions of traffic accidents. By using the decision tree algorithm [16] to study the causes of vehicle collision accidents, the results show that human factors are the most important factor causing traffic accidents. According to the research results of the driver's steering characteristics, an evaluation model used to improve the steering stability of the car is established [17]. In [18], the backpropagation neural network model and generalized linear mixed model were used to analyze multi-source traffic data, which showed that flow plays an important role in vehicle collision prediction. Thirdly, a variety of models were built to better predict vehicle safety. A traffic accident model based on collaboration theory [19] was proposed to analyze accident scene data by combining

driving comfort thresholds. The dynamic prediction model of vehicle operation trajectory based on vehicle trajectory data [20] can calculate the suspicious collision position of the vehicle. The perceived safety of self-driving cars and their application value in transportation and road safety [21] were derived due to the analysis of the driving habits of 1,205 regular vehicle drivers. A hidden Markov model [22] is proposed by analyzing a large amount of traffic trajectory data, and it is verified that the model can better predict the occurrence of traffic conflicts.

Related scholars have also carried out many studies on the safe operation and management of buses. Firstly, preventive measures [23] are proposed through the identification and risk analysis of bus drivers' dangerous behaviors. Risk assessment and analysis of hazard sources of road traffic safety risks are carried out through the application of the road traffic safety risk index evaluation method [24], and a corresponding road traffic safety risk monitoring index system is constructed. Besides, aiming at the main problems of safety management, traffic safety management countermeasures [25] are proposed to reduce driver unsafe behavior, improve vehicle safety level, reduce the accident rate, and ensure the safe operation of buses. Secondly, the safety of the driver's visual perception of dangerous areas is proposed by analyzing the eye movement data of changing lanes, cornering driving, and straight driving [26]. An evaluation method based on the driver's visual perception of safety indicators is established. In [27], a psychological fatigue evaluation system for bus drivers was constructed, and the authors proposed targeted suggestions to reduce driving fatigue. A method [28] that can evaluate the driver's potential danger prediction ability and the rationality of the system was designed. In [29], a method to analyze the safety operation of buses was proposed based on big trajectory data. In particular, research on the clustering characteristics of road safety factors [30] such as driver, vehicle, road, and environment under different accident types was conducted. According to the actual situation of vehicle safety prediction, different research methods are proposed to make the prediction results more accurate. Thirdly, in the establishment of the bus speed model, parameters such as bus flow and bus ratio [31] were introduced, and a bus speed control system was designed, which realized the dynamic monitoring of the vehicle running speed. The driver evaluation system based on the principal component analysis method [32] was established through the analysis and investigation of the questionnaire information of bus drivers. The research results show that the driver's driving habits and individual characteristics have a significant impact on driving behavior. Finally, by introducing the practice of traffic congestion charging in Singapore and London [33], it is concluded that public transportation congestion charging should be based on scientific planning and supporting the sustainable development of public transportation. Besides, the analysis method and test method of the index system [34] are used to classify the sustainable development of urban transportation. The evaluation index system and evaluation model of urban transportation sustainable development based on the theory of urban transportation sustainable

TABLE 1: Study of the relevant factors affecting the safe operation of buses.

Author	Year	Research
Gibson and Lee	1986	Driver's reaction time when a collision occurs
Mercier et al.	1999	Correlation between the driver's age, gender, vehicle, road environment, and the severity of traffic accidents
Chen et al.	2000	Influence of time factors on the severity of collision injuries of bus drivers
Yang	2007	Perception and driving behavior
M. Staubach	2009	Factors affecting road traffic accidents
Cafiso	2013	Related factors affecting the severity of bus collisions
Park	2019	Road accident risk under different weather conditions

development are established. This research provides a new perspective on urban sustainable development research.

In summary, objective, real, comprehensive, and effective historical operation data are a prerequisite for the accurate study of bus safety operation situation and risk management. The existing research studies mainly use vehicle accident data, vehicle trajectory data, laboratory data, and questionnaire survey data to carry out related research on vehicle safety characteristics, dangerous driving behavior, or risk situation. Because of the contingency of vehicle accidents and the incompleteness of data collection, it is difficult to realize the comprehensive analysis of bus operation state and the accurate prediction of safety risks [35]. This paper will overcome the shortcomings of the existing research, make full use of the safety forewarning system installed on public vehicles, obtain the real mass historical data of all kinds of public transport forewarning, carry out model construction and simulation analysis, provide auxiliary decision-making for bus operation, dispatching, and safety management, and promote the healthy, green, and sustainable development of urban public transportation [36].

2. Data Acquisition Process

The bus forewarning system installed by Zhenjiang Public Transport Company integrates various technologies such as ADAS yaw forewarning [37], fatigue driving video analysis, and BDS terminal [38]. It can realize the real-time upload of vehicle operating data and ensure the accuracy and reliability of the data. The forewarning equipment is shown in Figure 1. This research makes full use of the vehicle forewarning equipment and vehicle forewarning data platform of Zhenjiang Public Transport Company to obtain historical operating data of the bus.

2.1. Forewarning Equipment

2.1.1. ADAS Vehicle Yaw Forewarning System. ADAS stands for the Advanced Driving Assistance System. The system uses a camera located on the windshield to monitor the lane markings on the road ahead. When the system detects that the vehicle has deviated from the lane [39], it will issue a forewarning to the driver.

2.1.2. Fatigue Driving Analysis Equipment. The fatigue driving analysis equipment uses advanced AI video analysis

technology [40] to accurately recognize the driver's facial characteristics. At the same time, it can record and warn the driver's fatigue characteristics.

2.1.3. BDS. The artificial satellite's multifrequency positioning signal can be accepted by the system to achieve precise positioning. The system can calculate the distance of the vehicle ahead, consider the relative speed of the vehicle, determine the possible collision time, and issue a forewarning to the driver.

2.2. Forewarning System and Data Platform. The forewarning system can realize real-time monitoring and summary of vehicle information [41], mainly including 7 forewarning types: eyes closed, yawn, glance about, lane departure, rapid acceleration, rapid deceleration, and forward collision. This paper classifies the types of forewarnings, classifies eyes closed, yawn, and glance as driver fatigue forewarnings, and classifies rapid acceleration, rapid deceleration, forward collision, and lane departure as vehicle abnormal state forewarnings, as shown in Figure 2.

Data platforms mainly include current online, forward forewarning, driver forewarning, the total number of abnormalities, vehicle distribution, forewarning type distribution, forewarning occurrence trend, and other data. This paper obtained 297,189 forewarning data from November 2019 to March 2020 through the forewarning platform system of Zhenjiang Public Transport Company. The original forewarning data mainly include information such as license plate number, forewarning time, forewarning type, forewarning level, forewarning speed, latitude and longitude coordinates of forewarning points, location of forewarning points, driver names, and other information.

2.3. Research Period and Weather Conditions. Since the system started trial operation at Zhenjiang Public Transport Company in October 2019, this paper selected a 27-day official operation period from November 2019 to March 2020 to conduct research, as shown in Table 2.

2.4. Data Cleaning. Since the actual data obtained may have data missing, disordered format, abnormal data, and other phenomena, cleaning the data is an indispensable link. The principle of data cleaning [42] should ensure the accuracy, completeness, consistency, uniqueness, timeliness, and

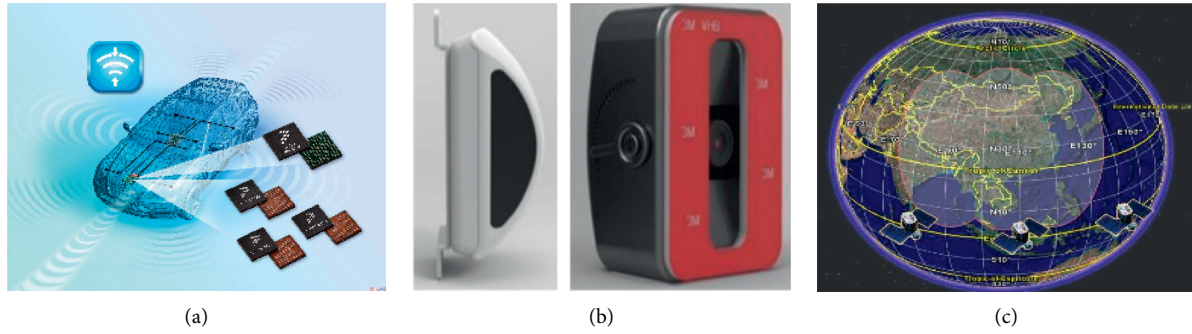


FIGURE 1: Forewarning equipment of buses: (a) ADAS yaw forewarning system; (b) fatigue driving analysis equipment; (c) BDS.

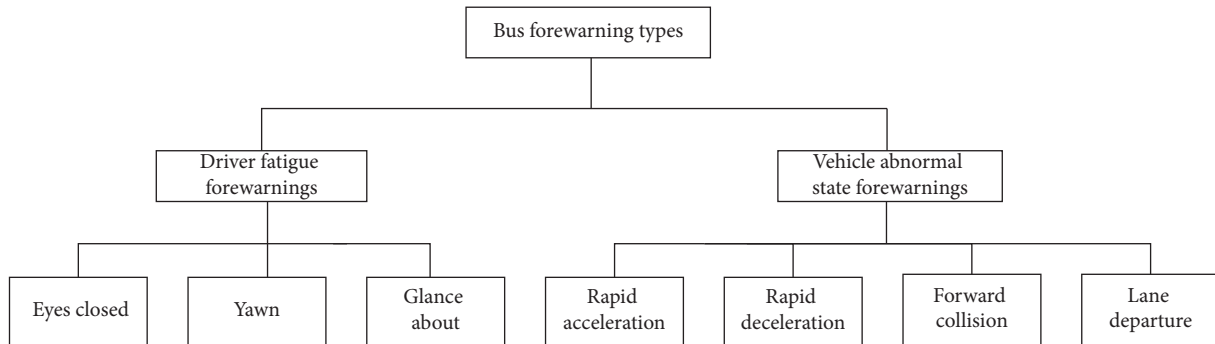


FIGURE 2: Classification of forewarning types.

TABLE 2: Weather and period of the retrieval date.

Date	Weather	Period
2019.11.01	Sunny	06:00–20:30
2019.11.02	Foggy	00:00–24:00
2019.12.01	Rainy	10:00–22:30
2019.12.02	Sunny	05:30–19:00
2019.12.04	Sunny	06:00–23:30
2019.12.05	Sunny	00:00–24:00
2019.12.06	Sunny	00:00–24:00
2019.12.07	Sunny	01:00–24:00
2019.12.15	Sunny	07:30–19:00
2019.12.16	Sunny	06:30–18:00
2019.12.17	Rainy	00:30–24:00
2019.12.18	Rainy	00:00–24:00
2019.12.20	Sunny	12:30–18:30
2019.12.21	Rainy	01:00–24:00
2020.01.01	Snowy	12:30–18:30
2020.01.02	Sunny	07:30–15:30
2020.01.03	Rainy	11:00–15:00
2020.01.04	Rainy	07:30–11:00
2020.01.06	Rainy	16:30–19:30
2020.01.07	Rainy	10:30–18:00
2020.01.08	Rainy	09:00–23:00
2020.01.09	Snowy	01:00–24:00
2020.01.10	Cloudy	00:00–24:00
2020.01.11	Rainy	12:30–19:00
2020.01.12	Rainy	08:30–23:30
2020.01.13	Foggy	00:00–24:00
2020.01.14	Foggy	00:00–24:00

effectiveness of data. There are mainly the following 4 methods [43]:

- (1) Supplement incomplete data
- (2) Detection and resolution of error values or abnormal values
- (3) Detection and elimination of duplicate records
- (4) Detection and resolution of data inconsistencies

The forewarning data set obtained and the driver information data set are associated and fused with the data table [44]. Finally, 297189 forewarning samples are associated with 1435 driver data samples. The research data samples after the fusion are shown in Table 3.

3. Analysis of the Bus Forewarning Characteristics from Multiple Perspectives

There are many factors related to the bus safe operation, and different factors have different effects on bus forewarning [45, 46]. To study the bus forewarning characteristics in different weather conditions, sections, driver characteristics, and periods, this paper makes a holographic portrait of the bus operation from multiple perspectives such as weather, time, space, speed, and driver characteristics distribution [47], as shown in Figure 3. Make full use of various multisource forewarning data to study the influence mechanism of various factors on bus forewarning.

TABLE 3: Data sample after cleaning.

Bus number	Time	Type	Longitude	Latitude	Route	Type number	Speed
18200148	5:38:33	Eyes closed	119.46	32.16	No. 81 bus	8	20
1709270416	8:18:53	Smoking	119.47	32.19	No. 35 bus	12	34
1709270762	8:19:54	Smoking	119.44	32.14	No. 95 bus	12	43
1709270416	8:21:29	Smoking	119.46	32.19	No. 35 bus	12	41
1709270041	8:21:58	Smoking	119.42	32.21	No. 23 bus	12	42
1709270762	8:22:11	Smoking	119.44	32.13	No. 95 bus	12	50

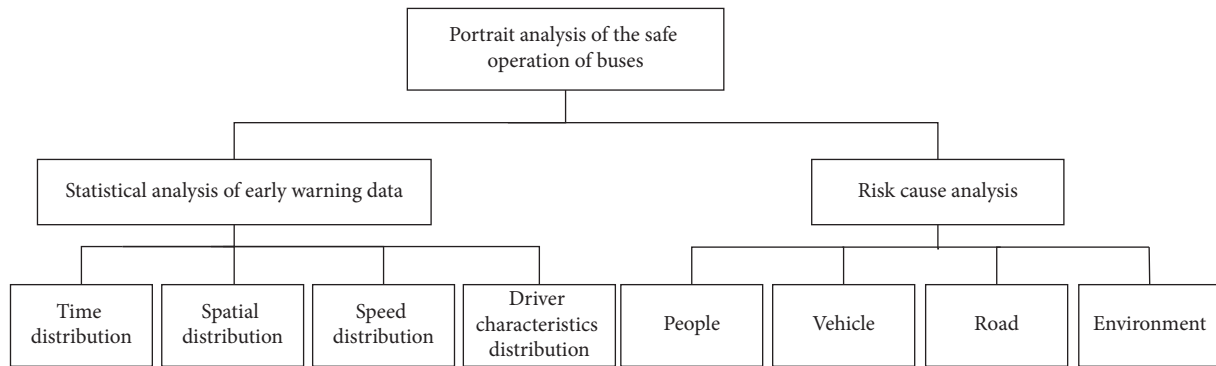


FIGURE 3: Portrait analysis of the safe operation of buses.

3.1. Weather Distribution. Vehicle operation safe is closely related to bad weather conditions [48]. This paper compares and analyzes the forewarning data of buses according to the four weather conditions of sunny, rain, fog, and snow. The results are shown in Table 4.

From the analysis of Figure 4, it can be seen that the proportion of forewarnings on sunny and foggy days is relatively large. The total proportion of forewarnings on sunny days reaches 31.29%. It is mainly due to the glare of the sun and dizziness. Drivers are easily sleepy and fatigued. The total proportion of forewarnings on foggy days reached 31.27%, mainly due to low air visibility, obstructed line of sight, and low road adhesion coefficient. Drivers need to maintain a high degree of attention for a long time and are prone to fatigue.

The vehicle's abnormal state forewarnings are greater than the number of driver fatigue forewarnings under all weather conditions. The vehicle's abnormal state forewarnings mainly refer to situations such as rapid acceleration, rapid deceleration, forward collision, and lane departure, which are not only closely related to the driver's bad driving behavior but also affected by road facilities, traffic environment, and other restrictive factors, resulting in a higher proportion.

3.2. Time Distribution. According to the forewarning data of buses, statistics are summarized by time, and the result is shown in Figure 5. Analysis shows the following:

- (1) Whether it is the forewarnings of driver fatigue state or the forewarnings of vehicle abnormal state, it shows a three-stage change rule of rising, local fluctuations, and falling over time.

- (2) The first stage is a rapid rise period. At this time, the driver fatigue forewarning period is [4:00, 7:00], and the vehicle abnormal state forewarning period is [4:00, 9:00], which is 2 hours longer than the fatigue forewarning, mainly due to complicated traffic environment and other factors restrict.
- (3) The second stage is a period of partial fluctuation. The driver fatigue forewarning and the vehicle abnormal state forewarning period are generally similar, within the range of [7:00, 19:00], and the vehicle abnormal state forewarning period is [9:00, 16:00].
- (4) The third stage is the partial descent period, and the overall is divided into 2 changes. During the period of [16:00, 20:00], the reduction range is relatively large; during the period of [20:00, 22:00], the range of change is relatively small.
- (5) The vehicle abnormal state forewarning is in [10:00, 11:00] and [16:00, 17:00] peaks, appearing in the two periods, and the driver fatigue forewarning is in the peak hours at [06:00, 09:00].

3.3. Spatial Distribution. The driver fatigue forewarning and vehicle abnormal state forewarning data are imported into the electronic map of Zhenjiang, and the locations corresponding to the relevant forewarning samples are all mapped to the map, as shown in Figure 6.

Using the kernel density analysis method [49], the density distribution corresponding to the driver fatigue forewarning is obtained. From Figure 7, the following holds:

- (1) The two forewarning types are generally consistent in the spatial distribution of urban road networks, but

TABLE 4: Distribution of bus forewarning types under different weather conditions.

Feature name	Feature coding	Total number		Driver fatigue		Vehicle abnormal state	
		Quantity	Percentage	Quantity	Percentage	Quantity	Percentage
Weather	Sunny	92994	31.29	40830	31.48	52164	31.14
	Rainy	85610	28.81	37852	29.19	47758	28.51
	Foggy	92936	31.27	40245	31.03	52691	31.46
	Snowy	25649	8.63	10766	8.3	14883	8.89

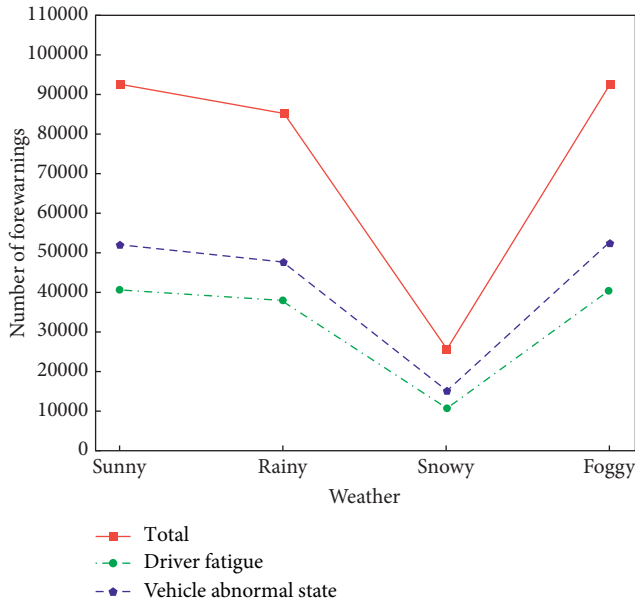


FIGURE 4: Distribution of forewarning types corresponding to different weathers.

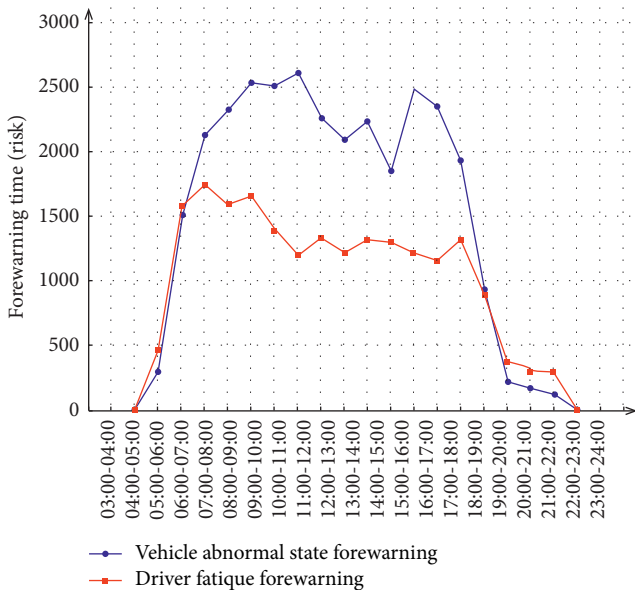


FIGURE 5: Time distribution characteristics of different forewarning types and number of buses.

there are large differences in local areas, as shown in Figure 7.

- (2) The driver fatigue forewarning density center is concentrated on Zhongshan Road (Jiuhuashan Road-Jiefang Road), as shown in Figure 7(a). Zhongshan Road is the main road of Zhenjiang, and most of it is commercial land nearby. This area has a high density of people and traffic, which can easily cause vehicle congestion. Drivers need to maintain a high degree of tension for a long time in this complex traffic environment. It is prone to fatigue characteristics.
- (3) The forewarning of vehicle abnormal state is mainly concentrated at the intersection of Dongwu Road and Mengxi Road, which is located in the Beigu Mountain Scenic Area, as shown in Figure 7(b). Beigu Mountain is an AAAAA-level tourist scenic spot in Zhenjiang, Jiangsu. The traffic volume of buses, private cars, tourist buses, and walking tourists is large, and the surrounding road network traffic congestion is serious. In this traffic environment, drivers are easy to make emergency operations and induce forewarning of abnormal vehicle status.

3.4. *Speed Distribution.* Select the period from December 2019 to January 2020 as the research period, analyze the corresponding vehicle speed when various forewarning events occur, obtain a total of 297189 data samples, and make summary statistics according to the speed, as shown in Table 5. Study the speed characteristic law under different forewarning types, as shown in Figure 8.

It can be seen from Figure 8 that as the speed increases, the number of driver fatigue forewarnings and the number of vehicle abnormal state forewarnings both fluctuate to a certain extent. The number of driver fatigue forewarnings reaches the peak at 30 km/h, and the number of driver forewarnings is less when the speed is less than 15 km/h or greater than 70 km/h. Since most buses operate in urban areas, the speed of running on urban roads is not high. When the speed of the vehicle is greater than 60 km/h, the number of driver fatigue forewarning and vehicle abnormal state forewarnings are kept at a low level. Both driver fatigue forewarning and vehicle abnormal state forewarnings have some abnormal values. The corresponding speed when the



FIGURE 6: Spatial distribution of forewarnings: (a) location of driver fatigue forewarning; (b) location of vehicle abnormal state forewarning.

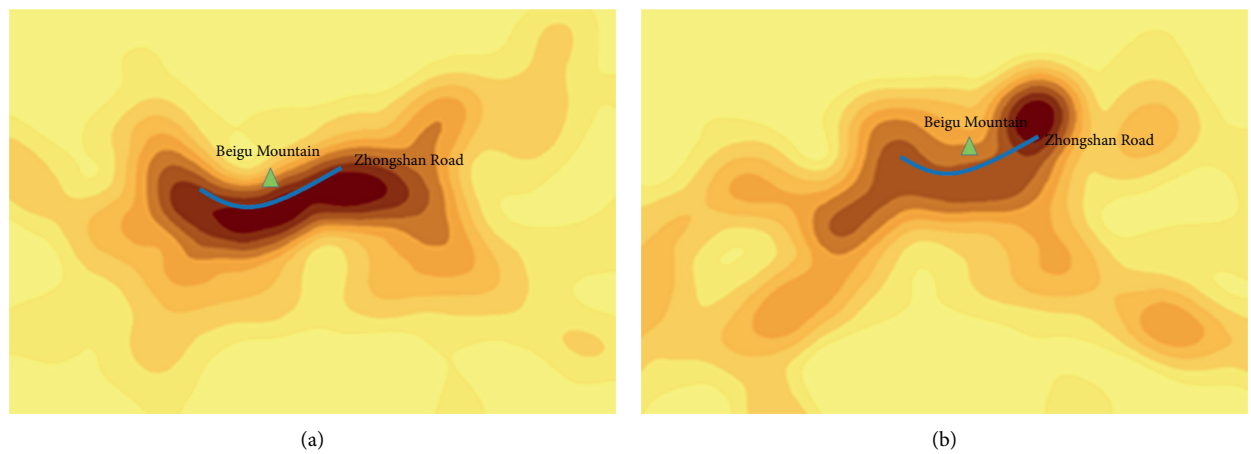


FIGURE 7: Comparative analysis of partial forewarning areas: (a) driver fatigue forewarning; (b) vehicle abnormal state forewarning.

TABLE 5: Distribution of bus forewarning types under different speed conditions.

Feature name	Feature coding	Total number		Driver fatigue		Vehicle abnormal state	
		Quantity	Percentage	Quantity	Percentage	Quantity	Percentage
Speed	Below 10 km/h	26225	8.82	7003	5.40	19222	12.96
	10–19 km/h	4307	1.45	511	0.39	3796	2.56
	20–29 km/h	46660	15.70	41571	32.05	5089	3.43
	30–39 km/h	124333	41.84	42301	32.62	82032	55.32
	40–49 km/h	65313	21.98	24469	18.87	40844	27.55
	50–59 km/h	23701	7.98	10172	7.84	13529	9.12
	60 km/h and above	6650	2.24	3666	2.83	2984	2.01

driver fatigue state forewarning occurs is generally greater than the speed when the vehicle abnormal state occurs.

To facilitate the analysis of the vehicle speed distribution characteristics under different forewarning density areas, this paper divides the forewarning occurrence areas into three types: low, medium, and high. The correlation analysis of the speed when the forewarning occurs in the three regions is carried out, and the characteristic law of the speed is studied, as shown in Figures 9 and 10.

It can be seen from Figure 9 that the low forewarning density area has the largest proportion when the speed is 30 km/h-39 km/h, and the smallest proportion when the speed is below 20 km/h. In areas with low forewarning

density such as suburban areas, there are fewer vehicles, smooth roads, and a small number of forewarnings. The number of forewarnings is the highest when the speed of buses reaches about 35 km/h. The medium forewarning density area has the largest proportion when the speed is 30 km/h-39 km/h, and the smallest proportion when the speed is above 60 km/h; the high forewarning density area has the largest proportion when the speed is 20 km/h-29 km/h, and the smallest proportion when the speed is above 60 km/h. In high forewarning density areas such as the city center, due to traffic congestion, the speed of buses is slow, and a large number of forewarnings are generated. The number of forewarnings reaches a peak when the speed is

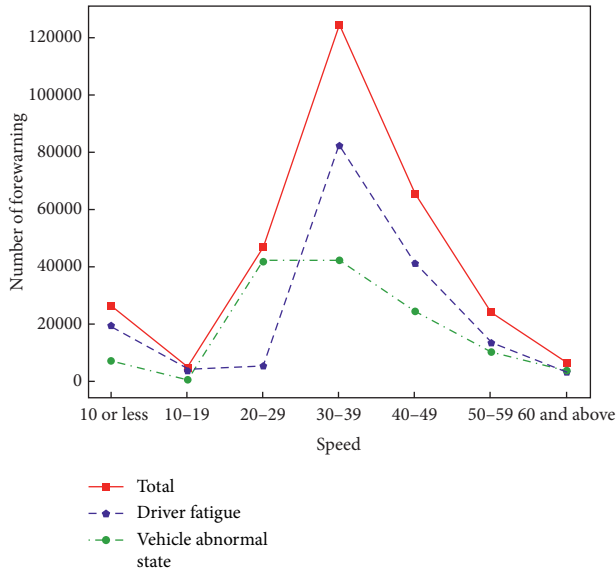


FIGURE 8: Distribution of forewarning types corresponding to different speeds.

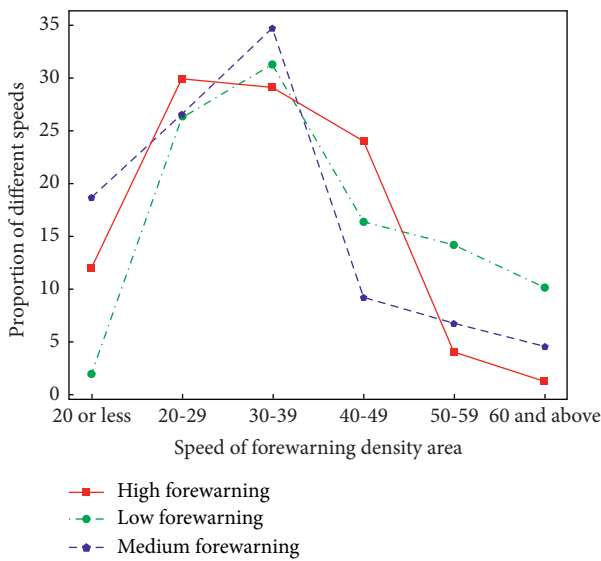


FIGURE 9: The proportion of different speeds in each forewarning density area.

about 25 km/h. Through observation and comparison, it can be seen that, due to different road congestion conditions, the speed of vehicles in high forewarning density areas is relatively low, and the speed of vehicles in low forewarning density areas is relatively high.

To be able to analyze the number of forewarnings that occur per unit area in each region more reasonably, this paper proposes the definition of unit forewarning density, that is,

$$\text{unit forewarning density} = \frac{\text{number of forewarnings}}{\text{forewarning area}} \quad (1)$$

It can be seen from the analysis of Figure 10 that the forewarning frequency of each speed in the low warning

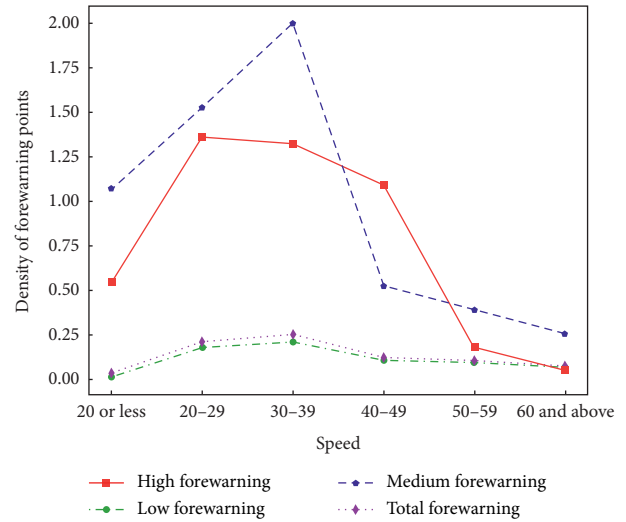


FIGURE 10: Density of forewarning points corresponding to different speeds in each forewarning density area.

density area is low. In the medium forewarning density area, the forewarning frequency reaches the peak when the speed is 30 km/h–39 km/h. In the high forewarning density area, when the speed is 20 km/h–29 km/h, the forewarning frequency is highest.

3.5. Driver Characteristics. This paper takes 324 drivers of Zhenjiang Public Transport Company as the research object, analyzes the influence of drivers’ age, driving years, gender, and educational background on the forewarning of buses [50], and conducts research on the distribution law of forewarning under the action of various factors.

3.5.1. Driving Years. The statistical analysis of the forewarning data of bus drivers of different driving years is shown in Table 6; in terms of the total number of forewarnings, drivers with driving experience between 15 and 19 years of the four driving years have the most forewarnings, accounting for about 35.66% of the total forewarnings, and; drivers with a driving experience of fewer than 5 years have the least number of forewarnings, accounting for about 0.68% of the total number of forewarnings.

As shown in Figure 11, drivers with a driving experience of 15 to 19 years have the largest number of driver fatigue forewarnings and vehicle abnormal state forewarnings. Drivers in this age group are more daring after having certain driving experience, have more aggressive driving styles, and are prone to aggressive operations, so they are more prone to forewarning of abnormal vehicle conditions.

3.5.2. Age. The statistical analysis of the forewarning data of bus drivers of different ages is shown in Table 7. In terms of the total number of forewarnings, drivers in the 40–44 age group of the eight age groups have the most forewarnings, accounting for about 23.13% of the total forewarnings. Drivers under the age of 25 have the least proportion, about 0.58%.

TABLE 6: Distribution of bus forewarning types for drivers of different driving years.

Feature name	Feature coding	Total number		Driver fatigue		Vehicle abnormal state	
		Quantity	Percentage	Quantity	Percentage	Quantity	Percentage
Driving years	Less than 5 years	2009	0.68	855	0.66	1154	0.69
	5–9 years	65889	22.17	26811	20.67	39078	23.33
	10–14 years	30452	10.25	13351	10.29	17101	10.21
	15–19 years	105964	35.66	46778	36.07	59186	35.34
	20–24 years	68677	23.11	31030	23.93	37647	22.48
	25–29 years	19281	6.49	8716	6.72	10565	6.31
	More than 30 years	4917	1.65	2152	1.66	2765	1.65

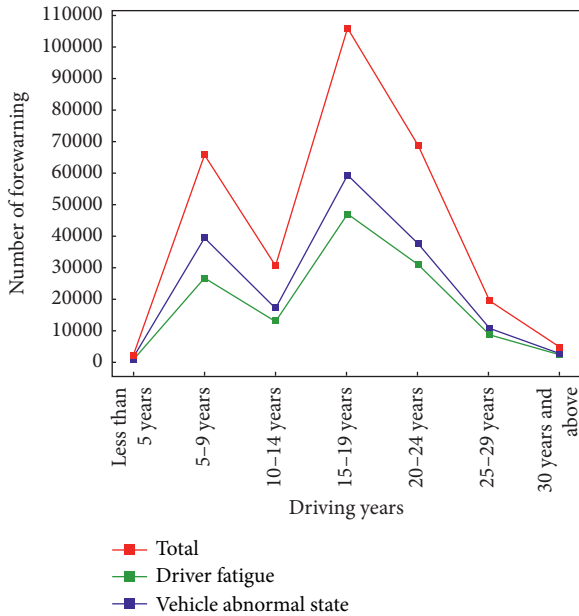


FIGURE 11: Distribution of forewarning types corresponding to drivers of different driving years.

As shown in Figure 12, from the perspective of different forewarning types, drivers in the 40–44 age group have the largest number of fatigue driving forewarnings, and drivers in the 30–34 age group have the largest number of vehicle abnormal state forewarnings. This is because 30–34 years old drivers have a more aggressive driving style, are more daring after having certain driving experience, and are easier to make aggressive operations. Drivers of different ages are generally more likely to have forewarnings of abnormal conditions than driver fatigue forewarnings. This is related to the fact that drivers are more aggressive in driving operations on the premise that they are safe.

3.5.3. Gender. Statistical analysis of the forewarning data of bus drivers of different genders is shown in Table 8; from the total number of forewarnings, male drivers have a much higher probability of having forewarnings than females. Among them, males account for approximately 91.44%, and the proportion of driver fatigue forewarning is about 91.26%, which has a certain relationship with the high proportion of male drivers in public transportation companies. As shown in Figure 13, comparing the number of warnings for male

and female drivers, it can be seen that the number of abnormal state forewarnings for drivers is higher than the number of fatigue forewarnings, while the numbers of fatigue forewarnings and abnormal state forewarnings for female drivers are very similar.

3.5.4. Degree. Statistical analysis of the forewarning data of bus drivers with different educational levels is shown in Table 9; drivers with junior high school and below have the most forewarnings, accounting for about 64.28% of the total number of forewarnings; drivers with high school education account for the least, about 12.98% of the total number of forewarnings. As shown in Figure 14, as the driver's educational background changes, the number of driver fatigue forewarnings and the number of vehicle abnormal state forewarnings show roughly the same changes.

4. Research on Risk Prediction of Public Transportation Safety Based on BP Neural Network Model

BP neural network is a concept proposed by Rumelhart and McClelland et al. It is a multilayer feedforward neural network with error backpropagation. The model has arbitrary complex pattern classification ability and excellent multibit function mapping ability and is suitable for complex nonlinear systems such as bus safety risk prediction.

4.1. Basic Principle

4.1.1. Structure of BP Neural Network. The topological structure of the BP neural network is shown in Figure 15, $\{x_1, x_2, \dots, x_n\}$ is the input vector of BP neural network, $\{y_1, y_2, \dots, y_n\}$ is the output vector of BP neural network, and w_{ij} and w_{jk} is the weight of BP neural network.

BP neural network can be regarded as a nonlinear function, and the network input value and predicted value are the independent variables and dependent variables of the function. When the number of input nodes is n and the number of output nodes is m , BP neural network expresses the functional mapping relationship from n independent variables to m dependent variables [51].

4.1.2. Error Backpropagation Algorithm. As a multilayer feedforward neural network, BP neural network is

TABLE 7: Distribution of forewarning types of buses for drivers of different ages.

Feature name	Feature coding	Total number		Driver fatigue		Vehicle abnormal state	
		Quantity	Percentage	Quantity	Percentage	Quantity	Percentage
Age	Less than 25 years	1726	0.58	822	0.63	904	0.54
	25–29-year-old	52493	17.66	21007	16.20	31486	18.80
	30–34-year-old	68495	23.05	26302	20.28	42193	25.19
	35–39-year-old	46036	15.49	22649	17.46	23387	13.96
	40–44-year-old	68730	23.13	31137	24.01	37593	22.44
	45–49-year-old	45843	15.43	21206	16.35	24637	14.71
	50–54-year-old	12107	4.07	5831	4.50	6276	3.75
	55-year-old and above	1759	0.59	739	0.57	1020	0.61

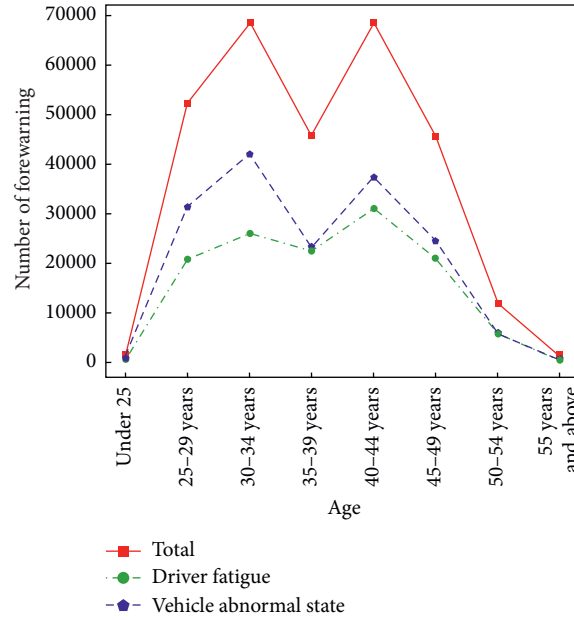


FIGURE 12: Distribution of forewarning types for drivers of different ages.

TABLE 8: Distribution of forewarning types of buses for drivers of different genders.

Feature name	Feature coding	Total number		Driver fatigue		Vehicle abnormal state	
		Quantity	Percentage	Quantity	Percentage	Quantity	Percentage
Gender	Male	271454	91.34	118594	91.44	152860	91.26
	Female	25735	8.66	11099	8.56	14636	8.74

characterized by signal forward transmission and error backpropagation. In forward transmission, the input signal is processed layer by layer from the input layer through the hidden layer until the output layer. The neuronal states of each layer only affect the next layer of the neuron state. If the output layer cannot get the expected output, it will switch to backpropagation and continuously adjust the network weights according to the prediction error so that the predicted value of the model will converge gradually. The error backpropagation algorithm of the BP neural network [52] can be expressed as follows:

$$\begin{aligned} \delta^L &= (t - y)f'(X^L - W^L), \\ \delta^l &= \delta^{l+1}(W^{l+1})^T f'(X^l W^l). \end{aligned} \quad (2)$$

In formula (2), δ^l is the learning signal of layer l , δ^L is the learning signal of the output layer, t is the label value, y is the predicted value, X^l is the output signal of layer l , X^L is the output signal of the penultimate layer, W^l is the weight vector between the layer l and $l + 1$, and W^L is the weight vector between the penultimate layer and the last layer.

The weight adjustment function of the BP neural network [53] is as follows:

$$\begin{aligned} \Delta W^L &= -\eta \frac{\partial E}{\partial W^L}, \\ \Delta W^l &= -\eta \frac{\partial E}{\partial W^l}. \end{aligned} \quad (3)$$

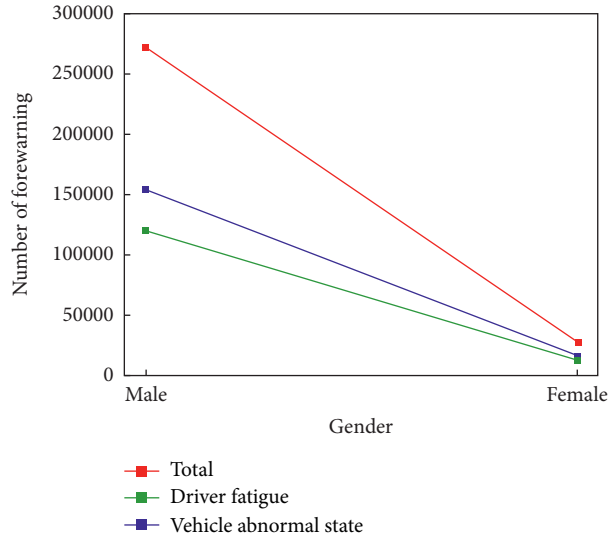


FIGURE 13: Distribution of forewarning types corresponding to drivers of different genders.

TABLE 9: Distribution of forewarning types of buses for drivers with different degree.

Feature name	Feature coding	Total number		Driver fatigue		Vehicle abnormal state	
		Quantity	Percentage	Quantity	Percentage	Quantity	Percentage
Education	Junior high school and below	191030	64.28	84208	64.93	106822	63.78
	High school diploma	67590	12.98	28030	21.61	39560	23.62
	University degree	38569	22.74	17455	13.46	21114	12.61

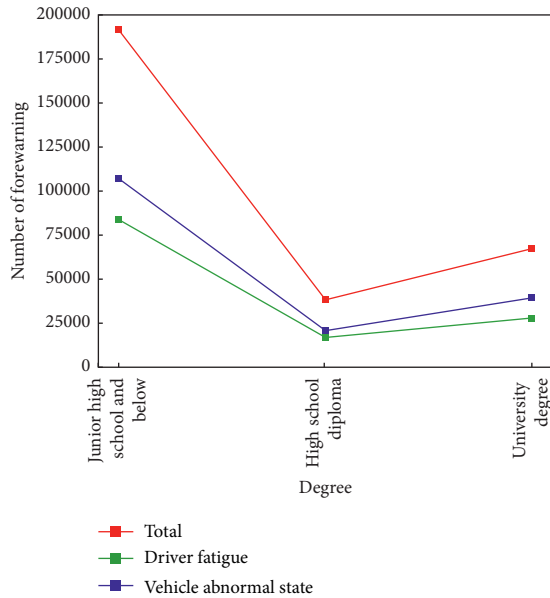


FIGURE 14: Distribution of forewarning types for drivers with different degrees.

In formula (3), ΔW^L is the adjustment value of the weight vector between the penultimate layer and the last layer of the BP neural network, ΔW^l is the adjusted value of the weight vector between the layer l and $l+1$, η is the learning rate, and E is the cost function.

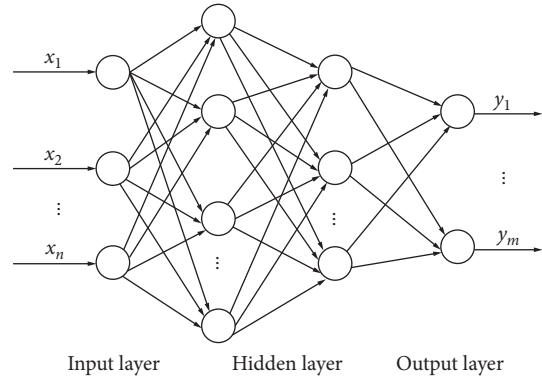


FIGURE 15: Topological structure diagram of BP neural network.

4.2. Model Building

4.2.1. *Establish a Network Structure.* Determining the network structure is an important part of constructing a BP neural network, which directly determines the training speed and prediction accuracy of the model. Generally speaking, the more hidden layers and nodes in the network topology structure, the stronger the generalization ability of the model, and the higher the accuracy of the model. However, the excessively complex network will lead to a slow training rate of the model and the more prone to overfitting; too simple network topology will make it difficult to establish a complex mapping relationship between feature variables and predictions, and it is difficult to achieve good

prediction results. Based on experience and repeated attempts, this paper confirms that the prediction results are good with the double hidden layer structure with node number of 100 and 50, respectively [54].

4.2.2. Selection of Learning Rate. The learning rate is an important parameter in the process of model optimization, which determines the speed of model learning and the convergence effect of the model. Too much learning rate will cause the model accuracy to oscillate and be difficult to converge. Too small learning rate will lead to slow model adjustment. In this paper, 0.01 is selected as the learning rate of the model. At this time, the model converges faster and the oscillation amplitude is smaller [55].

4.2.3. Activation Function Selection. The activation function in the BP neural network can increase the nonlinearity of the neural network so that the model has sufficient complex function mapping capabilities, and the applicability of different activation functions is also different [56].

(1) *tanh Function.* In this paper, the \tanh function is selected as the transfer function of the model. The \tanh function is the hyperbolic tangent function. It can maintain the non-linear monotonic rise and fall relationship on the output and input, which conforms to the gradient solution requirements of the BP network and has good fault tolerance and bounds. Besides, compared with the sigmoid activation function, \tanh function alleviates the problem of gradient disappearance to a certain extent, and its formula is as follows:

$$\tan h(x) = \frac{e^x - e^{-x}}{e^x + e^{-x}} \quad (4)$$

In formula (4), $\tan h(x)$ is the function value of the hyperbolic tangent function, x is the input variable, and e is the natural constant.

(2) *Softmax Function.* In this paper, the softmax function is selected as the classifier of the model output. The softmax function is the normalized exponential function, which can normalize the gradient logarithm of the finite item discrete probability distribution. Its characteristic is to normalize the vector, highlight the maximum value, suppress other components far below the maximum value, and visually show that the sample is a certain type of confidence; the formula is as follows [57]:

$$\text{softmax}(X)_i = \frac{e^{x_i}}{\sum_{j=1}^n e^{x_j}}, \quad j = 1, 2, \dots, n. \quad (5)$$

In formula (5), X is the input vector; $\text{softmax}(X)_i$ is the i -th function value of the vector softmax function for the vector X ; x_i and x_j are the i and j values of the vector X , respectively; n the length of vector X ; and the meaning of e is the same as above.

4.2.4. Cost Function Selection. The cost function is mainly divided into two types: quadratic cost function and cross-entropy cost function [58]. The quadratic cost function is

mainly used for regression problems. For the classification problems mentioned in this paper, the cross-entropy cost function is generally selected (labels are processed by one-hot encoding), and the formula is as follows:

$$E = -t(t \ln y + (1-t)\ln(1-y)). \quad (6)$$

In formula (6), E is the cost function value, t is the true label value, and y is the predicted value of the model.

Besides, the cross-entropy cost function also avoids the quadratic cost function: when the error is larger, the gradient of the activation function is smaller, resulting in slow convergence.

4.2.5. Data Preprocessing

(1) *Normalization.* To reduce the influence of the initialization value and accelerate the convergence speed of the BP neural network, the normalized preprocessing method can be generally adopted. In this paper, the maximum-minimum method is used to normalize the continuous characteristic variables [59], and the formula is as follows:

$$x_k = \frac{x_k - x_{\min}}{x_{\max} - x_{\min}} \quad (7)$$

In formula (7), x_{\min} is the minimum value of the feature in all samples, x_{\max} is the maximum value of the feature in all samples, and x_k is the eigenvalue after normalization.

(2) *One-Hot Encoding.* To digitize classification and discrete variables into the model, it is necessary to map such features to Euclidean space. One-hot encoding is one of the most effective ways to achieve this function. One-hot encoding is also known as one-bit effective encoding and uses multibit status registers to encode multiple states: for a feature, if it has m values, it becomes m binary features after one-hot encoding.

4.3. Construction and Application of the Prediction Model.

According to the BP neural network model constructed in Section 4.2, 13 features such as weather conditions, driver data, driving period, and driving speed are taken as the input of the model, and the alarm of the driver is taken as the output of the model. The network topology structure of "13-100-50-2" is adopted, and the \tanh function and softmax function are used as the transfer function and activation function of the model, respectively. The cross-entropy cost function is selected as the cost function of the model, and after repeated attempts, the learning rate of the model is 0.01, which ensures the stable convergence of the model. The specific form of the model is shown in Figure 16 [60].

4.3.1. Fatigue Driving Prediction Model

(1) *Investigation of Convergence and Dispersion.* Randomly select 2/3 of the samples as the training set and the remaining 1/3 as the test set. Perform 500 cycles of iterative training on

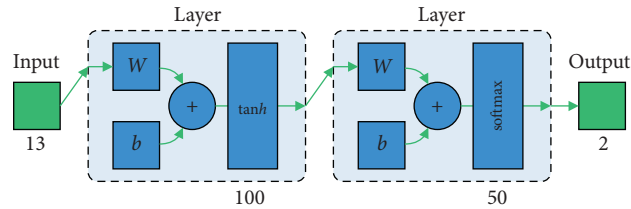


FIGURE 16: Safety state of buses model based on BP neural network.

the BP neural network. The learning curve of the fatigue driving prediction model is shown in Figure 17 [61].

As shown in Figure 17, the analysis shows the following: the fatigue driving prediction model has good convergence, and the learning curve tends to be flat around the 100th training cycle; during the whole 500-cycle iteration process, there was no large-scale oscillation and the fluctuation amplitude gradually decreased with the training cycle; the model performs well on the test set and can still reach an accuracy of 79% based on using a large number of static features; the model has no obvious overfitting in the training process, and there is only a 0.0034 accuracy difference between the set and the test set.

(2) *Sample Inspection*. Since the sample label adopts the form of one-hot encoding, with position 0 representing forewarning and position 1 representing no forewarning. Therefore, a single sample error can be obtained by randomly selecting the predicted value of the model with 200 samples and subtracting the true value, as shown in Figure 18.

It can be seen from Figure 18 that among the randomly selected prediction samples, the number of samples with correct forewarning accounts for 79%, 18% of the false positives are forewarnings, and only 3% of the samples are falsely reported as no forewarnings, which shows that the whole model is partial to safety and has high prediction accuracy under the application of state prediction.

4.3.2. Driving Risk Prediction Model

(1) *Investigation of Convergence and Dispersion*. Similar to the fatigue driving prediction model, 2/3 of the samples are randomly selected as the training set, and the remaining 1/3 are used as the test set. The BP neural network is trained iteratively for 300 cycles. The learning curve of the driving risk prediction model is shown in Figure 19.

From Figure 19, the following is obtained: the driving risk prediction model has good convergence. The learning curve tends to be flat around the 120th training cycle, but it fluctuates greatly from the 170th to the 210th cycle, which may be caused by the transformation of the model from the local optimal solution to the global optimal solution; The model reaches the highest state after 300 cycles of the iterative process, and the convergence speed was faster than that of fatigue driving risk forewarning model. The model is slightly weaker than the previous model in the test set, but it can still achieve a higher accuracy rate of 78%. The model has

no overfitting phenomenon in the training process, and the performance of the model in the test set is even better than that in the training set.

(2) *Sample Inspection*. Randomly select the predicted value of 200 samples from the model, and subtract the true value from it to get a single sample error, as shown in Figure 20.

As can be seen from Figure 20, among the randomly selected prediction samples, the number of samples with correct forewarning accounts for 78%, 14.5% of the false positives are forewarnings, and 7.5% of the samples are falsely reported as no forewarnings. The model is generally safe and has high prediction accuracy.

4.4. Research on Simulation of Risk Probability Prediction Based on the BP Model

4.4.1. *Typical Driver Selection*. This paper conducts a statistical analysis of 1565 drivers of the Zhenjiang Public Transport Company. For continuous features such as driving age and age, the mean value (16, 39) is used as the feature value of the virtual driver; for the classification features such as educational background and gender, the mode (high school, male) is taken as the characteristic value of typical drivers. An example of normalized virtual driver sample data is shown in Table 10.

4.4.2. *Risk Probability Analysis during Peak Hours*. The fatigue driving prediction model constructed in this paper is used to calculate the fatigue confidence of the virtual driver's sample data under different weather, periods, and speeds. The simulation results are shown in Figure 21.

It can be seen from the graph analysis that whether it is fatigue driving forewarning or driving risk forewarning, the probability of occurrence is positively increasing with the driving speed value; when the vehicle speed range is (18, 20) km/h and (42, 45) km/h, the probability of fatigue driving risk forewarning and driving risk forewarning, respectively, raises sharply; when the vehicle speed is lower than 17 km/h or 41 km/h, the probability of fatigue driving risk forewarning and driving risk forewarning, respectively, occurring is almost zero; under the same speed conditions, the probability of fatigue forewarning in snowy days is greater than that of foggy days, rainy days, and sunny days and the probability of driving forewarning in foggy days is greater than that of snowy days, rainy days, and sunny days.



FIGURE 17: Learning curve of fatigue driving prediction model.

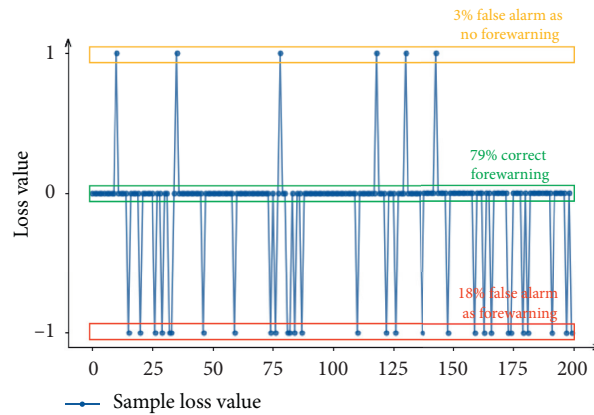


FIGURE 18: Analysis diagram of sample loss value of fatigue forewarning prediction model.

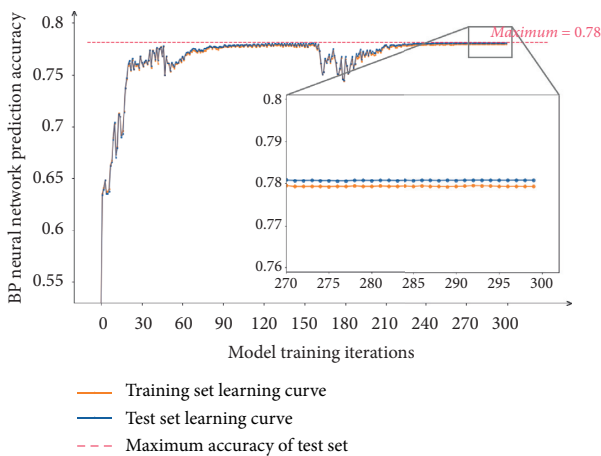


FIGURE 19: The learning curve of driving risk prediction model.

4.4.3. Risk Probability Analysis during Low Peak Hours. According to Figure 22, based on different speed conditions, the change characteristics of fatigue driving risk forewarning

and driving risk forewarning probability are generally consistent with those in peak hours, indicating that high attention should still be paid to safe driving of vehicles in low peak hours; under the same speed conditions, the probability of fatigue forewarning in rainy days is about 30% lower than that in peak hours, and the difference in other weather conditions is small.

4.4.4. Risk Probability Analysis during Flat Peak Hours. According to the analysis in Figure 23, the change characteristics of fatigue driving risk forewarning and driving risk forewarning probability are generally consistent with peak hours and flat peak hours; under the same speed conditions, the probability of driving forewarning in four weather conditions is 15% higher than that in low peak hours and 10% lower than that in peak hours; at the same driving speed, the sequence of driving risk probability is foggy, snowy, rainy, sunny, and speed, indicating that driving risk is significantly related to weather conditions.

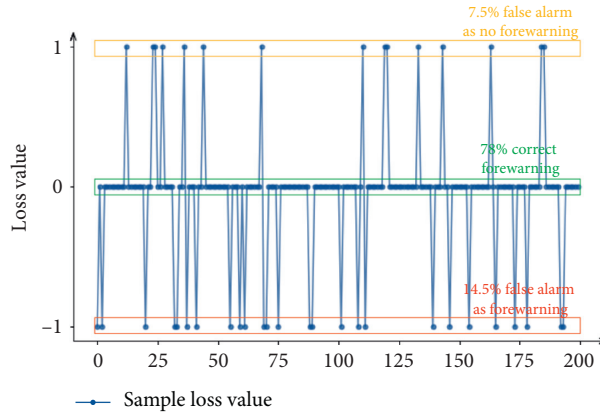
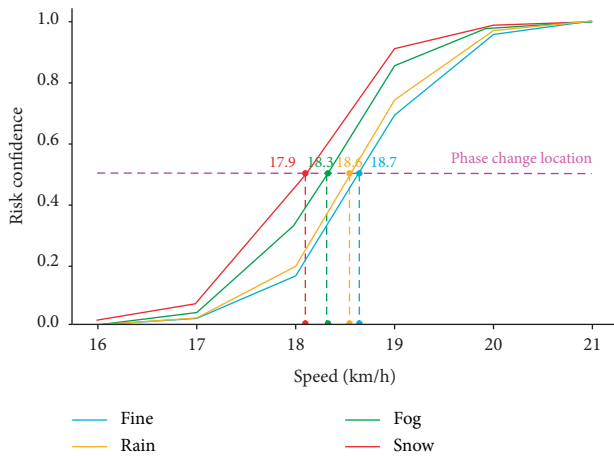


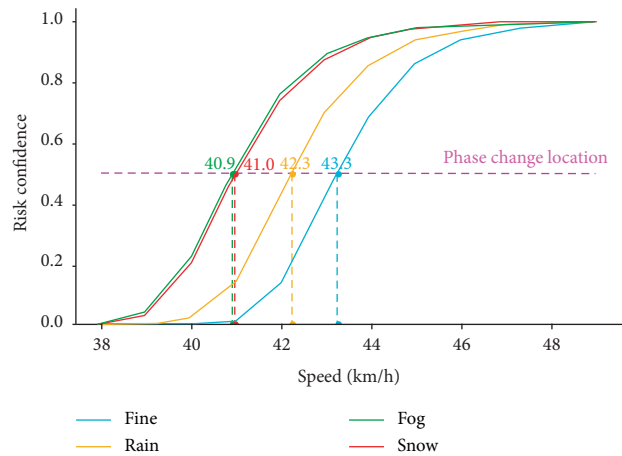
FIGURE 20: Analysis diagram of sample loss value of driving risk prediction model.

TABLE 10: Samples of typical drivers (partial).

	Fine	Rain	Fog	Snow	PeakT	FlatT	LowT	Male	Female	Age	DrivingY	Edu	Speed
0	1	0	0	0	1	0	0	1	0	0.66	0.47	0.67	0.0051
1	1	0	0	0	1	0	0	1	0	0.66	0.47	0.67	0.0102
2	1	0	0	0	1	0	0	1	0	0.66	0.47	0.67	0.0152
80	1	0	0	0	0	1	0	1	0	0.66	0.47	0.67	0.0051
81	1	0	0	0	0	1	0	1	0	0.66	0.47	0.67	0.0102
160	1	0	0	0	0	0	1	1	0	0.66	0.47	0.67	0.0051
161	1	0	0	0	0	0	1	1	0	0.66	0.47	0.67	0.0102
240	0	1	0	0	1	0	0	1	0	0.66	0.47	0.67	0.0051
241	0	1	0	0	1	0	0	1	0	0.66	0.47	0.67	0.0102
242	0	1	0	0	1	0	0	1	0	0.66	0.47	0.67	0.0152
480	0	0	1	0	1	0	0	1	0	0.66	0.47	0.67	0.0051
481	0	0	1	0	1	0	0	1	0	0.66	0.47	0.67	0.0102
482	0	0	1	0	1	0	0	1	0	0.66	0.47	0.67	0.0152



(a)



(b)

FIGURE 21: (a) Comparison of fatigue driving risk. (b) Comparison of driving risk probability under different weather conditions.

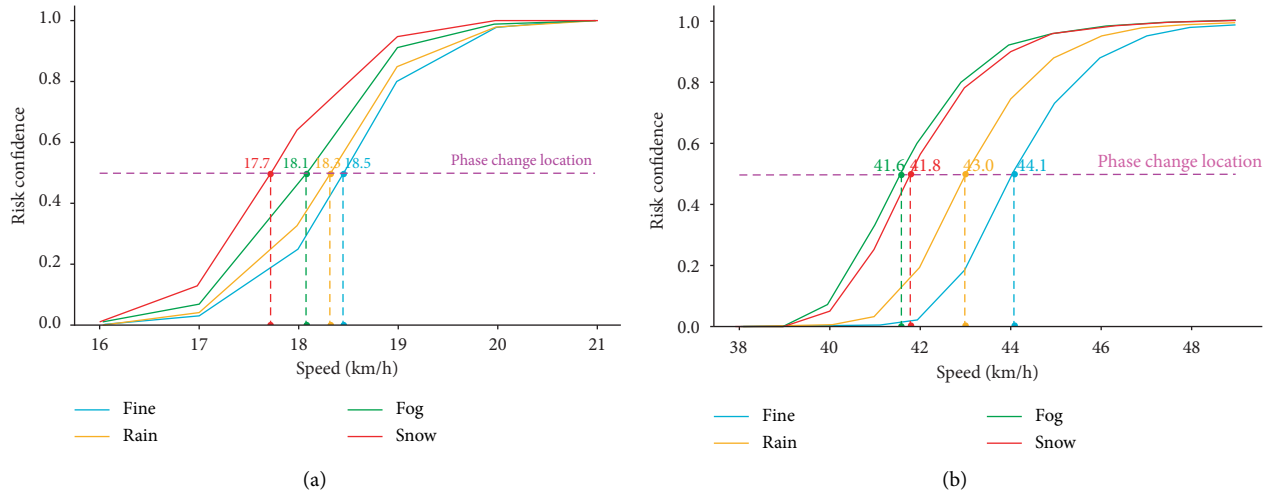


FIGURE 22: (a) Comparison of fatigue driving risk. (b) Comparison of driving risk probability under different weather conditions.

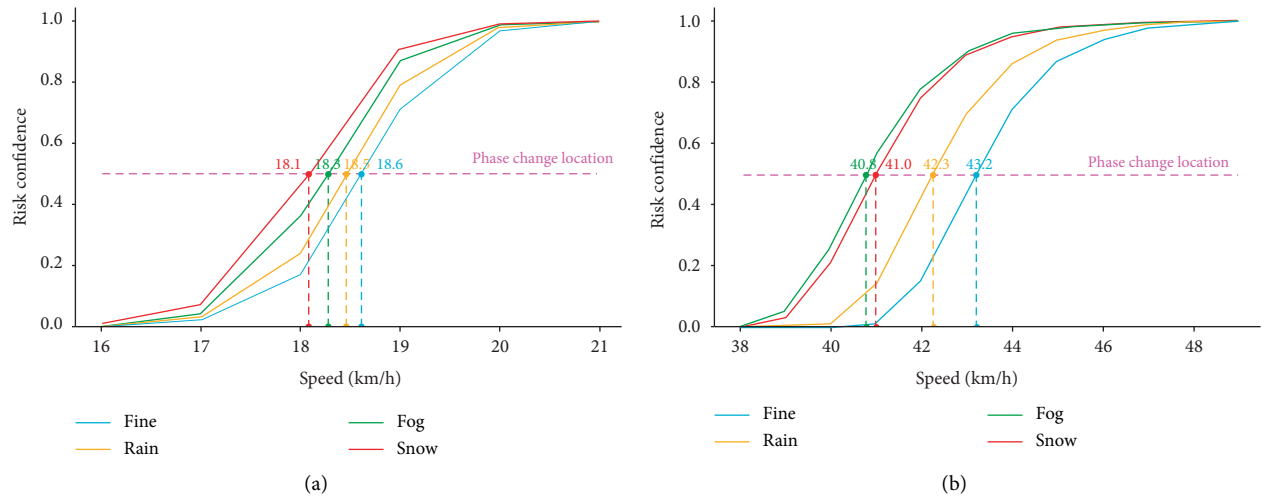


FIGURE 23: (a) Comparison of fatigue driving risk. (b) Comparison of driving risk probability under different weather conditions.

5. Conclusions

5.1. Research Result. This paper selects 297189 various types of forewarning data of Zhenjiang buses to carry out the analysis of hidden risks and characteristic laws. The distribution characteristics of bus forewarnings of different weather conditions, speeds, periods, spaces, and driver characteristics are studied. We get the following conclusions: firstly, on sunny days from 7:00–8:00 am in the morning, the probability of driver fatigue forewarning is greatest. On foggy days from 11:00 am–12:00 noon, the probability of vehicle abnormal state forewarning is the greatest. Secondly, when the vehicle is running at 30 km/h, the proportion of driver fatigue forewarning is the largest. Urban core areas are prone to trigger forewarning of driver fatigue, while tourist attractions are prone to trigger vehicle abnormal forewarning. Finally, drivers with 15–19 years of driving experience have the largest proportion of fatigue forewarnings and vehicle abnormal forewarnings. Drivers aged 40–44 years have the largest proportion of fatigue forewarnings. Drivers aged 30–34 years have the largest proportion of

vehicle abnormal forewarnings; male drivers have the largest proportion of fatigue forewarnings and vehicle abnormal forewarnings.

The fatigue driving and driving risk prediction model based on BP neural network are constructed, and simulation analysis is performed. The results show that, at the same driving speed, the sequence of occurrence of driving risk probability is foggy, snowy, rainy, and sunny days. During peak hours, the probability of fatigue forewarning in snowy days is greater than that of foggy, rainy, and sunny days; the probability of driving forewarning in foggy days is greater than that of snowy, rainy, and sunny days. When the vehicle speed range is (18, 20) km/h and (42, 45) km/h, the probability of fatigue driving risk and driving risk forewarning increases sharply; when the vehicle speed is lower than 17 km/h or 41 km/h, the probability of fatigue driving risk and driving risk forewarning, respectively, is almost zero. The probability of fatigue forewarning during low peak hours on rainy days is about 30% lower than that during peak hours. The probability of driving forewarning during

flat peak hours is 15% higher than that during low peak hours and about 10% lower than that during peak hours.

5.2. Practical Implications. The relevant research conclusions of this paper are of great practical significance for improving the passenger transportation capacity of buses and enhancing the management level. At the same time, it can improve the auxiliary decision-making for the safe operation and emergency management of buses, promoting the sustainable and healthy development of urban public transport safety.

5.3. Limitation and Future Research Scope. This study was not free from limitations. Firstly, we selected 297189 samples from November 2019 to March 2020 with a total of 27 days, and the sample size is relatively small. Secondly, when studying the forewarning characteristics of different gender bus drivers, male drivers accounted for a larger proportion of the selected 324 drivers. Therefore, the conclusion that male drivers have a much higher forewarning rate than female drivers needs further verification. Finally, public transportation safety risk probability prediction is multifactor. Currently, it is only based on the actual data obtained by the forewarning equipment to predict.

Although the constructed model has certain accuracy, more influencing factors such as the type of road facilities, road traffic conditions, and types of bus stations need to be fully considered in the follow-up research.

Although the sample size is insufficient and there are some of the above shortcomings in the research, this paper realizes for the first time the use of real forewarning data of buses in the full time, the whole region, and full cycle to carry out research and the use of real data for objective evaluation, which is representative and innovative.

Data Availability

The data used to support the findings of this study are included within the article.

Conflicts of Interest

The authors declare that there are no conflicts of interest.

Authors' Contributions

S. D. and H. Y. conceptualized the study and prepared methodology. C. L. and H. Y. analyzed using software and investigated and visualized the study. S. D., C. L., and H. Y. validated the study. C. L. and S. D. performed data curation and wrote the original draft. S. D. supervised the study, administrated the project, did formal analysis, managed resources, obtained funding acquisition, and reviewed and edited the article.

Acknowledgments

This study was supported by the Research planning fund for humanities and social sciences of the Ministry of Education

(19YJAZH011), support for the Open Project of Key Laboratory of Intelligent Traffic Technology and Traffic Industry (F262019016), Science and Technology Project of Traffic Department of Jiangsu Provincial Department of Communications (KY2018049), and Jiangsu Provincial Department of Science and Technology industry-university-research cooperation project "Traffic safety-oriented intelligent supervision and decision support system platform research and development" (BY2019263).

References

- [1] J. Tang, J. Liang, C. Han, Z. Li, and H. Huang, "Crash injury severity analysis using a two-layer stacking framework," *Accident Analysis and Prevention*, vol. 122, pp. 226–238, 2019.
- [2] J. Tang, L. Zheng, C. Han et al., "Statistical and machine-learning methods for clearance time prediction of road incidents: a methodology review," *Analytic Methods in Accident Research*, vol. 27, pp. 1–16, Article ID 100123, 2020.
- [3] Y. Wang, X. Ma, Z. Li, Y. Liu, M. Xu, and Y. Wang, "Profit distribution in collaborative multiple centers vehicle routing problem," *Journal of Cleaner Production*, vol. 144, pp. 203–219, 2017.
- [4] Y. Yan, Y. Zhang, X. Yang, J. Hu, J. Tang, and Z. Guo, "Crash prediction based on random effect negative binomial model considering data heterogeneity," *Physica A*, vol. 547, pp. 1–12, Article ID 123858, 2020.
- [5] C. Salvatore, D. G. Alessandro, and P. Giuseppina, "Road safety issues for bus transport management," *Accident Analysis and Prevention*, vol. 60, pp. 324–333, 2013.
- [6] C. Y. D. Yang and Noblis, "Trends in transit bus accidents and promising collision countermeasures," *Journal of Public Transportation*, vol. 10, no. 3, pp. 077–291X, 2007.
- [7] M. Staubach, "Factors correlated with traffic accidents as a basis for evaluating advanced driver assistance systems," *Accident Analysis & Prevention*, vol. 41, no. 5, pp. 1025–1033, 2009.
- [8] J. J. Gibson, *The Ecological Approach to Visual Perception*, Routledge, Abingdon, UK, 1986.
- [9] D. N. Lee, "A theory of visual control of braking based on information about time-to-collision," *Perception*, vol. 5, no. 4, pp. 437–459, 1976.
- [10] S. J. Park, S. Y. Kho, S.-Y. Kho, and H.-C. Park, "The effects of road geometry on the injury severity of expressway traffic accident depending on weather conditions," *The Journal of the Korea Institute of Intelligent Transport Systems*, vol. 18, no. 2, pp. 12–28, 2019.
- [11] C. R. Mercier, M. C. Shelley, G. H. Adkins, and J. M. Mercier, "Age and gender as predictors of injury severity in broadside and angle vehicular collisions," *Transportation Research Record: Journal of the Transportation Research Board*, vol. 1693, no. 1, pp. 50–61, 1999.
- [12] W. Chen and P. P. Jovanis, "Method for identifying factors contributing to driver-injury severity in traffic crashes," *Transportation Research Record*, vol. 1717, no. 9, pp. 1–9, 2000.
- [13] K. Sigal and G. P. Carlo, "Risk factors associated with bus accident severity in the United States: a generalized ordered logit model," *Journal of Safety Research*, vol. 43, pp. 171–180, 2012.
- [14] F. Zong, H. Y. Zhang, and H. G. Xu, "Predicting severity and duration of road traffic accident," *Mathematical Problems in Engineering: Theory, Methods and Applications*, vol. 2013, Article ID 547904, 9 pages, 2013.

- [15] N. Kuge, T. Yamamura, O. Shimoyama, and A. Liu, "A driver behavior recognition method based on a driver model framework," *SAE International Journal of Engines*, vol. 109, pp. 469–476, 2000.
- [16] R. Vesna, B. Milan, and B. Branko, "Identifying the key risk factors of traffic accident injury severity on Slovenian roads using a non-parametric classification tree," *Transport*, vol. 32, no. 3, pp. 272–281, 2017.
- [17] M. Abe and Y. Kano, "A study oil vehicle handling evaluation by model based driver steering behavior," in *Proceedings of the FISITA World Automotive Congress 2008, Congress Proceedings—Vehicle Concepts, Boay Design, Chassis Development*, pp. 377–384, Munich, Germany, June 2008.
- [18] L. Mussone, M. Bassani, and P. Masci, "Analysis of factors affecting the severity of crashes in urban road intersections," *Accident Analysis & Prevention*, vol. 103, pp. 112–122, 2017.
- [19] F. Chen, S. L. Chen, and Y. Y. Cheng, "Research on the model of road traffic safety evaluation based on synergetics theory," *Advanced Materials Research*, vol. 779-780, pp. 1028–1035, 2013.
- [20] I. Md Tazul and E. B. Karim, "Full Bayesian evaluation of the safety effects of reducing the posted speed limit in urban residential area," *Accident Analysis and Prevention*, vol. 80, pp. 18–25, 2015.
- [21] L. Montoro, S. A. Useche, F. Alonso, I. Lijarcio, P. Bosó-Seguí, and A. Martí-Belda, "Perceived safety and attributed value as predictors of the intention to use autonomous vehicles: a national study with Spanish drivers," *Safety Science*, vol. 120, pp. 865–876, 2019.
- [22] K. Xie, K. Ozbay, H. Yang, and C. Li, "Mining automatically extracted vehicle trajectory data for proactive safety analytics," *Transportation Research Part C: Emerging Technologies*, vol. 106, pp. 61–72, 2019.
- [23] C. Dai, *Research on the Post Characteristics of Modern Bus Drivers and Preventive Measures for Unsafe Behaviors*, Shandong University, Jinan, China, 2013.
- [24] X. G. Zhao, *Research on Key Technologies of Dynamic Warning of Traffic Safety Risks in Regional Road Networks*, Chang'an University, Xi'an, China, 2010.
- [25] M. Peng, *Research on Safety Management and Emergency Response of Urban Public Transport Operation*, Chang'an University, Xi'an, China, 2012.
- [26] Y. Li, *Research on Multi-Attribute Evaluation Method and Application of Driving Behavior Safety*, Jilin University, Changchun, China, 2016.
- [27] Y. Sang, *Research on the Mental Fatigue Evaluation of Beijing Public Transport Drivers*, Capital University of Economics and Business, Beijing, China, 2011.
- [28] G. Q. Yan, *Evaluation of Drivers' Potential Hazard Predictive Ability*, Chang'an University, Xi'an, China, 2011.
- [29] H. J. Ren, T. Xu, and X. Li, "Driving behavior analysis based on trajectory data collected with vehicle-mounted GPS receivers," *Geomatics and Information Science of Wuhan University*, vol. 39, no. 6, pp. 739–744, 2014.
- [30] T. X. Sun, *Analysis of Road Traffic Accidents Based on Data Mining*, Beijing Jiaotong University, Beijing, China, 2014.
- [31] C. W. Ren, *Research on Dynamic Supervision System of Bus Drivers*, Chang'an University, Xi'an, China, 2014.
- [32] T. Yi, "Investigation and characteristic analysis of bad driving behavior of bus drivers——taking Chengdu as an example," *Heilongjiang Transportation Science and Technology*, vol. 260, no. 10, pp. 166–168, 2015.
- [33] Y. Sun, "Research on urban road traffic congestion charging based on sustainable development," *Physics Procedia*, vol. 24, pp. 1567–1572, 2012.
- [34] Y. Xing, H. Liang, and D. Xu, "Sustainable development evaluation of urban traffic system," *Procedia-Social and Behavioral Sciences*, vol. 96, pp. 496–504, 2013.
- [35] Y. Yan, Y. Dai, X. Li, J. Tang, and Z. Guo, "Driving risk assessment using driving behavior data under continuous tunnel environment," *Traffic Injury Prevention*, vol. 20, no. 8, pp. 807–812, 2019.
- [36] Y. Wang, S. Peng, X. Zhou, M. Mahmoudi, and Z. Lu, "Green logistics location-routing problem with eco-packages," *Transportation Research Part E: Logistics and Transportation Review*, vol. 143, Article ID 102118, 2020.
- [37] Z. C. Guo, *Research on Lane Line Recognition and Lane Departure Judgment Method in ADAS*, Chang'an University, Xi'an, China, 2018.
- [38] G. Chen and C. Zhao, "Design and implementation of vehicle monitoring platform based on Beidou high precision location," *Electronic Design Engineering*, vol. 28, no. 04, pp. 52–55, 2020.
- [39] Y. Q. Xie, Z. B. Li, J. Qi, K. Zhang, B. X. Zhang, and F. Qi, "Optimal video communication strategy for intelligent video analysis in unmanned aerial vehicle applications," *Chinese Journal of Aeronautics*, vol. 33, no. 11, 2020.
- [40] X. Q. Xue, *Research on Traffic Safety Early Warning Methods in the Environment of Internet of Vehicles*, Beijing Institute of Technology, Beijing, China, 2016.
- [41] Y. Liang, K. L. Li, F. H. Bi, K. Zhang, and J. Yang, "Research on LFM CW radar velocity ranging optimization system based on FPGA," *Procedia Computer Science*, vol. 166, pp. 187–194, 2020.
- [42] Y. F. Wang, C. Z. Zhang, B. B. Zhang, and T. T. Wu, "Overview of data cleaning research," *New Technology of Library and Information Service*, vol. 12, pp. 50–56, 2007.
- [43] D. C. Corrales, A. Ledezma, and J. C. Corrales, "A case-based reasoning system for recommendation of data cleaning algorithms in classification and regression tasks," *Applied Soft Computing Journal*, vol. 90, 2020.
- [44] H. J. Wu, F. Liu, L. Zhao, Y. B. Shao, and R. Cui, "Application research of crawler and data analysis based on Python," *International Journal of Advanced Network. Monitoring and Controls*, vol. 5, no. 2, pp. 64–70, 2020.
- [45] H.-K. Chen, H.-W. Chou, J.-W. Su, and F.-H. Wen, "Structural interrelationships of safety climate, stress, inattention and aberrant driving behavior for bus drivers in Taiwan," *Transportation Research Part A: Policy and Practice*, vol. 130, pp. 118–133, 2019.
- [46] H. L. Sun and L. Liu, "Main factors and countermeasures affecting the safety of urban public transportation in my country," *Biotech World*, vol. 10, no. 10, p. 44, 2012.
- [47] B.-r. Cao, H.-H. Cao, and Y. Liu, "Research on construction and application of an evaluation system for regional road traffic safety," *Grey Systems: Theory and Application*, vol. 8, no. 4, pp. 527–538, 2018.
- [48] A. Theofilatos, "Incorporating real-time traffic and weather data to explore road accident likelihood and severity in urban arterials," *Journal of Safety Research*, vol. 61, pp. 9–21, 2017.
- [49] Y. Ge and K. Li, "Research on layout planning of automobile charging pile based on nuclear density analysis and space syntax——a case of Wuhan in hubei," *Urbanism and Architecture*, vol. 16, no. 34, pp. 41–45, 2019.
- [50] V. Petraki, A. Ziakopoulos, and G. Yannis, "Combined impact of road and traffic characteristic on driver behavior using

- smartphone sensor data,” *Accident Analysis and Prevention*, vol. 144, 2020.
- [51] J. Y. Sun and Y. F. Su, “Application of BP neural network based on matlab in public transport scheduling,” *Journal of Wuhan University of Technology (Transportation Science & Engineering)*, vol. 35, no. 3, pp. 599–602, 2011.
- [52] Y. F. Zhang, S. Y. Kuang, J. Liang, and J. Xu, “A recognition method for multi-reconnaissance data based on error back propagation algorithm,” *Electronic Warfare Technology*, vol. 34, no. 6, pp. 18–22, 2019.
- [53] P. Chen, *Research on Intelligent Real-Time Dispatching Model and System Implementation of Public Transport Based on BP Neural Network*, Beijing Jiaotong University, Beijing, China, 2008.
- [54] L. Wang and Y. J. Kuang, “Research of BP neural network optimizing method based on ant colony algorithm,” *New Industrialization Strategy*, vol. 2, no. 4, pp. 8–15, 2012.
- [55] J. Li, C. P. Chen, H. M. Deng, and Y. Ma, “Short-term traffic flow prediction based on improved variable learning rate BP algorithm,” *Automation & Instrumentation*, vol. 1237, no. 2, pp. 182–184, 2016.
- [56] Y. Xuan and R. L. Wang, “Research on the improvement of dual optimization on BP neural network,” *Journal of Guangxi Teachers Education University (Natural Science Edition)*, vol. 35, no. 1, pp. 60–65, 2018.
- [57] Y. D. Zhang, “Simulation of real-time management of orderly access information for urban traffic in big data,” *Computer Simulation*, vol. 35, no. 12, pp. 139–142, 2018.
- [58] L. Chen, W. He, and L. Q. Han, “Radial basis function neural network modeling of the traffic path cost function,” *CAAI Transactions on Intelligent Systems*, vol. 06, no. 5, pp. 424–431, 2011.
- [59] L. Yu, “Rolls-like algorithm of self-driving cars——whether the principle of “maximum minimum” can be used as the moral decision-making principle of “tramcar problem”” *Philosophical Trends*, vol. 10, pp. 100–107, 2019.
- [60] C. J. Cai, “Research on short-term traffic flow forecast model of BP neural network,” *Fujian Computer*, vol. 3, pp. 14–15, 2015.
- [61] W. Liu, H. X. Liu, and T. Zhu, “BP neural network for vehicle state estimation was based on ROC curve optimization,” *Journal of Xi’an University of Architecture & Technology*, vol. 46, no. 4, pp. 593–597, 2014.